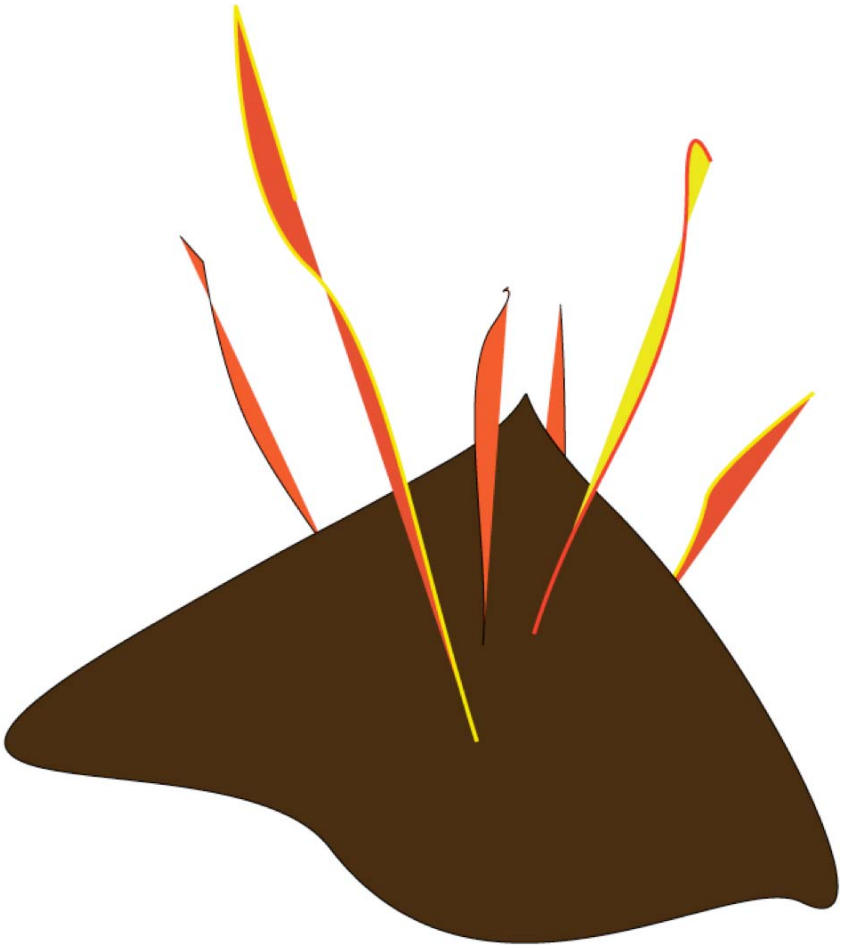
Petrographic, geochemical and age characterisation of crustal xenoliths from Coliban Dam, central Victoria, with implications for the early evolution of southeastern Australia, pre Lachlan Orogen

Allchurch, S.A.,
40643204



Presented to the Department of Earth and Planetary Sciences,
Division of Environmental and Life Sciences
In Partial Fulfilment of the requirements of the Degree of

Honours, BSc

Macquarie University, Sydney

November, 2008

STATEMENT OF ORIGINALITY

All the work submitted in this thesis is the original work of the author except where otherwise acknowledged. No part of this thesis has been previously submitted to any other university or institution.

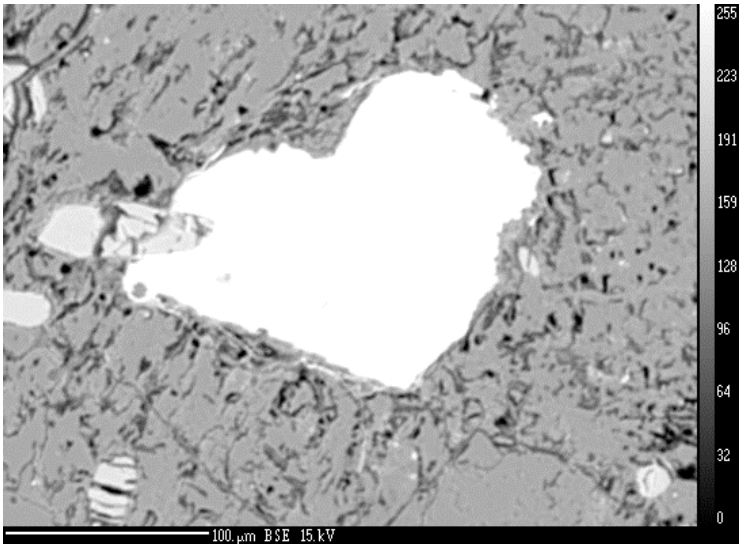
_____ _____

Signed *– Shelley Allchurch* ***Dated***

DEDICATION

To Grandma Allchurch

1921 to 2008



ACKNOLWEDGEMENTS

First and foremost thanks to my supervisors Nathan Daczko and Ian Graham. They have provided wonderful support and ideas throughout the year. Their enthusiasm never waned and they were always there when needed and willing to provide guidance. Nathan's door was always open! Thanks to Ross Pogson of the Australian Museum for access to the collection and permission to perform destructive analyses on samples from their collection and to the Australian Museum for the collections grant of $2,500 which paid for some analyses.

A big thank you to Peter Wieland at the GAU, Macquarie University who taught me so much in the laboratory - preparing solution and columns, running Nd and Sr on the TIMS, running solution on the MC etc and most importantly how to have a laugh. His hard work is much appreciated. Thank you to Norm for being so patient, understanding, flexible, knowledgeable etc etc etc etc and to Justin for his support and a big smile in the laboratory. Thanks to the Department of Earth and Planetary Sciences and GEMOC for their support. Thanks to Radd Flossman at UNSW for preparing polished sections at short notice and Irene Wainwright of UNSW Analytical Centre for the XRF analyses. Much appreciated funding from the NSW Division of the Geological Society of Australia allowed attendance at the 2008 Australian Earth Sciences Convention in Perth with a poster presentation of the thesis.

Thanks Christoph Beier for his great support, ideas and motivation and to Kevin Grant for his cheerful demeanour. Elena Belousova has been so patient and supportive and willing to spare time for questions. Melissa Murphy provided much appreciated guidance and support having just handed her thesis in and it was wonderful having Chuck to grumble with. Dick Flood's assistance and input was much valued and Carol McMahon's ability to help with just about anything is amazing and much appreciated.

My parents (Julie and David) and sister (Prue) have been so supportive of everything that I have undertaken, whether it be wayward travels or dropping a career to study and I couldn't ask for a better family. To the rest of my family, including the nephews and niece who think it strange that aunty is going to school, thank you so much - your love and understanding is much appreciated. My special friend, Sharon Phillips has also been a wonderful support, always bright and happy and providing distractions to free the mind. My close friends (Claire, Darren, Karen, Rick, Gerrit, Michael, Steph, Ang and Josie) have been so understanding in my absence from social events and/or bush regeneration! My flatmates,

Sarah and Peter, have been patient and not taken me up on the lack of housework during the last couple of months!!

Almost last, but not least my sincere thanks to dear John whose sensibility, support, laughs and input have been tremendous even whilst studying his PhD.

Finally, I thank Grandma for the wonderful memories and for she and Grandpa being so interested in and supportive of my studies.

PUBLICATION

Allchurch, S.A., Graham, I., Daczko, N.D., 2008. Petrographic and geochemical characterisation of charnokitic and cumulate gabbro xenoliths from Coliban Dam, central Victoria, with implications for the evolution of the Lachlan Orogen. Abstract with Programs, Australian Earth Sciences Convention. Perth, Geoscience Society of Australia.

TABLE OF CONTENTS

1 INTRODUCTION 1

1.1 Geological context ... 1
1.2 Review of xenolith studies ... 2
1.3 Aims of this study ... 4

2 REGIONAL SETTING AND LOCAL GEOLOGY 5

2.1 Regional Setting ... 5
2.1.1 Eastern Australia ... 6
2.1.2 Selwyn Block ... 7
2.2 Local Geology ... 10
2.2.1 Newer Volcanics Province (NVP) ... 10
2.3 Xenoliths of the NVP ... 13
2.4 Xenoliths of this study ... 14

3 FIELDWORK AND PETROGRAPHY 16

3.1 Fieldwork ... 16
3.1.1 Coliban Dam ... 16
3.1.2 Stewart Hill Location ... 19
3.2 Petrography ... 20
3.2.1 Upper Coliban Dam Suite ... 20
(a) Petrography - Coliban Dam Mafic Group ... 20
(b) Upper Coliban Dam Mafic Group Summary ... 40
(c) Petrography – Upper Coliban Dam Intermediate Group ... 42
(d) Upper Coliban Dam - Intermediate Group Summary ... 49
(e) Petrography – Upper Coliban Dam Felsic Group ... 50
(i) Felsic Group 1 with distinct glass banding ... 50
(ii) Felsic Group 2 with less distinct glass bands (sample #17915) ... 60
(f) Upper Coliban Dam Felsic Groups 1 and 2 Summary ... 68
(g) Upper Coliban Dam Massive Quartz Rich Felsic Group 3 ... 68
(h) Upper Coliban Dam Felsic Group 3 Summary ... 69
3.2.2 Petrography - Stewart Hill Suite ... 69
3.2.3 Stewart Hill Suite Summary ... 76

4 METHODS 77

4.1 Wholerock major and trace element analysis by XRF and ICP-MS ... 77
4.2 Wholerock isotope geochemistry ... 79
4.3 Mineral major element analysis by Electron Microprobe ... 82
4.4 LAM-ICP-MS Mineral Trace Element Analyses ... 82
4.5 Zircon U-Pb geochronology, trace element and Hf isotope analysis ... 84

5 RESULTS 88

5.1 Wholerock major and trace element geochemistry 88
5.1.1 Upper Coliban Dam Mafic Group 91
5.1.2 Upper Coliban Dam Intermediate Group 94
5.1.3 Upper Coliban Dam Felsic Group 95
5.1.4 Stewart Hill Suite 97
5.2 Mineral geochemistry 102
5.2.1 Upper Coliban Dam Mafic Group 102
5.2.2 Upper Coliban Dam Intermediate Group 106
5.2.3 Upper Coliban Dam Felsic Group 107
5.2.4 Stewart Hill Suite 108
5.3 Zircon U-Pb geochronology, trace element and Hf isotope analysis 128
5.3.1 Morphology – Coliban Dam Mafic Group 128
5.3.2 Morphology - Coliban Dam Felsic Group 129
5.3.3 Dating – Coliban Dam Mafic Group 130
5.3.4 Dating – Coliban Dam Felsic Group A 131
5.3.5 Hf isotope analysis – Coliban Dam Mafic Group 135
5.3.6 Hf isotope analysis – Coliban Dam Felsic Group A 135
5.3.7 Trace element analysis – Coliban Dam Mafic Group 137
5.3.8 Trace element analysis – Felsic Group A 137

6 DISCUSSION 141

6.1 Xenoliths from this study 142
6.1.1 Upper Coliban Dam Mafic Group 142
(a) Petrography 142
(b) Geochemistry 143
(c) Geothermometry 145
(d) Mafic Group U-Pb Zircon Dating 146
(e) Comparison to the NVP and Selwyn Block 147
6.1.2 Upper Coliban Dam Intermediate Group 149
(a) Petrography 149
(b) Geochemistry 149
(c) Comparison to the NVP and/or Selwyn Block 150
6.1.3 Upper Coliban Dam Felsic Group 151
6.1.4 Felsic Groups A and B 151
(a) Petrography 151
(i) Injection by host material 152
(ii) Equilibrium melt 152
(b) Geochemistry 153
(c) Sample #17915 Comparison to Felsic Groups A and B 155
(d) Geothermometry 156

(e) Felsic Group A U-Pb Zircon Dating 156
(f) Comparison with NVP and/or Selwyn Block 158
6.1.6 Sample #17917 (Petrographic Felsic Group 3) 159
6.1.7 Stewart Hill 159
(a) Stewart Hill Suite 159
(b) Comparison to NVP and/or Selwyn Block 160
6.2 Timeline 160
7 CONCLUSION 162

LIST OF FIGURES

Fig. 1.1 Map of Gondwana..... 2

Fig. 2.1 Tasmanides and NVP coverage and Selwyn Block. 5

Fig. 2.2 Tectonic model for the western Lachlan Fold Belt..... 7

Fig. 2.3 Regional aeromagnetic data..... 9

Fig. 3.1 Map showing the location of Coliban Dam..... 16

Fig. 3.2 Regional Map..... 17

Fig. 3.3 Coliban Dam site..... 17

Fig. 3.4 Coliban Dam site..... 17

Fig. 3.5 Stratigraphy at Coliban Dam 18

Fig. 3.6 Stewart Hill cone..... 19

Fig. 3.7 Xenolith collection at Stewart Hill..... 19

Fig. 3.8 Field photo of *in situ* xenoliths. 20

Fig. 3.9 Photo of mafic group xenolith, sample #15199..... 21

Fig. 3.10 Photo of mafic group xenolith, sample #17922. 21

Fig. 3.11 15199 thin section photo 24

Fig. 3.12 15199 thin section photo 25

Fig. 3.13 17913 thin section photo 26

Fig. 3.14 15199 thin section photo 27

Fig. 3.15 17914 thin section photo 28

Fig. 3.16 17914 thin section photo. 29

Fig. 3.17 17914 thin section photo 30

Fig. 3.18 17914 thin section photo 31

Fig. 3.19 17914 thin section photo 32

Fig. 3.20 17914 thin section photo 33

Fig. 3.21 18001 thin section photo 34

Fig. 3.22 18002 thin section photo 35
Fig. 3.23 15199 thin section photo 36
Fig. 3.24 17919 thin section photo 37
Fig. 3.25 17919 thin section photo 37
Fig. 3.26 17922 thin section photo 38
Fig. 3.27 17919 thin section photo 39
Fig. 3.28 17919 thin section photo 40
Fig. 3.29 Quartz-Alkali feldspar-Plagioclase Igneous classification..... 41
Fig. 3.30 Mafic Igneous classification 42
Fig. 3.31 Photo of intermediate group sample #17916 43
Fig. 3.32 18003 thin section photo 45
Fig. 3.33 18003 thin section photo 46
Fig. 3.34 17916 thin section photo 47
Fig. 3.35 18003 thin section photo 48
Fig. 3.36 18003 thin section photo 49
Fig. 3.37 Photo of felsic group 1 xenolith..... 50
Fig. 3.38 17918 thin section photo 53
Fig. 3.39 17918 thin section photo 54
Fig. 3.40 17918 thin section photo 55
Fig. 3.41 17911 thin section photo 56
Fig. 3.42 17921 thin section photo 57
Fig. 3.43 17921 thin section photo 58
Fig. 3.44 17912 thin section photo 59
Fig. 3.45 17920 thin section photo. 60
Fig. 3.46 Photo of felsic group 2 sample #17915 61
Fig. 3.47 17915 thin section photo 62
Fig. 3.48 17915 thin section photo 63

Fig. 3.49 17915 thin section photo 64

Fig. 3.50 17915 thin section photo 65

Fig. 3.51 17915 thin section photo 66

Fig. 3.52 17915 thin section photo. 67

Fig. 3.53 Photo of massive quartz rich felsic sample #17917. 68

Fig. 3.54 Photo of Stewart Hill Suite sample #19004. 70

Fig. 3.55 19002 thin section photo. 71

Fig. 3.56 19002 thin section photo 72

Fig. 3.57 19002 thin section photo 73

Fig. 3.58 19004 thin section photo. 74

Fig. 3.59 19004 thin section photo 75

Fig. 3.60 19002 thin section photo 76

Fig. 5.1 TAS plutonic volcanic diagrams. 89

Fig. 5.2 Wholerock oxides and trace elements vs SiO2. 90

Fig. 5.3 Wholerock oxides and trace elements vs Mg# 91

Fig. 5.4 Wholerock REE diagram. 92

Fig. 5.5 Wholerock spider diagrams 92

Fig. 5.6 Glass REE and spider diagrams. 93

Fig. 5.7 (a) Initial Hf vs Nd; (b) Initial Nd vs Sr 94

Fig. 5.8 (a) Initial Nd vs Age. 94

Fig. 5.9 (a) Ternary feldspar plot; (b) Quadrilateral pyroxene plot. 103

Fig. 5.10 Orthopyroxene charts - various elements vs Mg# 104

Fig. 5.11 Clinopyroxene charts - various elements vs Mg#; vs Al. 105

Fig. 5.12 Pyroxene REE and spider diagrams. 106

Fig. 5.13 Mafic sample #17913-03 BSE of zircon 128

Fig. 5.14 Mafic sample 15199-04 BSE of zircon 128

Fig. 5.15 Mafic sample #15199-02 BSE of zircon 128

Fig. 5.16 Felsic sample #17912-37 BSE of zircon. 129

Fig. 5.17 Felsic sample #17911-70 BSE of zircon 129

Fig. 5.18 Sample #17912-14 BSE of zircon..... 130

Fig. 5.19 Sample #17912-36 BSE of zircon..... 130

Fig. 5.20 Sample #17912-21 BSE of zircon..... 130

Fig. 5.21 Sample #17912-27 BSE of zircon..... 130

Fig. 5.22 Mafic U-Pb Concordia plot 131

Fig. 5.23 Felsic sample #17911 U-Pb Concordia; Inverse Concordia plots; Weighted average; Probability..... 132

Fig. 5.24 Felsic sample #17912 U-Pb Concordia; Inverse Concordia plots; Weighted average; Probability..... 133

Fig. 5.25 Felsic combined MSWD and relative probability 134

Fig. 5.26 Zircon Th/U ratio v Age..... 135

Fig. 5.27 Zircon eHf and iHf v age..... 136

Fig. 6.1 Wholerock spider diagrams. 144

Fig. 6.2 Tectonic discrimination plots for basalts..... 145

Fig. 6.3 Zircon Th/U ratios v U-Pb Age and Initial Hf v Age 147

Fig. 6.4 Kb/Nb vs K..... 148

Fig. 6.5 Tectonic discrimination plots for granites 154

Fig. 6.6 Tectonic discrimination plots for granites 154

Fig. 6.7 Timeline 154

LIST OF TABLES

Table 2.1 Geochronology of Cainozoic igneous activity in Victoria 11

Table 4.1 LLD of XRF analysis. 77

Table 4.2 ICP-MS Operating Conditions – Agilent 7500cs. 78

Table 4.3 Measured and reported values of BHVO-2 and BIR-1 – trace elements. 80

Table 4.4 LLD and errors for the CAMECA SX100 EMP 82

Table 4.5 LA-ICP-MS Operating Conditions – Agilent 7500s 83

Table 4.6 Measured and reported values of BCR2G – trace elements 83

Table 4.7 Values reported for 91500 zircon standard 85

Table 4.8 LAM-MC-ICP-MS Operating Conditions – Nu Plasma MC. 86

Table 5.1 Wholerock major element results and CIPW Norm calculations 98

Table 5.2 Wholerock trace element results. 99

Table 5.3 Isotope analysis results. 101

Table 5.4 Average plagioclase compositions 110

Table 5.5 Plagioclase range 112

Table 5.6 Average alkali feldspar compositions 112

Table 5.7 Alkali feldspar range 113

Table 5.8 Average orthopyroxene compositions 114

Table 5.9 Orthopyroxene range 116

Table 5.10 Average clinopyroxene compositions 117

Table 5.11 Clinopyroxene range 118

Table 5.12 Pyroxene trace element concentration (ppm) for all analyses 118

Table 5.13 Average amphibole compositions 120

Table 5.14 Average glass compositions 121

Table 5.15 Glass trace element concentration for all analyses 121

Table 5.16 Mica composition, with cations based on 24 oxygen 123

Table 5.17 Average ilmenite compositions 125

Table 5.18 Average magnetite compositions 126

Table 5.19 Average titanomagnetite compositions 127

Table 5.20 Zircon U-Pb analysis results 138

Table 5.21 Zircon Hf Isotope Analysis Results 139

Table 6.1 Geothermometry results 146

APPENDICES

Appendix 1 Table of Acronyms

Appendix 2 Seismic sections from the Lachlan Orogen

Appendix 3 Physical volcanology and geochemistry of the NVP

Appendix 4 List of samples collected, size, analyses undertaken and a petrographic summary, in groups determined by petrography

Appendix 5 EMP Major Element Geochemistry Results

Appendix 6 U-Pb Zircon Dating Results

Appendix 7 Zircon Hf Isotope Analysis Results

Abstract

Xenoliths brought up by igneous activity provide insight into underlying geology which may otherwise be inaccessible. In this study wholerock major and trace element geochemistry, zircon U-Pb geochronology and Sr-Nd-Hf isotope data are presented for xenoliths hosted by the Newer Volcanics Spring Hill Complex (~ 3 Ma) at Upper Coliban Dam. These xenoliths provide insight into underlying basement known as the Selwyn Block.

The xenolith suite includes two dominant groups: a mafic group with gabbroic texture and composition; and a felsic gneiss with granitic composition and glass bands interlayed between quartz-feldspar rich bands. Rarer xenoliths include trachyandesites, a massive quartz rich meta-sedimentary rock and basaltic icelandites from nearby Stewart Hill. Such diversity reflects the complex nature of the crust and mantle within the region.

Zircons separated from the felsic gneiss were examined by backscattered imaging and found to be of the magmatic type, with narrow metamorphic overgrowths. They have a Neoproterozoic crystallisation age of 553 Ma with Hf isotope compositions representative of a mixed source with juvenile and crustal input. Geochemical data support an upper crustal signature. These findings extend on limited knowledge of the Selwyn Block, including a history of formation and deformation. The data also unleashes a potential source for the extensive Lachlan Orogen granites and regional sedimentary terrains.

Five zircons from the mafic group xenoliths were also analysed and they provide a timeline of magmatic events within the region. The mafic and intermediate xenoliths share Sr isotope composition with the Newer Volcanic Province but heterogeneous trace element signatures suggest that they are not related.

1 Introduction

1.1 Geological context

In Earth's 4.5 Ga history, supercontinents have been formed and broken up in what is now known as the Wilson Cycle. Most prominent are Rodinia (~1.35 Ga to 0.8 Ga) which preceded the formation of Gondwana (~ 0.6 Ga to ~ 0.1 Ga), Pangea (~0.3 Ga to 0.18 Ga) and Laurasia (0.33 Ga to 0.06 Ga) (Li and Powell, 1993; Condie *et al.*, 2000; Veevers, 2000; Li and Powell, 2001; Condie, 2004).

During Rodinian times, at ~ 1 Ga, Australia was attached to east Antarctica and South China Block (SCB), lying ~ 30 °N of the equator (Li and Powell, 2001). By ~ 0.76 Ga, the breakup of Rodinia was at its peak, Australia was separated from the SCB and east Gondwana had been formed. The fragments of Gondwana began converging at ~ 0.6 Ga with the subduction of Indo-Antarctica (India) beneath west Gondwana (Africa, South America), forming the Mozambique Suture (Li and Powell, 2001; Boger and Miller, 2004). The ocean between west and east Gondwana then began to close at ~ 0.56 Ga by subduction of east Gondwana, forming the Kuunga suture. The completion of convergence at ~ 0.53 Ga marked the complete formation of Gondwana (Veevers, 2000; Boger and Miller, 2004) (Fig. 1.1).

During the final stages of Gondwanan formation (~ 0.58 – 0.52 Ga), small scale rifting was occurring to the east of Australia, resulting in the Kanmantoo Marginal Basin. Meanwhile the Proto Pacific plate was being subducted below east Gondwana on a larger scale, forming the Ross-Delamerian Orogeny (Boger and Miller, 2004; Miller *et al.*, 2005). Plate reorganisation then occurred at ~ 0.52 Ga causing orogenesis along the entire Gondwana/Pacific margin, a subduction arc and turbidite deposition signalling the beginning of the Lachlan-Robertson Orogen (Boger and Miller, 2004; Miller *et al.*, 2005).

Pangea began forming at ~ 0.32 Ga, with the convergence of Gondwana and Laurussia (Li and Powell, 1993). At ~0.15 Ga Pangea began to breakdown, followed quickly by the separation of Gondwana at ~ 0.13 Ga, particularly sea-floor spreading between Australia and Antarctica. Australia became an independent plate at ~ 96 Ma (Li and Powell, 1993).

The period from 0.6 Ga to 0.5 Ga is of interest in this study, particularly the small scale rifting to the east of Australia (see Fig. 1.1 for Australia's location at that time). This study aims to better understand the nature of the crust being rifted. The felsic xenoliths of this study are a sample of that crust, now known as the Selwyn Block. Also of interest is the final breakup of Gondwana at ~ 0.096 Ga, which coincides with the beginning of Cretaceous-Tertiary volcanism in eastern Australia which hosts the xenoliths (Price *et al.*, 1997; Price *et al.,* 2003).

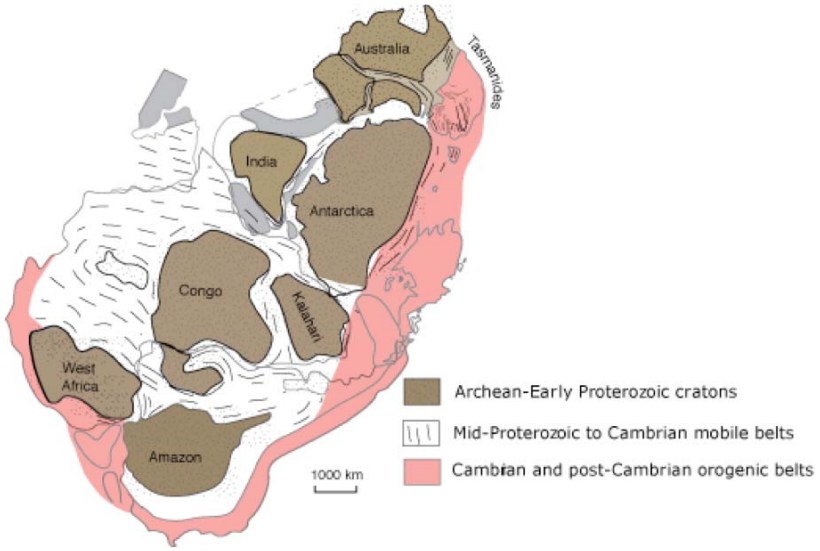


Fig. 1.1 Map of Gondwana illustrating the Tasmanides and Archean-Early Proterozoic cratons modified, based on Li and Powell (1993) and Foster and Gray (2000).

1.2 Review of xenolith studies

Xenolith A fragment of rock that is entrained in volcanic or intrusive material during igneous activity. A xenolith may be country rock not associated with the igneous activity within which it is entrained or part of the igneous system, such as from the wall of a magma chamber, and classed as a cognate xenolith (Allaby and Allaby, 2003).

Xenoliths provide abundant information on subsurface physical and chemical characteristics of the crust and mantle. Extensive worldwide studies have been undertaken on a variety of xenolith suites, ranging from ultramafic to silicic (O'Reilly and Griffin, 1985; Dodge *et al.*, 1986; Griffin and O'Reilly, 1986; O'Reilly and Griffin, 1990;

Wysoczanski *et al.*, 1995; Aguirre-Diaz *et al.*, 2002; Weber *et al.*, 2002; Dessai *et al.*, 2004; Sutherland *et al.*, 2004; Dai *et al.*, 2008). Authors of such studies have been able to infer, amongst other things, crustal thickness, tectonic processes, magma mixing and regional geotherms with information obtained from xenoliths. When tied with geophysical data, such information provides strong evidence for subsurface processes.

Most xenoliths studied within southeastern Australia to date have been mantle derived and ultramafic to mafic in composition, as summarised by O'Reilly *et al.* (1989b). Few lower crustal xenoliths of predominantly mafic composition have also been studied and consist mainly of plagioclase and pyroxene (O'Reilly *et al.*, 1989a).

Several authors (Ellis and Green, 1979; O'Reilly and Griffin, 1985; O'Reilly *et al.*, 1997; Sutherland *et al.*, 1998) created a Cenozoic geotherm for southeastern Australia using garnet websterite, garnet lherzolites, garnet pyroxenites and garnet granulite xenoliths suites. This geotherm has since been used with other suites in the region to constrain crystallisation, crustal depth information and subsurface magmatic processes. For example, Griffin and O'Reilly (1985) use geochemical, petrological and geophysical data to infer an approximate crustal base of 30-25 km for eastern Australia, with the lower crust formed by episodic intrusion of basaltic material and tectonic accretion in an intraplate environment. They also used geophysical data with gradients observed between 45-20 km to suggest a large transitional zone between crust and mantle.

Other studies (Dai *et al.,* 2008; Dodge *et al,* 1986) have used isotope systems such as Rb-Sr, Lu-Hf and Sm-Nd to infer crustal thickness, magma mixing and source signatures.

1.3 Aims of this study

The aims of this study are to:

- Characterise the xenoliths, including:
  - rocktype and microstructures
  - the relationship, if any, with the host lava
  - tectonic setting of the xenolith sources.
- Create a timeline of events associated with the formation, evolution and entrainment of the xenoliths.
- Establish if a geochemical and physical relationship exists with current information on the Selwyn Block.
- Establish if a geochemical and physical relationship exists with geology of Antarctica.

2 Regional setting and local geology

2.1 Regional Setting

Australia may be divided into two distinct geological regions: the cratonic Proterozoic and Archaean geology of the western two thirds and the Phanerozoic Tasmanides of the east, divided by the Tasman Line (Scheibner, 1974; Veevers and Powell, 1984; Shaw *et al.*, 1996). The Tasmanides geology formed progressively in an easterly direction by accretionary processes and consists of four orogenic belts (from west to east): Delamerian, Lachlan, Thompson and New England orogens (Fig. 1.1). The Lachlan Orogen extends from southern Victoria to central New South Wales and is overlain in central and western Victoria by deposits of the Cenozoic Newer Volcanics Province (**NVP**) (Fig. 2.1). The Spring Hill Complex of the NVP hosts the xenoliths of this study, which are interpreted to be derived from the Lachlan Orogen basement geology (Griffin and O'Reilly, 1986; Cas and Simpson, 1993; Nicholls *et al.*, 1993; Graham *et al.*, 2003; Gray and Foster, 2004).

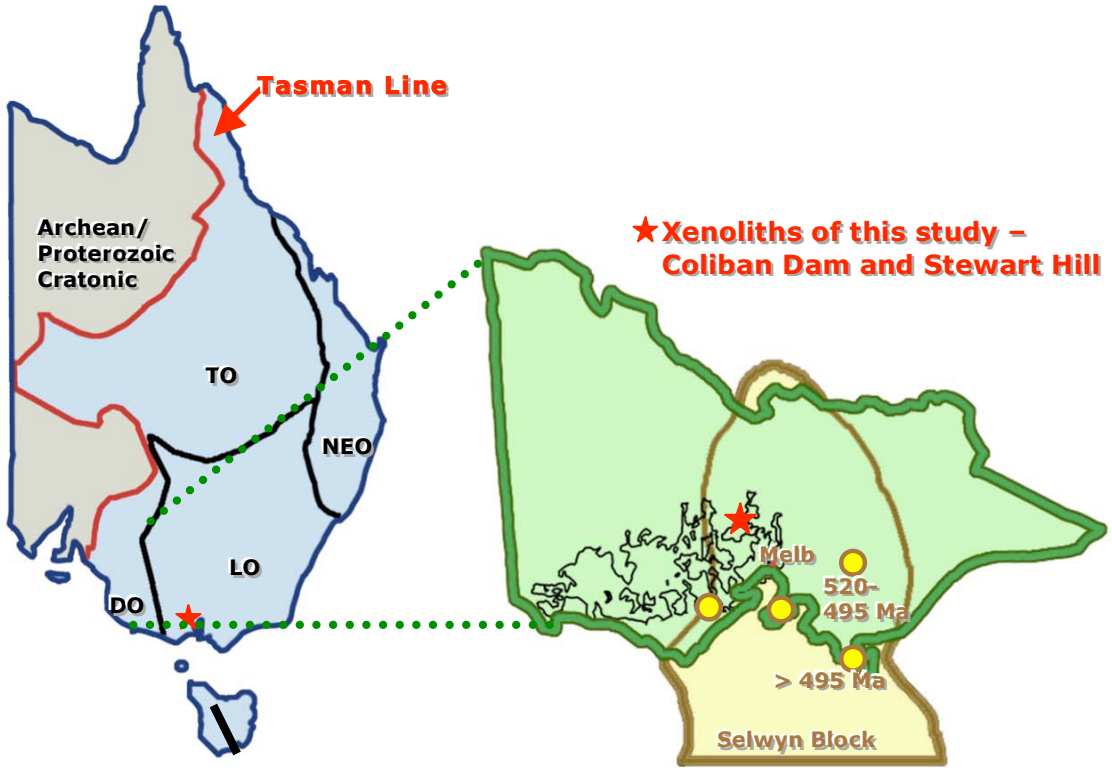


Fig. 2.1 **Left** - Tasmanides with the four orogens: DO – Delamerian Orogen; TO – Thomson Orogen; LO – Lachlan Orogen; NEO – New England Orogen; Tasman Line (red) - divides the Archean/Proterozoic craton of the west with the thin Phanerozoic crust of the east; and the location of the xenoliths in this study (red star) (Modified based on Shaw *et al.*, 1996; Gray and Foster, 2004). **Right** - Newer Volcanic Province coverage (black line: Cartwright, 2002); underlying Selwyn Block (brown line; Cayley *et al.*, 2002); Outcrops of the Selwyn Bock (circles with brown line/yellow fill); Victoria (green line/fill).

2.1.1 Eastern Australia

(a) Delamerian Orogen

The Delamerian Orogen is located to the west of the Lachlan Orogen. It formed part of a large orogeny that ran along the eastern margin of Gondwana, from Australia to Antarctica, with the Ross Orogen being the Antarctic counterpart (Boger and Miller, 2004; Miller *et al.*, 2005; Foden *et al.*, 2006). The main orogenic phase of the Delamerian Orogeny occurred between ~ 515 and 490 Ma relating to subduction of the Palaeo Pacific plate (Boger and Miller, 2004; Miller *et al.*, 2005; Foden *et al.*, 2006). This activity was in response to major plate reorganisation following the convergence of west and east Gondwana from 540 to 500 Ma (Boger and Miller, 2004; Miller *et al.*, 2005; Foden *et al.*, 2006). Convergence in the Ross Orogen (Antarctica) began ~ 25 Ma earlier (540 Ma), when the east of Australia was still in a state of extension and sediments were being deposited on a passive margin in the Kanmantoo Basin.

(b) Lachlan Orogen

There is great debate over the formation and evolution of the Lachlan Orogen from ~525 to 320 Ma, particularly with regard to the involvement of continental crust (Scheibner, 1973; Chappell and White, 1974; Rutland, 1976; Scheibner, 1985). However, it is agreed that the orogen formed eastward in a predominantly oceanic setting as a result of the amalgamation of accretionary complexes, volcanic arcs, submarine fans and oceanic crust. The upper crustal geology is dominated by turbidites, calcalkaline volcanic rocks and granites. The various turbidite sequences are comparable with the modern-day Bengal Fan and were derived from the Gondwanan Ross-Delamerian Orogen and Transantarctic Mountains, with age peaks between 600 to 500 Ma (Foster and Gray, 2000; Fergusson, 2003; Gray and Foster, 2004; Veevers, 2004; Veevers *et al.*, 2005; Veevers and Saeed, 2008; Veevers *et al.*, 2008).

Glen (2005) discussed orogenies in terms of tectonic cycles, from rift to a possible drift phase, convergence followed by collisional deformation and possible post collision phases. It was proposed that the Lachlan supercycle occurred from ~490 Ma to 320 Ma, with diachronous, orogen-wide contractional deformation and heating from Early to Middle

Cambrian that affected surrounding geology, such as the Delamerian Orogeny both on the mainland and in Tasmania.

Continental accretion in the eastern region was driven by subduction whilst in the west, extensional processes such as rifts and grabens were the predominant processes, resulting in crustal thicknesses of ~35-40 km. Thin skinned tectonic structural processes have deformed the upper 12-15 km of the crust by large-scale listric faulting, whilst the lower crust is mafic and of oceanic origin (Foster and Gray, 2000; Gray *et al.*, 2003).

The Lachlan Orogen is separated into three structural subprovinces: Western, Central and Eastern, and then into smaller zones (Foster and Gray, 2000). The xenoliths of this study were collected from within the Bendigo Zone of the western Lachlan Orogen, ~ 20 km west of the Heathcote Fault (Cayley *et al.*, 2002; Miller *et al.*, 2005). A tectonic model for the Western Lachlan Orogen is given in Fig. 2.2.

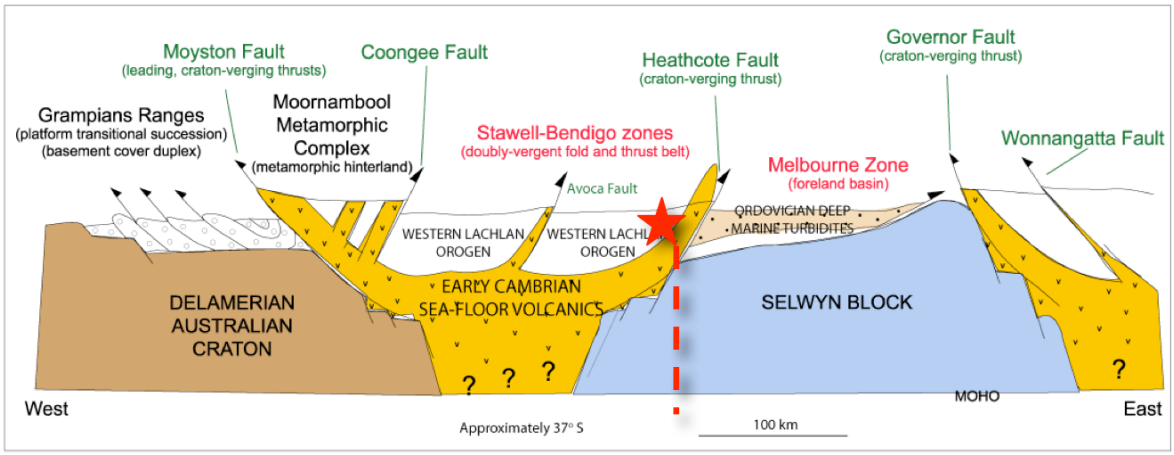


Fig. 2.2 Tectonic model for the western Lachlan Fold Belt, modified based on Cayley *et al.* (2002) and Miller *et al.* (2005). Red star = Location of the xenoliths in this study. This model is at ~ 37ºS, which is very close to the latitude of the xenoliths at 37°17'4.77"S.

2.1.2 Selwyn Block

The presence of a crustal block beneath Victoria, particularly the Melbourne Zone, was initially proposed as an underthrust, thin continental crustal block (Crawford *et al.*, 1984) or a submarine plateau (Powell, 1983). It is believed that the block, initially called 'Victorian Microcontinent' (Scheibner, 1985; Scheibner, 1992), was present as far back as 840 Ma when it was attached to eastern Australia. At ~ 590 Ma it was located offshore of

southeastern Australia before being rifted by the Kanmantoo Marginal Basin. The Mount Arrowsmith volcanics have been associated with such extension at ~ 586 Ma (Crawford *et al.*, 1997)). Sedimentary components of the Lachlan Orogen were deposited upon the Selwyn Block from ~ 525 Ma before its final convergence with the Australian craton in the Ordovician-Silurian that caused deformation in the western Lachlan Orogen. This convergence is close to the estimated convergence of the Mount Arrowsmith volcanics at ~ 400 Ma during the Bindian Orogeny (Scheibner, 1992; Scheibner and Veevers, 2000; Rossiter and Gray, 2008).

Proterozoic-Cambrian meta-igneous outcrops on the south coast of central Victoria at Waratah Bay, Phillip Island, Barrabool Hills and inland near Licola are particularly important in comparison of Victorian and Tasmanian geology. Also, greenstone at Waratah Bay has been traced along a belt to King Island and Tasmania via magnetic data (Cayley *et al.*, 2002) (Fig. 2.3). Seismic profiles (Cayley *et al.*, 2008) have also identified the Selwyn Block, placing it between 12 km and 39 km depth, where it meets with the geophysical MOHO (Appendix 2). The depth to the Selwyn Block varies, from depths of 15 km at the north west of the Melbourne Zone to possible surface expression near the Victorian coast (Cayley *et al.*, 2002). The extent of the Selwyn Block based on geophysical methods as proposed by Cayley *et al.* (2002) is debated by Rossiter and Gray (2008) who use Ba concentration in granites and structural processes to reassess the boundaries.

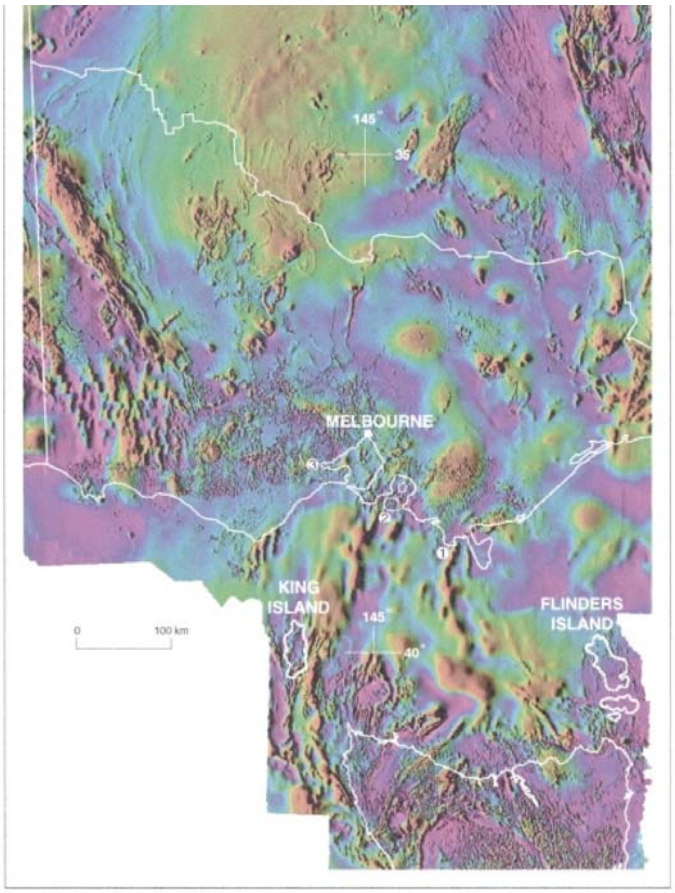


Fig. 2.3 Regional aeromagnetic data showing a continuous magnetic anomaly from Victoria down through King Island to Tasmania. Outcrops of the Selwyn Block are marked: 1 – Waratah Bay; 2 – Phillip Island; 3 – Barrabool Hills (Cayley *et al.*, 2002).

Isotopic and geochemical data differentiate the granites in the area overlying the Selwyn Block (Central Granite Superprovince) from others in the Lachlan Orogen (Gray, 1990; Cayley *et al.*, 2002). A Cambrian and recycled Proterozoic source is suggested by Nd and Sr isotope signatures, whilst the presence of cordierite infers a more silicic source for these granites compared to other parts of the Lachlan Fold Belt (Elburg, 1996). The granites also share similarities with the 395 Ma Bassian Granite Province which spans from Wilsons Promontory to northeastern Tasmania (Chappell and White, 1985; Stump *et al.*, 1986; Clemens, 1988).

2.2 Local Geology

2.2.1 Newer Volcanics Province (NVP)

(a) Overview

The NVP extends from central Victoria to southeastern South Australia, with activity ranging from approximately 9 Ma to 5 ka (Fig. 2.1). The NVP represents the most recent major igneous phase in Victoria and southeastern South Australia. It follows earlier phases including Early Jurassic to Early Cretaceous activity in central Victoria (191 to 130 Ma) and extensive Late Cretaceous to Mid-Miocene (95 to 10 Ma) activity across Victoria (The Older Volcanics) (Graham *et al.*, 2003). Currently, there is debate over the nomenclature of these provinces, with suggestion that the Cenozoic Older Volcanics and NVP should not be separated as they represent continued volcanism rather than different volcanic episodes (Price *et al.*, 2003; Vandenberg, 2007). Peaks with younger ages are dominant within the province, however this may simply be due to the greater number of younger samples gathered due to greater preservation and better exposure (Price *et al.*, 2003).

Price *et al.* (2003) proposed a time-based division of the Cenozoic igneous activity in Victoria (Table 2.1), rather than using the Newer and Older Volcanics. The Western District Province includes most of the Newer Volcanics and encompasses the Macedon-Trentham Province. Vandenberg (2007) and Price *et al.* (2003) discussed the original NVP nomenclature, particularly the issue of whole lava flows being split into different provinces. It was resolved that GeoScience Victoria will no longer use the Newer Volcanics and Older Volcanics categories but rather follow the modified proposal by Price *et al.* (2003; Vandenberg, 2007) (Table 2.1). This new nomenclature is still being debated so the NVP nomenclature will continue to be used in this paper. The Spring Hill host of the xenoliths in this study is located within the Macedon-Trentham Province, which will be reviewed in more detail in this paper (Cas and Simpson, 1993; Graham *et al.*, 2003). Greater detail on the NVP overall is given in Appendix 3.

Table 2.1 Geochronology of Cainozoic igneous activity in Victoria

	New Nomenclature (Price *et al.*, 2003)	Age of activity
Older Volcanics	**Latrobe Province**	**59-56 Ma**
	Eastern Province	
	Toombullup Subprovince	37-44 Ma
	Howitt Subprovince	36-33 Ma
	Bogong Subprovince	31-37 Ma
	Gelantipy Subprovince	39-43 Ma
	Flinders Subprovince	40-48 Ma
	South Coast Province	
	Aberfeldy subprovince	min 28 Ma
	Neerim Subprovince	21-26 Ma
	Thorpdale subprovince	18-23 Ma
	Gellibrand subprovince	27-30 Ma
Newer Volcanic Province	**Macedon-Trentham Province**	**8-3 Ma**
	Western District Province	
	Central Highlands Subprovince	6.2-0.5 Ma
	Western Plains Subprovince	4.6-0.0 Ma
	Uplands Province	4 to 2 Ma

(b) Physical volcanology

The 8.3 to 2.9 Ma Macedon-Trentham Province commonly has basaltic valley infilling with flows up to 20 m thick in outcrops with columnar jointing. The volcanic centres for basaltic rocks occur in clusters and are represented by low hills. The silicic nepheline and quartz-bearing trachytes on the other hand form small lava flows and steep-sided domes and plugs (Price *et al.*, 2003). Mt Macedon is an example of a complex volcanic centre within the province. It has three eruption points and nine recognised lava flows with varying composition from olivine basalts to Na trachyte (Price *et al.*, 2003).

The NVP covers ~ 20,000 km^2 with over 400 volcanic centres (Joyce, 1975; Ewart, 1985; Johnson, 1989). Characteristic features of the NVP include lava shields, lava flows, scoria cones, maars, tuff rings and composites. There are two types of lava flows within the NVP: *sheet lava flows* which form an extensive 5-7m thick veneer of low viscosity lava, seemingly by repeated thin flow sheets; and *constricted lava flows* which move along pre-existing valleys thus resulting in a thicker and narrower morphology (Nicholls *et al.*, 1993;

Graham *et al.*, 2003; Price *et al.*, 2003). See Appendix 3 for more information on physical NVP details.

(c) Volcanic products

The Macedon-Trentham Province features the most silicic rock types within the NVP, which is otherwise predominantly mafic. The rock types include: transitional basalt (alkali olivine basalt), trachyte, basanite, nepheline hawaiite, nepheline trachyte and tholeiitic (K and Na) trachytes (Ewart *et al.*, 1985). The xenoliths in this study are hosted by basaltic icelandites (Price *et al.*, 1997; Graham *et al.*, 2003).

The lavas in the NVP range from alkalic nephelinites and basanites to transitional hawaiites and tholeiitic icelandites (Price *et al.*, 2003).

(d) Geochemistry of the basaltic icelandite

Representative basaltic icelandite samples discussed by Price *et al.* (1997) have SiO_2 of ~ 52 wt %, relatively high MgO (8.64 wt %) and Fe (Fe_2O_3 3.10; FeO 7.09 wt %) and low K_2O (0.96 wt %). They are enriched in HREE compared to chondrite, decreasing in the LREE (Price *et al.*, 1997). Based on the relatively high MgO of the basaltic icelandite compared to the less evolved compositions studied, Price *et al.* (1997) determined that the basaltic icelandite had not evolved from other compositions observed within the NVP. Ratios such as Pb/Ce and K/Nb ratios and relatively high SiO_2 were indicative of crustal contamination. However, Price *et al.* (1997) concluded that the basaltic icelandites result from heterogeneity within the shallow mantle, which was also reflected in heterogeneous strontium isotope values for basaltic icelandite within the NVP, ranging from $^{87}Sr/^{86}Sr$ 0.70429 (in the east) to 0.70548 (in the west). $^{87}Sr/^{86}Sr$ values between 0.70388 and 0.70494 were detected for other compositions within the Macedon-Trentham complex. For more details of NVP geochemistry, see Appendix 3.

(e) Tectonic Setting

The source of igneous activity has been debated. For the basalts, similarities with OIB have been observed in isotope and geochemical data, although this varies between series in the NVP (the basalts have been geochemically divided into tholeiitic and transitional plains and alkalic cones series by Vogel and Keays (1997)). A cogenetic relationship has

been noted between the cones series and transitional plains series, both being derived from an enriched, mantle source (Vogel and Keays, 1997). However, there is still debate as to the source, ie plumes, lithospheric mantle or a mixture of the both (McDonough *et al.*, 1985; Price *et al.*, 1997). Some authors suggest hot spot intraplate volcanism following the northward migration of the Australian Plate (Wellman and McDougall, 1974). However this is doubted due to the unsuitable location of Mt Macedon silicic volcanism, which should lie west of the trace (Lister and Etheridge, 1989; Price *et al.*, 1997). Also, the longevity of volcanism suggests a continuous period of volcanism has occurred rather than transient sessions.

Recent studies suggest that the activity relates to asthenospheric uplift due to continental extension/rifting and mantle instability related to the break-up of Gondwana (Price *et al.,* 1993; Price *et al*., 2003). Initial volcanic activity postdates the separation of Australia and Antarctica by approximately 10 Ma and it is suggested that this activity instigated the rise of a chain of diapirs. The late NVP and Macedon-Trentham Province may then represent a new cluster of diapiric volumes at the base of the lithosphere (Price *et al.*, 2003). The diapirs may have risen from 200-400 km depth at approximately 5-10 km/year, reaching mantle solidus P-T conditions 100 Ma after extension.

2.3 Xenoliths of the NVP

Within the NVP, lower crustal and mantle xenoliths have been extensively observed and studied at 30 locations. However, they are mostly mafic in composition and limited study has been undertaken within the Macedon-Trentham Province. Sutherland *et al.* (2004) reported on xenoliths from Hepburn Lagoon (~ 37 km WSW from the Coliban Dam site), which are predominantly pyroxenite and websterite cumulate xenoliths, with less dominant gabbros, gabbronorites and norites. They are derived from Hy and Ne-normative basaltic melts.

The Western Plains Subprovince of NVP in the Colac Mortlake area has the highest concentration of xenoliths within proximity of the Mortlake Discontinuity, east of which xenolith observations are limited (Graham *et al.,* 2003; Price *et al.*, 2003). Ultramafic xenoliths are associated with maars and tuff rings, like Lakes Bullenmerri and Gnotuk, though they are typically found within basaltic scoria cones, such as Mount Leura, Mount Noorat and Mount Shadwell (Graham *et al.,* 2003; Price *et al.*, 2003). These locations are

within the Western Plains Subprovince, with Mt Franklin and Mt Fraser being the most significant sites within the Central Highlands Subprovince (Price *et al.*, 2003).

The xenoliths typically occur in SiO_2 undersaturated alkalic host rocks, such as nephelinites, basanites, nepheline hawaiites and nepheline mugearites (Nicholls *et al.*, 1993; Price *et al.*, 2003). However, rocktype is not necessarily a controlling factor on xenolith occurrence (Nicholls *et al.*, 1993; Graham *et al.*, 2003). Xenoliths are predominantly peridotitic, particularly spinel lherzolite which forms part of a chromian diopside series, together with less common harzburgites (with Cr diopside), dunites and wehrlites (Wilshire and Shervais, 1975; Graham *et al.*, 2003; Price *et al.*, 2003). A less common Al- and Ti-rich augite series distinguished by Al-rich spinel instead of Cr- and black Al- and Ti- rich augites, consists of wehrlites, websterites, and clinopyroxenites. A garnet pyroxenite series is also reported and common at some locations, such as Lake Bullenmerri and Lake Gnotuk (Graham *et al.*, 2003; Price *et al.*, 2003).

The series described above is most likely derived from the upper mantle, near the crust mantle boundary, with some granulites from mid to deep crustal origin (Griffin and O'Reilly, 1986; Nicholls *et al.*, 1993). Clasts of close-lying surface material, like limestone, sandstone, granite and metamorphic rocks, have also been observed (Graham *et al.*, 2003).

2.4 Xenoliths of this study

Xenoliths from two sites are being studied in this paper: the Upper Coliban Dam site with dominant felsic and mafic suites along with less dominant intermediate samples; and the Stewart Hill site with a mafic-intermediate suite.

Graham *et al.* (2003 and 2006) undertook a preliminary study on the dominant suites from the Coliban Dam site. The felsic xenoliths had geochemistry representative of charnockites with ~75 wt% SiO_2 and K_2O+Na_2O of ~7 wt%, low TiO_2 (0.3 wt%) and LREE enriched (Le Maitre *et al.*, 1989). SHRIMP U-Pb zircon ages of 580 Ma (Neoproterozoic) and 400 Ma (Devonian) were determined. Thorium/U ratios between 0.3 and 0.6 were identified in the Neoproterozoic age group whilst a range of 0.01 to 0.05 was present in the Devonian age group. The low Th/U ratios possibly relate to metamorphism, which was also identified in thin-section. These are the oldest ages to be found in the

3 Fieldwork and petrography

3.1 Fieldwork

Xenoliths were collected from two locations: predominantly Upper Coliban Dam, near Kyneton and a few from Stewart Hill, ~ 30 km WNW of Upper Coliban Dam.

3.1.1 Coliban Dam

The Coliban Dam samples were collected from the Upper Coliban Dam at Kyneton, central Victoria (37°17'4.77"S 144°23'45.97"E), approximately 500 m above sea level (Figs. 3.1 and 3.2). A total of 19 samples were analysed in this study, 13 of which were collected in 1980 by Australian Museum personnel during construction of the wall at Upper Coliban Dam. Current low water levels and limited vegetation growth at the site allowed access for collection of an additional six samples in this study (Figs. 3.3 and 3.4).

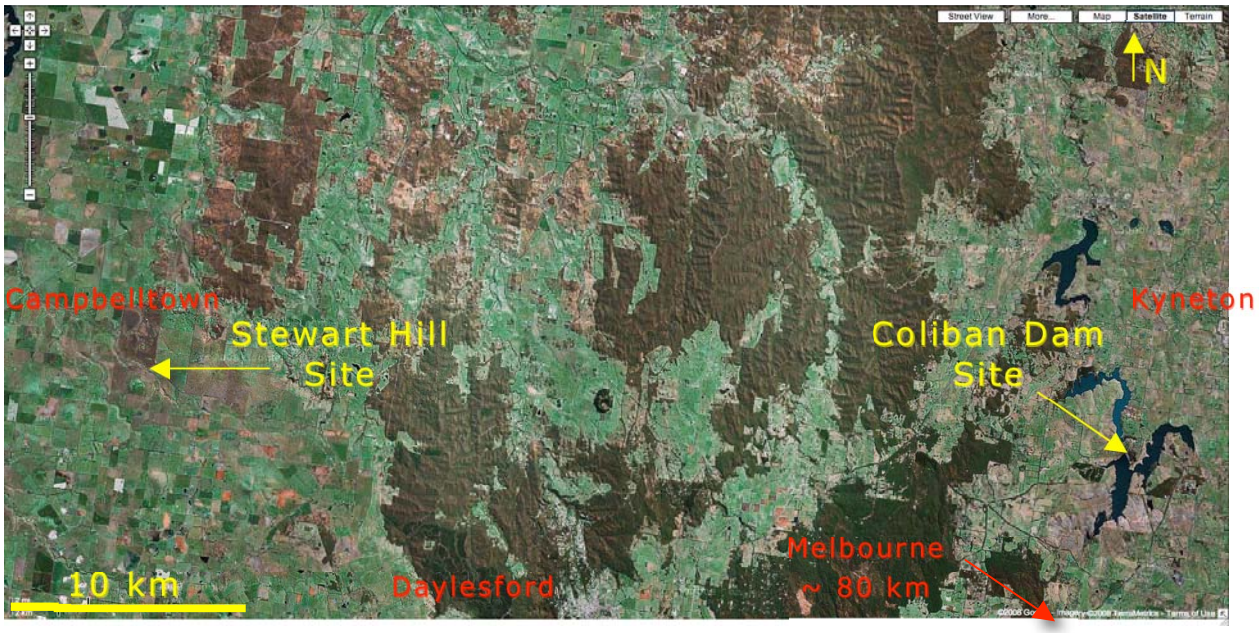


Fig. 3.1 Map showing the location of Coliban Dam and Stewart Hill sites (Image: Google Earth, 2008)

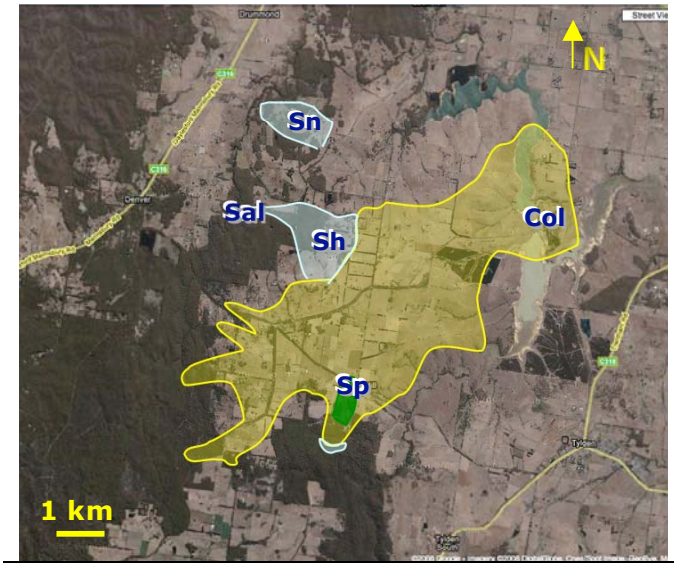


Fig. 3.2 Map in the region of the Coliban Dam Site, including approximate coverage of the Spring Hill Complex (modified: Graham *et al.*, 2003): Yellow = basaltic icelandite (trachyandesite); Blue = olivine basalt; Green = pyroclastics. Sn = Snowden Hill; Sal = Salisbury; Sh = Shepherds; Sp = Spring Hill; Col = Coliban Dam Site. (Image: Modified, Google Earth, 2008).



Fig. 3.3 Coliban Dam site, showing the dam and current low water levels (Photos: Allchurch, 2008).



Fig. 3.4 Coliban Dam site, including the xenolith-bearing basaltic icelandite (left) (Photos: Graham, 2008).

The xenoliths are hosted within the Spring Hill Complex which encompasses the Spring Hill Township at 37°18'50.82"S 144°21'2.41"E . Approximately 16 km^2 of tholeiitic differentiates have been identified within the complex, ranging from trachyandesite to alkaline dacite in composition (Graham *et al.*, 2003). The complex provides the most acidic and silicic end members within the NVP with ages ranging from ~ 8.3 to 2.9 Ma (Wellman, 1974; Graham *et al.*, 2003; Sutherland and Hollis, unpublished Geotrack Reports). Samples were collected from ~ 100 m exposure with stratigraphy consisting of the xenolith bearing basaltic icelandite overlying a platy basalt which in turn overlies Permian glacial deposits (Fig. 3.5). Xenoliths were only observed within the basaltic icelandite. It is difficult to constrain the topography due to changes made during construction of the dam. A list of the samples including size, analyses and a summary of petrography is included in Appendix 4.

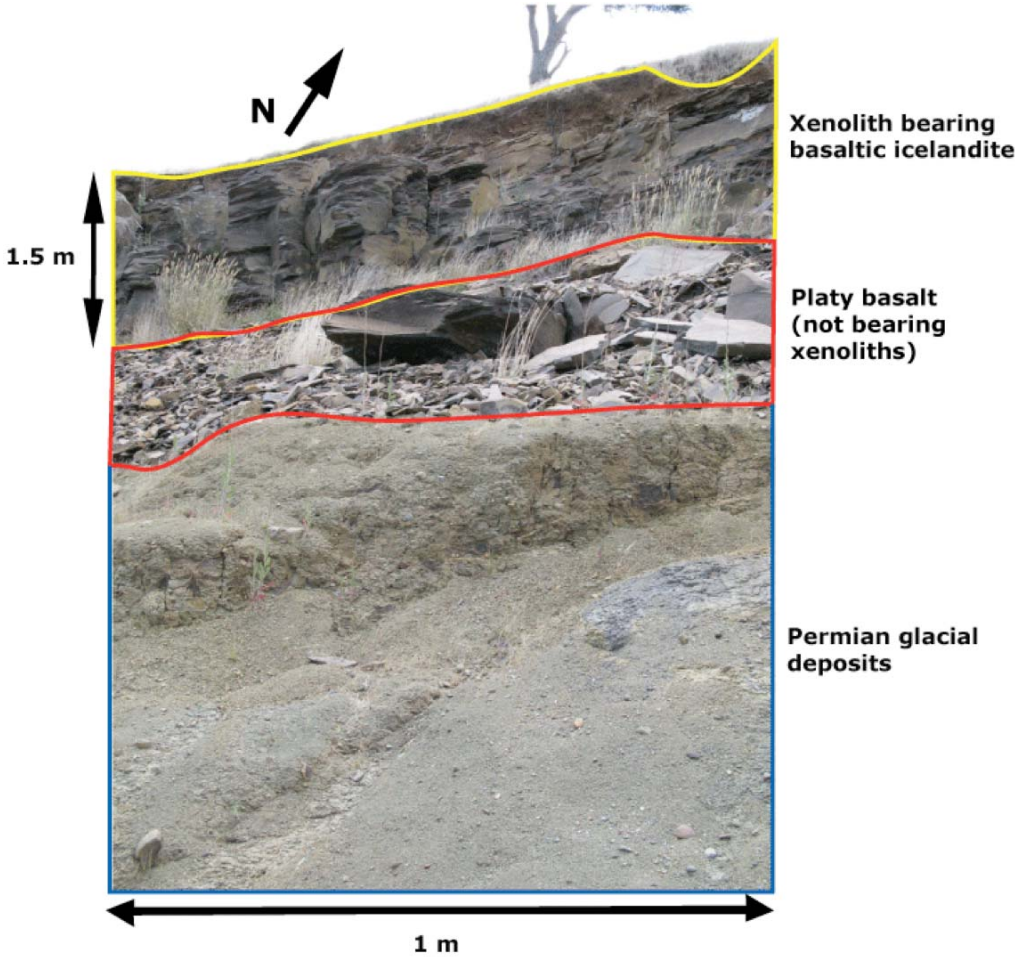


Fig. 3.5 Stratigraphy at Coliban Dam consisting of the xenolith-bearing basaltic icelandite overlying platy basalt (with no xenoliths) which unconformably overlies Permian glacial deposits (Image: modified Graham, 2008).

3.1.2 Stewart Hill Location

Six xenolith samples were collected from Stewart Hill, which is located ~ 30 km WNW from the Upper Coliban Dam site. Stewart Hill is a scoria cone with tholeiitic composition and is part of the Clover Hill Complex. The xenoliths were collected from the base of the cone and range in size from ~ 100 mm x 100 mm to 200 mm x 200 mm (Figs. 3.6 and 3.7). A sharp contact is noted between the xenoliths and host material in hand sample.



Fig. 3.6 Stewart Hill site showing the cone in the left hand background.



Fig. 3.7 Xenolith collection at Stewart Hill (Photo: Graham, 2008).

3.2 Petrography

3.2.1 Upper Coliban Dam Suite

Based on their mineralogy and textures, the Coliban Dam xenoliths can be divided into two main groups: a mafic and felsic group, with a rarer intermediate group and a single massive quartz rich sample. This group subdivision has been used throughout this thesis. The xenoliths range in size from ~ 20 mm x 20 mm to 200 mm and are predominantly rounded, although some are angular, as in Fig. 3.8.



Fig. 3.8 Field photo of rounded *in situ* xenoliths exhibiting a sharp contact with the host basaltic icelandite. Each xenolith is ~3 cm wide (Photos: Graham, 2008).

(a) Petrography - Coliban Dam Mafic Group

Mineral modes have been estimated by thorough visual inspection of thin sections, see Appendix 4 for modes. This Group is predominantly composed of plagioclase feldspar (40 to 60 vol. %); pyroxene (40 to 60 vol. %); magnetite – titanomagnetite (<5 to 10 vol. %). Accessory minerals include biotite, a pseudomorphed mineral and minor apatite. Glass / fine-grained material is present in varying mode from 5 to 10 vol. %, with some devitrified.

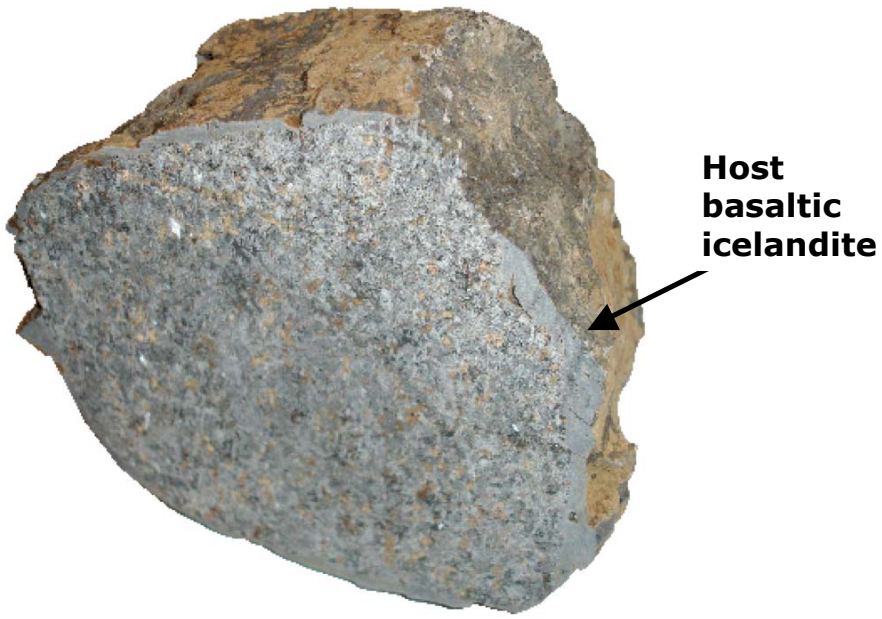


Fig. 3.9 Photo of a mafic group xenolith, sample #15199 ~ 15 cm across with attached basaltic icelandite (Image: Allchurch, 2008).



Fig. 3.10 Photo of a mafic group xenolith, sample #17922 showing the complex nature of the xenolith, including changes in colour and grain size of the texture (Image: Allchurch, 2008).

The plagioclase grains range from 0.5 to 4 mm are euhedral to subhedral and lathlike (Figs. 3.11-3.14 and 3.15); the pyroxene grains (80 % clinopyroxene and 20 % orthopyroxene) range from 0.4 to 3.2 mm are predominantly euhedral although some have

irregular crystal faces (Figs. 3.11-3.14 and 3.15); magnetite - titanomagnetite ranges from 0.04 to 2 mm are subhedral to anhedral (Figs. 3.11-3.13 and 3.15). Biotite, up to 0.4 mm is subhedral to anhedral (Fig. 3.14), apatite up to 0.05 mm is euhedral, and altered, while the pseudomorphed mineral ranges up to 2 mm long and is euhedral to subhedral (Fig. 3.23). Glass / fine-grained material up to 3 mm is interstitial (Figs. 3.11 and 3.12).

Igneous textures and deformation twinning are observed within the plagioclase grains (Figs. 3.11-3.14; 3.15). Both the long axis and twinning orientation in plagioclase grains are aligned in some samples, particularly #15199 (Figs. 3.13 and 3.23). Recrystallisation textures and bent deformation twins are observed in the plagioclase grains (Figs. 3.22, 3.25 -26) of some rocks. Rarely, plagioclase segments that share optical continuity with proximal larger grains are surrounded by glass and isolated from the other parts of the mineral. The outer boundaries of plagioclase and pyroxene grains have inclusions of plagioclase and pyroxene (Fig. 3.11). Biotite inclusions are also observed within pyroxene grains, and usually aligned within the cleavage of the pyroxene (Fig. 3.14).

A reverse ophitic texture is observed (particularly in samples #17914 and 18001), with euhedral pyroxene grains (up to 3.2 mm) enveloped by oikocrystic plagioclase grains (Fig. 3.15). Within this texture, the pyroxenes are typically well-spaced. However, when plagioclase is absent, the pyroxenes are present as subhedral crystal shapes surrounded by interstitial glass and in other zones in tight grain clusters (Figs. 3.16 and 3.17). Glass within these samples is usually found in discrete zones (Fig. 3.17).

The opaque minerals, magnetite and ilmenite, are present as small rounded inclusions (to 0.4 mm) within plagioclase and as small clusters along pyroxene grain boundaries (Figs. 3.13 and 3.15). Sample #18002 has an interesting vermiform texture of the opaque minerals. No reaction rim is evident between these minerals and pyroxene and plagioclase. However, within the glass, particularly in #18002, a corona texture is observed around the opaques with pyroxene (to 0.04 mm) and plagioclase (to 0.04 mm) grains. In sample #18001, the opaque minerals have a mode up to 10 vol. % and reach 2 mm, again showing corona rims (Fig. 3.21).

The contact between the host material and primary mineral phases is relatively sharp with little reaction observed (Fig. 3.16). Typically, the glass/fine-grained material is interstitial

with a micro doleritic texture with little or no reaction observed by the minerals. In other areas such material is finer-grained, orange/red in colour and is observed near altering minerals. The pseudomorphed mineral has a well developed reaction rim with alteration occurring along fractures (Fig. 3.23).

Biotite is also present within interstitial glass throughout the samples (Fig. 3.19). In addition to the textures mentioned above, sample #17919 has domains with well developed metamorphic textures including bent deformation twins and undulose extinction (Fig. 3.24). Within these domains, there is a mixture of fine grained size textures (< 0.02 to 0.5 mm). Examples of axialites (elongate spherulitic textures) and crystallites are present within the glass and along grain boundaries/fracture lines <1 mm (particularly #17919, Figs. 29 and 30).

The reverse ophitic texture is finer grained (<0.05 mm) in sample #17922 (Fig. 3.26) and a large feldspar grain (1.5 cm) is observed. There are domains consisting of coarser (<1 mm) feldspar grains with recrystallisation textures and brokendown pyroxene grains.

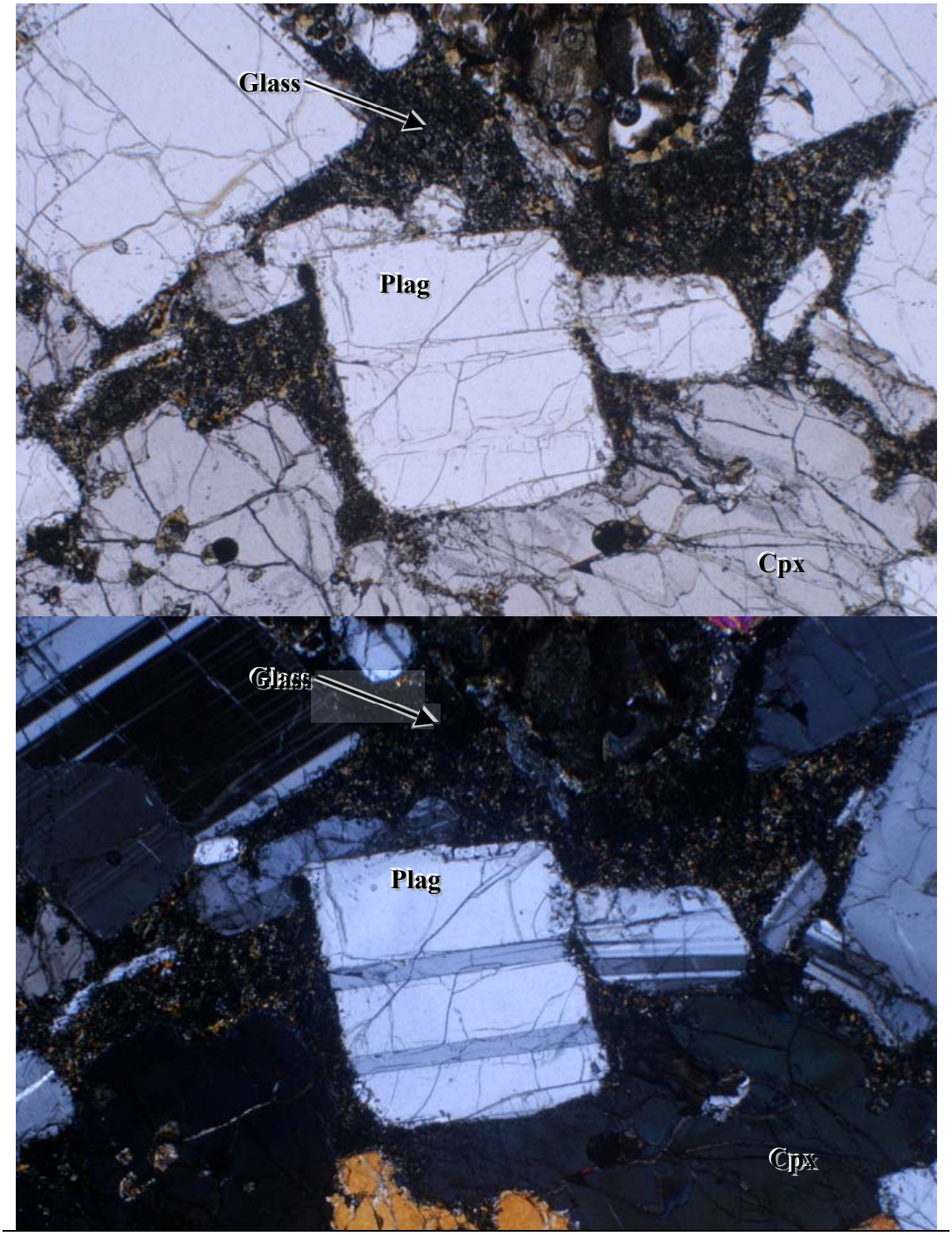


Fig. 3.11 15199 (a) PPL (b) XPL Base of photo: 3.5 mm - euhedral plagioclase with pyroxene and plagioclase inclusions within the rim and subhedral pyroxene grains surrounded by interstitial glass.

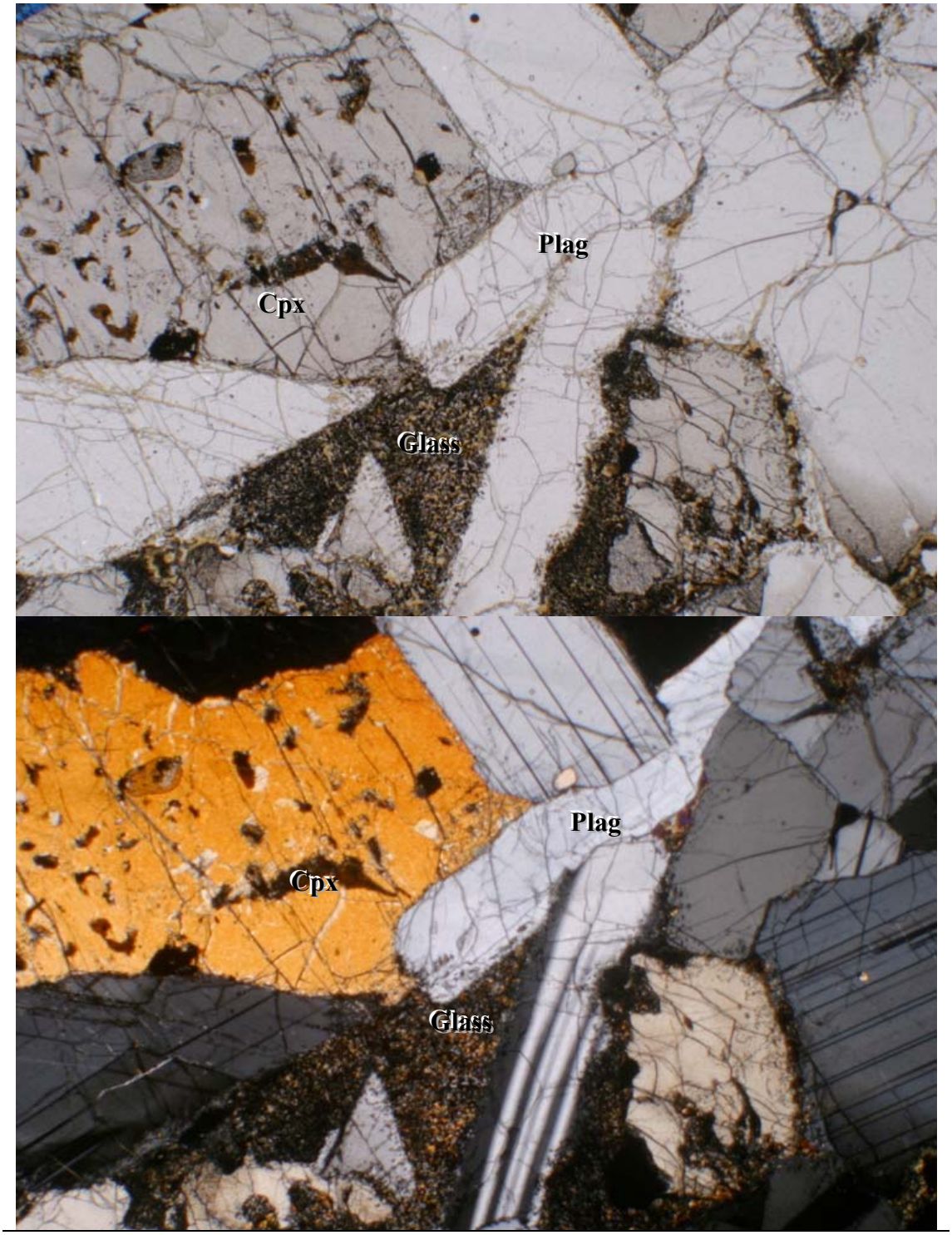


Fig. 3.12 15199 (a) PPL (b) XPL Base of photo: 3.5 mm – plagioclase grains exhibiting 'moth eaten' boundary textures, interstitial glass, interstitial pyroxenes and inclusions within the pyroxenes.

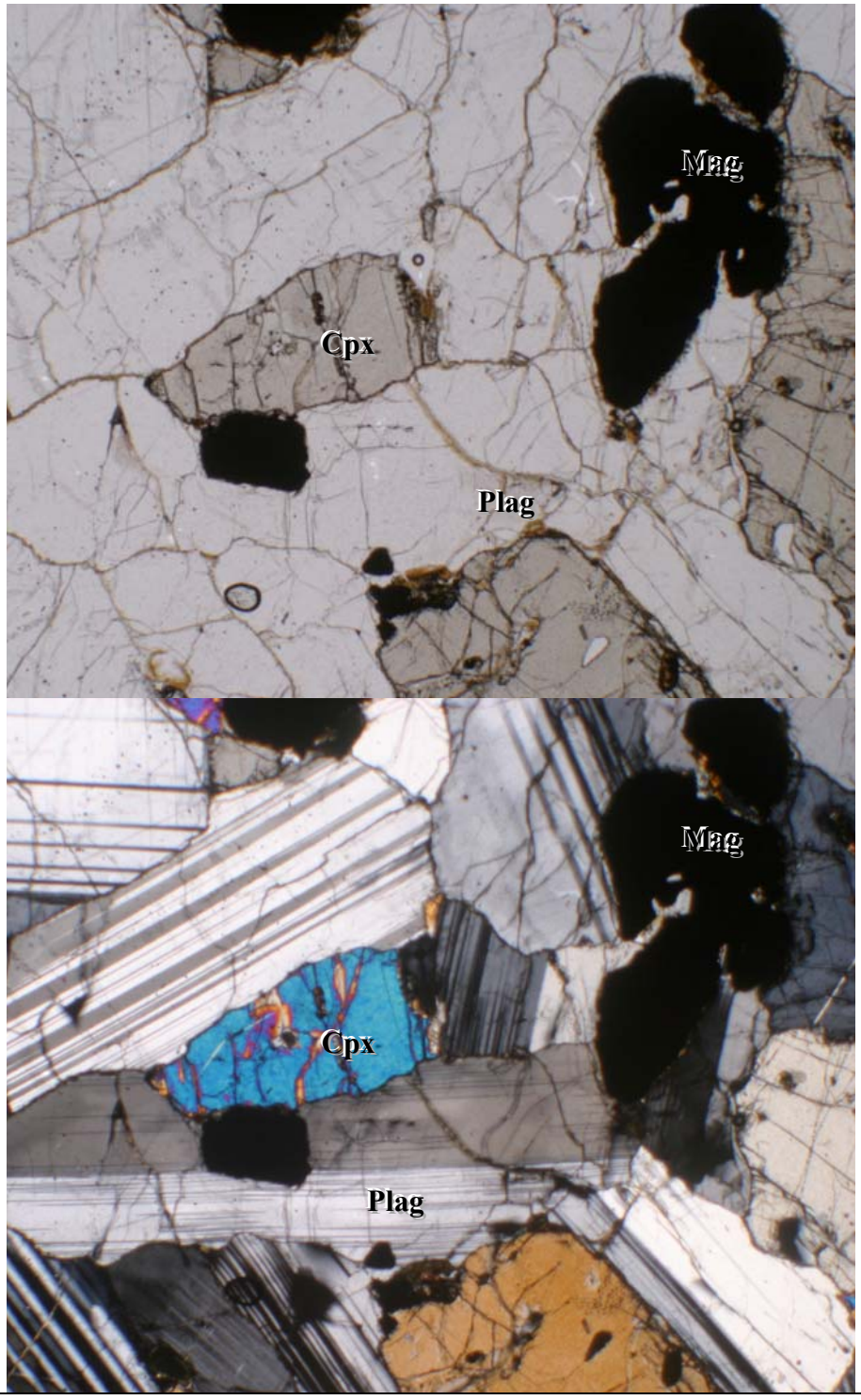


Fig. 3.13 17913 (a) PPL (b) XPL Base of photo: 2.8 mm – plagioclase laths and interlocking texture with pyroxene and magnetite grains.

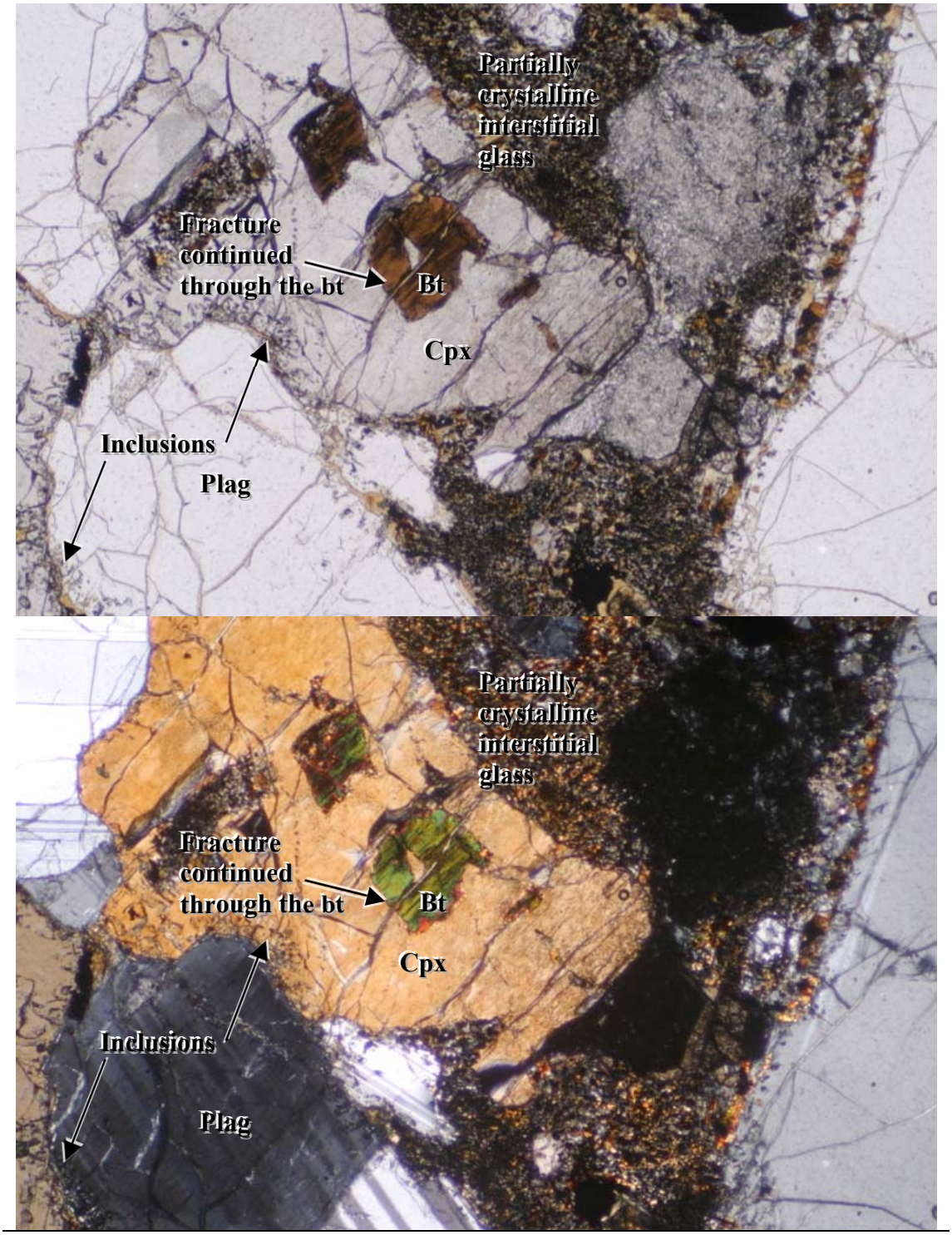


Fig. 3.14 15199 (a) PPL (b) XPL Base of photo: 1.75 mm – Biotite inclusions within a pyroxene grain which are aligned with the cleavage of the pyroxene. Also notable are the pyroxene and plagioclase inclusions within the plagioclase and pyroxene rims. A fracture within the pyroxene grain is continued through the biotite inclusion.

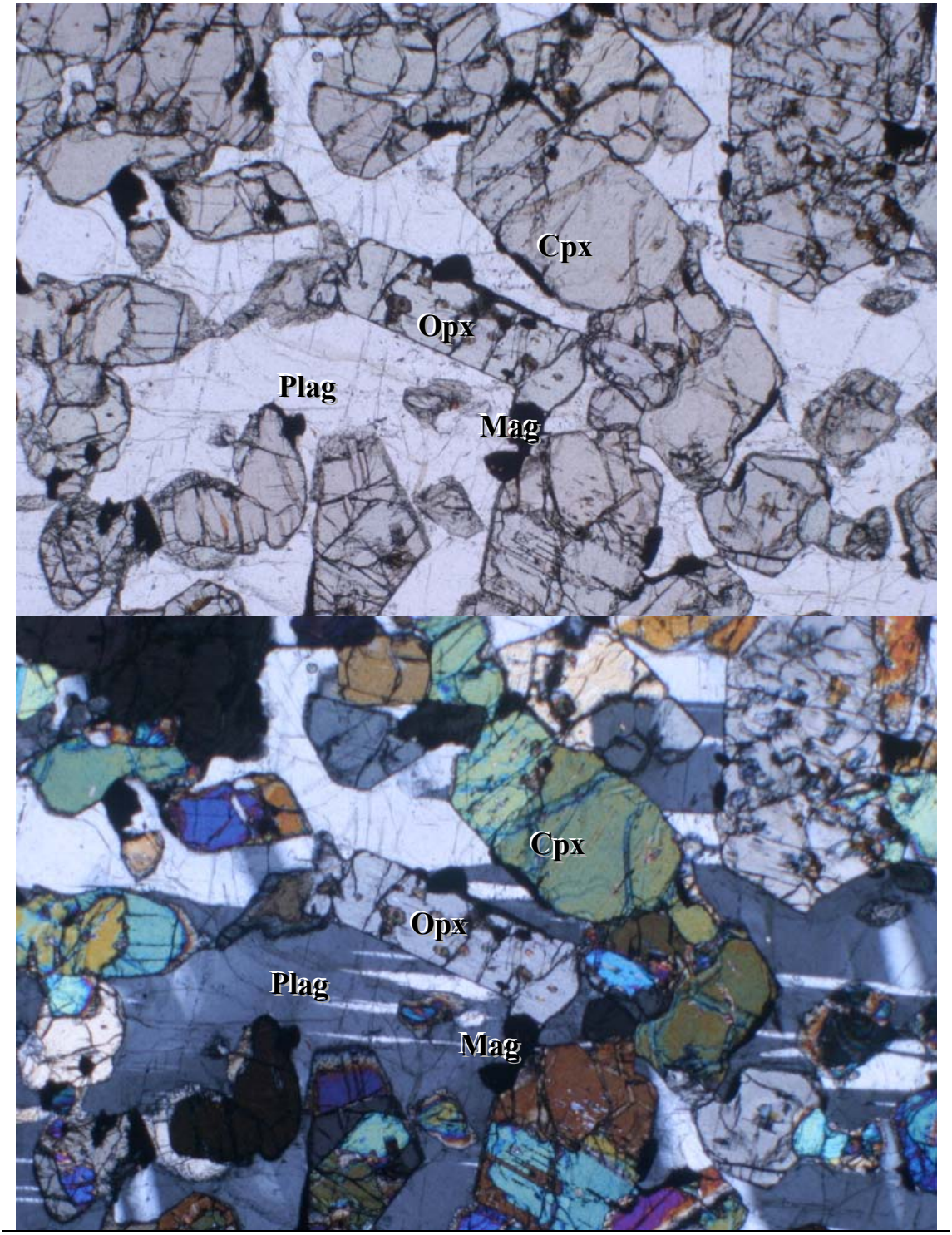


Fig. 3.15 17914 (a) PPL (b) XPL Base of photo: 3.5 mm – Reverse ophitic texture with euhedral pyroxene grains enveloped by an oikiocrystic plagioclase grain with deformation twinning. Also note the magnetite grains along the pyroxene grain boundaries.

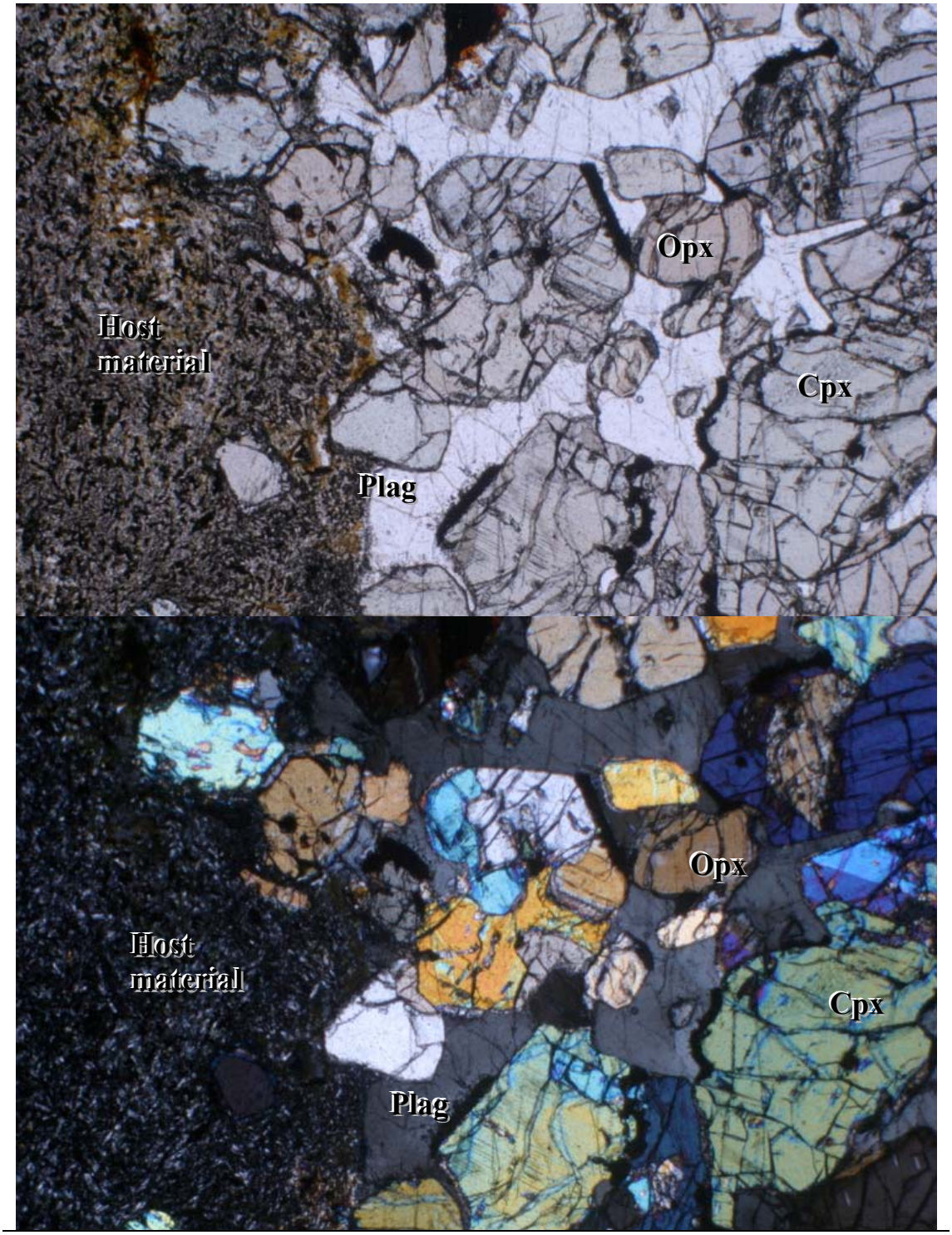


Fig. 3.16 17914 (a) PPL (b) XPL Base of photo: 3.5 mm – Reverse ophitic texture exhibiting euhedral pyroxene grains and the sharp contact with the host lava.

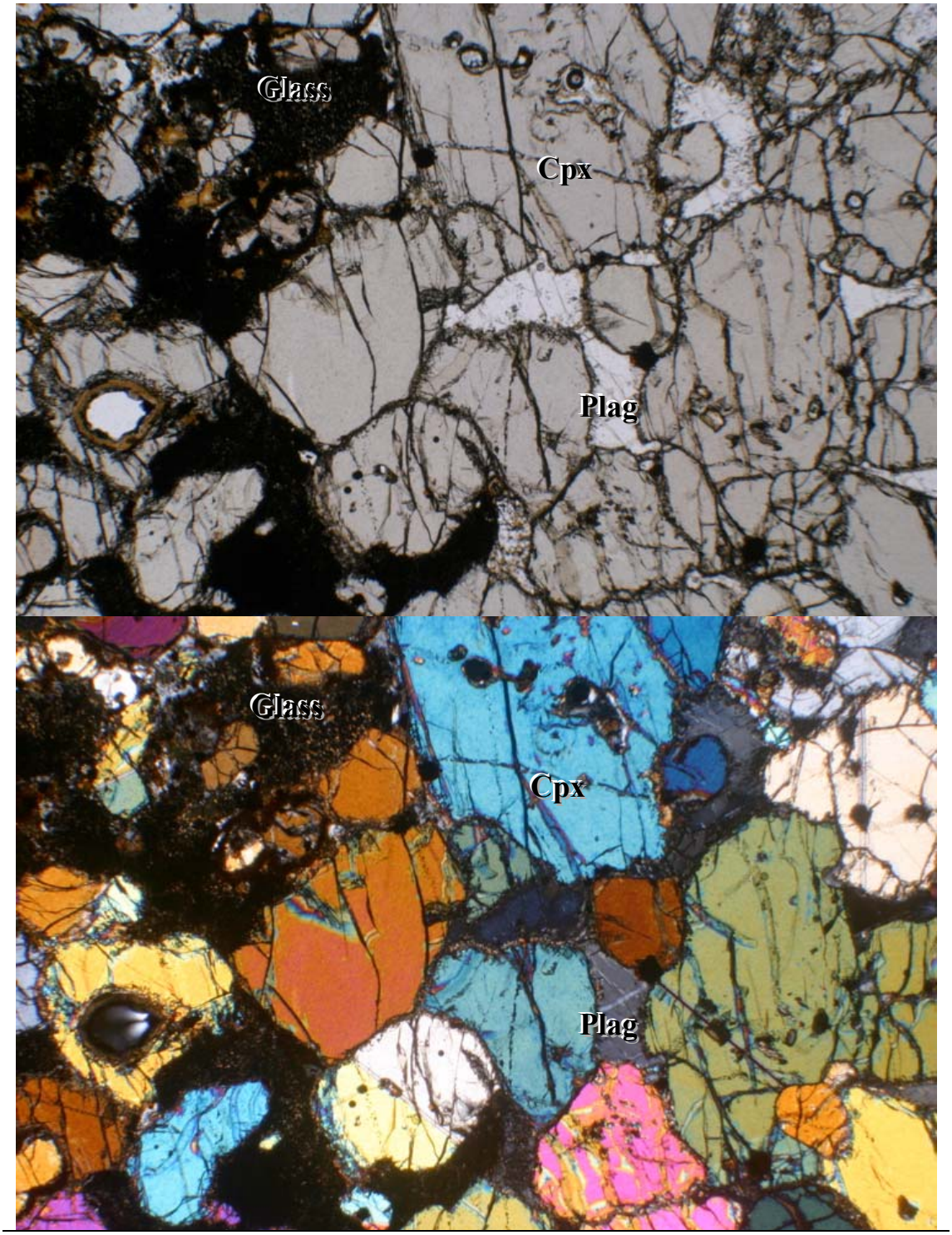


Fig. 3.17 17914 (a) PPL (b) XPL Base of photo: 3.5 mm – Change in zones from the reverse ophitic texture with an oikocrystic plagioclase (on the right) to interstitial glass (on the left) and tight pyroxene cluster (bottom right).

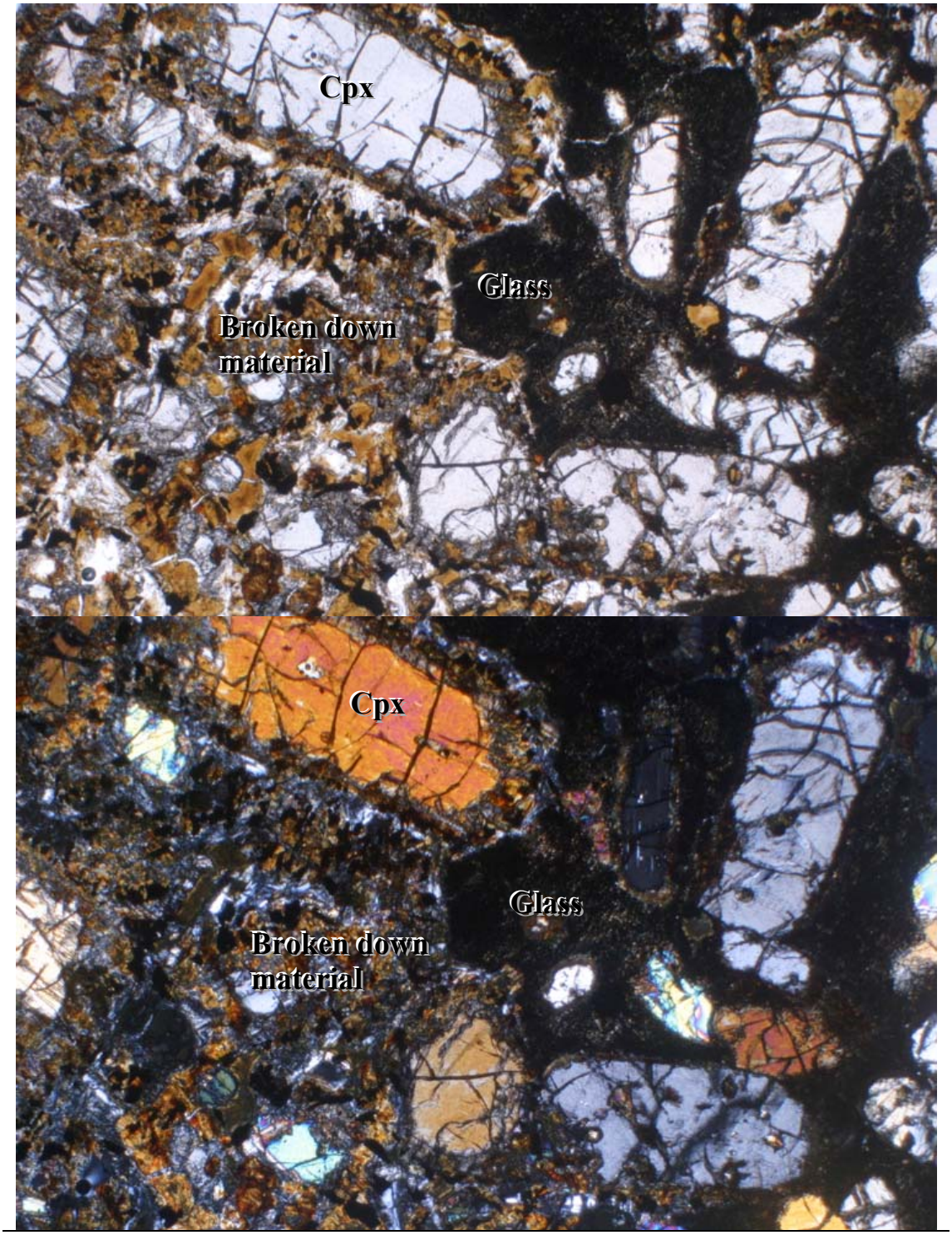


Fig. 3.18 17914 (a) PPL (b) XPL Base of photo: 3.5 mm– alteration textures at the rim of a pyroxene grain and the sharp contact of altered material with the glass.

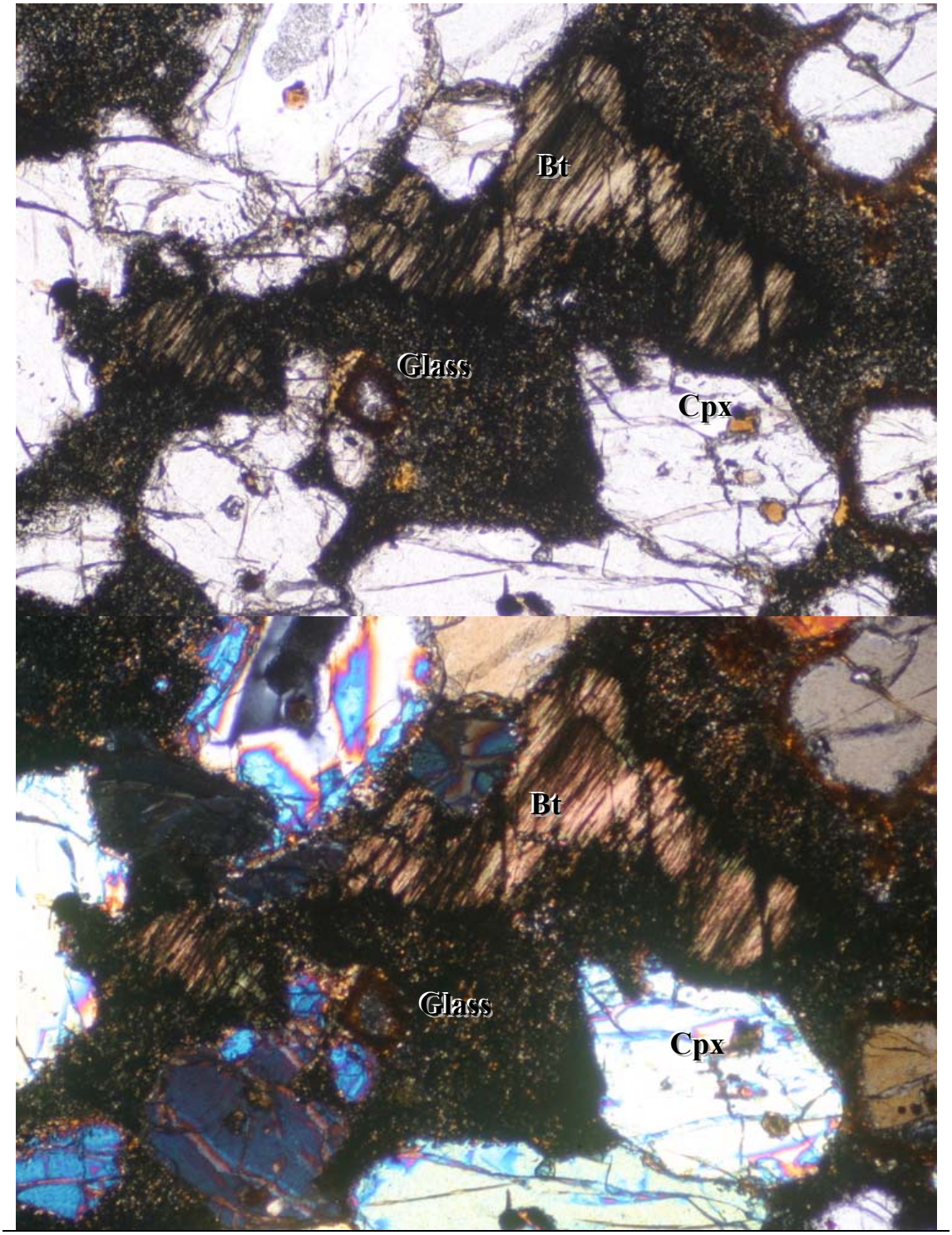


Fig. 3.19 17914 (a) PPL (b) XPL Base of photo: 1.75 mm – Biotite formation within glass.

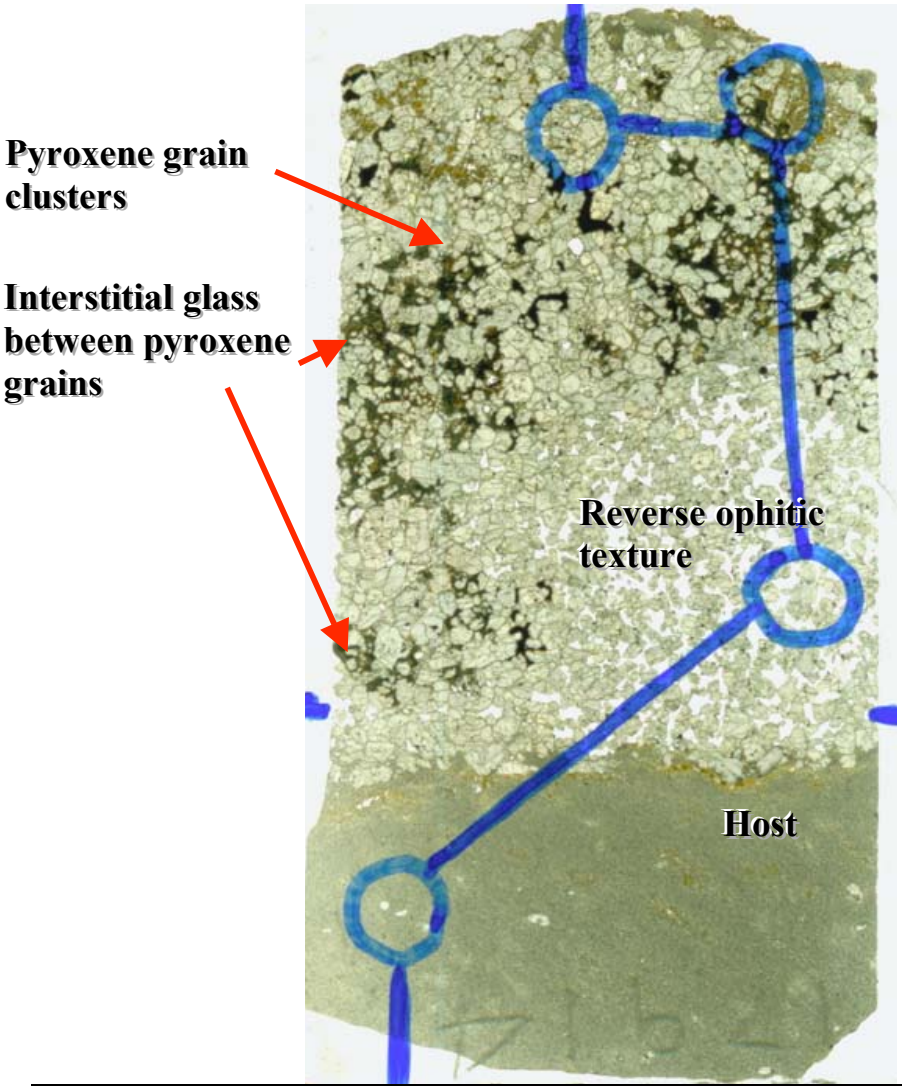


Fig. 3.20 17914 (a) Base of photo: 8 cm – Spatial relationship between the reverse ophitic texture, interstitial glass and tight pyroxene clusters.

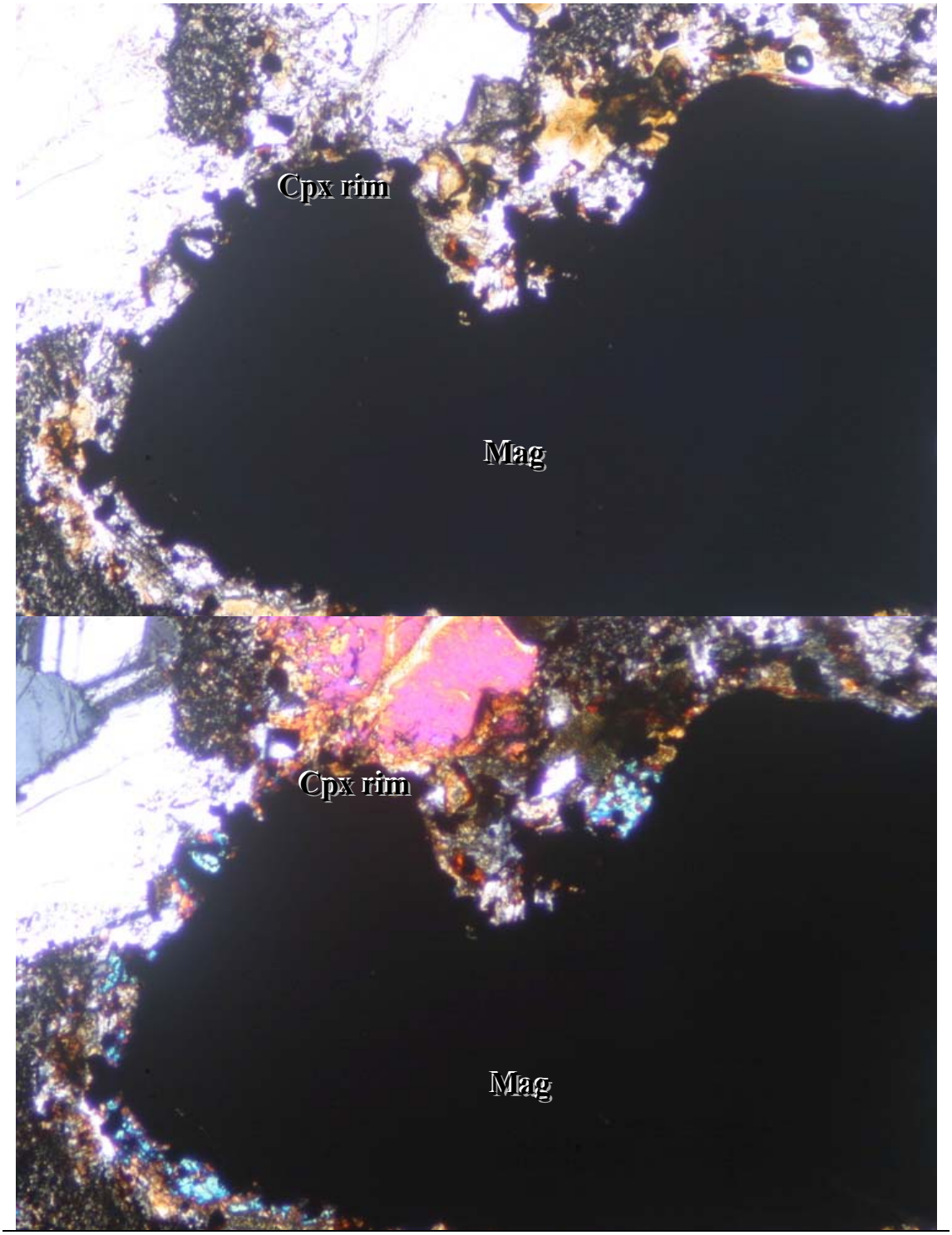


Fig. 3.21 18001 (a) PPL (b) XPL Base of photo: 1.75 mm – rim of pyroxene grains around a magnetite grain.

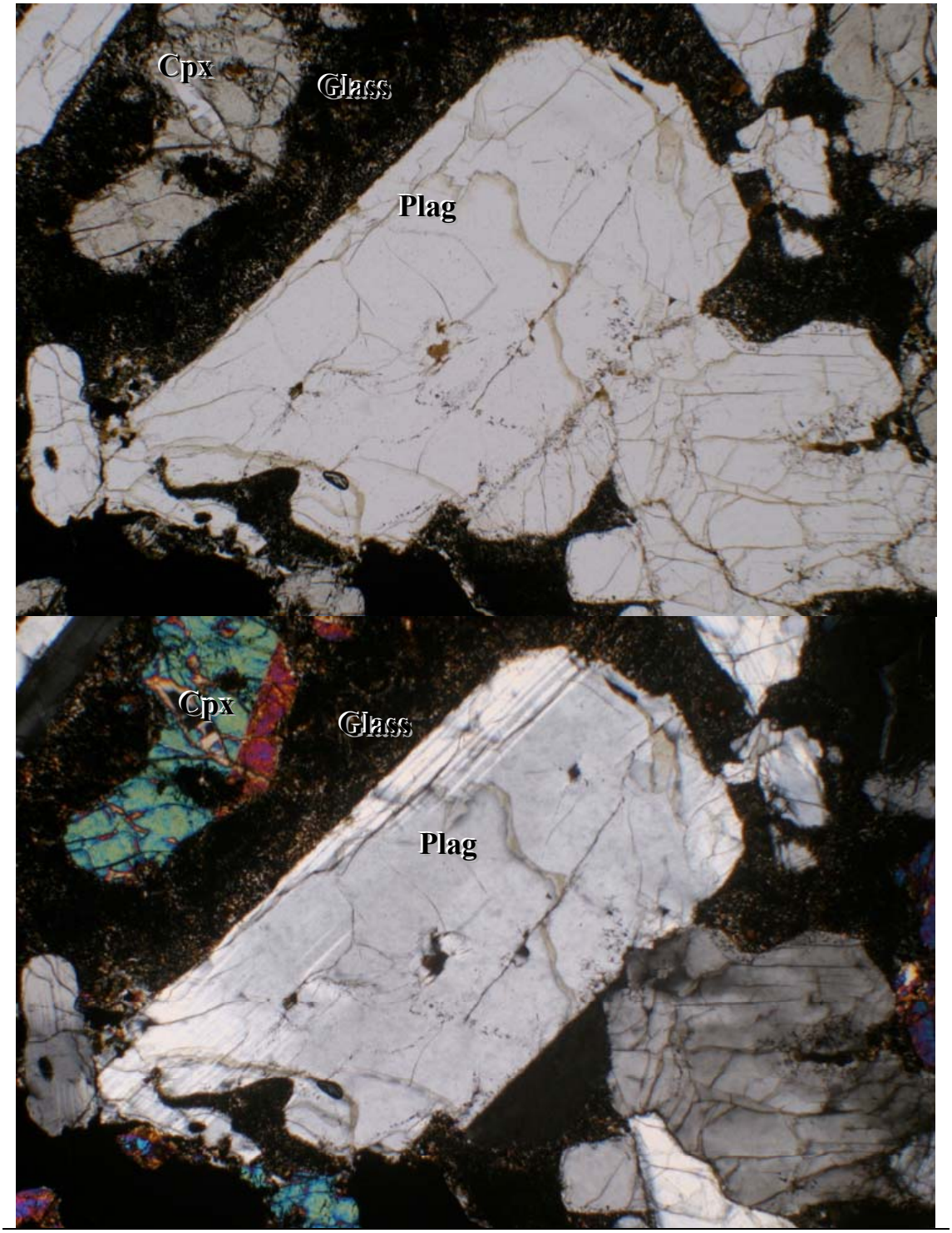


Fig. 3.22 18002 (a) PPL (b) XPL Base of photo: 3.5 mm – Large euhedral plagioclase grain surrounded by interstitial glass and undulose extinction of a plagioclase grain in the bottom right hand corner.

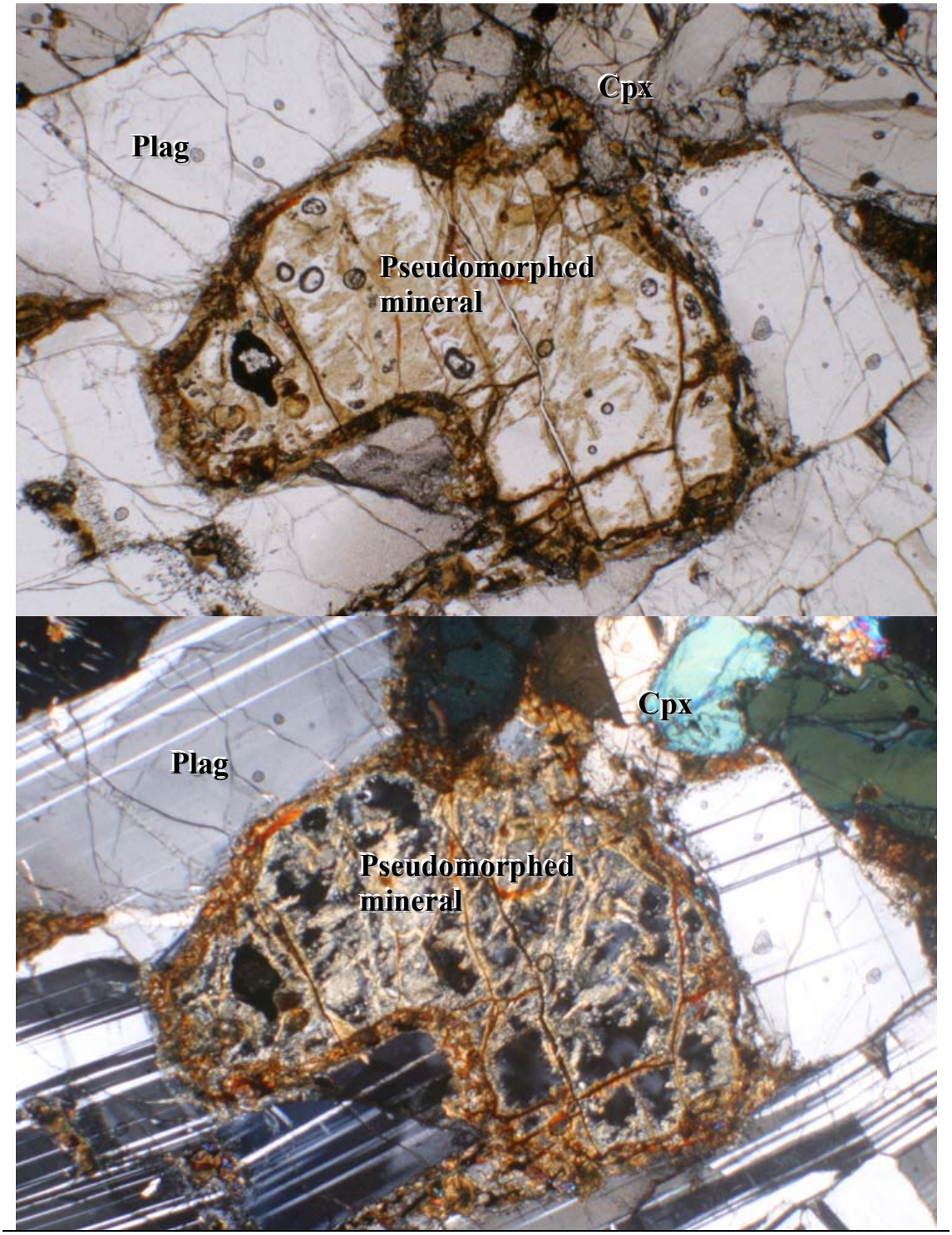


Fig. 3.23 15199 (a) PPL (b) XPL Base of photo: 3.5 mm – Pseudomorphed mineral with a well developed rim and alteration along fracture lines.

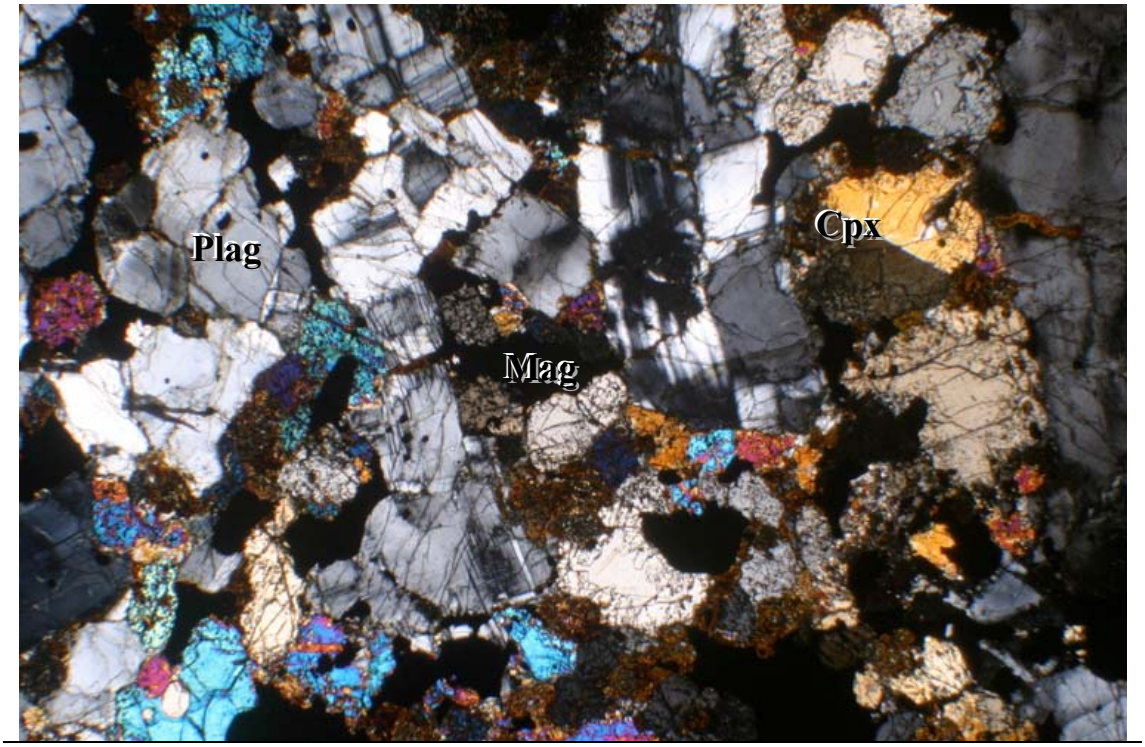


Fig. 3.24 17919 XPL Base of photo: 3.5 mm – Reaction rims, alteration and deformation textures (bent deformation twins, undulose extinction) within plagioclase grains and polygonal shape of the pyroxene grains.



Fig. 3.25 17919 XPL Base of photo: 0.9 mm – Intermingling of fine and coarse grained material, with weak brecciated texture including coarse plagioclase (up to 0.2 mm) and biotite (0.2 mm).

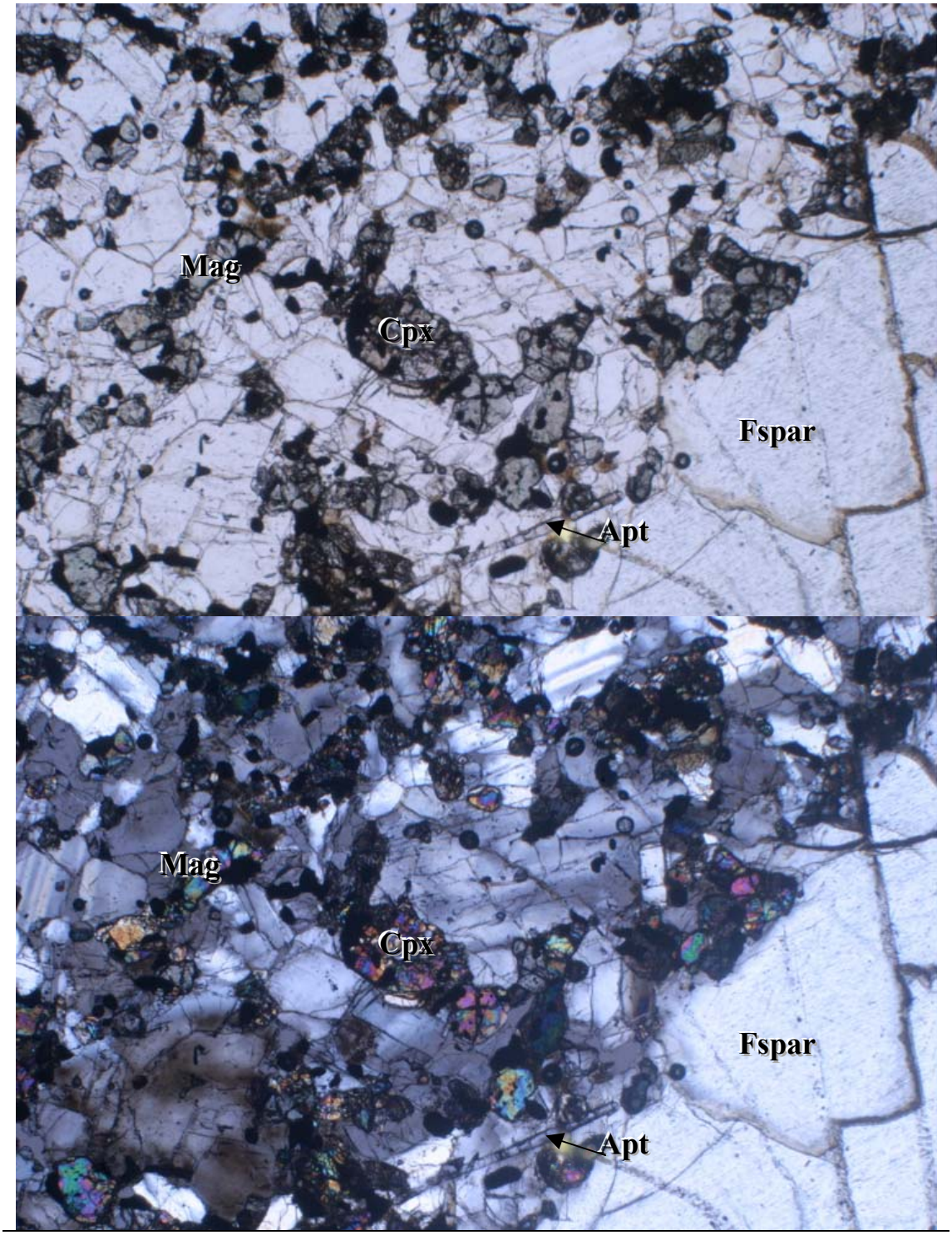


Fig. 3.26 17922 (c) PPL (d) XPL Base of photo: 3.5 mm – Contact between large euhedral feldspar grain (1.5 cm width) and fine grained, almost reverse ophitic texture. Deformation textures are also apparent within the feldspar grains.

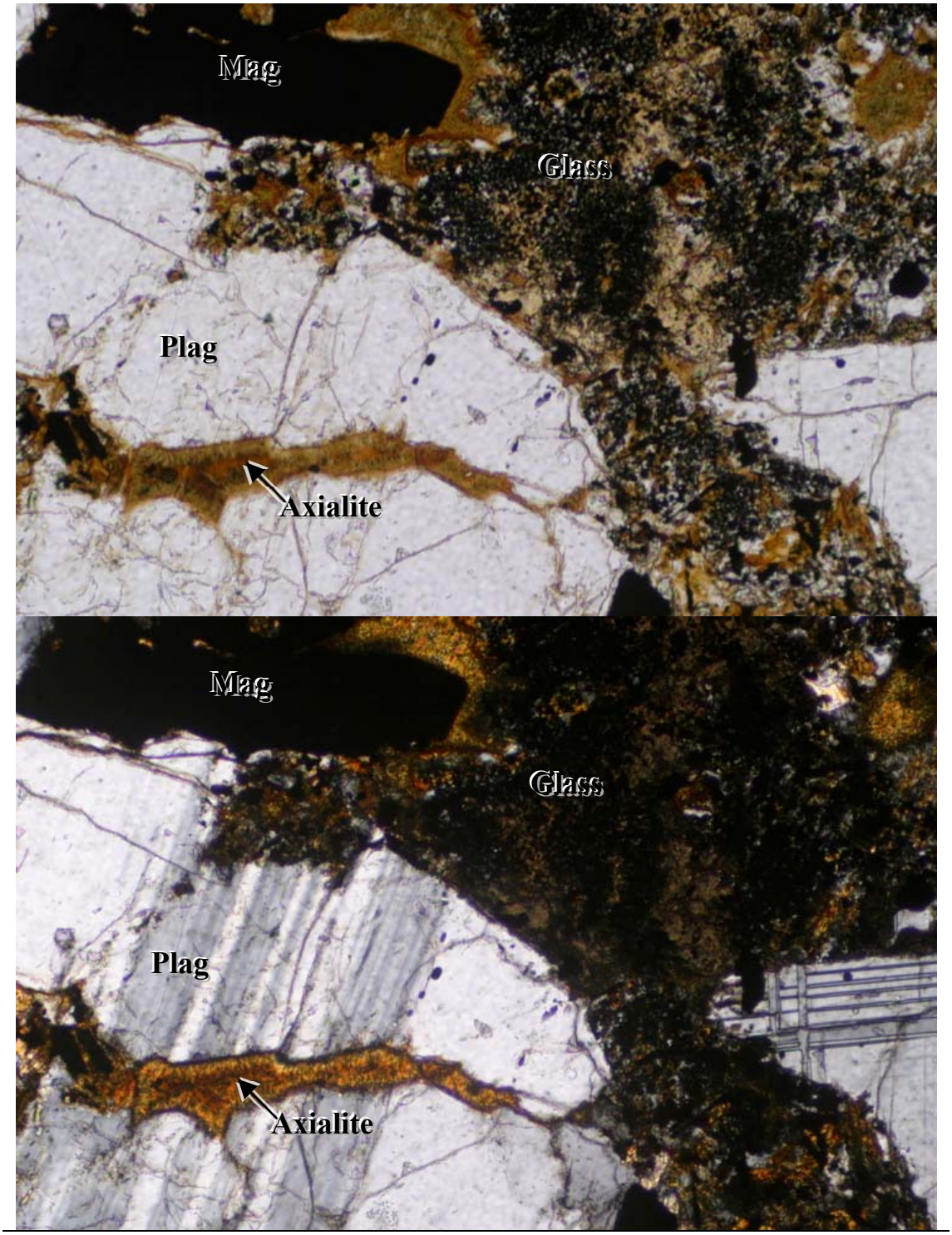


Fig. 3.27 17919 (a) PPL (b) XPL Base of photo: 0.7 mm – Axialite vein within a plagioclase grain and axialite formation at the rim of an opaque grain.

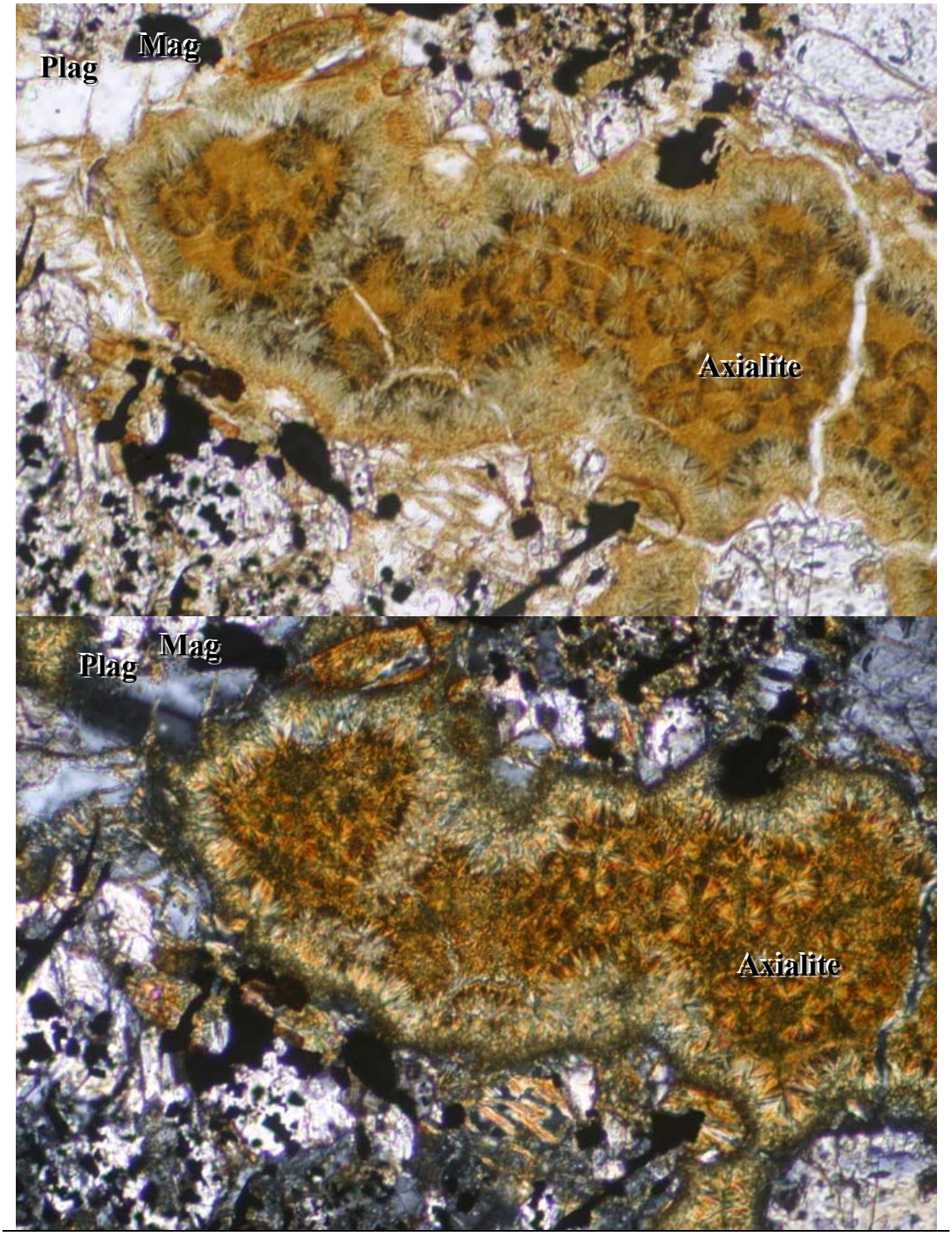


Fig. 3.28 17919 (a) PPL (b) XPL Base of photo: 0.45 mm – Axialites and rounded opaque grains.

(b) Upper Coliban Dam Mafic Group Summary

The euhedral crystal shapes, grain size, parallel lamellae twinning (inferred as growth twinning), interlocking texture and alignment of plagioclase twins and the long axes of grains suggests that this group is igneous in origin, with gabbroic compositions and

grainsize of >1 mm (Streckeisen (1974, 1976); Fig. 3.29). Two different textural groups are noted based on grain size: a coarse texture with a dominant grainsize of ~2 mm; and a finer grained texture with a dominant grainsize of ~ 1 mm. The morphological nature of the pseudomorphed mineral, including shape and alteration along fractures, is most suggestive of olivine. This provides important information on the primary nature of the gabbro (Figs. 3.11 and 3.12).

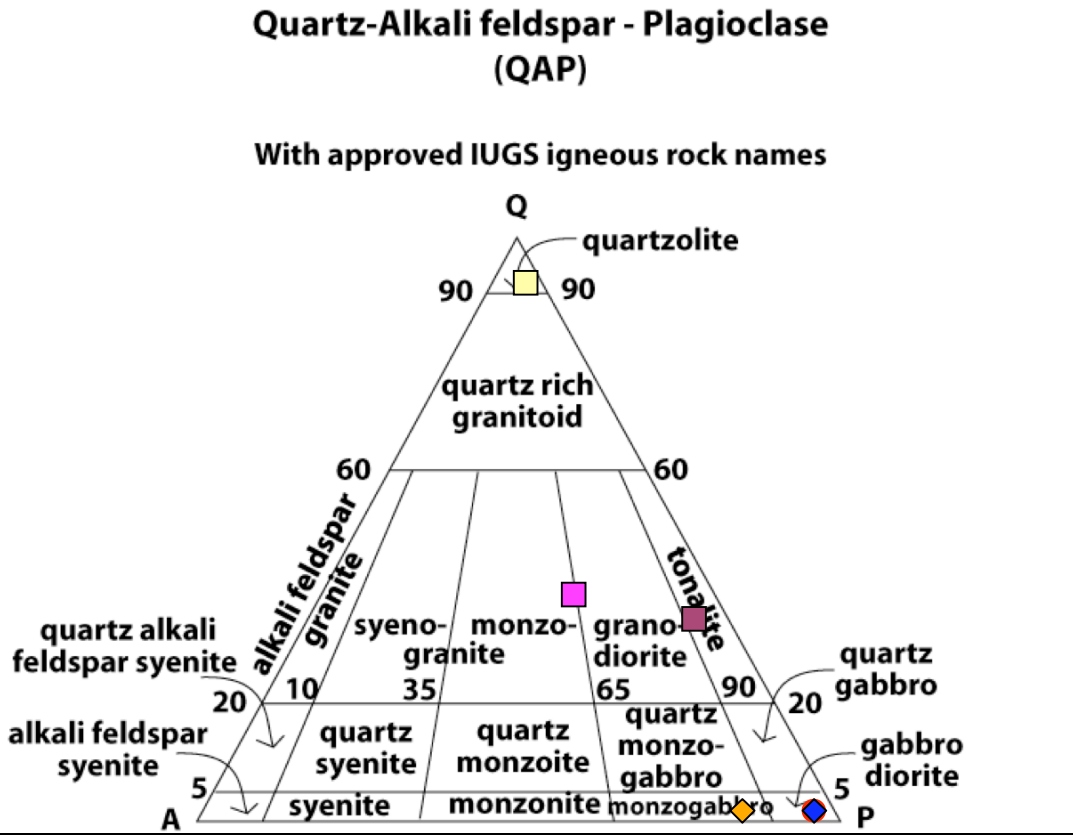


Fig. 3.29 Igneous classification based on Le Maitre (2002) using average values for each group (pink square: felsic group 1; plum square: felsic group 2 (#17915); yellow square: felsic group 3 (#17917); blue diamond: mafic group; orange diamond: mafic group 3; red circle: Stewart Hill).

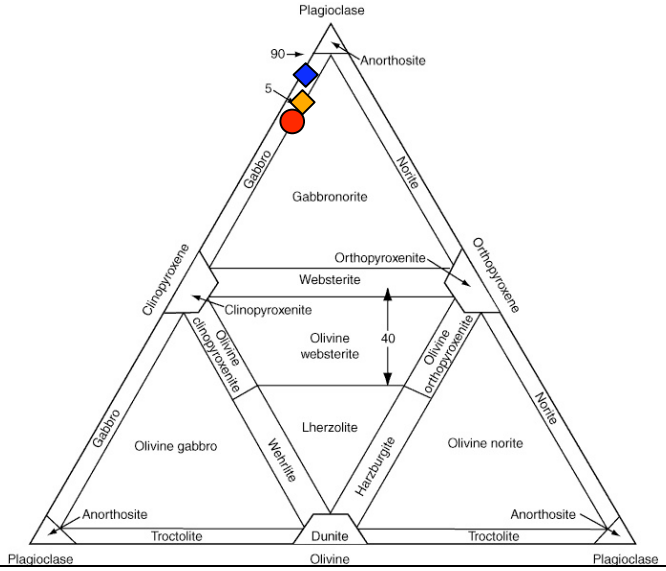


Fig. 3.30 Igneous classification of the mafic suite using modes based on Streckeisen (1976) (blue diamond: mafic group; blue diamond: Intermediate; red circle: Stewart Hill).

(c) Petrography – Upper Coliban Dam Intermediate Group

The xenoliths in this group are finer grained compared to the other groups, see Fig. 3.31 for a hand sample photo. This subgroup is predominantly composed of plagioclase (70 vol. %), alkali feldspar (15 vol. %) and pyroxene (10 vol. %), along with accessory magnetite – titanomagnetite, apatite and zircon. Glass / fine-grained material is present in varying mode from up to 5 vol. %, with some devitrified.



Fig. 3.31 Hand sample photo of intermediate group sample #17916 exhibiting the dikelet through the centre of the sample (0.5 mm to 2 mm across).

Plagioclase and alkali feldspar grains range from 0.08 mm to 2 mm, are subhedral with relic laths just visible. The pyroxene grains are from 0.04 mm to 1 mm, subhedral with irregular edges; magnetite and titanomagnetite up to 0.08 mm is subhedral; apatite up to 0.3 mm is euhedral; and zircon up to 0.8 mm is subhedral, with smooth irregular edges in a boudinaged form. The glass / fine-grained material is irregular in shape (Fig. 3.33 and Fig. 3.34).

Cross-hatched twinning is noted within the alkali feldspar grains. Feldspar grains are present as polygonal aggregates and exhibit well developed sieve textures, some extending throughout the entire grains (Fig. 3.32). The pyroxene grains are strongly altered, almost beyond recognition with some fully pseudomorphed (Fig. 3.33). Opaque minerals occur only along the grain boundaries of pyroxene.

Glass is found throughout the sample as interstitial areas and films along grain boundaries (Fig. 3.33 and Fig. 3.34).

Contact with the host lava is complex in both samples (Fig. 3.35). Sample #18003 has a particularly complex contact with a coarse band running between the xenolith and the host. A segment of the xenolith (~ 1 mm across) has been completely separated and entrained by the host.

Sample #17916 hosts multiple dykelets up to 1 mm wide and some up to 60 mm long, running from the contact with the host and pinching-off towards the centre. In thin section these consist entirely of euhedral feldspar grains up to 0.2 mm in length (Fig. 3.34).

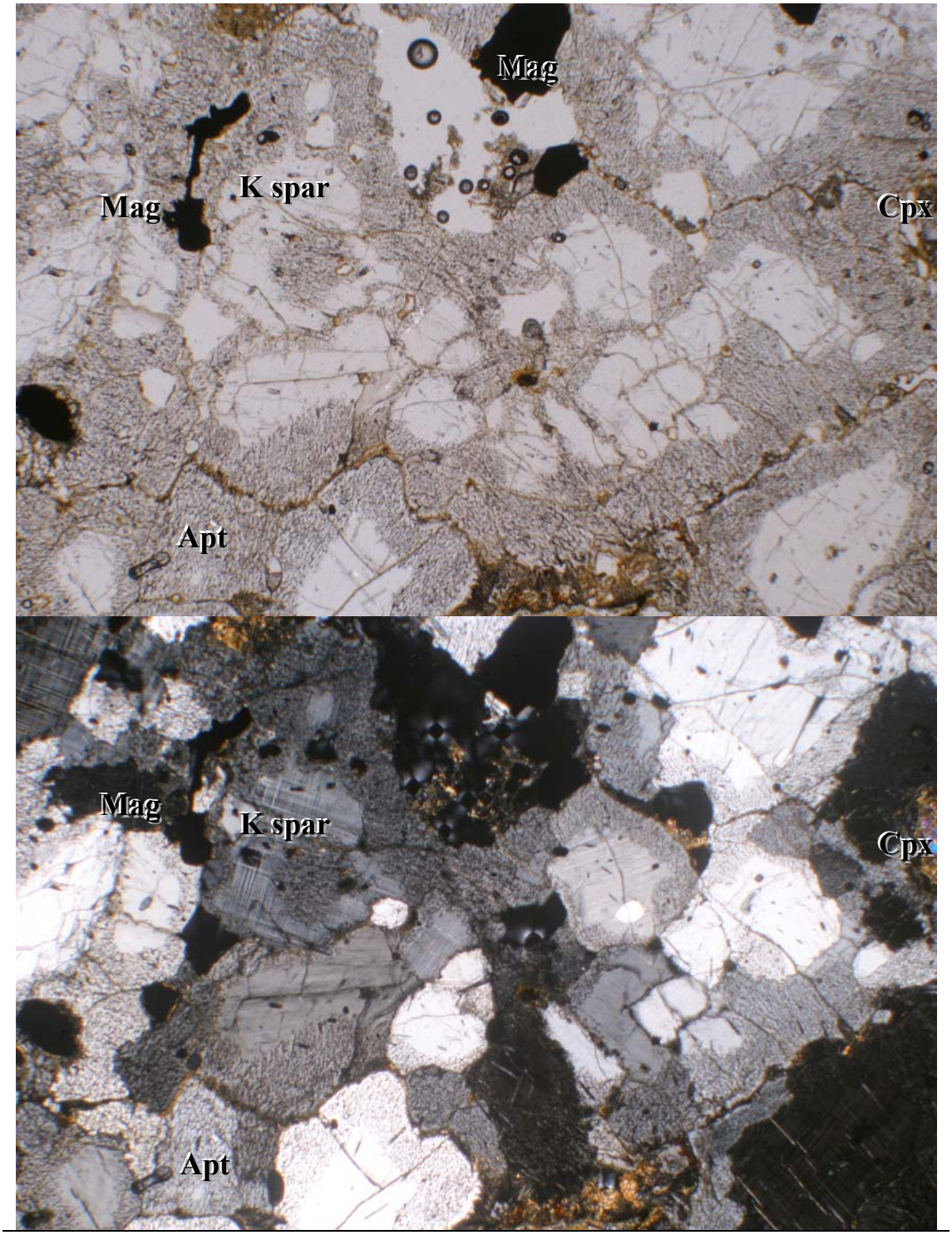


Fig. 3.32 18003 (c) PPL (d) XPL Base of photo: 3.5 mm – polygonal feldspar grains, some exhibiting cross hatch twinning. Also obvious are reaction rim textures and apatite inclusion.

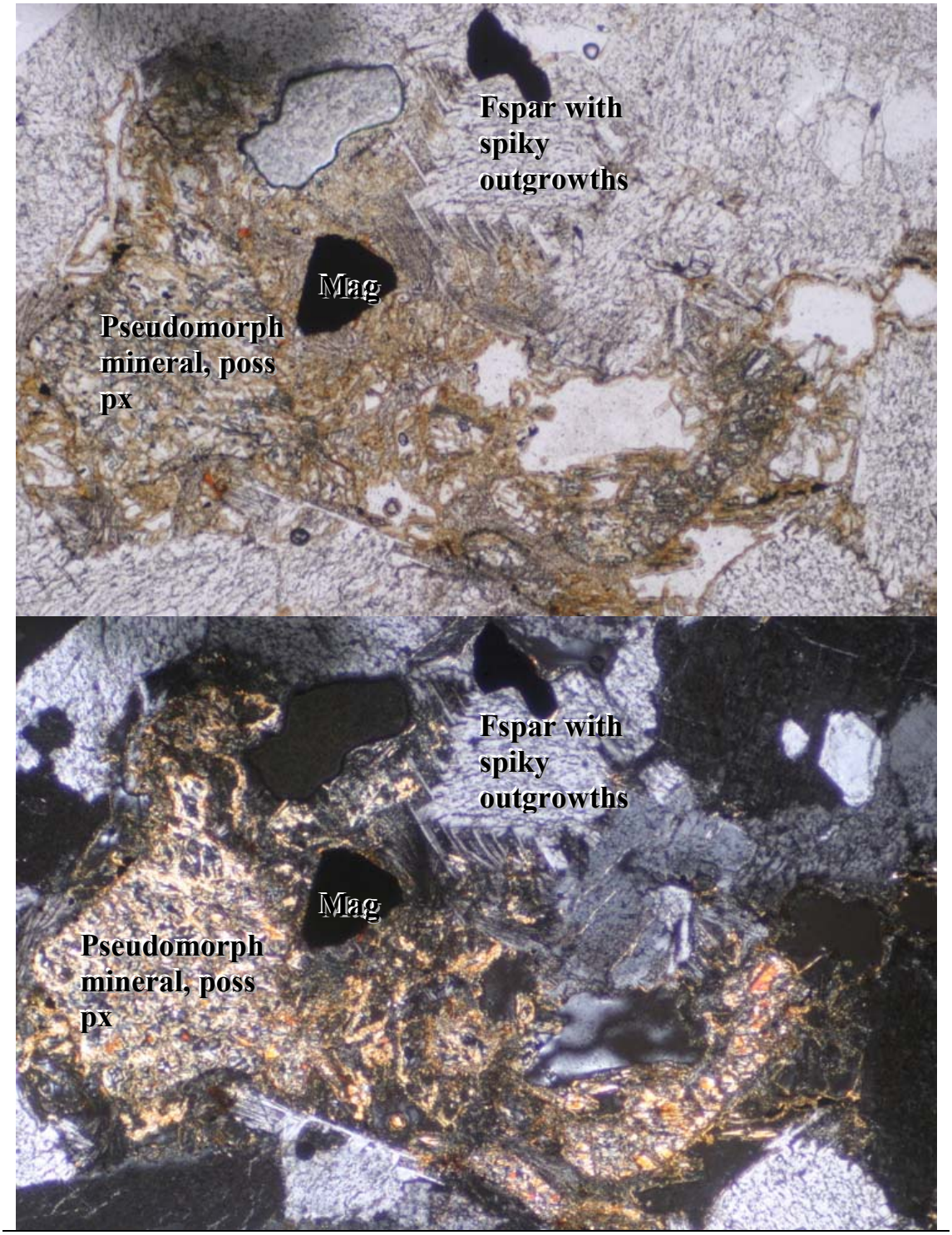


Fig. 3.33 18003 (a) PPL (b) XPL Base of photo: 1.75 mm - Spiky outgrowths of plagioclase and possible pyroxene surrounded by altered material. A pseudomorph, possibly pyroxene, is present to the left of the photo.

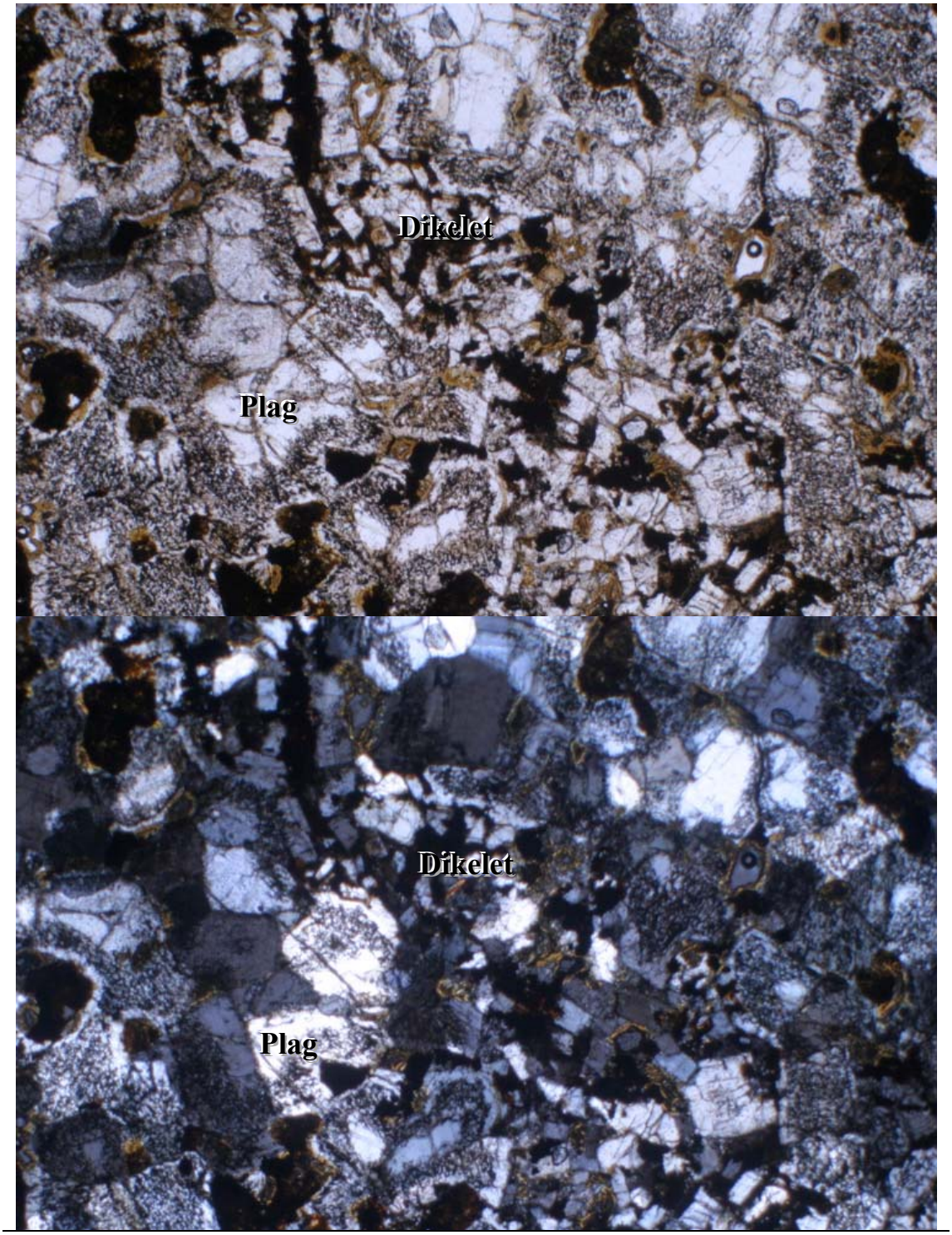


Fig. 3.34 17916 (a) PPL (b) XPL Base of photo: 3.5 mm – Weathered texture with altered and polygonal plagioclase grains. A dikelet up to 1 mm across with euhedral feldspar runs from top left to bottom right. This also highlights the extent of alteration within the sample, evident by the orange/red glass.

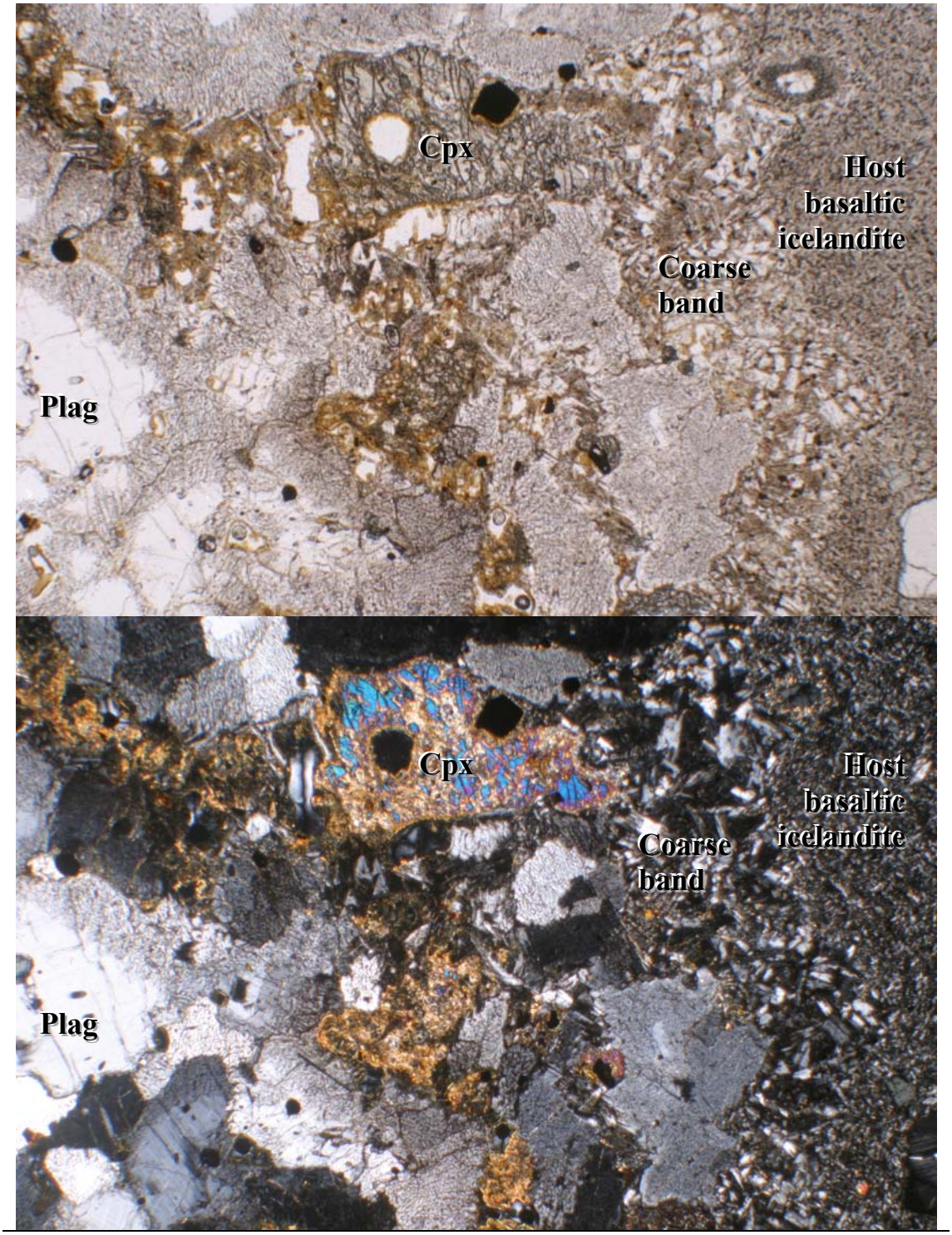


Fig. 3.35 18003 (b) PPL (c) XPL Base of photo: 3.5 mm – Intensely broken down minerals, particularly clinopyroxene which is only just identifiable. The complex contact with the host basaltic icelandite (right) including a coarse band between the xenolith and the host basaltic icelandite.

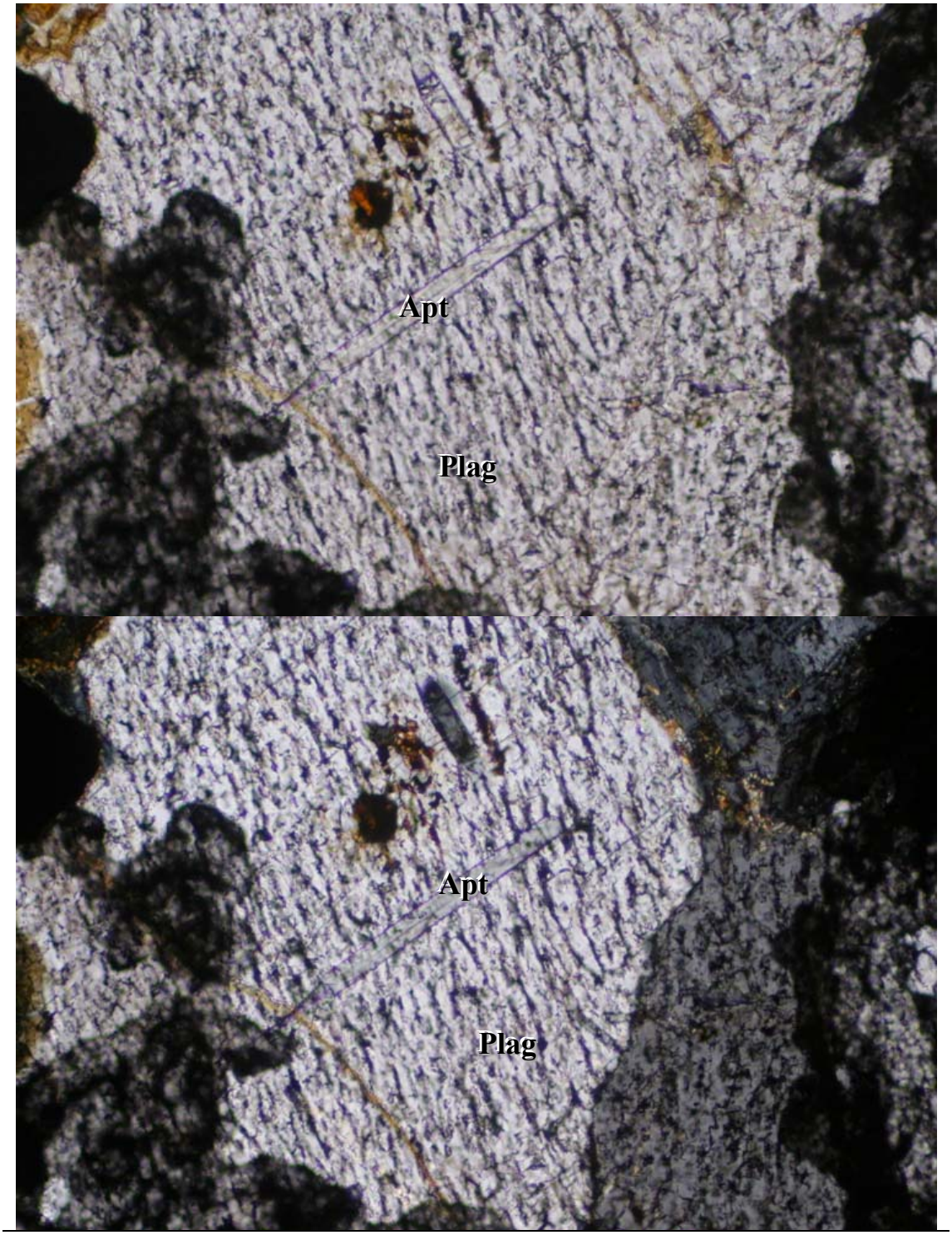


Fig. 3.36 18003 (a) PPL (b) XPL Base of photo: 0.45 mm – Broken down plagioclase grain with apatite inclusions.

(d) Upper Coliban Dam - Intermediate Group Summary

Extensive weathering (evident by the orange glass) and metamorphism make it difficult to fully characterise these samples. Evidence for an igneous protolith includes euhedral

crystal shapes, relict plagioclase laths, simple twinning and a pseudomorphed mineral with straight edges. The composition and dominant grainsize of <1 mm would classify it as a meta-monzodiorite ((Streckeisen, 1974; Streckeisen, 1976); Fig. 3.29).

(e) Petrography – Upper Coliban Dam Felsic Group

The felsic samples are divided into three groups: (1) the most abundant, with distinct glass banding between quartz and feldspar rich layers; (2) a group with less distinct glass domains; and (3) one sample with a massive texture. The xenoliths range in size from ~ 2 cm to 20 cm and are typically rounded with a sharp contact with host basaltic icelandite (Fig. 3.8).

(i) Felsic Group 1 with distinct glass banding

These samples have a coarsely banded texture defined by distinctive alternating glass-rich with glass-poor (quartz and feldspar rich) bands. Plagioclase (35 to 40 vol.%), alkali feldspar (20 to 25 vol.%) and quartz (35 to 40 vol.%) are prominent within the samples. Accessory minerals include orthopyroxene, zircon, apatite and magnetite - titanomagnetite.



Fig. 3.37 Photo of a felsic group 1 xenolith ~10 cm across (Image: Allchurch, 2008) with glass bands between quartz-feldspar rich layers.

Glass (~ 5 %) is present in continuous planar sinuous bands throughout the samples, up to 1 mm wide and between 0.5 mm and 1 mm apart (Fig. 3.38-3). The feldspar grains (0.2 to

4 mm) are predominantly subhedral with smooth irregular edges. When in contact with glass bands, the feldspar grains are rounded and exhibit reaction rims with sieve textures (Fig. 3.38-39). Rare coarse feldspar grains (up to 4 mm) are euhedral (Figs. 3.40 and 3.44) Quartz (0.1 to 1.6 mm) is present as equant grains with smooth irregular faces similar to fracture lines within the grains (Figs. 3.38-39). The pyroxene (0.02 to 2 mm), magnetite – titanomagnetite (0.01 to 0.8 mm) grains are predominantly anhedral with smooth irregular edges although in places the pyroxene has rare straight boundaries (Figs. 3.39 and 3.45) and some magnetite grains are present as blades (Figs. 3.38-39 and 3.45). Apatite (0.02 to 0.5 mm) and zircon (0.02 to 0.1 mm) are euhedral to subhedral (Fig. 3.45).

The glass bands are evenly distributed throughout the samples forming a film along crystal boundaries. These bands appear to broaden against quartz rims (Fig. 3.38 to Fig. 3.43). In some samples (i.e. #17921 and 17920), the glass is more dominant and more abundant at grain boundaries in the quartz and feldspar rich layers. Sample #17920 has quartz and feldspar grains completely isolated in glass in the two-dimensional section of the thin-section. Zones in sample #17920 retain polygonal aggregates of quartz and plagioclase (Fig. 3.42 and Fig. 3.45).

Two spatially discreet textures are observed within glass in the samples: (1) within mm of the contact with the host lava: a matrix consisting of rectangular feldspar grains (up to 0.02 mm) similar to that observed within the host basaltic icelandite (Fig. 3.40); and (2) within the bands throughout the sample: microphenocrysts of feldspar grains including swallow tails and spiky dendrils up to 0.3 mm that splay-out from the reaction rims on feldspar grains (Fig. 3.42).

Both growth and deformation twins are observed within the feldspar grains (Fig. 3.38- Fig. 3.42). Rare perthitic textures are also observed within the coarser, euhedral grains mentioned above (Fig. 3.40). The quartz grains are embayed and rimmed by glass, especially when within mm of glass bands (Fig. 3.38-6). The zircon grains are also moderately embayed (Fig. 5.17).

The pyroxene and magnetite grains are spatially associated with glass bands and, particularly pyroxene, occur along the rim of quartz grains (Figs. 3.39 and 3.45). Magnetite and pyroxene grains are typically intergrown (Fig. 3.39). This relationship is

most prominent within the larger grains of these minerals, between 0.5 to 1 mm (Fig. 3.39). The apatite and zircon grains are embedded within quartz and feldspar grains and rarely within glass, or on the border of both (Fig. 3.45).

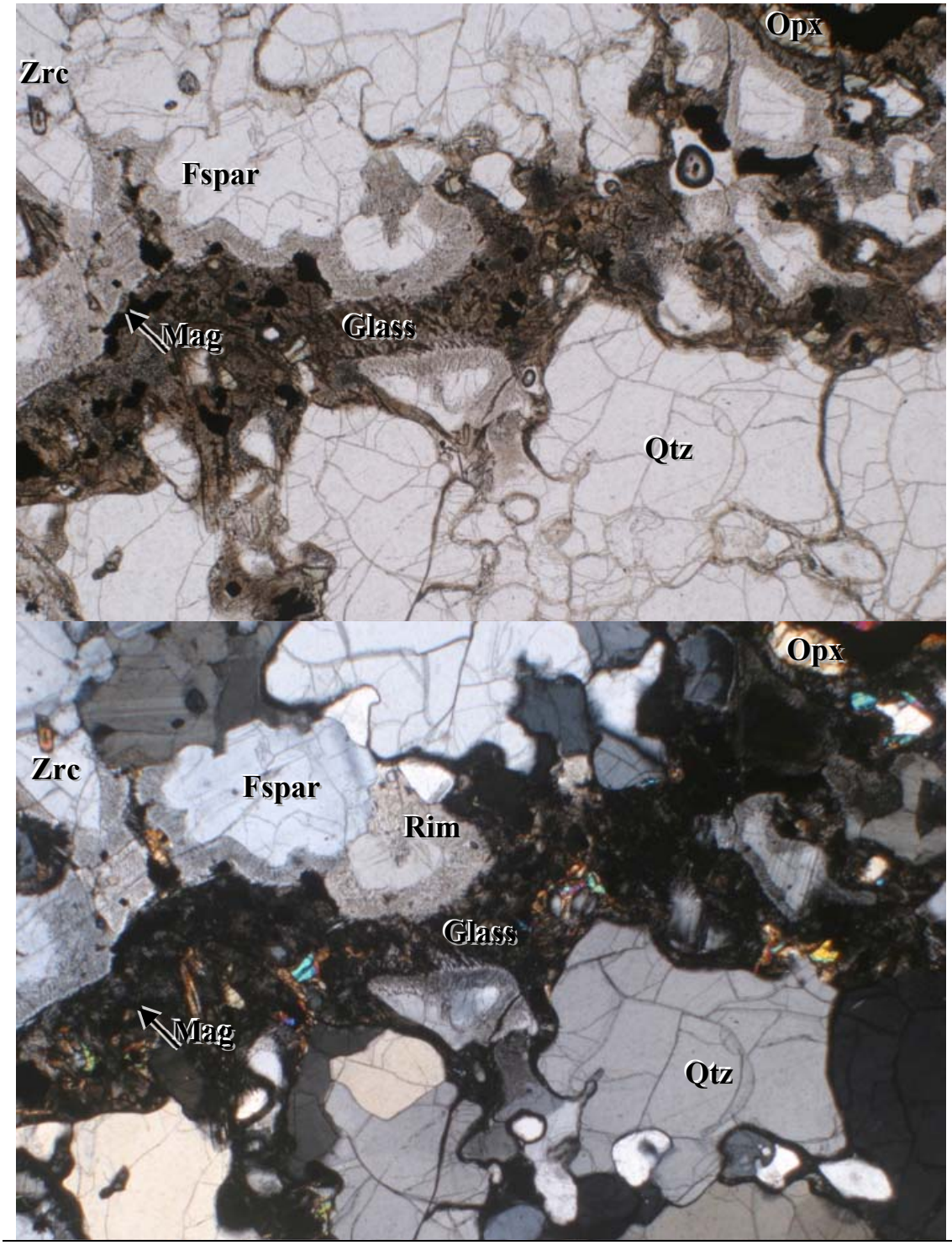


Fig. 3.38 (a) 17918, PPL (b) 17918 XPL, Base of photo: 3.5 mm– Overview of the felsic minerals and texture, with a glass band running lower left to upper right (~ 1 mm maximum width). The reaction rim of the feldspar proximal to the glass is prominent, as is the location of the pyroxenes and opaque minerals within the glass.

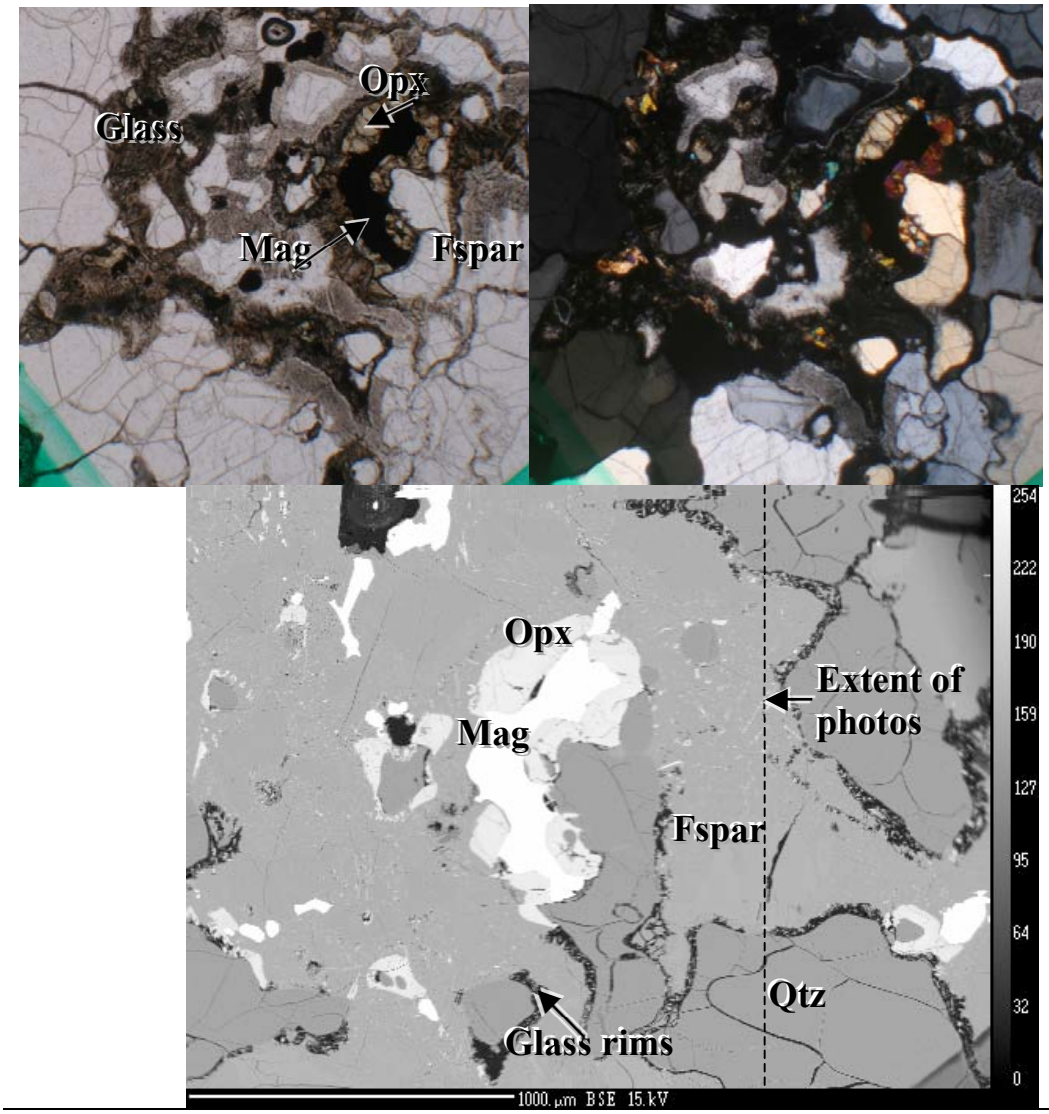


Fig. 3.39 17918 (a) PPL (b) XPL Base of photo: 2 mm and (c) BSE Base of photo: 2.5 mm– illustrating the relationship of quartz with glass rims and orthopyroxene and opaque minerals within the partially crystalline glass and feldspar reaction rims.

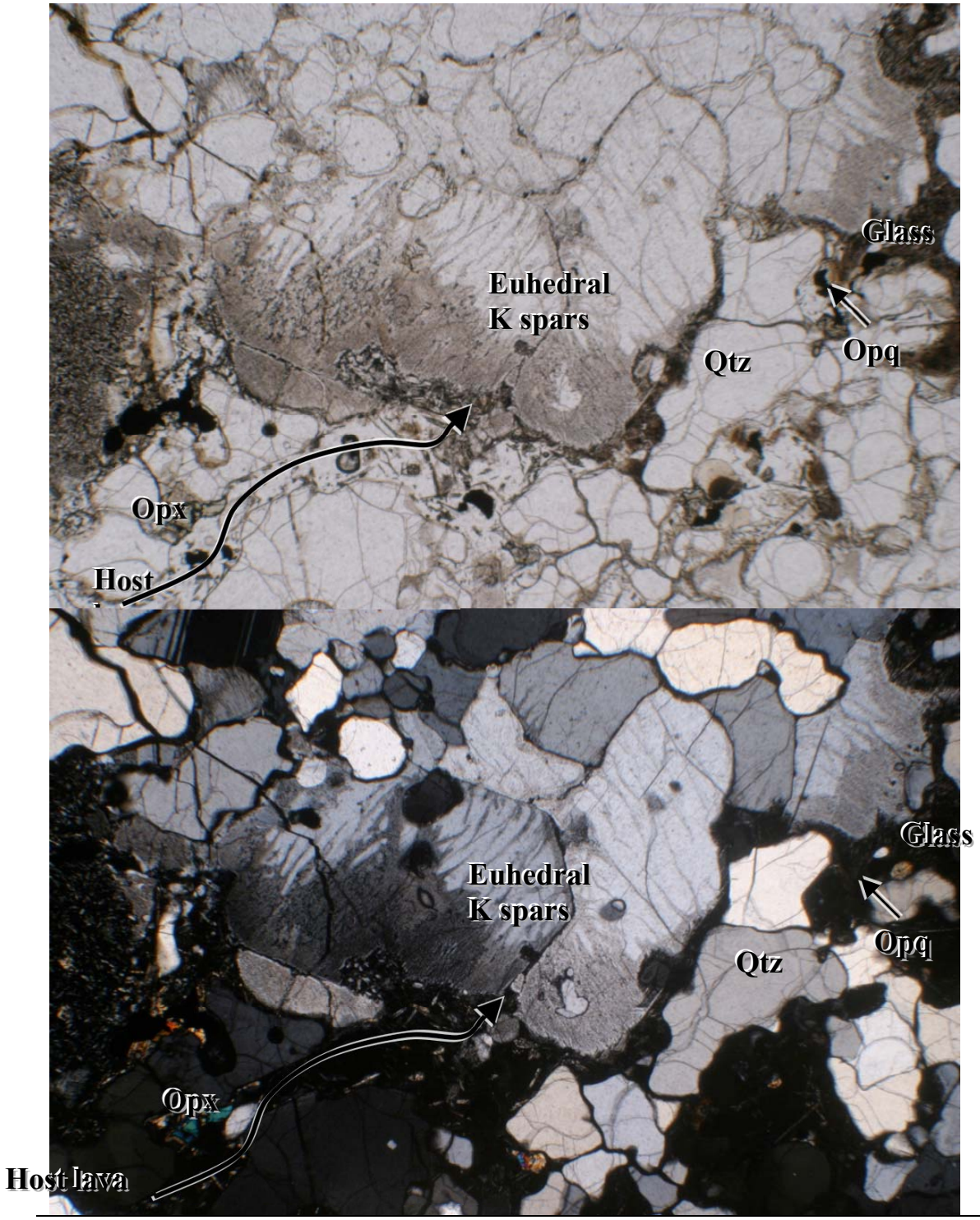


Fig. 3.40 17918 (a) PPL (b) XPL, Base of photo: 3.5 mm – Coarse euhedral feldspar grain with perthitic textures and reaction with the host lava. Irregular crystal edges of other feldspar and quartz grains are also shown. The path of the host lava is also shown. The host lava contact is approximately 1 mm to the left

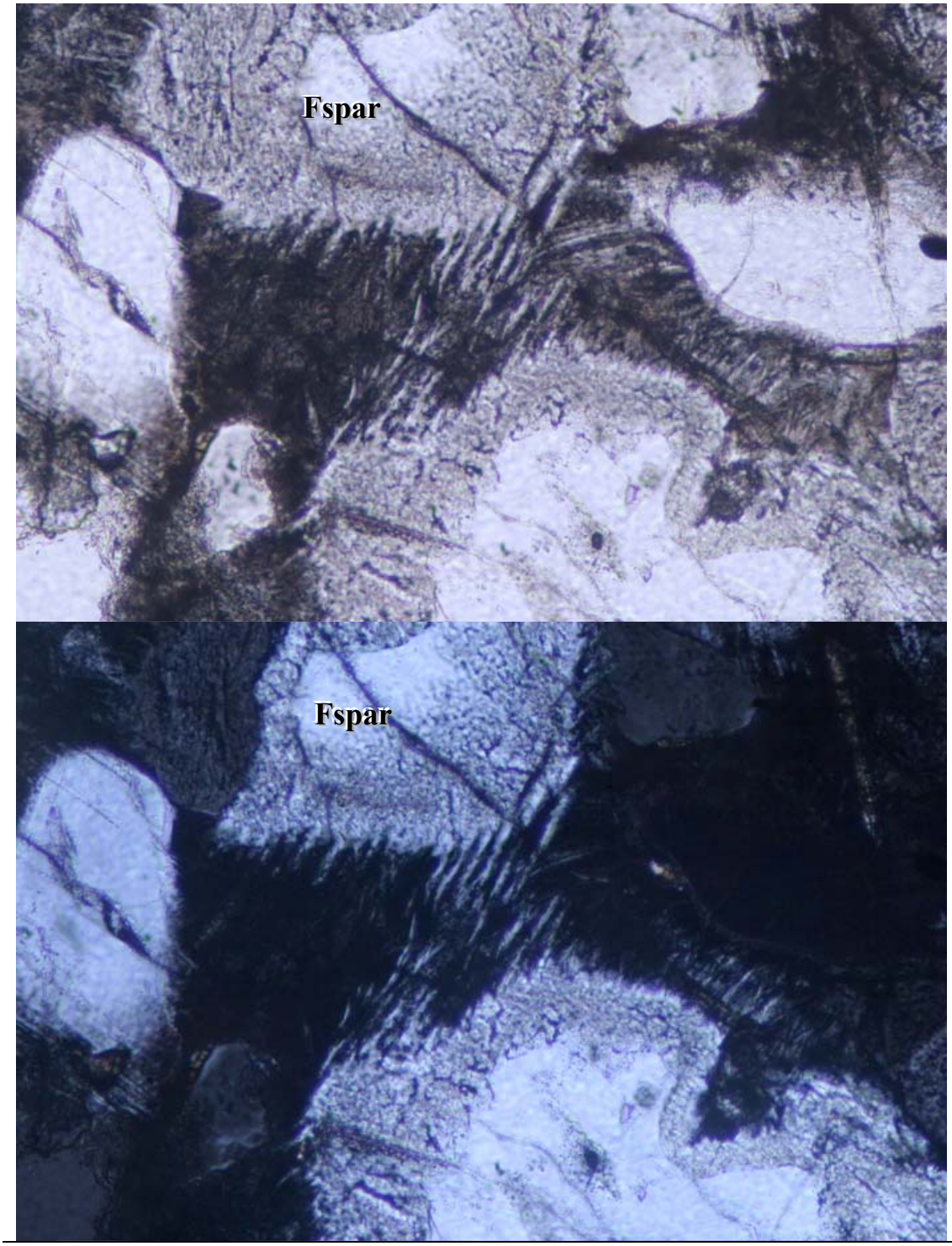


Fig. 3.41 17911 (a) PPL (b) XPL Base of photo: 0.9 mm – quench textures within the glass and growing from feldspars at reaction rims

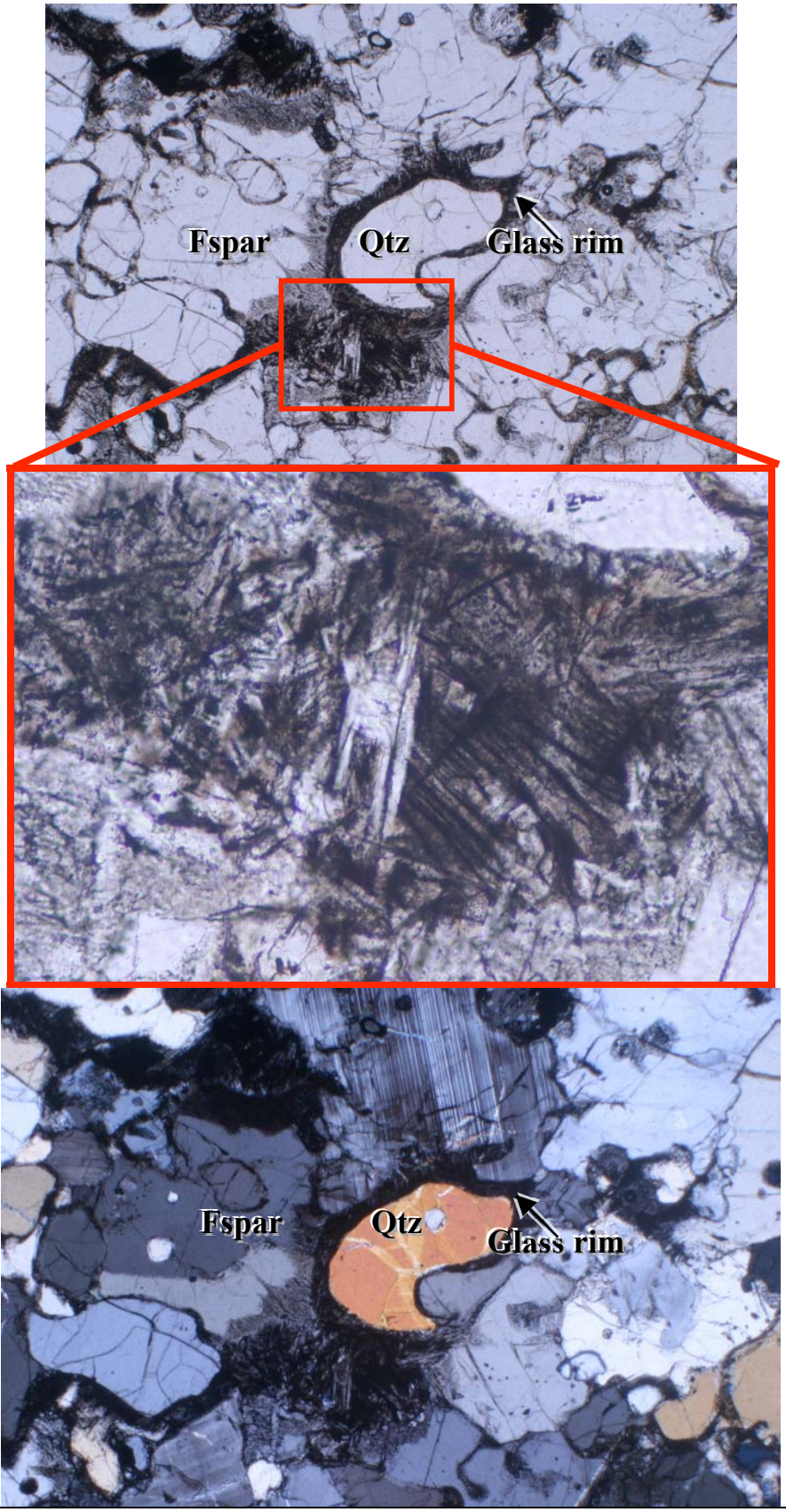


Fig. 3.42 17921 (a) PPL Base of photo: 3.5 mm (b) PPL Base of photo: 0.9 mm (c) XPL Base of photo: 3.5 mm – Microphenocrysts within the glass including swallow tail feldspars and spiky dendrils. It also shows twinning within the feldspar (top centre).

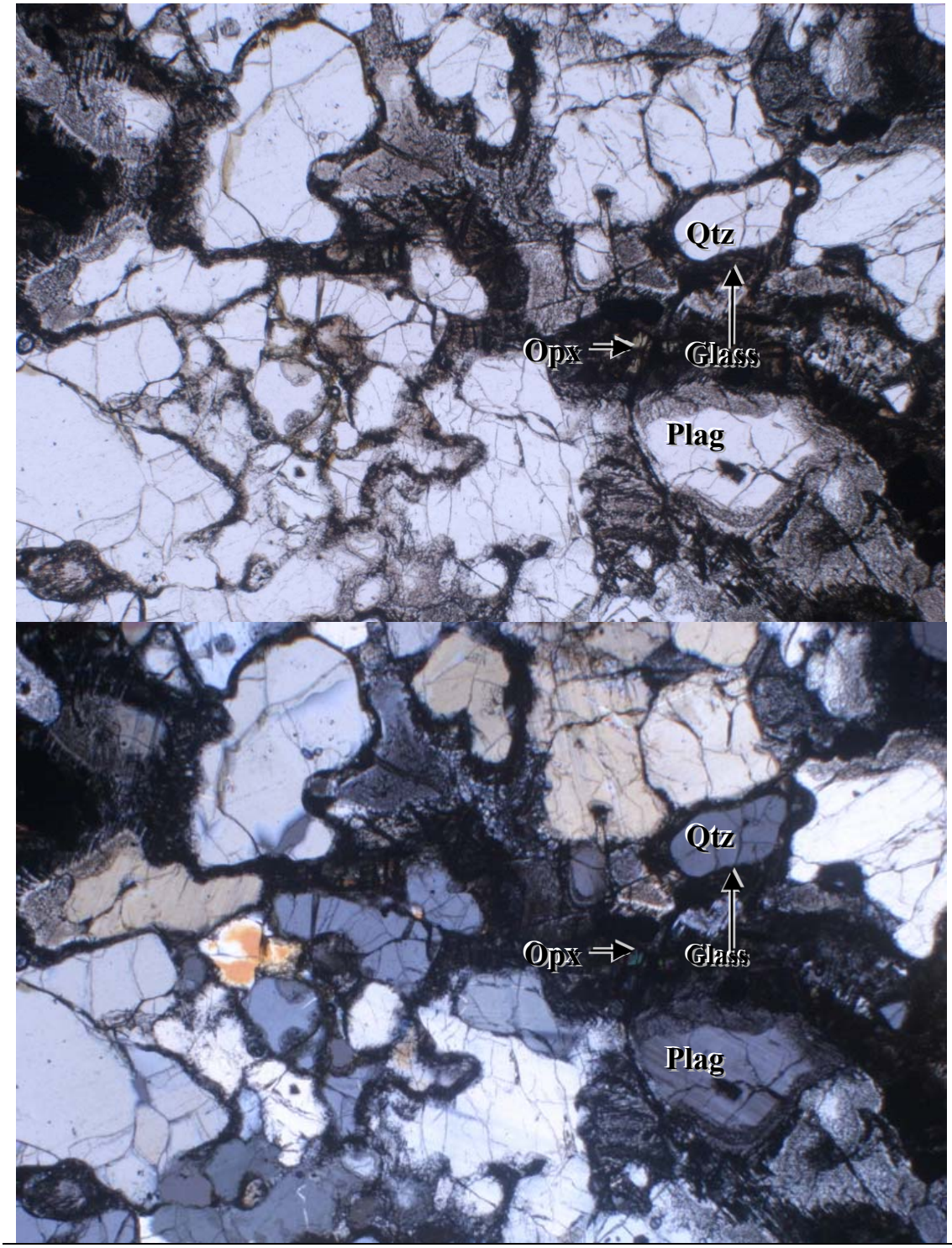


Fig. 3.43 17921 (a) PPL (b) XPL Base of photo: 3.5 mm – glass rim around quartz outside of the main band and embaying quartz and feldspar grains (lower centre).

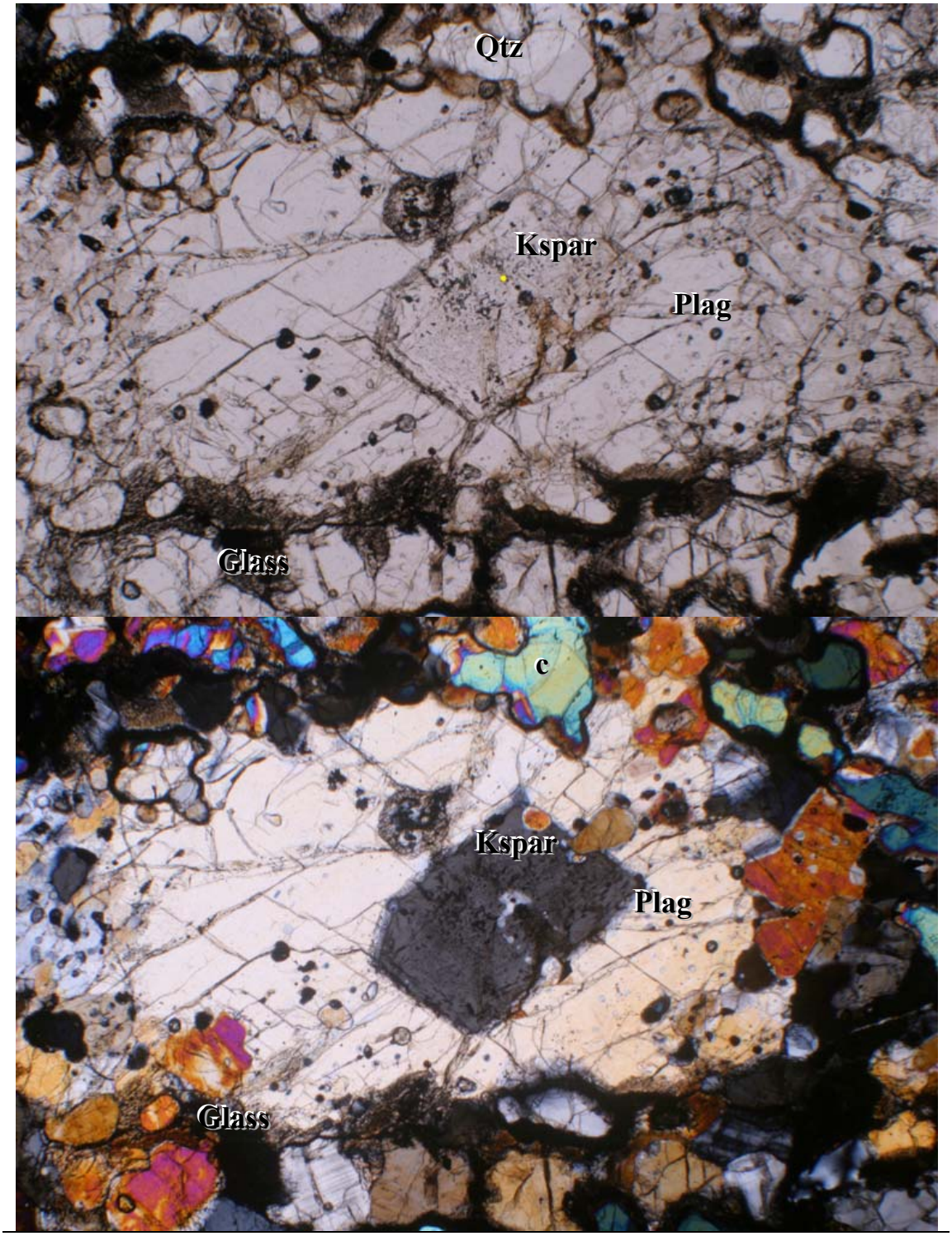


Fig. 3.44 17912 (a) PPL (b) XPL Base of photo: 3.5 mm – large euhedral plagioclase encasing a smaller feldspar and quartz grains.

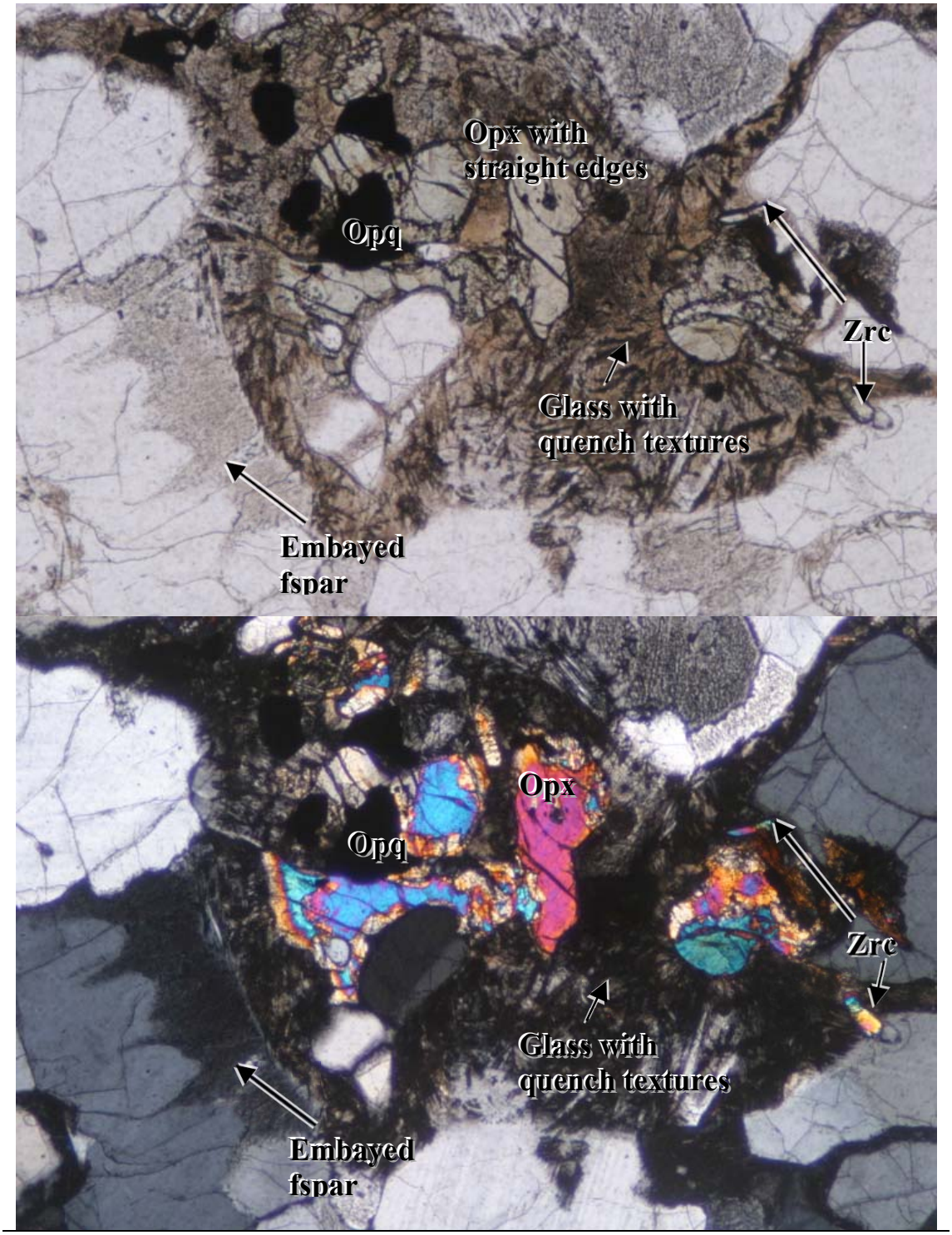


Fig. 3.45 17920 (a) PPL (b) XPL Base of photo: 1.75 mm – Quench texture and opaque grains within the glass, orthopyroxene with straight edges. Also note two zircons (right hand side) embedded within a partly brokendown plagioclase and glass.

(ii) Felsic Group 2 with less distinct glass bands (sample #17915)

This sample is similar to felsic group 1 discussed above. However there are two main differences: 1) rather than glass bands, this sample has discreet zones of glass and a fine

grained texture consisting of intergrown plagioclase, orthopyroxene and magnetite (Figs. 3.48 and 3.51) the feldspar grains are predominantly plagioclase with greater occurrence of euhedral crystal shapes (Figs. 3.47-48) and clinopyroxene is dominant over orthopyroxene in the primary intergrown quartz-feldspar texture. The lack of glass bands is immediately visible in hand sample compared to felsic group 1 (Fig. 3.46).



Fig. 3.46 Hand sample photo of felsic group 2 sample #17915, with attached basaltic icelandite host to the left with minor glass zones

Grain size and shape is similar to felsic group 1. Glass is present as a fine film around grains and in small pockets up to 0.5 mm. A fine-grained texture is present with symplectite orthopyroxene and magnetite (up to 0.03 mm) included within plagioclase. This texture is observed in irregular zones up to 2 mm long (Fig. 3.49 and Fig. 3.51), some of which have straight edges (Fig. 3.49). Clinopyroxene grains (up to 0.03 mm) rim quartz grains (Fig. 3.49 and Fig. 3.50). Exsolution textures are visible within the magnetite grains (Fig. 3.52).

A band of massive coarser-grained material up to 20 mm wide occurs at one end of the xenolith, with a relatively sharp contact against the bulk of the xenolith as described above.

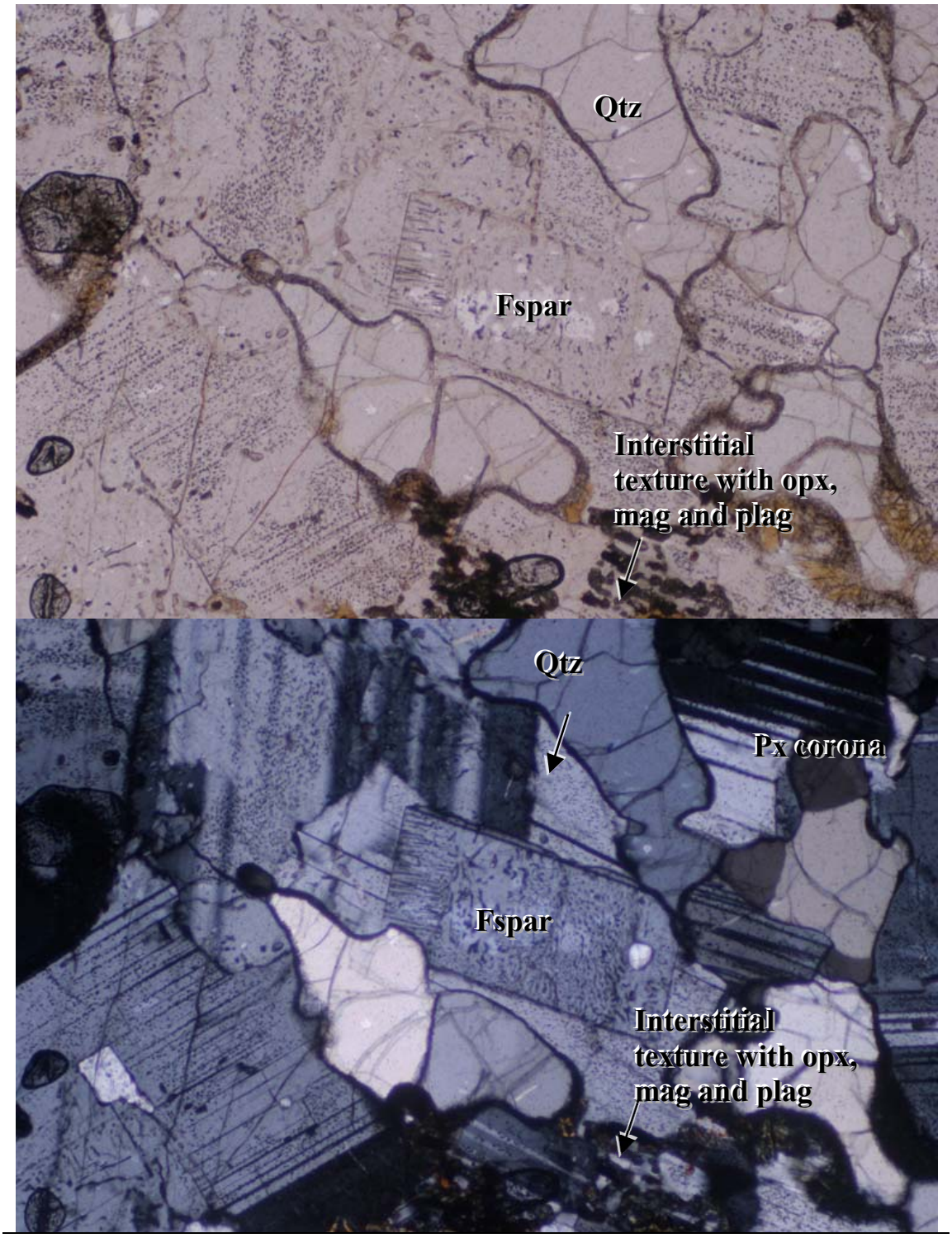


Fig. 3.47 17915 (a) PPL (b) XPL Base of photo: 3.5 mm – euhedral feldspar grains exhibiting a symplectic texture and intergrown texture with quartz.

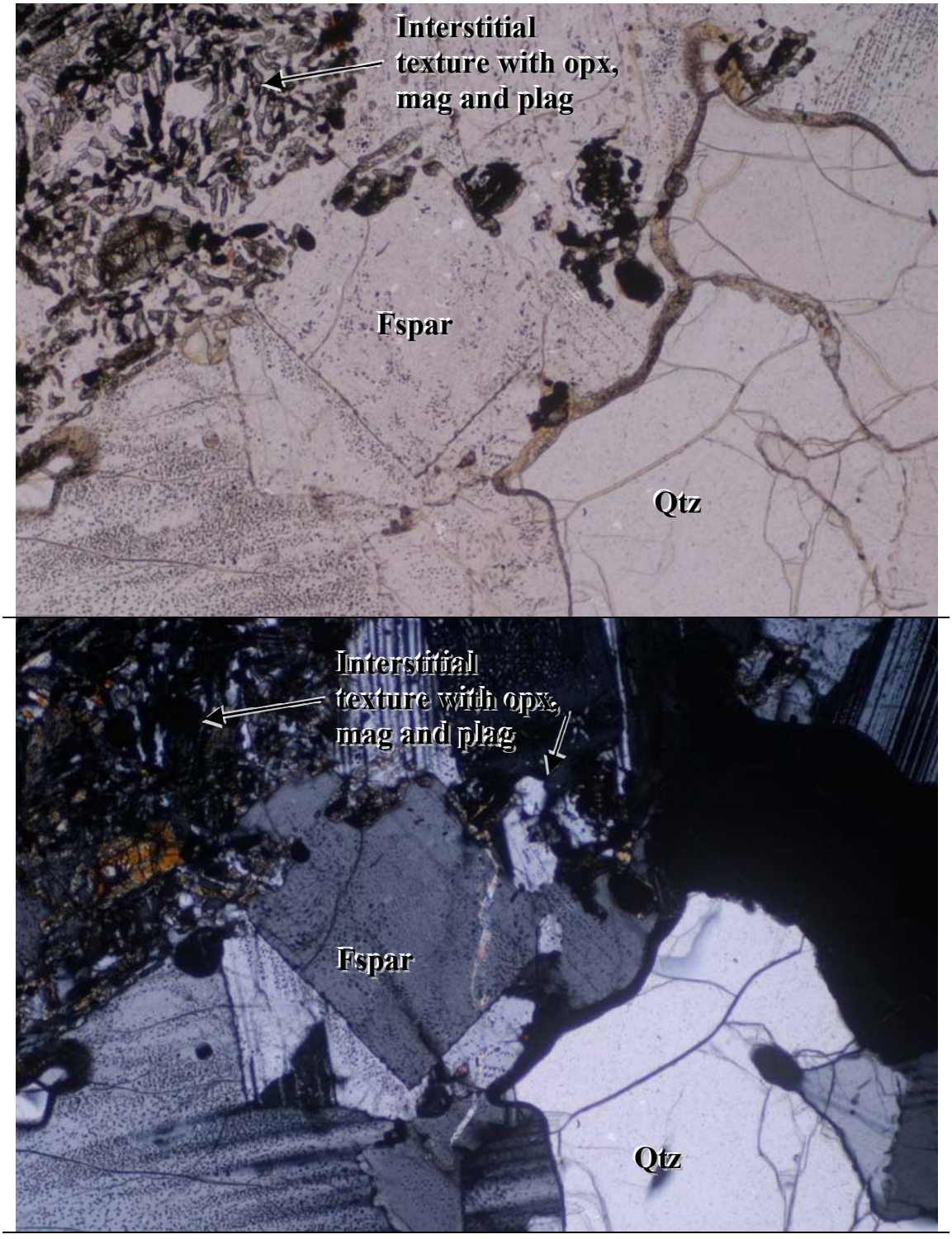


Fig. 3.48 17915 (a) PPL (b) XPL Base of photo: 3.5 mm – intergrown texture of euhedral feldspar and quartz grains and relationship with the interstitial texture.

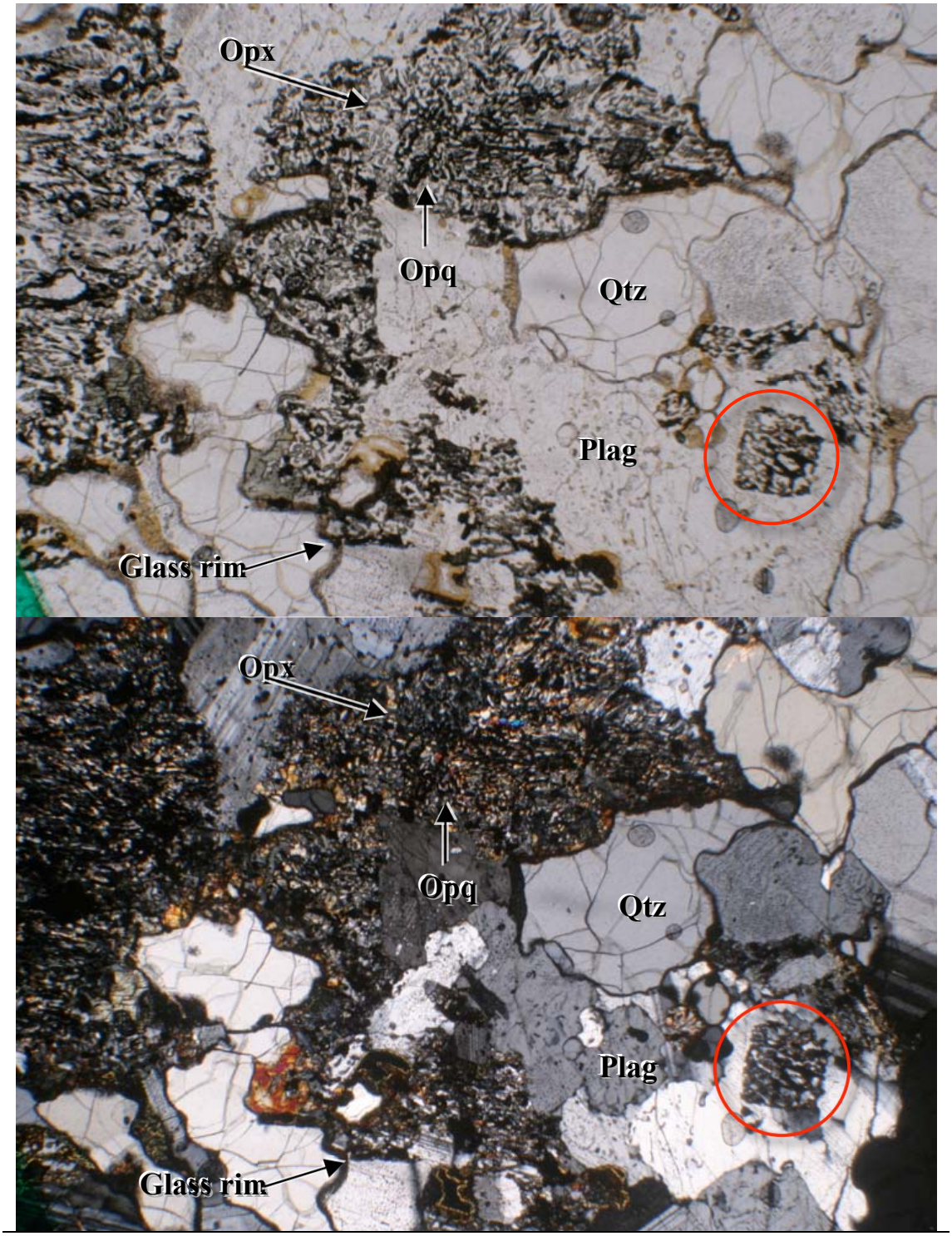


Fig. 3.49 17915 (a) PPL (b) XPL Base of photo: 3.5 mm – symplectite texture including with intergrown orthopyroxene and magnetite enveloped by plagioclase. An example with straight edged boundaries is circled in the bottom right hand corner. Also shown is the film of glass around quartz grains

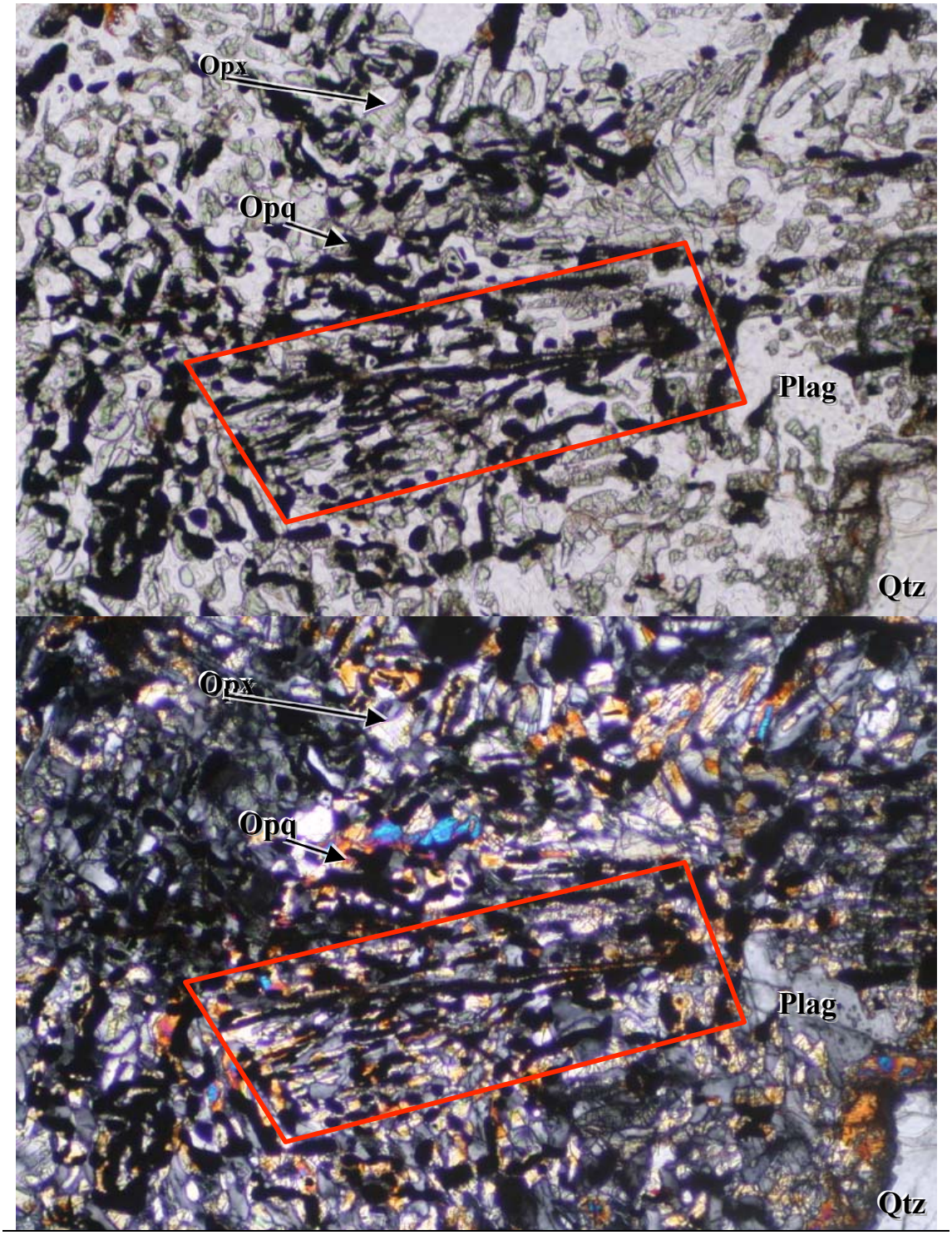


Fig. 3.50 17915 (a) PPL (b) XPL Base of photo: 0.9 mm – symplectite texture, including orthopyroxene and opaque grains enveloped by plagioclase. In the rectangle are grains with similar orientation.

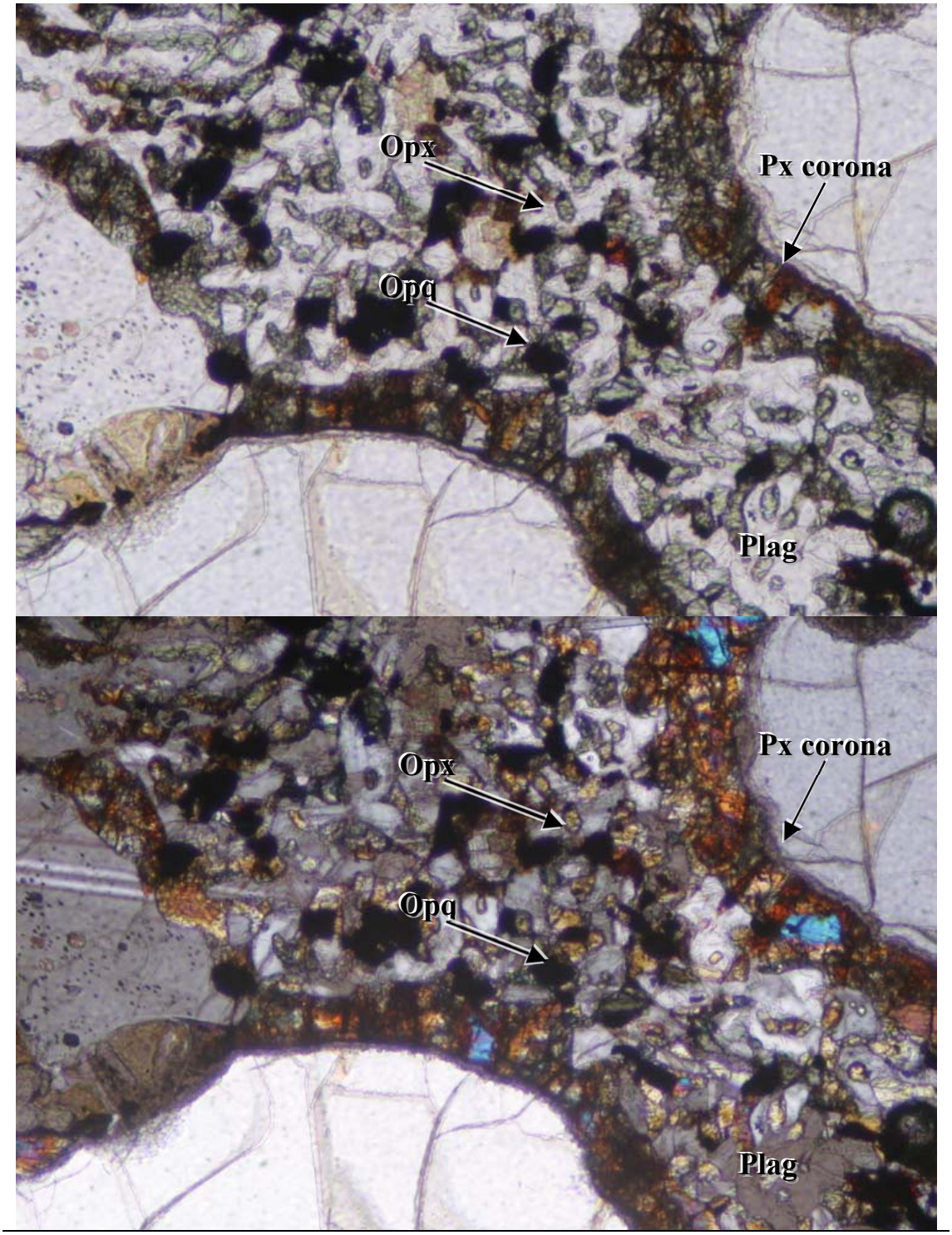


Fig. 3.51 17915 (a) PPL (b) XPL Base of photo: 0.5 mm – pyroxene corona around quartz grains and interstitial doleritic texture.

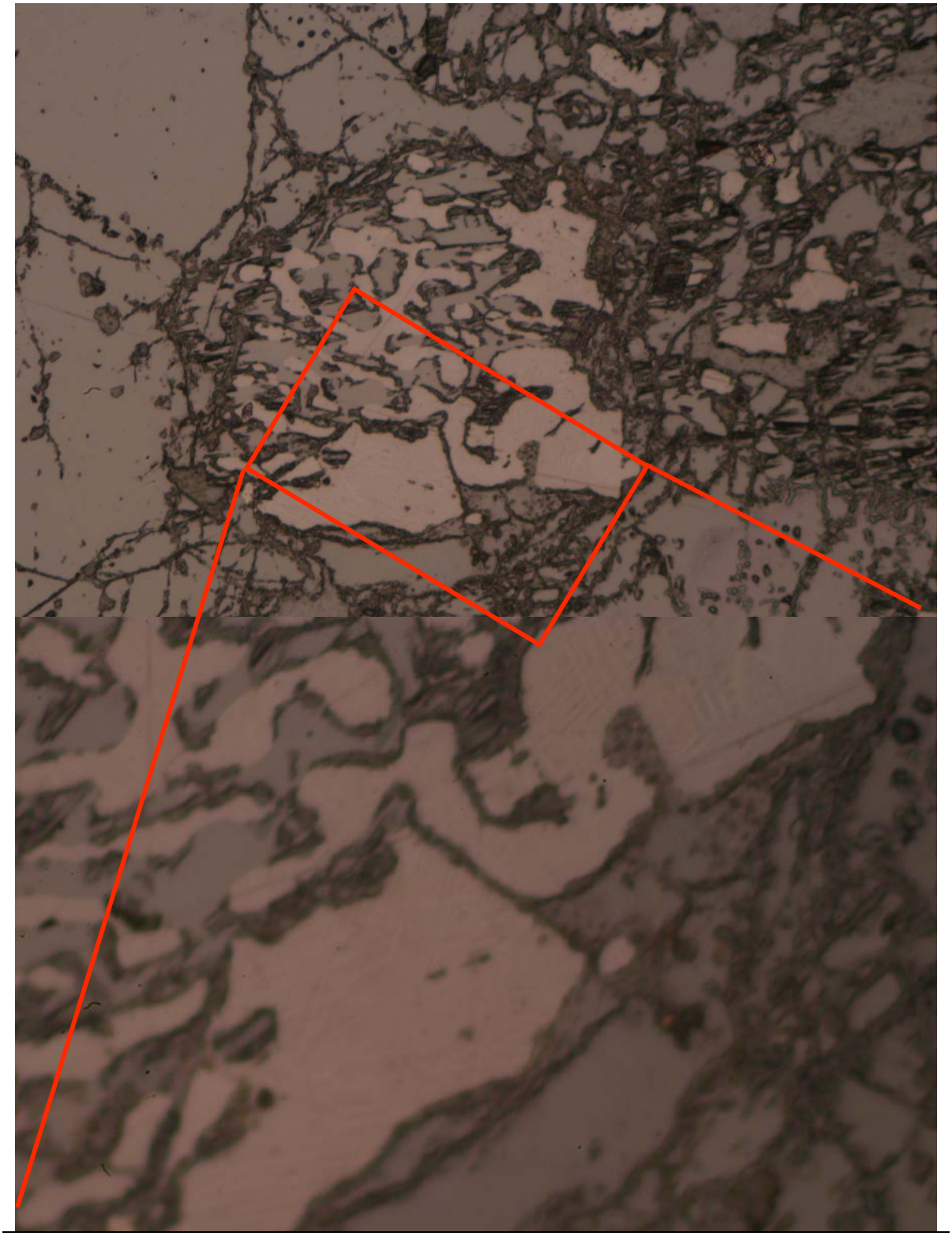


Fig. 3.52 17915 (a) Reflected light Base of photo: 0.5 mm (b) Reflected light Base of photo: 0.2 mm – relationship of magnetite and orthopyroxene in interstitial texture and magnetite exsolution (just visible).

(f) Upper Coliban Dam Felsic Groups 1 and 2 Summary

Deformation twinning, banding and smooth irregular grain shapes provide evidence for both metamorphic and igneous affinities. Further evidence for a metamorphic affinity include recrystallisation textures and quartz and feldspar aggregates, whilst rare euhedral grain shapes and parallel equal width twinning support an igneous affinity (Fig. 3.40 and Fig. 3.44). It may thus be termed a meta-igneous rock. Uniform modes between the samples suggest that these rocks are derived from a homogeneous composition, consistent with a granite / granodiorite on a Quartz—Alkali Feldspar—Plagioclase (QAP) ternary plot ((Le Maitre, 2002); Fig. 3.29). The sieve-like texture at the feldspar rims may be due to peritectic behaviour causing the plagioclase to dissolve (Nekvasil, 1990; Shelley, 1992). As for felsic group 1, sample #17915 may be termed a meta-igneous rock.

(g) Upper Coliban Dam Massive Quartz Rich Felsic Group 3

This rock is predominantly composed of quartz (90 % vol.), with minor plagioclase, calcite, pyroxene and epidote. The quartz mode in Appendix 4 may be deceiving due to the coarse nature of the grains. See the hand sample photo in Fig. 3.53.



Fig. 3.53 Massive quartz rich felsic sample #17917.

The quartz (0.08 mm to 4 mm) is anhedral. The plagioclase (0.04 mm to 0.08 mm) and pyroxene (0.06 mm to 0.10 mm) are subhedral to anhedral, whilst the calcite is commonly present in veins and rarely as anhedral aggregates up to 0.04 mm.

Quartz typically encloses plagioclase and pyroxene grains. Strained lattices undulose extinction is observed within the quartz grains. Calcite is present throughout the sample in veins and at points of breakdown in plagioclase grains. The large calcite aggregate occurs at the contact with the host lava. The plagioclase grains have igneous twinning and rarely form quench textures.

(h) Upper Coliban Dam Felsic Group 3 Summary

Extensive metamorphism as evidenced by lattice strain within the quartz grains and grain shape, make it difficult to infer a protolith for this sample. The high mode of quartz suggests that the protolith is sedimentary (classified as a quartzarenite (Folk, 1974) rather than igneous (classified as a quartzolite (Le Maitre, 2002; Fig. 3.29)). However, such homogeneity may also represent the protolith to be a quartz vein. There is no evidence of euhedral grain shapes to suggest an igneous protolith.

3.2.2 Petrography - Stewart Hill Suite

These samples are predominantly equigranular, although grain size varies within samples, as seen in hand sample (Fig. 3.54). They are predominantly composed of plagioclase (40 to 50 vol. %) up to 2 mm and pyroxene (40 to 60 vol. %) up to 1.2 mm, with accessory kaersutite and opaque minerals.



Fig. 3.54 Hand sample photo of Stewart Hill Suite sample #19004, with obvious variation in grain size.

The plagioclase and pyroxene grains are both subhedral with the plagioclase displaying strong magmatic twinning (Figs. 3.55-57). The pyroxenes have abundant inclusions/exsolution along cleavage planes. The kaersutite is subhedral whilst the opaque minerals occur as small rounded inclusions (Fig. 3.55-38). Glass is present interstitially with spindle outgrowths of plagioclase and as fine rims around pyroxene and plagioclase grains (Fig. 3.60). The textures vary in grain-size between and within samples (Fig. 3.54) from the coarsest size given above to maximum size of plagioclase of 0.6 mm and pyroxene 0.8 mm.

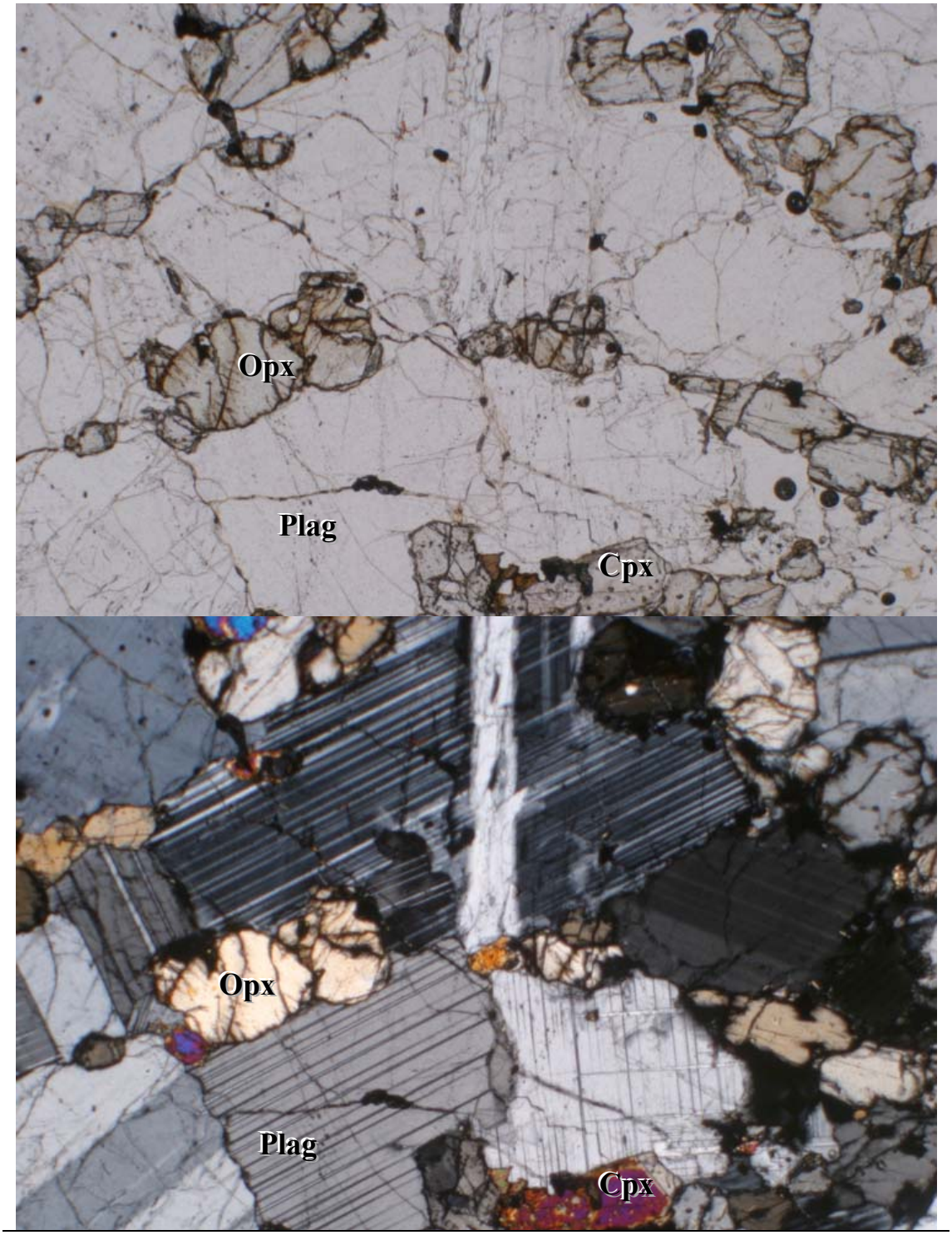


Fig. 3.55 19002 (Stewart Hill) (a) PPL (b) XPL 3.5 mm Base of photo: Interlocking texture of plagioclase and pyroxene grains with clear twinning.

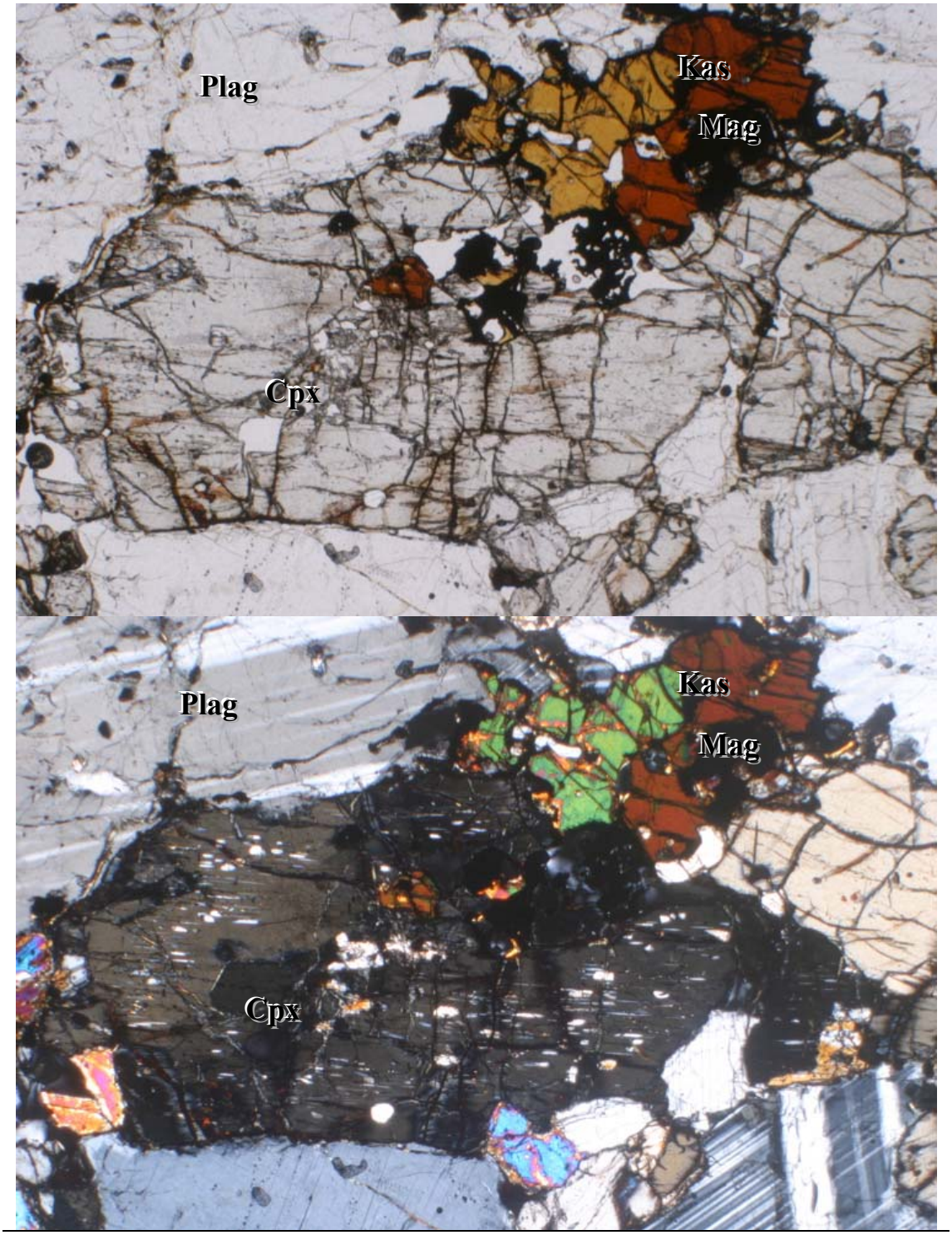


Fig. 3.56 19002 (a) PPL (b) XPL Base of photo: 3.5 mm – Pyroxene grain with lamellae blebs, kaersutite (top right hand corner) and opaque minerals.

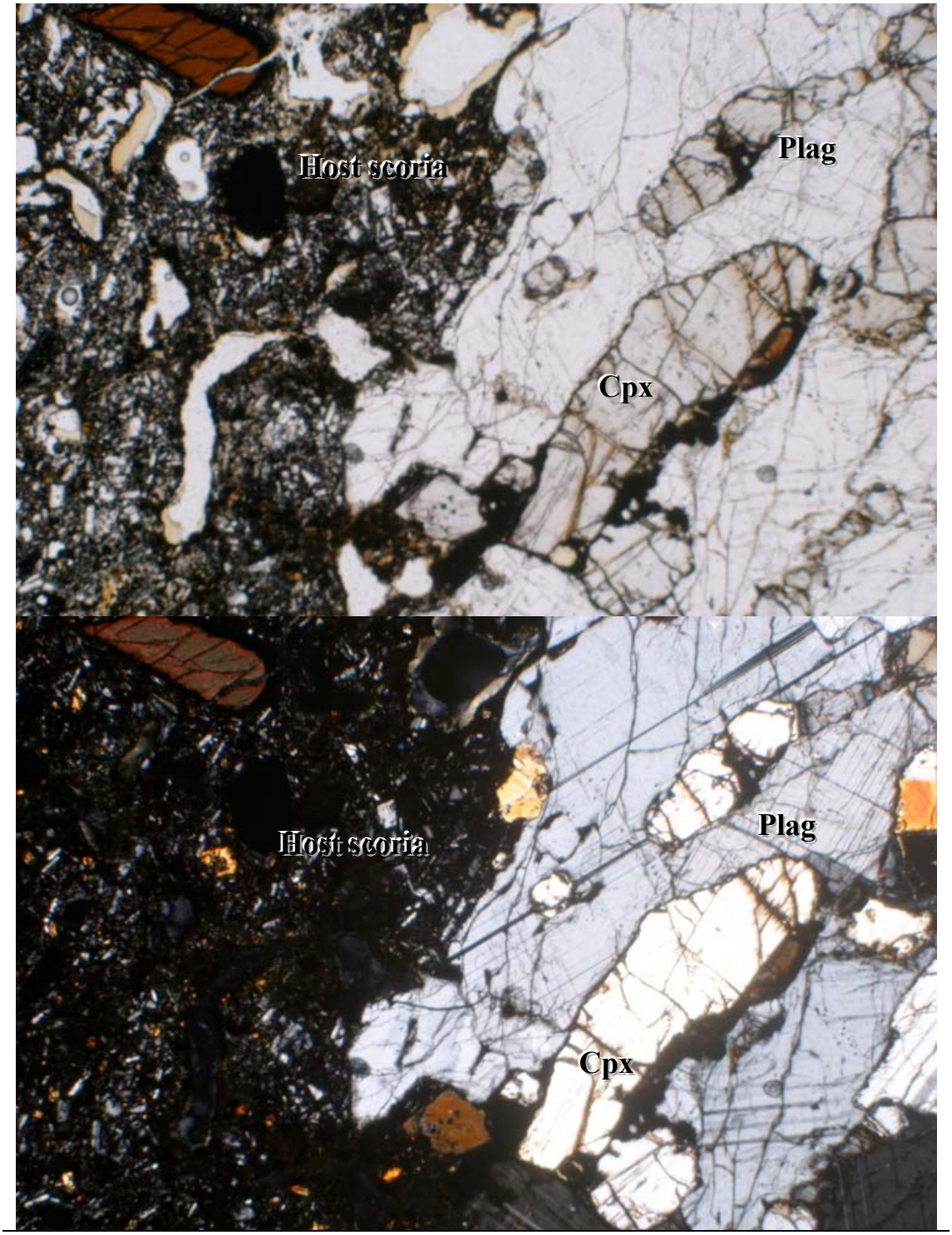


Fig. 3.57 19002 (a) PPL (b) XPL 3.5 mm Base of photo: Interlocking pyroxene and plagioclase grains and contact with the host scoria.

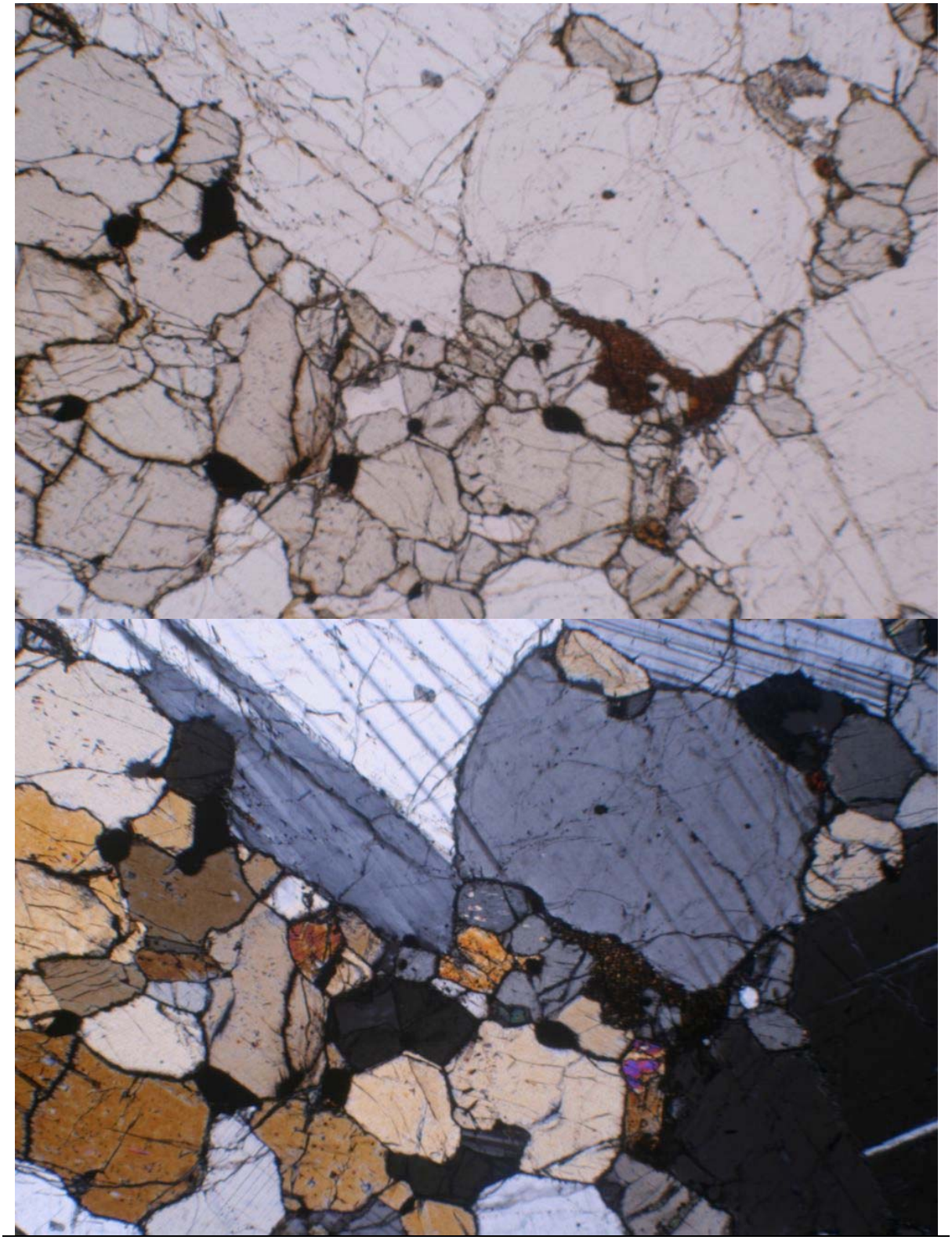


Fig. 3.58 19004 (a) PPL (b) XPL 3.5 mm Base of photo: Polygonal orthopyroxene and plagioclase grains and contact with the host scoria.

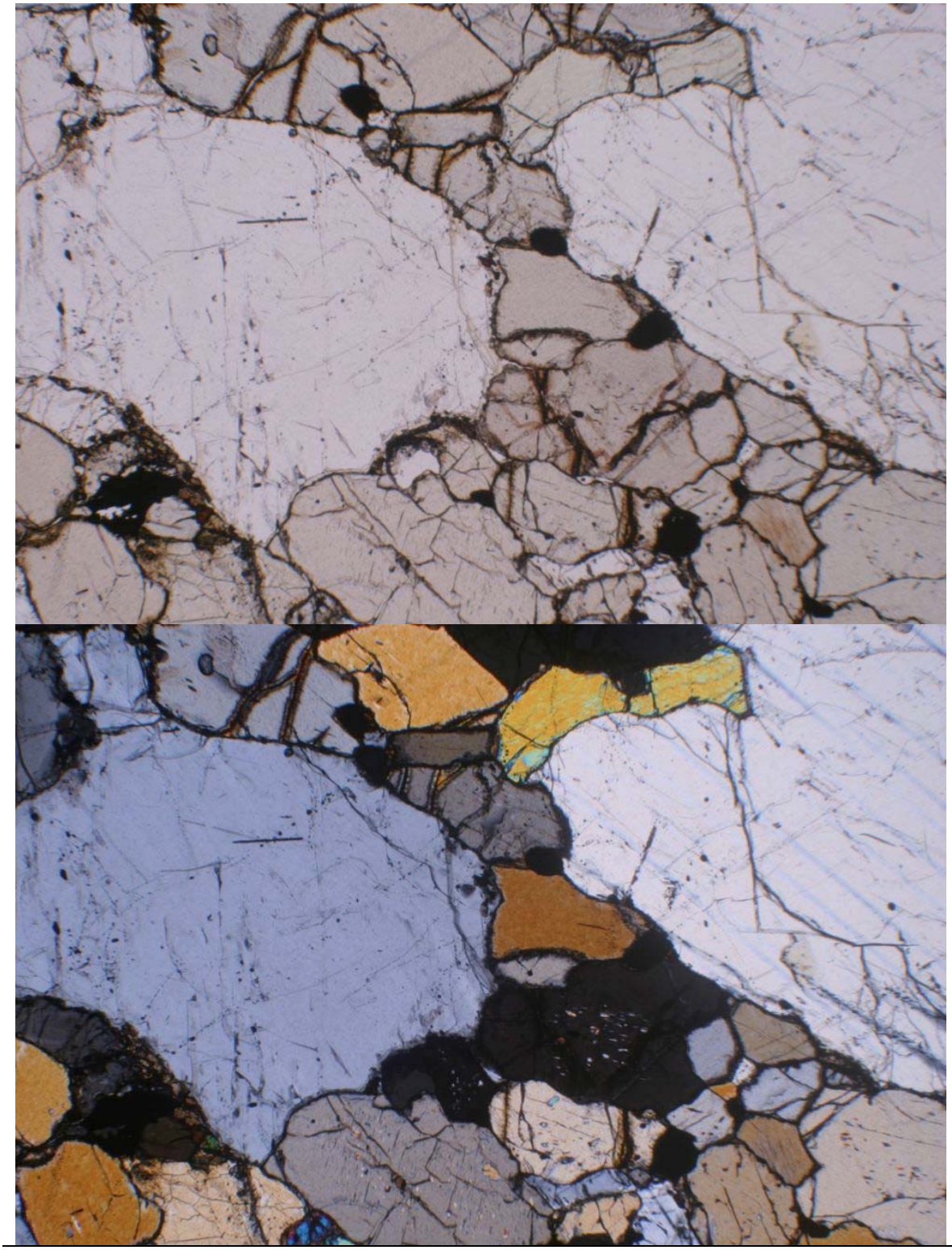


Fig. 3.59 19004 (a) PPL (b) XPL 3.5 mm Base of photo: Polygonal orthopyroxene grains and coarser plagioclase grains.

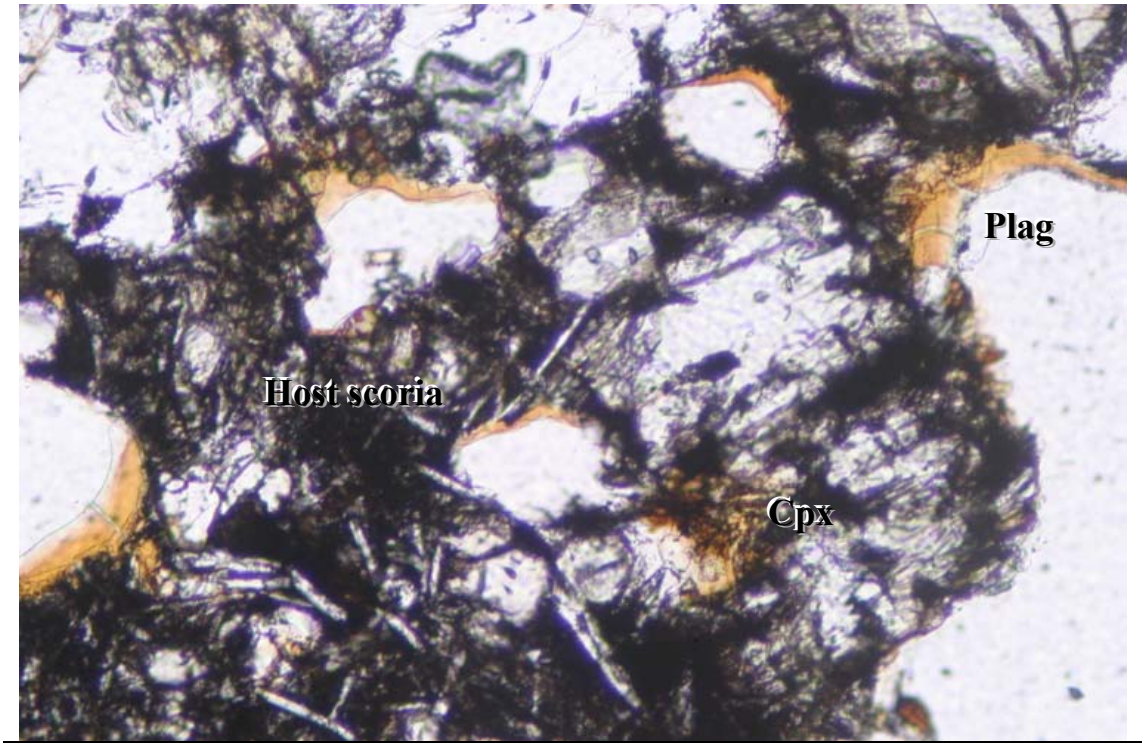


Fig. 3.60 19002 PPL Base of photo: 0.9 mm – Microphenocrysts of plagioclase in glass.

3.2.3 Stewart Hill Suite Summary

The euhedral crystal shapes, grain size, parallel lamellae twinning (inferred as growth twinning) and alignment of plagioclase twins and the parallel alignment of the long axis of grains suggest that this group is of igneous origin, with gabbroic compositions and grainsize of >1 mm (Streckeisen (1974, 1976); Figs. 3.29-30).

4 Methods

4.1 Wholerock major and trace element analysis by XRF and ICP-MS

Fresh sample cores of all samples were firstly cut using a circular rock saw. Outer surfaces were removed to avoid incorporation of weathered and altered material. Host material was also removed to provide a representative sample of the xenoliths. The samples were then crushed using a hydraulic press and powdered using a tungsten carbide ringmill. The press and mill were thoroughly cleaned between each sample, using MQ water and ethanol.

Thirteen xenolith samples were analysed for major and trace elements by X-ray fluorescence (**XRF**) and inductively coupled plasma mass spectrometer (**ICP-MS**). For major element analysis by XRF, a 40 mm glass disc was prepared using a sample flux ratio of ~1:5.4. For trace element analysis by XRF, a pressed pellet was created using ~ 10 g of crushed sample and ~ 1.75 ml of elvanol solution. Analyses were performed on a Panalytical PW2400 XRF Spectrometer at the UNSW Analytical Centre SSEAU, Sydney. See Norris and Hutton (1969) for full details of the method. Loss of ignition was also measured. Lower levels of detection are given in Table 4.1.

Table 4.1 Lower levels of detection of major and trace elements analysed by XRF.

Major elements	wt %	Trace elements	ppm
P_2O_5	0.0029	V	2.9
SiO_2	0.0132	Cr	2.9
TiO_2	0.0046	Co	2.9
Al_2O_3	0.0048	Ni	2.0
Fe_2O_3	0.0017	Cu	2.0
MnO	0.0018	Zn	1.8
MgO	0.0099	Ga	1.0
CaO	0.0017	As	2.5
ZnO	0.0013	Rb	1.0
Na_2O	0.0221	Sr	0.9
K_2O	0.0012	Y	1.0
SO_3	0.0051	Zr	1.0
		Nb	1.0
		Mo	1.8
		Cd	3.0
		Sn	3.9
		Sb	2.9
		Ba	8.0
		Ce	15.4
		Pb	2.0
		Th	2.8
		U	2.9

For trace element analysis by ICP-MS, powdered samples (~ 0.1 g) were digested by standard digestion using HNO_3 and HF. A random sample duplicate (Felsic Group sample #17921) and a method blank were also prepared separately to ensure that contamination did not occur during sample preparation and as a measure of precision. Each of the samples were spiked with 15 μL of an internal standard consisting of Li, As, Rh, In, Tm and Bi in 2% HNO_3. 1/1000 and 1/5000 dilutions were used to measure trace elements on an Agilent 7500cs ICP-MS at GEMOC Analytical Unit (**GAU**) Macquarie University. The operating conditions are detailed in Table 4.2 below. Analyses were undertaken in runs of seven samples, bracketed by BCR-2 in 1/1000, 1/2000 and 1/5000 dilutions, with a set of BIR-1 and BHVO-2 standards at the beginning and end of the sequence.

Table 4.2 ICP-MS Operating Conditions – Agilent 7500cs.

Condition	Property
Type of ICPMS	Octopole Reaction System
Brand and model	Agilent 7500cs
Type of nebuliser	Self aspirating concentric
Brand and model	Agilent micro flow
Nebuliser pump	0.1 rps
Sample depth	5.5 mm
Torch H	-0.2 mm
Torch V	0.5 mm
Carrier gas	1.13 L/min
Make up gas	0.23 L/min
Carrier Gas(es)	Ar
External standard used	BCR-2A
Reference Sample used to determine accuracy	BHVO-2 and BIR-1
Lowest levels of detection (LLD)	$< 10^{-3}$
Counting time	3 x 70 s repetition

The average values obtained for the reference material and duplicate sample are detailed in Table 4.3. The data was corrected using BCR-2 to measure sensitivity and drift, with the HNO_3 rinse as background counts. XRF values have been used for Cr, Ti, As and Zr due to high Cr and Ti values for the standards, As being used as an internal standard and Zr being biased by the dissolution properties of zircon. Hafnium and Lu have been calibrated to the XRF values, using the ratios vs Zr obtained by ICP-MS. Tungsten values have been omitted due to potential contamination from the tungsten carbide mill used for powdering samples.

4.2 Wholerock isotope geochemistry

The samples were once again digested using a repeat of HNO_3 (2mL; Ajax) and HF (2 mL, 27N; Merck, suprapur grade). Once dried down $HClO_4$ (10-15 drops Merck suprapur grade) was added, followed by HCl (4 mL 6N; Merck) and H_2O_2. Finally the samples were dissolved in HCl (6N), dried, HCl and HF solution added and the samples centrifuged. The samples were then eluted through Teflon columns. Hafnium was first collected after 5.4 mL of 2.5N HCl/ 0.1N HF (Blichert-Toft, 2001), followed by 29.5 mL, before collecting Sr. The remaining sample was dried and Nd collected using an Ln.Spec column, following the method described in Pin *et al.* (1997). Sr and Nd isotope analysis was undertaken on a Thermo Finnigan Triton thermal ionisation mass spectrometer (**TIMS**) at GAU, Macquarie University. Samples were loaded onto rhenium filaments and analysed for 200. For Sr, samples produced signals of between 4 - 20 volts at 1380 °C to 1450 °C. Neodymium was run at between 0.5 to 20 volts at 1200 to1800 MA. Hafnium isotope analysis was undertaken on a Nu Instruments 34 MC-ICP-MS also at GAU, Macquarie University, Sydney using standard JMC 475 to monitor precision. BHVO-2 was analysed in each method.

Table 4.3 Measured and reported concentration (ppm) of trace elements for reference material BHVO-2 and BIR-1 as well as the duplicate sample #17921 analysed by ICP-MS solution.

Element	BHVO-2 Reported (ppm)	2SE	BHVO-2 Measured (ppm) Ave (n=12)	2SE	BIR-1 Reported (ppm)	2SE	BIR-1 Measured (ppm) Ave (n=14)	2SE	17921 Ave (n=2)	17921B Ave (n=2)
Be			1.29	0.08	0.58		0.13	0.02	3.54	3.55
Sc	32	2	34.8	1.8	44.0	2	45.6	6.6	3.60	3.24
Ti	16366	480	17153	422	5755		5938	312	1076	1050
V	317	22	316	8	313	22	318	15.3	6.81	6.54
Cr	280	38	337	14	382		455	28	1.63	1.52
Mn	1290	80	1368	38			1377	78	327	318
Co	45	6	46.29	3	52	4	53.8	4.54	57.4	55.9
Ni	119	14	137	6	170	12	195	14.9	5.23	5.19
Cu	127	14	126	12	126	8	119	13.04	4.10	4.19
Zn	103	12	107	10	71	18	68.6	9.56	48.7	45.2
Ga	21.7	1.8	20.6	0.8	16		14.9	0.72	17.7	17.3
Rb	9.8	2	9.03	0.32	0.24		0.18	0.02	151	144
Sr	389	46	383	12	110	4	106	5.98	72.1	68.9
Y	26	4	28.0	1.4	16.5	2	16.7	0.84	60.1	58.3
Zr	172	22	177	4.96	14.5		15.1	0.74	26.0	25.9
Nb	18	4	18.4	1.2	0.55		0.53	0.02	27.8	28.5
Mo			4.08	0.2	0.50		0.05	0.02	0.42	0.39
Cd			0.11	0.02	0.11		0.08	0.02	0.15	0.16
Sn	1.9		2.18	0.12	0.54		0.86	0.1	6.05	6.70
Sb			0.09	0	0.58		0.44	0.04	0.03	0.03
Cs			0.10	0	0.01		0.01	0	1.11	1.10
Ba	130	26	130	4	6.40		6.45	0.36	663	655
La	15	2	15.6	0.6	0.58		0.61	0.04	49.7	50.9
Ce	38	4	38.2	1.8	1.85		1.89	0.1	101	105
Pr	5.0	1.2	5.46	0.14	0.37		0.39	0.04	11.7	12.3
Nd	25	3.6	24.9	0.6	2.35		2.41	0.16	43.7	45.7
Sm	6.2	0.8	6.28	0.16	1.10		1.14	0.06	9.50	9.73
Eu	2.0	0.4	2.09	0.08	0.52		0.53	0.02	1.76	1.69
Gd	6.3	0.4	6.30	0.2	1.80	0.8	1.75	0.1	9.59	9.76
Tb	0.9		0.98	0.04	0.38		0.37	0.02	1.59	1.62

Element	BHVO-2 Reported (ppm)	2SE	BHVO-2 Measured (ppm) Ave (n=12)	2SE	BIR-1 Reported (ppm)	2SE	BIR-1 Measured (ppm) Ave (n=14)	2SE	17921 Ave (n=2)	17921B Ave (n=2)
Dy	4.9	1.6	5.41	0.2	2.50		2.65	0.16	9.60	9.70
Ho	1.04	0.08	1.04	0.04	0.57		0.61	0.04	2.02	2.03
Er	2.3	0.8	2.64	0.1	1.70		1.81	0.1	5.82	5.80
Yb	2.0	0.4	2.02	0.08	1.70	2	1.69	0.12	5.32	5.35
Lu	0.28	0.02	0.28	0.02	0.26		0.25	0.02	0.75	0.75
Hf	4.1	0.6	4.39	0.1	0.60	0.16	0.59	0.02	0.96	0.94
Ta	1.4		1.14	0.02	0.06		0.03	0.02	3.17	3.34
W			0.44	0.32			0.20	0.52	893	492
Pb			1.47	0.04	3.00		2.91	0.12	19.38	18.93
Th	1.2	0.6	1.19	0.06	0.03		0.03	0.00	19.3	21.5
U			0.81	0.84	0.01		0.02	0.01	1.79	1.90
$^{87}Sr/^{86}Sr$ (n=1)	0.703487	19	0.703507	8					0.761908±7	0.761910±6
$^{143}Nd/^{144}Nd$ (n=1)	0.512981	10	0.512968	4					0.512495±7	0.512498±5
$^{176}Hf/^{177}Hf$ (n=1)	0.283096	20	0.283047	15					0.282517±8	0.283318±14

USGS BHVO-2 values (Wilson, 1997; Gao *et al.*, 2002; Weis *et al.*, 2005); BIR-1 values (Flanagan, 1984; Gladney and Roelandts, 1988; Govindaraju, 1994). The value for sample #17921 is out of error compared to the duplicate for $^{176}Hf/^{177}Hf$ due to an erroneous analysis.

4.3 Mineral major element analysis by Electron Microprobe

Polished thin-sections of ~ 30 μm were prepared from fresh cuts of the xenolith suite. Major element mineral data of the xenoliths were then obtained using a CAMECA SX100 electron microprobe (**EMP**) at the GAU, Macquarie University, Sydney. Operating conditions were 15 kV accelerating voltage and 20 nA beam current. Digital images were captured using backscattered electron (**BSE**) and a LINK analysis system. The following standards were used for calibration: albite for Na, Fe_2O_3 for Fe; kyanite for Al, olivine for Mg; wollastonite for Si, Ca; chromite for Cr, spessartine garnet for Mn; orthoclase for K; and rutile for Ti. Lower limits of detection (LLD) are < 0.03 wt % for all elements except ZrO_2, which is 0.09 wt %. The relative standard distribution (as a percentage) is detailed in Table 4.4.

Table 4.4 LLD and errors for the CAMECA SX100 EMP

CAMECA SX100 ELECTRON MICROPROBE **Large area LIF, PET and TAP** **Lower limits of detection for 15 kV accelerating voltage are < 0.03 wt % for all elements, except ZrO2 which is 0.09 wt %**	
Elements measured on Clinopyroxene	**% relative standard deviation per element**
SiO_2	0.27
TiO_2	0.19
Al_2O_3	0.18
Cr_2O_3	0.56
FeO	0.34
MnO	0.55
MgO	0.22
CaO	0.27
Na_2O	0.56
K_2O	0.49
NiO	0.30
P_2O_5	0.65
Elements measured on Zircon	
SiO_2	0.19
HfO_2	0.19
ZrO_2	0.30
Y_2O_3	0.34

4.4 LAM-ICP-MS Mineral Trace Element Analyses

Polished thick sections of ~ 100 μm were prepared from fresh cuts of the xenolith suite. Trace element mineral data of the xenoliths were then obtained using an Agilent 7500s

laser-ablation microprobe independently coupled plasma mass spectrometer (LAM-ICP-MS) attached to a New Wave 213nm Nd:YAG laser at GAU, Macquarie University (see Table 4.5 for the operating conditions). Measured values for BCR2G fell within error of published values. Calcium from EMP analysis was used as an internal standard, whilst reported values Price *et al.* (1997) were used for the basaltic icelandite host material.

Table 4.5 LAM-ICP-MS Operating Conditions – Agilent 7500s

Condition	Property
Type of ICP-MS	Quadrupole
Brand and model	Agilent 7500s
Type of Laser	Nd:YAG
Brand and model	New Wave UP213
Laser Wavelength (nm)	213
Beam Diameter (µm) or	55 µm: Mineral Trace Element Analysis 30-40 µm: Zircon U-Pb Dating and Zircon Trace Element Analysis
Pit depth estimate	30 – 55 µm
Carrier Gas(es)	He; He only in laser cell; Ar added downstream from laser cell
Gas flow rate	0.8 L/min
Laser power	0.08mJ; 6 J/cm^2
Laser Pulse Rate (Hz)	5
External standard used	NIST610: Mineral Trace Element Analysis GEMOC GJ Zircon: Zircon U-Pb Dating
Reference Sample used to determine accuracy	BCR2G: Mineral Trace Element Analysis 91500 Zircon: Zircon U-Pb Dating
Data reduction software used	Glitter v4.4.1
Typical length of signal for background	60
Typical length of signal for age calculation	100-120
Sensitivity on mass 238U in laser mode	2000 cps/ppm (measured on GJ-1 zircon)
Isotope dwell times	^{206}Pb 15 ms; ^{207}Pb 30 ms; ^{208}Pb 10 ms; ^{232}Th 232 10 ms; ^{238}U 15 ms All else 30 ms

Table 4.6 Measured and reported concentration (ppm) for reference material BCR2G analysed by LAM-ICP-MS

	BCR2G Reported (ppm)		BC2RG Measured (n=3)	
Element	**Ave**	**StDev**	**Ave**	**StDev**
Li			9.7	0.2
Sc	33	0.8	32.6	0.04
Ti*	1.4	0.03	14574	461
V	414	8	434	11
Co	35.8	1.3	36.4	0.72
Ni	10.8	0.7	11.4	0.48
Cu	19	1	20.5	1.12

	BCR2G Reported (ppm)		BC2RG Measured (n=3)	
Element	**Ave**	**StDev**	**Ave**	**StDev**
Zn	147	12	140	13
Ga	22.7	0.9	23	1
Rb	49	2	49.7	0.84
Sr	342	6	351	4
Y	35.3	0.7	34.6	0.30
Zr	194	4	202	12
Nb	12.8	0.4	13.7	0.57
Mo	244	7	256	12
Cs	1.13	0.08	1.18	0.08
Ba	660	19	695	24
La	25	0.7	25.35	0.88
Ce	50.5	1.6	53	3
Pr	6.8	0.3	7.10	0.20
Nd	29	1	30.09	1.31
Sm	6.6	0.4	6.76	0.19
Eu	1.92	0.12	2.03	0.10
Gd	6.5	0.4	6.58	0.13
Tb	NA		0.99	0.02
Dy	6.5	0.4	6.49	0.21
Ho	1.3	0.08	1.31	0.05
Er	3.6	0.2	3.64	0.03
Yb	3.5	0.2	3.68	0.08
Lu	0.51	0.03	0.53	0.03
Hf	5	0.3	5.22	0.14
Ta	0.8	0.05	0.82	0.02
Pb	11.5	0.6	10	1
Th	6.1	0.3	6.35	0.11
U	1.73	0.09	1.87	0.09

BCR2G Values Norman *et al.* (1998), * value in wt %

4.5 Zircon U-Pb geochronology, trace element and Hf isotope analysis

Zircons were separated by standard techniques using heavy liquids and a Frantz magnetic separator. They were then hand picked, mounted in epoxy and polished to expose the internal structure. Images of the grains were then taken on a CAMECA SX100 electron microprobe (**EMP**) using the backscattered electron (**BSE**) technique to image structural features at GAU, Macquarie University, Sydney. Digital images were captured using a LINK analysis system. Selected major and trace element analysis was also performed on the CAMECA SX100 using 15 kV accelerating voltage and 20nA beam current. A short list of the most useful major and trace elements were analysed including SiO_2, ZrO_2, Y_2O_3,

and HfO_2. Hafnium was used as an internal standard for LAM-ICP-MS trace element analysis.

The mount was cleaned in acid prior to analysis to avoid Pb contamination. *In situ* U-Pb dating and trace element analysis was undertaken simultaneously using an Agilent 7500s laser-ablation-microprobe inductively-coupled-plasma mass-spectrometer (LAM-ICP-MS) attached to a New Wave 213nm Nd:YAG laser at GAU, Macquarie University (see Table 4.5 for the operating conditions). Five isotopes were measured for U-Pb dating (^{206}Pb, ^{207}Pb, ^{232}Th, ^{238}U and ^{235}U) and 11 for trace element analysis as per methods described by (Norman *et al.*, 1996; Norman *et al.*, 1998; Jackson *et al.*, 2004). The data was reduced using GLITTER© (v4.4.1) software.

The analyses were undertaken in runs of 10 samples, bracketed by GEMOC-GJ as an external standard for the U-Pb dating (Jackson *et al.*, 2004) and NIST610 (Norman *et al.*, 1996) for the trace element analysis. Zircon 91500 (1064 Ma; Wiedenbeck *et al.*, 1995) was used as a reference standard in each run to monitor instrument accuracy. The values measured were within reported error (Table 4.7).

Table 4.7 Values reported for 91500 zircon standard

	Reported Age	**1SD**	**This study (n=10)**	**1SD**
$^{207}Pb/^{206}Pb$ Age (Wiedenbeck *et al.*, 1995)	1065 Ma	4	1069 Ma	20
Element (ppm)	**Average**	**1SD**	**Average**	**1SD**
Y	147	22	139	8
Ce	2.5	0.5	2.3	0.2
Sm	0.41	0.2	0.39	0.05
Eu	0.37	0.17	0.20	0.04
Gd	2.1	0.4	2.06	0.20
Yb	66	7	67	4
Lu	14	2	12.4	0.7
Hf	0.64	0.09	0.64	0.09
Th	31	5	29	2
U	88	15	82	7

HfO from EMP analysis was used as an internal standard; 91500 trace element values(Belousova *et al.*, 2002)

Hf isotope analysis was carried-out using a New Wave/Merchantek UP 213 nm laser ablation microprobe attached to a Nu Plasma 34 multi-collector ICP-MS at GAU, Macquarie University, Sydney. The operating conditions are given in Table 4.8 and the methodology used is as described by Griffin *et al.* (2000). Mud Tank (**MT**) zircon was used as reference material

which has an average $^{176}Hf/^{177}Hf$ ratio of 0.282522 ±42 (2SE) (Griffin *et al.*, 2007). MT analysed in this study was within reported range (weighted average 0.282538 ±12 (2SE); n=12). More details of these analytical techniques is described by Griffin *et al.* (2000; 2004).

Initial $^{176}Hf/^{177}Hf$ ratios were calculated using measured $^{176}Lu/^{177}Hf$ ratios, with a typical uncertainty on a single analysis of $^{176}Hf/^{177}Hf$ ± 1-2% (2SE). This error includes both analytical uncertainties and intragrain variance of Lu/Hf, as typically observed in zircons. The decay constant of Scherer *et al.* (2001) ($1.865x10^{-11}$) has been used for the calculation of ε_{Hf} values. A model of $(^{176}Hf/^{177}Hf)_i = 0.279718$ at 4.56 Ga and $^{176}Lu/^{177}Hf = 0.0384$ has been used to calculate model ages (T_{DM}) based on a depleted-mantle source, producing a present-day value of $^{176}Hf/^{177}Hf$ (0.28325) (Griffin *et al.*, 2000; Griffin *et al.*, 2004). As T_{DM} ages are calculated using measured $^{176}Hf/^{177}Hf$ of the zircon and give only the minimum age for the source material from which the zircon crystallised, we have also calculated a "crustal" model age (T_{DM}^{C}) for each zircon which assumes that the parental magma had the composition of average continental crust ($^{176}Lu/^{177}Hf = 0.015$) that was originally derived from depleted mantle.

Table 4.8 LAM-MC-ICP-MS Operating Conditions – Nu Plasma MC.

Condition	Property
Type of ICP-MS	Multi Collector
Brand and model	Nu Plasma 34
Type of Laser	Nd:YAG
Brand and model	New Wave UP213
Laser Wavelength (nm)	213
Beam Diameter (μm) or	40 / 55
Pit/raster depth estimate	50-60 μm
Carrier Gas(es)	He
Gas flow rate	1 L/min He; 0.7 L/min Ar
Laser power	0.1 mJ; 6 J/cm^2
Laser Pulse Rate (Hz)	5
Reference Sample used to determine accuracy	Mud Tank
Data reduction software used	Nu Instruments Time Resolved Analysis
Typical length of signal for background	30 s
Typical length of signal for age calculation	80-120 s

The source rock types have been determined using trace element data from the EMP and LAM-MC-ICP-MS and the CART (Classification and Regression Trees) analysis system of (Belousova, 2000; Belousova *et al.*, 2002).

5 Results

5.1 Wholerock major and trace element geochemistry

Major and trace element geochemical data are detailed in Tables 5.1 and 5.3 (at the end of this subchapter). Values for the basaltic icelandite host material are also included for comparison (Price *et al.*, 1997). Samples grouped petrographically (i.e. Upper Coliban Dam Felsic, Mafic and Intermediate) are supported in the total alkali vs silica (TAS) plot (Fig. 5.1), with the exception of sample #17922 which has an intermediate composition rather than mafic as suggested by petrography. The Felsic Group is classified as granitic. The Mafic Group and the Stewart Hill Suite are classified as gabbroic, although the Stewart Hill samples trend towards an intermediate composition of basaltic andesite composition. The intermediate samples are classified as trachyandesite / basaltic tranchyandesite. The Mafic and Intermediate groups are alkaline, whilst the Felsic Group and Stewart Hill Suite are subalkaline (Fig. 5.1).

The petrographic groups also nucleate within distinct domains on major and trace element vs SiO_2 (Fig. 5.2) and vs Mg# (Fig. 5.3), with the exception of V. However, the Felsic Group may also be subdivided into two groups by differences in Y and Nb vs SiO_2 (Fig. 5.2) and in Zr vs Mg# (Fig. 5.3).

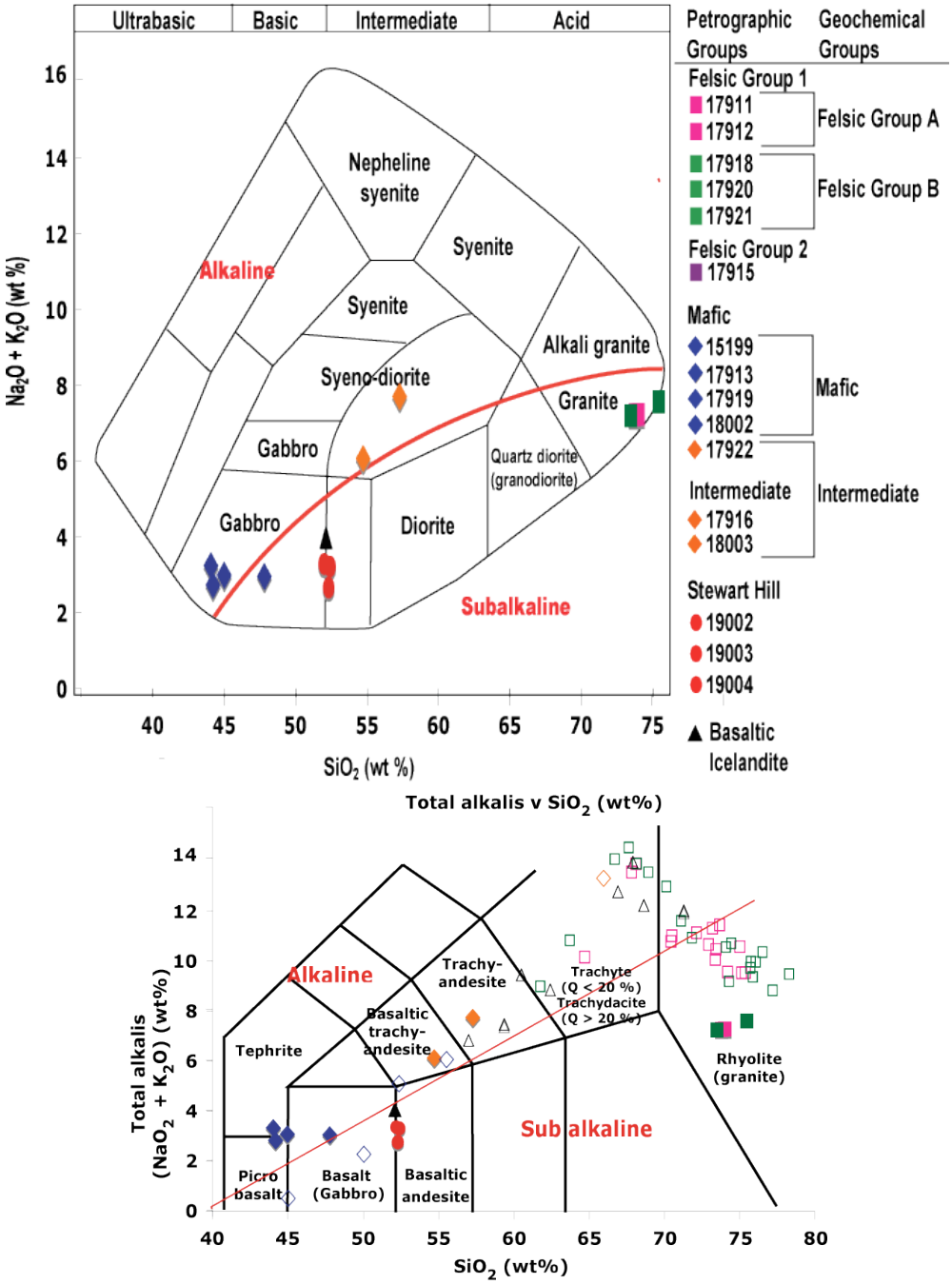


Fig. 5.1 Top: TAS plutonic diagram (Cox *et al.*, 1979; Wilson, 1989); and Bottom: TAS volcanic diagram (Le Maitre *et al.*, 1989); open symbols are analyses of glass within the samples (filled symbols).

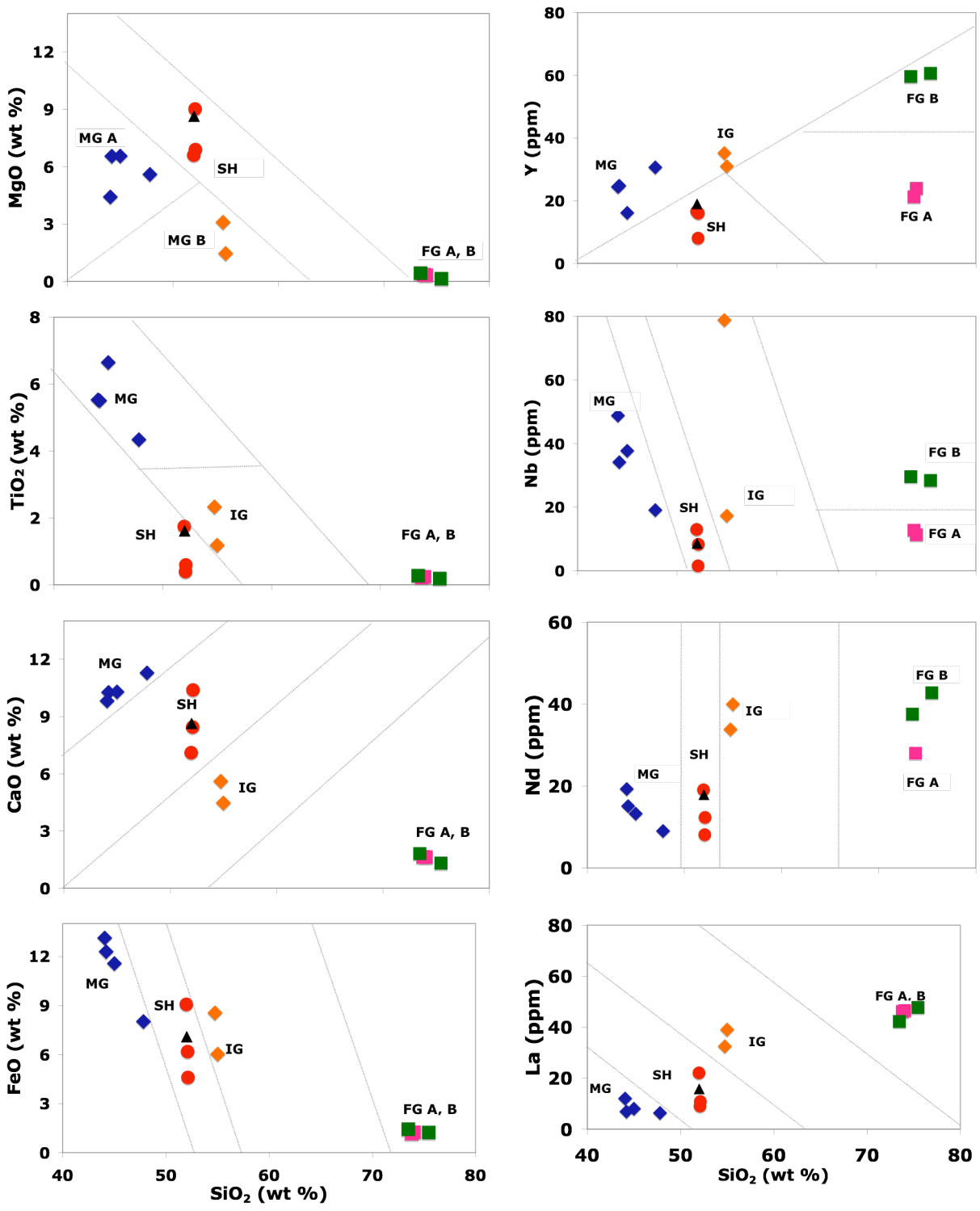


Fig. 5.2 Various wt % oxides and trace elements vs SiO_2. Grey lines subdivide the samples into geochemical groups. The slopes of the grey lines have no particular meaning except to subdivide the samples into geochemical groups. Key as for Fig. 5.1. Linear relationships are noted within the mafic group.

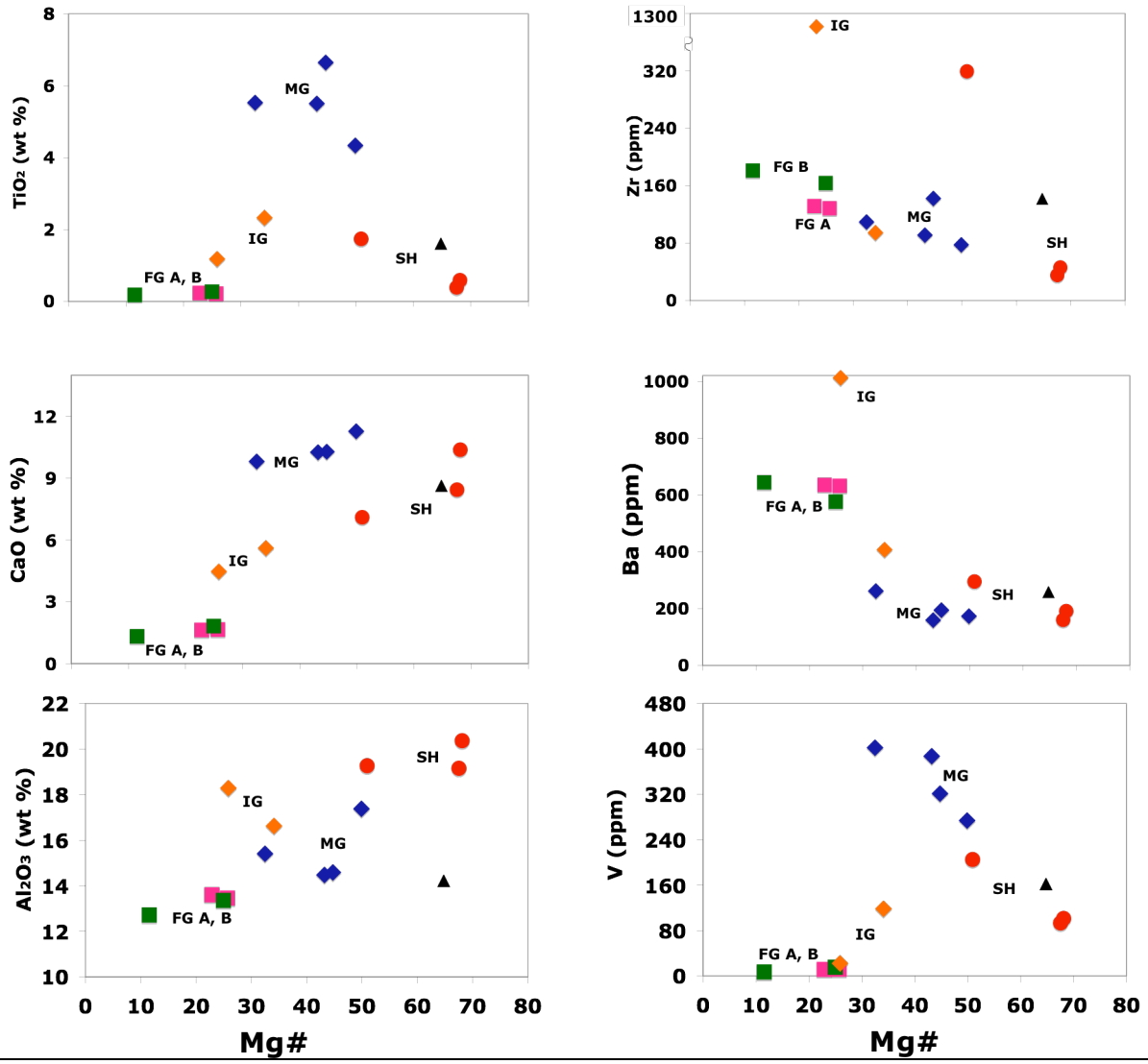


Fig. 5.3 Various wt % oxides and trace elements vs Mg#. Key as for Fig. 5.1. Once again, linear trends are noted within the mafic group.

5.1.1 Upper Coliban Dam Mafic Group

All samples in this group are classified as gabbro on the TAS chart (Fig. 5.1), with low SiO_2 and total alkalis (44 to 48 wt %; $Na_2O + K_2O$ 2.8 to 3.3 wt %). The analyses of glass domains (described in petrography) within samples form a positive linear relationship on the TAS chart (Fig. 5.1). Based on CIPW norm calculations (Table 5.1), #15199 may be classified as tholeiitic with >10 % normative hy+qtz (12.2 %) and <50 % SiO_2 (48 %). Samples #17913, 17919 and 18002 have transitional geochemistry, with normative <10 % hy+qtz (4.6 and 6.8 %) and <50 % SiO_2 (44 and 45 %) (Carmichael, 1964; Price *et al.*, 1997). As expected, the Mafic Group has the highest TiO_2, CaO and FeO (Fig. 5.2; TiO_2 4.3 to 6.7; wt % CaO 9.82 to 11.3 wt %), with a large range in Mg# (Fig. 5.3; Mg# 32 to 50). A positive linear relationship is seen for CaO and Y vs SiO_2, with a negative

relationship for La, TiO_2 and FeO (Fig. 5.2). There is a large variation in concentration for all elements vs Mg# (Fig. 5.3), a negative linear relationship is expressed for CaO, Al_2O_3, Ba and V.

The Mafic Group has ∑REE 47.2 to 85.2 (Table 5.2), with a positive Eu anomaly (Eu/Eu* 1.25 to 1.28) and a slight decreasing enrichment trend relative to chondrite towards the HREE (Fig. 5.4). The Group has slight enrichment in mobile element concentrations relative to chondrite (Fig. 5.5; Rb, 2.7 to 6.9 ppm; Th 0.27 to 0.31 ppm), increasing for K (2947 to 3461 ppm), with positive anomalous values in Nb, Ta, Sr and Ti (Fig. 5.5; Nb 19.1 to 49 ppm; Ta 1.3 to 2.9 ppm; Sr 798 to 988 ppm).

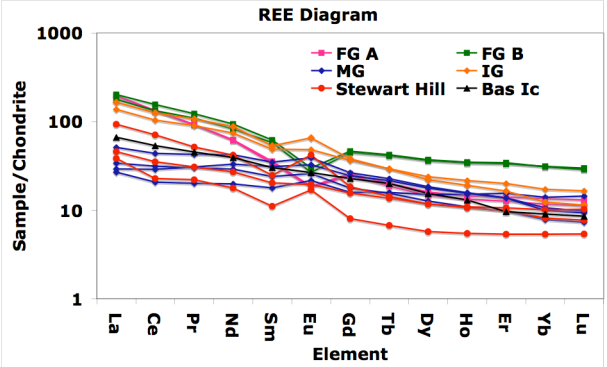


Fig. 5.4 REE diagram normalised to chondrite, with values from Sun and McDonough (1989). To note is greater enrichment of HREE felsic group B samples compared to felsic group A.

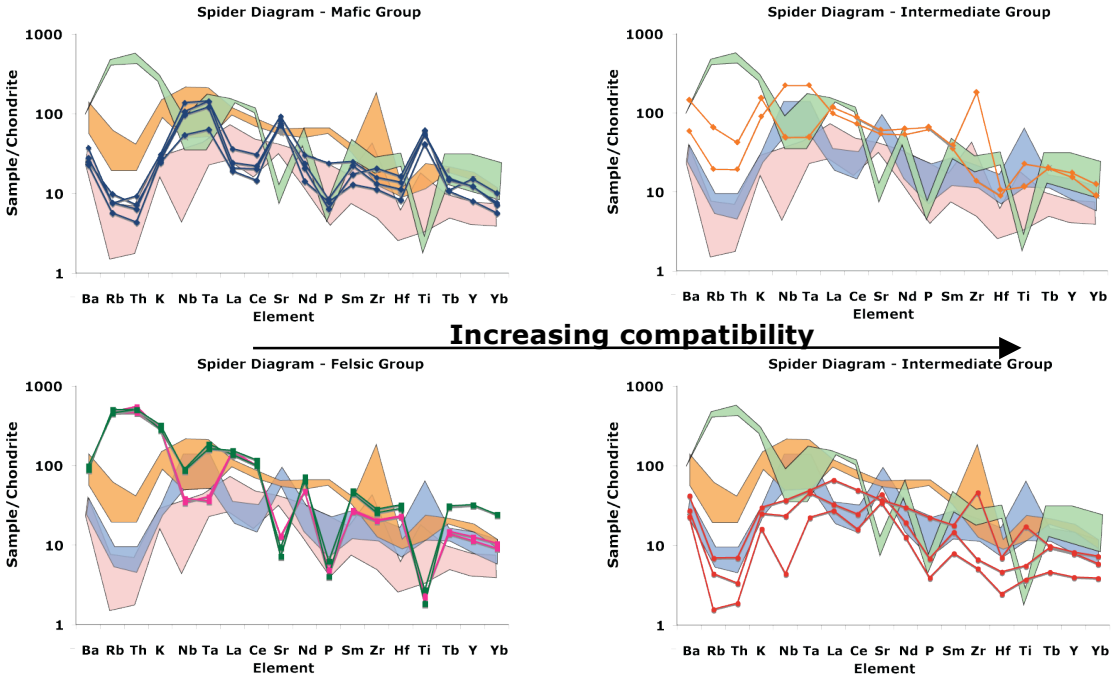


Fig. 5.5 Spider diagrams for each group normalised to the chondrite values of Thompson (1982).

Glass from within the Mafic Group samples has a similar REE trend to the wholerock analyses, with a decrease in the degree of enrichment towards the HREE (Fig. 5.6). However, a slight negative Eu anomaly is noted for most analyses. A similar pattern between the wholerock and glass is also seen in the spider diagram, except for a negative Sr anomaly in the glass (Fig. 5.6).

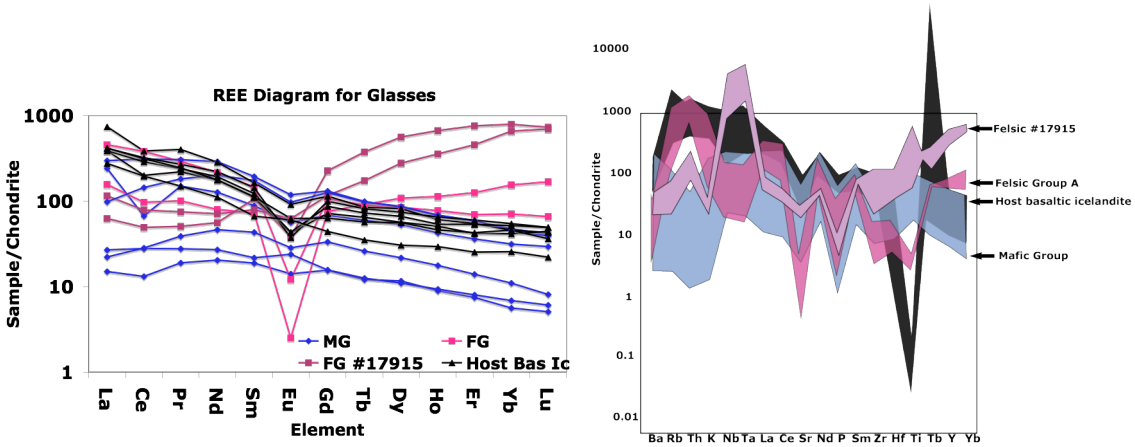


Fig. 5.6 REE and spider diagrams for glass located within samples of the felsic and mafic groups and the host basaltic icelandite normalised to the chondrite values from Thompson (1982). Key as for Fig. 1.

The range of isotope results are relatively tight in the Mafic Group for the Lu-Hf and Sm-Nd systems (Table 5.3; initial $^{176}Hf/^{177}Hf$ 0.282849 to 0.282959; initial $^{143}Nd/^{144}Nd$ 0.512730 to 0.512783; ε_{Nd} 1.87 to 2.45; (Nd) T_{DM} 1.64 to 1.01 Ga; Figs. 5.7 and 5.8). However, there is greater range within the Rb-Sr system ($^{87}Sr/^{86}Sr$ 0.704161 to 0.704912 (Fig. 5.7). An age of 3 Ma, the minimum age obtained from the mafic samples during U-Pb zircon dating (see 5.3 below), has been assumed for calculating the initial values. Such a variation in the Rb-Sr system is seen in all samples, suggesting superficial gain and/or loss or Rb and/or Sr due to weathering.

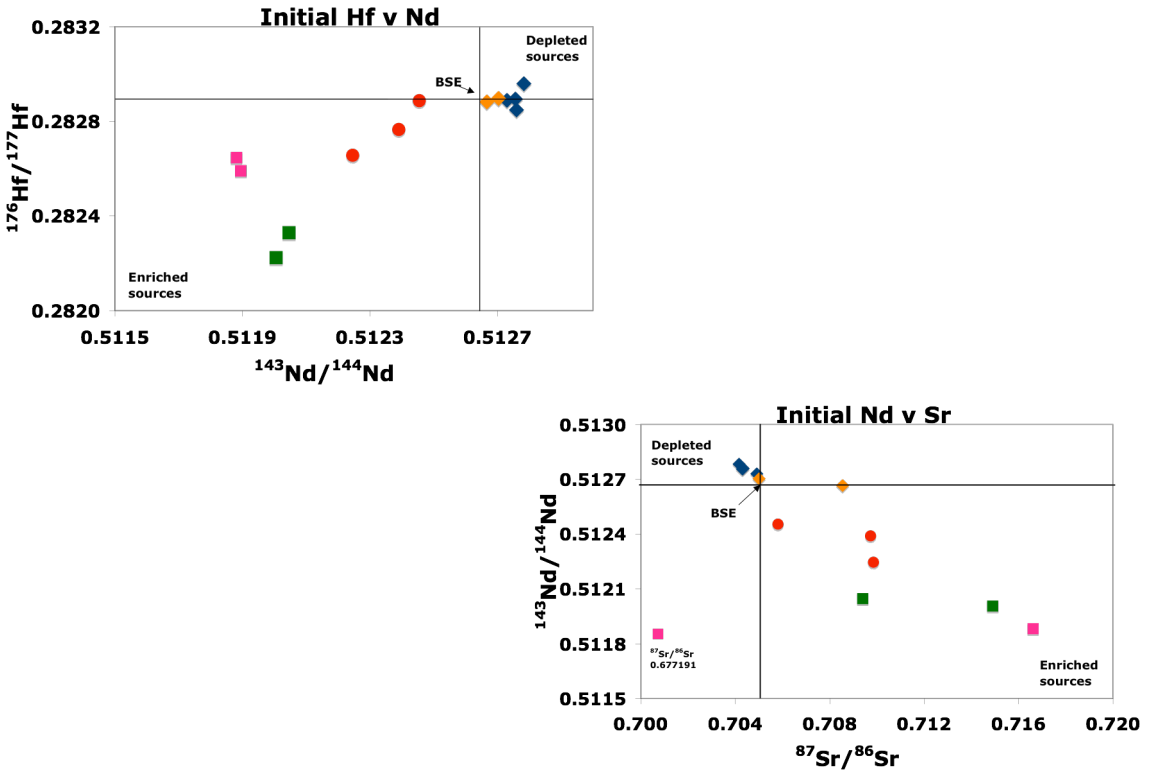


Fig. 5.7 (a) Initial Hf vs Nd (Salters and Hart, 1991; Dickin, 2005); (b) Initial Nd vs Sr showing average values for the Upper Coliban Dam Mafic and Intermediate Groups and a scatter towards enriched sources for the Upper Coliban Dam Felsic Group and Stewart Hill groups.

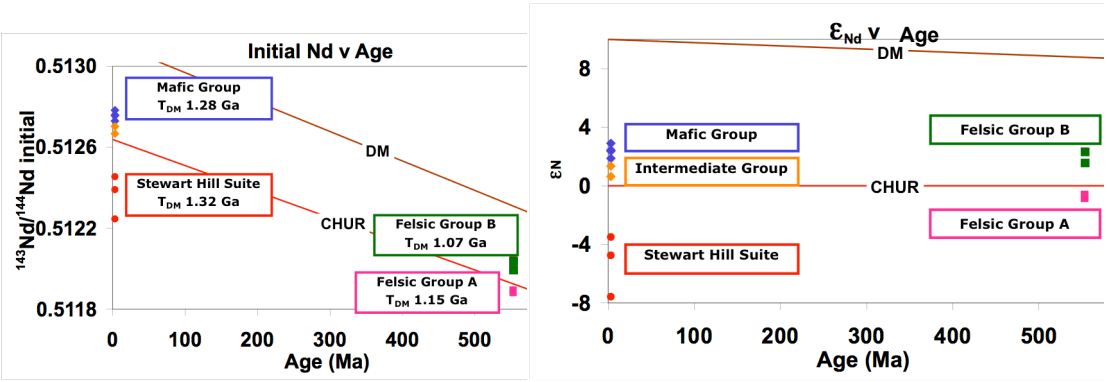


Fig. 5.8 (a) Initial Nd vs Age with T_{DM} marked for each group aside from the Intermediate Group for which it was not calculated; (b) ε_{Nd} vs Age. Once again the felsic subgroups form distinct clusters.

5.1.2 Upper Coliban Dam Intermediate Group

The Intermediate Group is classified as trachyandesite/basaltic trachyandesite (syeno-diorite on the plutonic chart) on the TAS chart (Fig. 5.1; SiO_2 55 to 55 wt %; $Na_2O + K_2O$ 6.1 to 7.4 wt %). Based on CIPW norm calculations (Table 5.1), this group is classified as

having basaltic icelandite composition with >10 % normative hy+qtz (15 to 20 %) and >50 % SiO_2 (55 %) (Carmichael, 1964; Price *et al.*, 1997). The Intermediate Group is distinguished from the Mafic Group by CaO, FeO and La vs SiO_2 (Fig. 5.2) and V vs Mg# (Fig. 5.3). Sample #18003 has the highest LOI value (3.20). The Group has lower TiO_2, CaO and V compared to the Mafic Group, with higher La (Fig. 5.2 and Fig. 5.3).

The samples in this group all have a common trend in REE (Table 5.2; ∑REE 170 to 197 ppm;), with positive Eu anomalies (Eu/Eu* 1.2 to 1.5) and enrichment relative to chondrite decreasing towards the HREE (Fig. 5.4). They have negative mobile element anomalies (Fig. 5.6) and; Rb 6.9 to 23; Th 0.82 to 1.8 ppm; K 10883 to 18603 ppm) and follow a similar overall trend to each other in the spider diagram (Fig. 5.5), with decreasing enrichment relative to chondrite towards the compatible elements. Distinct differences between the samples include anomalous values of Ba and Zr in sample #18003 (Zr 1254 ppm; Ba 1013 ppm) and enriched values of Nb and Ta in #17922 (Fig. 5.5; Nb 79 ppm; Ta 4.5 ppm).

Within this group, initial $^{176}Hf/^{177}Hf$ (0.282883 to 0.282883) and $^{143}Nd/^{144}Nd$ (0.512667 to 0.512703; ε_{Nd} 0.63 to 1.35) values ((Nd) T_{DM} 0.77 to 0.64 Ga) are identical, plotting close to BSE (Figs. 4.7 and 4.8). However, $^{87}Sr/^{86}Sr$ varies considerably from 0.705008 to 0.708548 (Fig. 5.7(b)). An age of 3 Ma, the minimum age obtained from U-Pb zircon dating, has been assumed for calculating the initial values (see 5.3 below).

5.1.3 Upper Coliban Dam Felsic Group

The entire Felsic Group is classified as granitic on the volcanic and plutonic TAS charts, with high total alkali values (Fig. 5.1; SiO_2 73.5 to 75.5; $Na_2O + K_2O$ 7.26 to 7.58 wt %). Analyses of glass (as discussed in petrography results) from samples #17911 and #17921 are also included. The glass data are variable and plot predominantly within the granite field with a broad negative linear trend (Fig. 1). As expected, the Felsic Group has the lowest values in other major elements such as TiO_2, CaO and FeO (Fig. 5.2 and Fig. 5.3; TiO_2 0.18 to 0.27; CaO 1.31 to 1.82; FeO 1.16 to 1.43 wt %), whilst the low Mg# (12 to 26) is highlighted in the various oxide and trace element plots vs Mg# (Fig. 5.3). Apart from the particularly low Mg# of sample #17921, the group is not separable using major elements, which exhibit no discernable trend. However, trace elements such as Y and Nb vs SiO_2 (Fig. 5.2) and Zr vs Mg# (Fig. 5.3) show a clear division within the group, with

Felsic Group B displaying greater concentrations of these elements. Overall, the group is more enriched in Zr, Ba (Fig. 5.2) and Y (Fig. 5.3) compared to the mafic and intermediate groups. LOI is moderate (0.74 to 1.05).

The Felsic Group is enriched in REE compared to chondrite values (∑REE 187 to 241) (Fig. 5.4), particularly LREE. All plots of this group exhibit a negative Eu anomaly (Eu/Eu* 0.53 to 0.63). Felsic Group A has a high La/Yb ratio (14.6 and 16.7), compared to Felsic Group B (La/Yb 5.70 to 6.52), suggesting a more even spread across the elements for the latter (Fig. 5.4). The samples are highly enriched in mobile elements such as Rb, Th and K compared to chondrite values (Rb 150 to 167 ppm; Th 18.2 to 22.0 ppm; K 31919 to 36352 ppm) showing a clear hump in the spider diagram (Fig. 5.5). Strontium (71 to 121 ppm), P (175 to 271 ppm) and Ti (1085 to 1385 ppm) have negative anomalies, whilst Tb has a positive anomaly (0.67 to 1.52 ppm) (Fig. 5.5). There is a tight range in trace elements overall for the Felsic Group aside from Nb, Ta, Tb, Y and Yb as mentioned above (Fig. 5.5).

The glass within Felsic Group A (sample #17912) has a strong negative Eu, with more enrichment relative to chondrite for the rest of the REE (Fig. 5.6). A similar trace element pattern on the spider diagram is seen in the wholerock samples, with positive anomalies for Rb and Th and negative anomalies for Nb, Ta, Sr and P (Fig. 5.5). However, the glass in Felsic sample #17915 (which has differences observed in petrography) shows a different trend, with a less exaggerated Rb and Th anomaly, positive anomalies in Nb and Ta and an increase in enrichment compared to chondrite values towards the more compatible elements (Fig. 5.6). The glass in sample #17915 also has a negative Eu anomaly with enrichment of HREE compared to chondrite values.

Wholerock isotope results once again separate the Felsic Group into the same two subgroups identified using trace elements (Table 5.3). Felsic Group A has the following values: initial $^{176}Hf/^{177}Hf$ 0.282590 to 0.282646; $^{143}Nd/^{144}Nd$ 0.511881 to 0.511894; ε_{Nd} 0.84 to 0.59 and $^{87}Sr/^{86}Sr$ 0.677191 to 0.716569 and Felsic Group B $^{176}Hf/^{177}Hf$ 0.282217 to 0.282323; $^{143}Nd/^{144}Nd$ 0.512005 to 0.512045; εNd +1.58 to 2.37; and $^{87}Sr/^{86}Sr$ 0.709332 to 0.714820 (Figs. 4.7 and 4.8). Extreme variation is seen in $^{87}Sr/^{86}Sr$ values sample #17912 (Fig. 5.7). Initial ratios for each isotope system plot within enriched zones (Fig. 5.7). The group has tight (Nd) T_{DM} ages of 1.17 to 1.07 Ga, averaging 1.11 Ga.

5.1.4 Stewart Hill Suite

The Stewart Hill samples sit on the boundary of gabbro and basaltic icelandite on the TAS chart (Fig. 5.1) (Price *et al.*, 1997). However, further discrimination using CIPW norm calculations (Table 5.1) classify them as having basaltic icelandite composition with >10 % normative hy+qtz (21 to 33 %) and >50 % SiO_2 (52 %) (Carmichael, 1964; Price *et al.*, 1997). The Stewart Hill suite forms a group in all elements vs SiO_2 and Mg# (Fig. 5.2 and Fig. 5.3), although the low Mg# of 51 for sample #19003 distinguishes it from the rest of the group. The Group has low TiO_2, Nb and Y ((Fig. 5.2 and Fig. 5.3; TiO_2 0.38 to 1.7; Nb 1.56 to 8.3 ppm; Y 8.1 to 17 ppm) and high CaO (CaO 7.1 to 10 wt %), with the highest Mg# values (Mg # 51 to 68) of all the suites.

The suite has an intermediate REE range (Table 5.2; ∑REE 41.2 to 107), with a strong Eu positive anomaly (Eu/Eu* 1.1 to 2.0; Fig. 5.4). There is large scatter between the samples, possibly due to weathering, with an overall decrease in enrichment compared to chondrite values towards the HREE. This group has negative anomalies in Rb and Th (Rb 0.56 to 2.5 ppm; Th 0.08 to 0.14 ppm).

Within the Stewart Hill Suite, $^{143}Nd/^{144}Nd$ values are similar (0.512246 to 0.512455; εNd + 1.87 to 2.91), however $^{176}Hf/^{177}Hf$ (0.282657 to 0.282887) and $^{87}Sr/^{86}Sr$ (0.705813 to 0.709857; Figs 4.7 and 4.8) values vary considerably. The (Nd) T_{DM} ages vary from 1.59 Ga to 1.06 Ga. Initial values for each isotope system plot towards enriched sources (Fig. 5.7). An age of 3 Ma, the minimum age obtained from U-Pb zircon dating, has been assumed for calculating the initial values.

Table 5.1 Wholerock major element results by XRF and CIPW Norm calculations

	Felsic Group A		Felsic Group B		Mafic Group				Intermediate		Stewart Hill			Bas. Ice.
	17911	**17912**	**17920**	**17921**	**15199**	**17913**	**17919**	**18002**	**17922**	**18003**	**19002**	**19003**	**19004**	**(host)**
Majors – wt %														
SiO_2	74.0	73.8	73.5	75.5	47.8	44.1	44.2	45.0	54.7	55.0	52.1	52.0	52.1	52.0
TiO_2	0.23	0.21	0.27	0.18	4.34	5.53	5.51	6.65	2.33	1.18	0.59	1.74	0.39	1.61
Al_2O_3	13.6	13.5	13.4	12.7	17.4	15.4	14.5	14.6	16.6	18.3	20.4	19.3	19.2	14.2
Fe_2O_3^	1.98	1.84	2.27	1.96	9.92	16.2	15.2	14.3	10.6	7.44	5.69	11.2	7.64	
MnO	0.04	0.04	0.06	0.04	0.11	0.18	0.15	0.18	0.17	0.06	0.10	0.14	0.13	0.16
MgO	0.33	0.36	0.43	0.15	5.60	4.42	6.55	6.56	3.10	1.47	6.89	6.60	9.02	8.64
CaO	1.63	1.64	1.82	1.31	11.3	9.82	10.3	10.3	5.61	4.47	10.4	7.10	8.44	8.64
Na_2O	3.37	3.28	3.34	3.16	2.66	2.84	2.41	2.63	4.75	5.11	2.91	2.98	2.50	3.04
K_2O	3.85	3.92	3.85	4.38	0.36	0.45	0.38	0.42	1.31	2.24	0.37	0.44	0.24	0.96
P_2O_5	0.04	0.05	0.06	0.04	0.08	0.26	0.09	0.07	0.66	0.71	0.07	0.24	0.04	0.28
ZnO	<0.0013	0.003	0.01	0.004	0.01	0.02	0.01	0.01	0.02	0.02	0.004	0.01	0.004	^
SO_3	<0.005	<0.005	<0.005	<0.005	<0.005	<0.005	<0.005	<0.005	<0.005	<0.005	<0.005	0.03	<0.005	^
LOI%	1.02	1.05	1.01	0.74	0.13	0.20	0.50	0.30	0.10	3.20	0.63	0.20	0.33	^
Total	98.94	99.10	98.60	98.94	99.54	99.18	99.23	100.68	99.88	95.98	99.41	101.72	99.64	99.74
Fe_2O_3*	0.73	0.68	0.84	0.73	1.89	3.09	2.90	2.72	2.49	1.75	1.08	2.14	1.46	3.10
FeO*	1.24	1.16	1.43	1.23	8.03	13.1	12.3	11.6	8.08	5.69	4.60	9.07	6.18	7.09
Mg#	23	26	25	12	50	32	43	45	34	26	68	51	68	65
Total alkalis**	7.28	7.30	7.26	7.58	3.03	3.32	2.81	3.03	6.07	7.66	3.29	3.36	2.74	4.01
CIPW Norm														
Q	35	35	34	37	0.2	-	-	-	3.1	2.8	0.4	2.8	1.0	0.3
An	7.9	8.0	8.8	6.3	34	28	28	27	20	18	42	33	40	22
Ab	29	28	29	27	23	24	21	22	40	45	25	25	21	26
Or	23	24	23	26	2.2	2.8	2.3	2.5	7.9	14	2.3	2.7	1.5	5.8
Cor	1.0	0.9	0.5	0.4	-	-	-	-	-	0.9	-	1.5	-	
Di	-	-	-	-	17	16	19	19	3.0	-	8.0	-	1.1	15
Hy	2.4	2.4	2.7	1.8	12	4.6	6.8	6.8	17	12	20	28	32	22
Ol	-	-	-	-	-	8.4	8.6	6.0	-	-	-	-	-	

	Felsic Group A		Felsic Group B		Mafic Group				Intermediate		Stewart Hill			Bas. Ice.
	17911	**17912**	**17920**	**17921**	**15199**	**17913**	**17919**	**18002**	**17922**	**18003**	**19002**	**19003**	**19004**	**(host)**
Ilm	0.4	0.4	0.5	0.3	8.3	11	11	13	4.4	2.3	1.1	3.3	0.7	3.1
Mag	1.1	1.0	1.2	1.1	2.7	4.5	4.2	3.9	2.9	2.1	1.6	3.0	2.1	4.5
Ap	0.1	0.1	0.1	0.1	0.2	0.6	0.2	0.2	1.5	1.7	0.2	0.5	0.1	0.7
Zr	0.03	0.03	0.03	0.03	0.01	0.01	0.01	0.03	0.01	0.3	0.01	0.06	-	0.03
Total	**99.9**	**100.0**	**100.0**	**100.0**	**99.9**	**99.9**	**99.9**	**99.9**	**99.9**	**99.8**	**100.0**	**99.9**	**100.0**	**99.4**

^ Measured Fe_2O_3; * Fe_2O_3 and FeO values calculated using the following ratios Felsic: Fe_2O_3 = 0.3; Mafic 0.1; Intermediate 0.15 as suggested by Winter (2001); CIPW Norm calculated using the spreadsheet of Hollocher (2007); Mg# = 100*(MgO/40.31)/((MgO/40.31)/(FeO_{TOT}/71.85); ** total alkalis normalised to 100 wt % totals .

Table 5.2 Wholerock trace element results.

	Felsic Group A		Felsic Group B		Mafic Group				Intermediate		Stewart Hill			Bas. Ice. (Host)
	17911	**17912**	**17920**	**17921**	**15199**	**17913**	**18002**	**17919**	**17922**	**18003**	**19002**	**19003**	**19004**	
Be	2.65	2.61	3.67	3.38	3.30	1.54	1.05	1.35	1.80	2.28	1.16	2.08	0.85	
Sc	4.23	4.00	4.40	3.92	24.3	23.6	23.2	27.0	12.4	7.83	25.3	30.5	18.0	18.0
Ti	1385	1277	1589	1085	26006	33170	39873	33020	13956	7086	3513	10437	2326	
V	11.5	11.9	15.4	7.17	274	402	321	387	119	22.2	101	205	93.4	162
Cr	138	141	3.3	2.4	173	129	11.5	58.3	13.1	2.6	66.2	224	247	355
Mn	297	270	460	322	839	1440	1348	1213	1297	446	735	1103	894	
Co	2.93	2.82	81.8	55.6	44.2	47.6	63.0	87.6	41.7	21.8	50.9	59.4	65.1	
Ni	782	722	4.83	5.10	725	611	54.6	113	21.8	7.52	60.3	155	117	186
Cu	4.95	4.77	10.6	3.56	36.5	44.6	41.4	43.1	32.5	29.5	31.7	52.1	38.9	43.0
Zn	30.9	29.5	68.8	49.1	96.6	175	118	130	144	135	44.1	129	58.8	94.0
Ga	16.0	15.4	18.0	17.6	15.6	21.7	16.7	19.4	20.3	26.5	17.7	23.7	16.0	20.0
As	4.2	4.3	3.9	4.5	1.5	3.1	3.7	2.5	3.4	4.4	2.3	2.6	1.9	
Rb	155	151	167	150	3.49	2.65	2.71	2.01	6.87	23.2	1.56	2.45	0.56	258
Sr	129	126	92	71	868	988	798	755	577	642	467	391	364	402
Y	23.9	21.2	59.6	60.6	30.6	24.4	16.2	24.8	35.2	31.0	16.0	16.6	8.07	19.0
Zr	132	129	164	181	77.6	110	142	91.3	94.5	1254	46.1	320	35.5	142
Nb	11.4	12.8	29.6	28.4	19.1	48.8	37.8	34.2	78.8	17.4	8.34	13.02	1.56	20.0
Mo	0.80	0.82	9.16	0.43	0.50	1.45	0.94	1.06	6.75	3.58	0.18	0.89	0.11	

	Felsic Group A		Felsic Group B		Mafic Group				Intermediate		Stewart Hill			Bas. Ice. (Host)
	17911	**17912**	**17920**	**17921**	**15199**	**17913**	**18002**	**17919**	**17922**	**18003**	**19002**	**19003**	**19004**	
Cd	0.11	0.10	0.20	0.15	0.10	0.34	0.16	0.18	0.13	0.08	0.06	0.08	0.06	
Sn	4.50	4.29	6.78	5.94	1.28	1.98	2.75	2.14	1.04	2.02	0.74	0.37	0.68	
Sb	0.02	0.02	0.02	0.03	0.14	0.12	0.11	0.14	0.08	0.14	0.01	0.01	0.01	
Cs	2.47	2.37	2.45	1.10	0.89	0.40	0.31	0.32	0.35	0.38	0.01	0.02	0.01	0.98
Ba	635	632	577	644	173	262	195	159	407	1013	191	295	160	258
Hf	4.38	4.28	5.44	6.01	1.67	2.79	3.30	2.28	1.79	2.14	0.94	1.42	0.50	3.00
Ta	0.76	0.67	3.50	3.06	1.28	2.92	2.89	2.45	4.51	1.00	0.92	0.99	0.45	
Pb	20.5	20.2	18.9	19.4	1.31	1.55	2.78	1.72	4.88	12.9	3.90	7.85	3.25	3.30
Th	22.0	18.2	19.8	19.9	0.31	0.39	0.27	0.18	0.82	1.79	0.14	0.30	0.08	3.10
U	1.27	1.09	1.87	1.79	0.13	0.11	0.13	0.07	0.43	0.80	0.12	0.08	0.05	0.70
La	46.6	46.2	42.2	47.7	6.36	12.1	8.04	6.91	32.5	39.1	10.9	22.1	9.08	15.8
Ce	81.6	81.0	81.2	95.6	12.7	26.9	19.3	17.7	63.5	76.7	21.6	43.4	13.9	32.8
Pr	8.61	8.51	10.2	11.4	1.86	3.95	2.79	2.85	8.3	9.94	2.86	4.79	2.05	4.20
Nd	28.4	28.0	37.6	42.8	9.05	19.3	13.3	15.1	33.9	40.0	12.4	19.1	8.1	17.9
Sm	5.27	5.01	8.58	9.17	2.64	5.15	3.55	4.59	7.23	7.87	3.00	3.66	1.64	4.48
Eu	1.05	1.02	1.50	1.68	1.21	2.19	1.46	1.84	2.72	3.69	1.10	2.36	0.95	1.50
Gd	5.14	4.89	8.87	9.23	3.17	5.27	3.54	4.87	7.25	7.58	3.10	3.66	1.60	4.52
Tb	0.72	0.67	1.48	1.52	0.57	0.82	0.56	0.78	1.06	1.05	0.49	0.51	0.24	0.72
Dy	3.93	3.61	8.88	9.10	3.71	4.52	3.12	4.36	5.87	5.43	2.89	2.88	1.41	3.80
Ho	0.79	0.72	1.86	1.90	0.83	0.86	0.60	0.85	1.18	1.04	0.58	0.60	0.30	0.71
Er	2.25	2.02	5.33	5.50	2.48	2.20	1.55	2.19	3.19	2.63	1.58	1.70	0.86	1.54
Yb	2.17	1.87	5.03	4.97	2.25	1.71	1.26	1.60	2.77	1.99	1.31	1.63	0.86	1.46
Lu	0.32	0.28	0.73	0.71	0.35	0.24	0.18	0.23	0.41	0.28	0.19	0.25	0.13	0.21
∑REE	187	184	213	241	47.2	85.2	59.2	63.8	170	197	61.9	107	41.2	89.6
Eu/Eu*	0.61	0.63	0.53	0.56	1.28	1.28	1.25	1.18	1.15	1.46	1.09	1.96	1.79	1.02
Ce/Ce*	0.99	0.99	0.95	0.99	0.90	0.94	0.99	0.96	0.93	0.94	0.94	1.02	0.78	0.97
La/Yb	14.6	16.7	5.70	6.52	1.92	4.80	4.33	2.93	7.98	13.3	5.62	9.23	7.15	7.35

Eu/Eu* - Eu anomaly; Ce/Ce* - Ce Anomaly; La/Yb – Using chondrite normalised values. Values in red were obtained by XRF analysis (discussed above); Basaltic Icelandite values from Price *et al.* (1997).

Table 5.3 Isotope analysis results.

	Felsic Group A		Felsic Group B		Mafic Group				Intermediate		Stewart Hill		
	17911	**17912**	**17920**	**17921**	**15199**	**17913**	**18002**	**17919**	**17922**	**18003**	**19002**	**19003**	**19004**
Age	553	553	553	553	3	3	3	3	3	3	3	3	3
$^{87}Sr/^{86}Sr$	0.743471	0.703959	0.749680	0.761908	0.704334	0.704913	0.704161	0.704302	0.708549	0.705012	0.709731	0.709857	0.705814
2SE	0.000006	0.000007	0.000006	0.000007	0.000005	0.000009	0.000006	0.000007	0.000006	0.000008	0.000005	0.000005	0.000003
$^{87}Rb/^{86}Sr$	3.41	3.39	5.11	5.96	0.01	0.01	0.01	0.01	0.03	0.10	0.01	0.02	0.00
Sr (ppm)	1289	126	92.4	71.1	577	868	988	755	799	642	467	391	364
Rb (ppm)	155	151	167	150	3.49	2.65	2.01	2.71	6.87	23.20	1.56	2.45	0.56
Initial $^{87}Sr/^{86}Sr$	0.716618	0.677239	0.709405	0.714906	0.704334	0.704912	0.704161	0.704301	0.708548	0.705008	0.709730	0.709857	0.705813
$^{143}Nd/^{144}Nd$	0.51	0.51	0.51	0.51	0.51	0.51	0.51	0.51	0.51	0.51	0.51	0.51	0.51
2SE	0.00	0.00	0.00	0.00	0.00	0.00	0.00	0.00	0.00	0.00	0.00	0.00	0.00
$^{147}Sm/^{144}Nd$	0.12	0.11	0.14	0.14	0.18	0.17	0.19	0.17	0.13	0.12	0.15	0.12	0.13
Nd	28.4	28.0	37.6	42.8	33.9	9.05	19.3	15.1	13.3	40.0	12.4	19.1	8.11
Sm	5.27	5.01	8.58	9.17	2.64	5.15	4.59	3.55	7.23	7.87	3.00	3.66	1.64
Initial $^{143}Nd/^{144}Nd$	0.511882	0.511895	0.512046	0.512006	0.512760	0.512730	0.512783	0.512756	0.512667	0.512703	0.512391	0.512246	0.512455
ε_{Nd}	-0.85	-0.60	2.36	1.57	2.45	1.87	2.91	2.38	0.63	1.35	-4.75	-7.57	-3.49
T_{DM}	1.17	1.13	1.07	1.08	1.41	1.07	1.64	1.01	0.77	0.64	1.59	1.30	1.06
$^{176}Hf/^{177}Hf$	0.282667	0.282613	0.283424	0.283318	0.282850	0.282890	0.282960	0.282895	0.282884	0.282898	0.282767	0.282658	0.282889
2SE	0.000006	0.000010	0.000027	0.000015	0.000078	0.000015	0.000034	0.000067	0.000014	0.000007	0.000006	0.000012	0.000021
$^{176}Lu/^{177}Hf$	0.002	0.002	0.106	0.106	0.030	0.012	0.014	0.008	0.032	0.018	0.028	0.025	0.037
Hf (ppm)	4.38	4.28	5.44	6.01	1.67	2.79		2.28	3.30	2.14	0.94	1.42	0.50
Lu (ppm)	3.33	3.25	4.13	4.57	0.35	0.24	0.18	0.23	0.41	0.28	0.19	0.25	0.13
Initial $^{176}Hf/^{177}Hf$	0.282646	0.282590	0.282329	0.282224	0.282849	0.282889	0.282959	0.282894	0.282883	0.282897	0.282765	0.282657	0.282887

SE = Standard error, given to e^{-6} Note: 1. Nd isotopic ratios normalised to $^{146}Nd/^{144}Nd = 0.7219$; $^{86}Sr/^{88}Sr = 0.1194$; $^{179}Hf/^{177}Hf$ 0.7325. Parent system ratios calculated using abundances: $^{87}Rb/^{86}Sr$: ^{87}Rb 27.83 %; ^{86}Sr 9.86 %; $^{147}Sm/^{144}Nd$: ^{147}Sm - 14.99%, ^{144}Nd – 23.8%; $^{176}Lu/^{177}Hf$: ^{176}Lu 2.59 %; ^{177}Hf 18.60 %; Initial ratios have been calculated using the U-Pb Zircon Ages of 553 Ma for the Felsic Group and 3 Ma for all others. Decay rates for Sm = 6.54^{-12} (Lugmair and Marti, 1978); Rb = 1.42^{-11} (Davis *et al*., 1977); Lu = 1.865^{-11} (Scherer *et al*., 2001). DM_{Nd}: $^{147}Sm/^{144}Nd = 0.222$ and $^{143}Nd/^{144}Nd_{(0)} = 0.513114$: $CHUR_{Nd}$: $^{147}Sm/^{144}Nd = 0.1967$ and $^{143}Nd/^{144}Nd = 0.512638$; εNd: = ($^{143}Nd/^{144}Nd$ Sample/$^{143}Nd/^{144}Nd$ CHUR)-1)10^{-4}

5.2 Mineral geochemistry

Average major element mineral compositions for each sample are listed in Tables 5.4 to 5.17 at the end of this subchapter. A complete set of analyses is included Appendix 5. Feldspars are the most common phase within the samples, ranging from bytownite to Na-sanidine (Fig. 5.9) in composition. The average values per sample are detailed in Table 5.4 (plagioclase) and Table 5.6 (alkali feldspars) with compositional ranges in Table 5.5 (plagioclase) and Table 5.7 (alkali feldspars) and a ternary discrimination plot (Fig. 5.9).

The average pyroxene composition per sample is detailed in Table 5.8 (orthopyroxene) and Table 5.10 (clinopyroxene) with compositional ranges in Table 5.9 (orthopyroxene) and Table 5.11 (clinopyroxene) and a quadrilateral discrimination plot in Fig. 5.9. Oxides throughout the samples range from magnetite to titanomagnetite (ulvospinel) and ilmenite (Table 5.17 to Table 5.19). Major and trace element results for glass (as described in the petrography results) are given in Table 5.14 and Table 5.15. The major element values vary considerably within samples depending on the location of the analysis and proximity to certain minerals (Fig. 5.1). However, the trace elements form tight patterns (Fig. 5.6).

5.2.1 Upper Coliban Dam Mafic Group

Plagioclase is dominant in the mafic group, ranging from labradorite to andesine (Ab 35 to 66; Table 5.5; Fig. 5.9). Alkali feldspar grains were only identified in sample #15199 (Or 11; Ab 67; Table 5.7).

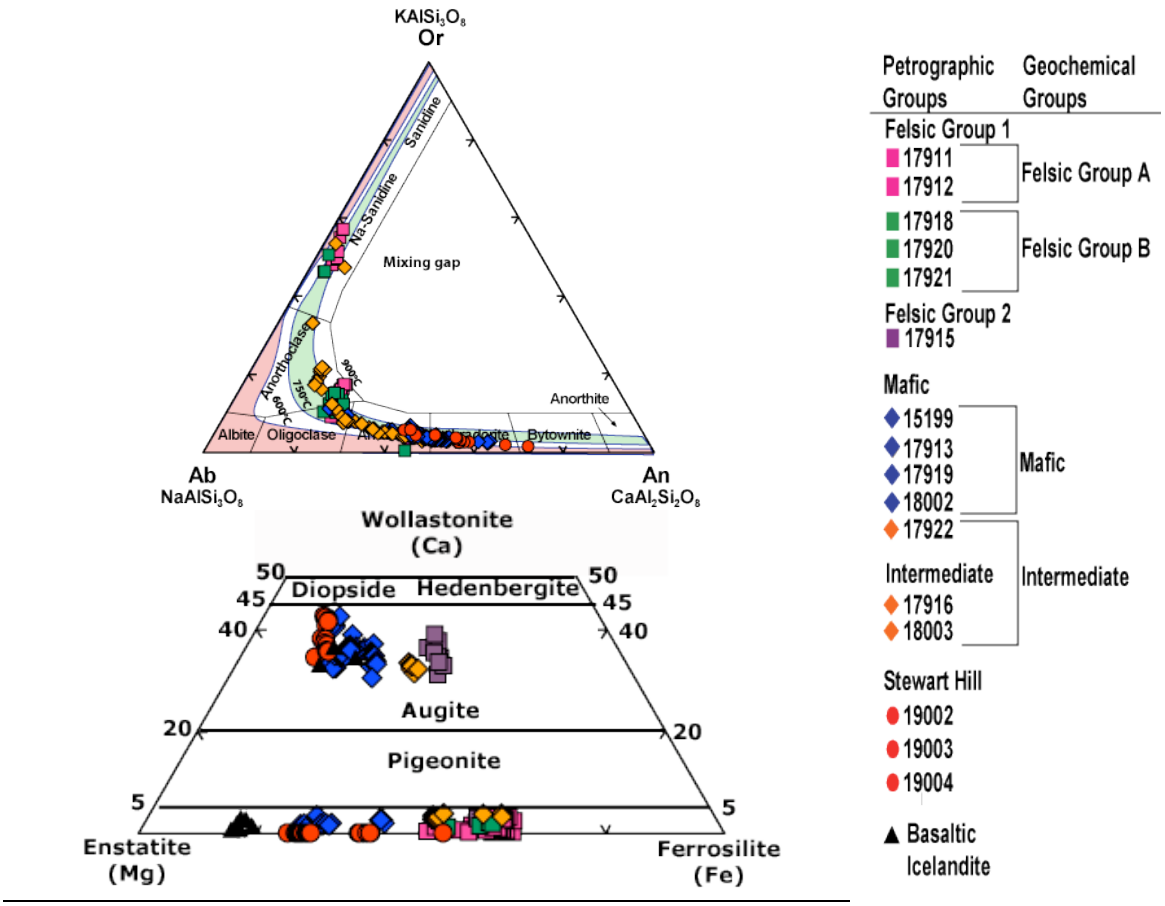


Fig. 5.9 (a) Ternary feldspar discrimination plot; (b) Quadrilateral pyroxene discrimination plot.

Within the Mafic Group, the orthopyroxene grains are present as enstatite (Fs 26 to 41, Mg# 58 to 73; Table 5.9). Sample #17914, with the highest Mg# values, has a spread in values for Al, Ti and Cr (Fig. 5.10). The group forms two tight clusters dominated by Mg# values - sample #17913 forms one group with the lowest Mg# values and samples #18002 and 17914 form the second with higher Mg# values (Fig. 5.10). The group has higher Ca, Na and significantly higher Ti values compared to the Stewart Hill Suite. A positive linear relationship is observed for the Mafic Group in Al vs Mg#, with a negative relationship in Mn vs Mg# (Fig. 5.10).

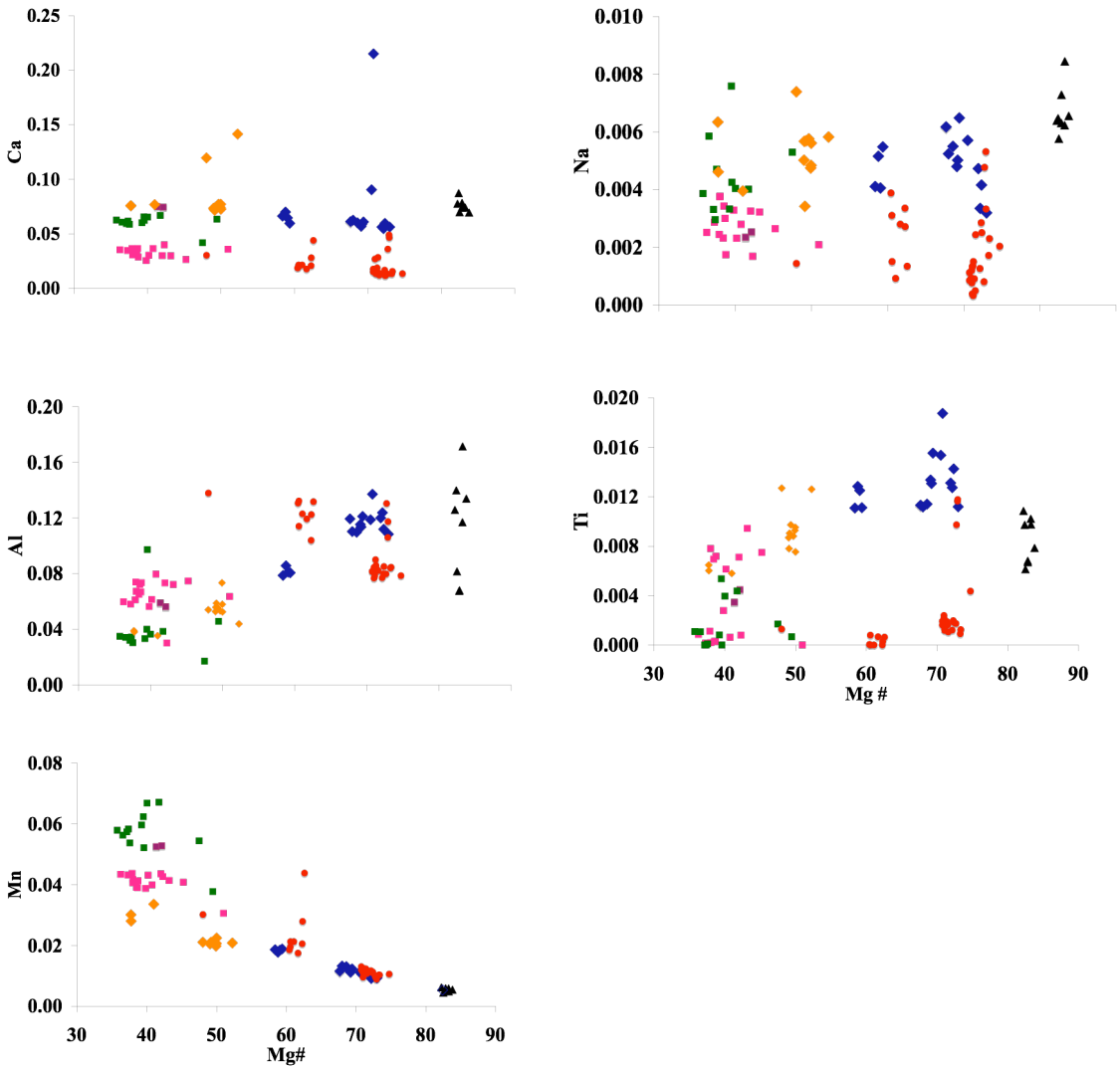


Fig. 5.10 Orthopyroxene charts with various elements vs Mg#. Key as in Fig. 1. Note the distinct clusters within each group, particularly in Ca, Al and Mn – these are formed by individual samples, rather than varied compositions within one sample. Intermediate sample #18003 plots very close to or within felsic group clusters. The basaltic icelandite pyroxenes have a distinct, high Mg# composition.

Clinopyroxene was dominant in the mafic samples (Wo 34 to 41 to Fs 43 to 49, Mg# 66 to 80; Table 5.11; Fig. 5.9). Positive linear trends are seen for Ca and Ti vs Mg# (Fig. 5.11) and Na vs Al(M1) and Ti vs Al (Fig. 5.11) and an elbow trend is observed in Al and Na vs Mg#. This group has the highest values in Na, Ti and Al (Fig. 5.11). The REE and trace element patterns are relatively flat, with negative Sr and Ga anomalies (Fig. 5.12).

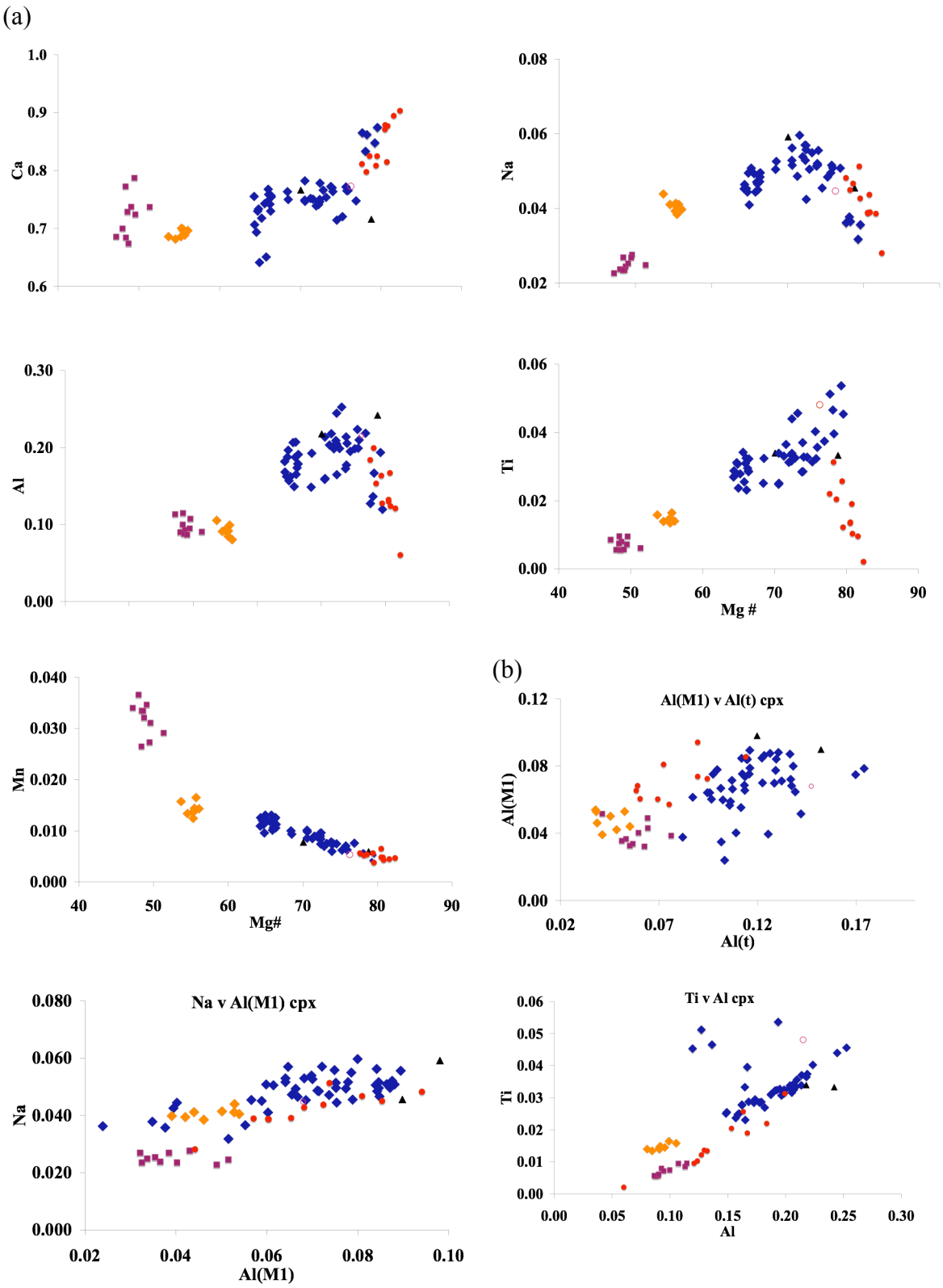


Fig. 5.11 Clinopyroxene charts with various elements (a) vs Mg#; (b) vs Al. Key as in Fig. 1. A linear relationship is seen from felsic to mafic samples, with the intermediate samples forming a distinct cluster.

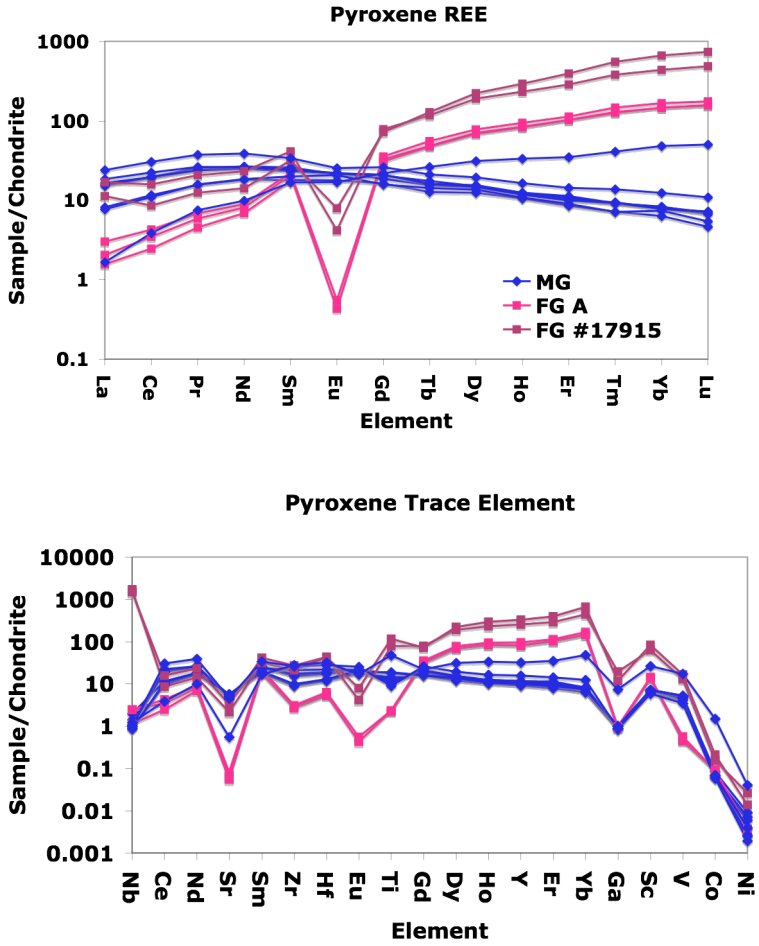


Fig. 5.12 Pyroxene trace element concentrations – REE and trace element diagrams normalised to chondrite (Taylor and McLennan, 1981). The analysed pyroxene grains are clinopyroxene for the mafic group and orthopyroxene for the felsic groups.

One grain of phlogopite-biotite and one ferropargasitic amphibole grain were identified in sample #17913 (Table 5.13 and Table 5.16).

5.2.2 Upper Coliban Dam Intermediate Group

There is a great range in feldspars within this group, from labradorite to Na-sanidine in composition (Fig. 5.9). Sample #18003 has the largest range overall (Or 5 to 53; Ab 44 to 68; Table 5.5 and Table 5.7) with compositions ranging from andesine to Na-sanidine and an almost linear range from andesine to anorthoclase (Or 5 to 17; Ab 60 to 67). Sample #17916 has alkali feldspars only (anorthoclase and Na-sanidine; Or to 19 to 47; Ab 45 to 65; Table 5.7) and #17922 had only plagioclase (oligoclase to labradorite; Or 3 to 9; Ab 48

to 66; Table 5.5). Several high temperature anorthoclase feldspar compositions are evident, with temperatures up to 900 ºC (Fig. 5.9).

The orthopyroxene grains within the Intermediate Group have ferrosilite composition, but in two clear groups (#17922: Wo 2 to 7; Fs 44 to 50 and #18003 Wo 3 to 4; Fs 54 to 60; Table 5.9; Fig. 5.9). Clinopyroxene was only identified in sample #17922 (Wo 29 to 31; Fs 22 to 31; Table 5.11). A tight cluster is formed vs Mg# in the clinopyroxene compositions, however there is more variability within the orthopyroxene compositions (Fig. 5.11). There is a large range in Na and Ti vs Mg#. The Intermediate Group, particularly #18003, sits close to the Felsic Group in most elements (Fig. 5.11), apart from Na and Ti.

5.2.3 Upper Coliban Dam Felsic Group

Plagioclase is the dominant feldspar within subgroup sample #17915 ranging from labradorite to andesine (Ab 46 to 53; Table 5.5; Fig. 5.9) but is less common in other samples within the group, ranging from andesine to oligoclase (Ab 46 to 68; n=3; Table 5.5). Alkali feldspar ranges from anorthoclase to Na-sanidine (Or 10 to 57; Ab 41 to 69; Table 5.7) in composition. Sample #17918 has the greatest range within the Felsic Group ranging from andesine to Na—sanidine (Or 11 to 56; Ab 50 to 67; Table 5.7). However, there are three distinct compositions rather than a gradual change. Several high temperature anorthoclase feldspar compositions are observed, up to 900 ºC (Fig. 5.9).

The orthopyroxene grains are predominantly ferrosilite (Fs 49 to 64, Mg# 38 to 51; Table 5.9; Fig. 5.9). The range in sample #17912 (Fs 49 to 64; Mg# 36 to 51; Table 5.9) dictates the whole range across the Felsic Group. The group has the lowest Mg# values (Fig. 5.10). There are clear clusters within the Felsic Group separated by Ca, Al and Mn (Fig. 5.10), with individual samples falling into one or the other. The pyroxene grains are depleted in Sr with a strong negatively Eu anomaly though enriched in HREE compared to the mafic samples (Table 5.12; Fig. 5.12). Two orthopyroxene grains analysed from sample #17915 within the symplectite texture (see petrography) were enriched in most trace elements compared to other samples, particularly in the HREE (Fig. 5.11).

Clinopyroxene was only identified in one felsic sample (#17915) where it was dominant over orthopyroxene (Wo 31 to 39; Fs 30 to 35; Mg#47 to 51; Table 5.11). This sample has the lowest range of Mg# values within the clinopyroxene measurements and forms a tight cluster in various plots vs Mg # (Fig. 5.11), with higher Mn values but lower Na, Al and Ti compared to the mafic and intermediate groups. A positive linear relationship is seen in Ti vs Al and there is an excess in Al(t) compared to Na, which is consistent throughout all samples, except for the Stewart Hill group (Fig. 5.11).

5.2.4 Stewart Hill Suite

Plagioclase ranges from bytownite to andesine in this group, with no alkali feldspar grains analysed (Ab 41 to 45; Table 5.5; Fig. 5.9). The composition of orthopyroxene within the Stewart Hill samples is predominantly enstatite (Fs 25 to 37, Mg# 63 to 75; Table 5.9; Fig. 5.10) with only one ferrosilite grain analysed (#19003; Fs 51.96, Mg# 48). Stewart Hill samples contain predominantly enstatite (Fs 25 to 37, Mg# 63 to 75; Table 5.9). This group has two distinct Mg # clusters, with low values in Ca and Ti and a spread in Na (Fig. 5.10). Mn follows the linear trend formed over all the groups. Clinopyroxene was only identified in #19002 as augite (Wo 35 to 43; Fs 10 to 14, Mg# 78 to 82; Table 5.11; Fig. 5.9). The high range in Ca observed may be due to exsolution within the pyroxene grains as described in the petrography chapter. The Stewart Hill Suite has the highest Mg# values. Ca and Mn follow the linear trends of the Upper Coliban Dam mafic group, however Na, Al and Ti form negative linear trends at the high Mg# extent (Fig. 5.11).

Amphiboles with kaesurtite composition are present within #19002, represented by a high TiO_2 (9 to 13 wt %) (Table 5.13). Biotite was also identified within this sample (Table 5.16).

Table 5.4 Average plagioclase compositions, with cation calculations based on 32 oxygens

Rock type	**Felsic Group A**	**Felsic Group B**		**Felsic Subgroup**		**Mafic Group**								**Intermediate Group**			
Sample	**17911**	**17918**			**17915**	**15199**		**17913**		**17914**		**18002**		**17922**		**18003**	
n =	**1**	**2**		**8**		**26**		**33**		**17**		**23**		**46**		**7**	
		Ave	**StDev**	**Ave**	**StDev**	**Ave**	**StDev**	**Ave**	**StDev**	**Ave**	**StDev**	**Ave**	**StDev**	**Ave**	**StDev**	**Ave**	**StDev**
Wt % O																	
SiO_2	63.19	61.21	1.88	57.37	0.91	54.61	1.62	56.75	0.80	56.17	0.75	55.92	0.84	57.36	1.82	64.84	2.06
TiO_2	0.06	-	-	0.01	0.01	0.12	0.04	0.06	0.02	0.07	0.02	0.08	0.02	0.05	0.04	0.05	0.08
Al_2O_3	22.73	24.04	1.63	25.55	0.71	28.15	1.16	26.44	0.54	26.83	0.64	27.03	0.50	25.93	1.17	20.70	2.02
FeO	0.29	0.39	0.25	0.44	0.02	0.37	0.20	0.25	0.03	0.36	0.17	0.31	0.07	0.28	0.10	0.33	0.30
CaO	5.02	6.44	1.82	9.76	0.57	11.16	1.38	9.28	0.61	9.99	0.55	9.96	0.63	9.12	1.37	3.14	1.64
Na_2O	7.92	6.53	1.70	5.58	0.29	5.09	0.64	5.98	0.28	5.57	0.23	5.61	0.29	5.98	0.61	7.07	1.12
K_2O	1.57	0.90	1.23	0.61	0.08	0.56	0.23	0.72	0.15	0.62	0.11	0.69	0.19	0.72	0.26	3.90	2.50
Total	100.78	99.55	1.09	99.37	0.45	100.09	0.38	99.51	0.32	99.65	0.34	99.61	0.32	99.47	0.35	100.08	0.19
Cations																	
Si^{4+}	11.17	10.94		10.40		9.88		10.27		10.17		10.13		10.37		11.57	
Ti^{4+}	0.01	-		-		0.02		0.01		0.01		0.01		0.01		0.01	
Al^{3+}	4.74	5.06		5.46		6.01		5.64		5.73		5.77		5.53		4.35	
Fe^{2+}	0.04	0.06		0.07		0.06		0.04		0.05		0.05		0.04		0.05	
Ca^{2+}	0.95	1.23		1.90		2.17		1.80		1.94		1.93		1.77		0.60	
Na^{+}	2.71	2.26		1.96		1.79		2.10		1.96		1.97		2.10		2.44	
K^{+}	0.35	0.20		0.14		0.13		0.17		0.14		0.16		0.17		0.89	
Z	15.96	16.06		15.92		15.96		15.96		15.96		15.97		15.95		15.97	
X	4.02	3.70		4.00		4.09		4.07		4.04		4.07		4.04		3.94	
Σcat	19.98	19.76		19.92		20.05		20.03		20.01		20.03		19.99		19.92	
Or	9	5		4		3		4		4		4		4		23	
Ab	68	61		49		44		52		48		48		52		62	
An	24	34		47		53		44		48		48		44		15	

Or = 100K/(Ca+Na+K); Ab = 100Na/(Ca+Na+K); An = 100Ca/(Ca+Na+K)

Table 5.4 cont… Average plagioclase compositions, with cation calculations based on 32 oxygens

Rock Type	**Stewart Hill**			
Sample	**19002**		**19003**	
n =	**10**		**5**	
	Ave	**StDev**	**Ave**	**StDev**
Wt % O				
SiO_2	53.77	2.28	55.04	1.21
TiO_2	0.02	0.03	0.01	0.01
Al_2O_3	28.28	1.46	27.86	0.98
FeO	0.15	0.04	0.20	0.04
CaO	11.77	1.74	10.83	1.08
Na_2O	4.81	0.90	5.25	0.50
K_2O	0.48	0.22	0.69	0.19
Total	99.32	0.32	99.89	0.21
Cations				
Si^{4+}	9.81		9.97	
Ti^{4+}	-		-	
Al^{3+}	6.09		5.95	
Fe^{2+}	0.02		0.03	
Ca^{2+}	2.30		2.10	
Na^{+}	1.70		1.84	
K^{+}	0.11		0.16	
Z	15.93		15.95	
X	4.12		4.11	
Σcat	20.05		20.06	
Or	3		4	
Ab	41		45	
An	56		51	

Table 5.5 Plagioclase range

	Felsic Group A	Felsic Group B		Felsic Subgroup		Mafic Group								Intermediate group			
Sample	**17911**	**17918**		**17915**		**15199**		**17913**		**17914**		**18002**		**17922**		**18003**	
n =	**1**	**2**		**8**		**26**		**33**		**17**		**23**		**46**		**8**	
		Low	**High**	**Low**	**High**	**Low**	**High**	**Low**	**High**	**Low**	**High**	**Low**	**High**	**Low**	**High**	**Low**	**High**
Or	9	0.21	10	3	4	2	9	3	6	3	4	3	4	3	9	11	53
Ab	68	55	66	46	53	35	64	47	56	45	52	46	52	48	66	44	67
An	24	24	44	44	51	27	62	38	49	43	52	42	51	25	49	12	24

Rock Type	**Stewart Hill**			
Sample	**19002**		**19003**	
n =	**10**		**5**	
	Low	**High**	**Low**	**High**
Or	1	6	3	6
Ab	27	53	42	51
An	42	71	43	55

Table 5.6 Average alkali feldspar compositions, with cation calculations based on 32 oxygens

Rock type	**Felsic Group A**				**Felsic Group B**				**Mafic Group**	**Intermediate Group**			
	17911		**17912**		**17918**		**17921**		**15199**	**18003**		**17916**	
n =	**12**		**10**		**6**		**6**		**1**	**5**		**6**	
Sample	**Ave**	**StDev**	**Ave**	**StDev**	**Ave**	**StDev**	**Ave**	**StDev**	**20 / 1 .**	**Ave**	**StDev**	**Ave**	**StDev**
Wt % O													
SiO_2	63.59	1.68	64.77	1.76	64.35	1.99	63.70	1.71	62.22	60.44	0.97	64.19	0.66
TiO_2	0.01	0.01	-	0.01	0.00	0.00	-	0.01	0.30	0.02	0.01	0.01	0.01
Al_2O_3	21.70	1.60	20.89	1.83	21.34	1.98	21.44	1.54	22.82	24.30	0.78	20.76	1.45
FeO	0.17	0.04	0.16	0.04	0.19	0.04	0.23	0.05	0.82	0.26	0.06	0.91	1.72
CaO	3.84	1.73	2.76	2.14	3.38	2.06	4.02	1.76	4.68	6.64	0.81	2.97	0.84
Na_2O	6.79	0.96	6.20	1.23	7.12	1.02	7.03	0.90	7.82	7.24	0.35	6.92	1.31
K_2O	4.12	2.70	6.10	3.43	4.18	3.04	3.32	2.60	1.96	1.19	0.26	4.19	1.26
Total	100.24	0.48	100.90	0.28	100.59	0.33	99.78	0.35	100.83	100.13	0.55	100.07	0.98
Cations													
Si^{4+}	11.37		11.55		11.45		11.40		11.06	10.80		11.50	

Rock type	Felsic Group A				Felsic Group B				Mafic Group	Intermediate Group			
	17911		17912		17918		17921		15199	18003		17916	
n =	12		10		6		6		1	5		6	
Sample	Ave	StDev	Ave	StDev	Ave	StDev	Ave	StDev	20 / 1 .	Ave	StDev	Ave	StDev
Ti^{4+}	-		-		-		-		0.04	-		-	
Al^{3+}	4.57		4.39		4.47		4.52		4.78	5.12		4.38	
Fe^{2+}	0.03		0.02		0.03		0.03		0.12	0.04		0.14	
Ca^{2+}	0.73		0.53		0.64		0.77		0.89	1.27		0.57	
Na^{+}	2.35		2.14		2.45		2.44		2.69	2.51		2.40	
K^{+}	0.94		1.39		0.95		0.76		0.44	0.27		0.96	
Z	15.96		15.96		15.96		15.96		16.00	15.97		16.02	
X	4.03		4.06		4.05		3.97		4.08	4.06		3.96	
Σcat	19.99		20.02		20.01		19.93		20.08	20.02		19.99	
Or	23		34		24		19		11	7		25	
Ab	58		53		61		61		67	62		61	
An	18		13		16		19		22	31		14	

Table 5.7 Alkali feldspar range

Rock type	Felsic Group A				Felsic Group B				Mafic Group	Intermediate Group B			
	17911		17912		17918		17921		15199	18003		17916	
n =	12		10		7		6		1	5		6	
Sample	Low	High	Low	High	Low	High	Low	High	20 / 1 .	Low	High	Low	High
Or	12	17	15	57	11	46	10	50	11	5	8	19	47
Ab	60	66	41	63	50	67	47	69	677	59	68	45	65
An	22	23	2	23	3	23	2	25	22	27	36	7	16

Table 5.8 Average orthopyroxene compositions, with cation calculations based on 6 oxygens

	Felsic Group A				Felsic Group B				Felsic Subgroup	
Sample	**17911**		**17912**		**17918**		**17921**		**17915**	
n =	**9**		**10**		**8**		**4**		**2**	
	Ave	**StDev**	**Ave**	**StDev**	**Ave**	**StDev**	**Ave**	**StDev**	**Ave**	**StDev**
Wt% O										
SiO_2	49.45	0.47	50.09	1.57	50.02	0.86	50.74	0.58	49.71	0.60
TiO_2	0.24	0.06	0.01	0.01	0.02	0.02	0.13	0.05	0.13	0.03
Al_2O_3	1.78	0.91	1.65	1.06	0.92	0.45	0.71	0.23	1.24	0.03
FeO	34.32	1.39	33.82	2.64	34.34	2.06	32.18	1.44	32.73	0.25
MnO	1.23	0.05	1.17	0.14	1.61	0.18	1.88	0.17	1.57	0.02
MgO	12.77	1.09	12.78	1.59	12.28	1.47	13.21	1.44	13.00	0.34
CaO	0.69	0.05	0.82	0.09	1.44	0.05	1.41	0.28	1.76	0.01
Na_2O	0.04	0.01	0.13	0.31	0.06	0.01	0.07	0.02	0.03	-
K_2O	0.03	0.03	0.10	0.30	0.01	0.01	0.05	0.07	0.02	-
Total	100.56	0.87	100.62	1.14	100.72	0.42	100.41	0.27	100.22	0.69
Cations (with Ferrous/ ferric correction)										
Si^{4+}	1.95		1.97		1.98		2.00		1.96	
Ti^{4+}	0.01		-		-		-		-	
Al^{3+}	0.08		0.08		0.04		0.03		0.06	
Fe^{3+}	0.03		0.01		0.01				0.01	
Fe^{2+}	1.11		1.10		1.13		1.06		1.07	
Mn^{2+}	0.04		0.04		0.05		0.06		0.05	
Mg^{2+}	0.75		0.75		0.72		0.77		0.76	
Ca^{2+}	0.03	-	0.03		0.06		0.06		0.07	-
Na^{+}	-	-	0.01		-	-	0.01		-	-
K^{+}	-	-	-		-	-	-		-	-
Σcat	4.00		4.00		4.00		4.00		4.00	
Mg #	0.40		0.40		0.39		0.42		0.42	
Al(t)	0.05		0.03		0.02		-		0.04	
Al(M1)	0.03		0.05		0.02		0.03		0.02	
Wo	0.01		0.01		0.02		0.01		0.03	
En	0.40		0.41		0.38		0.42		0.41	
Fs	0.60		0.60		0.60		0.57		0.57	
XFe	0.60		0.60		0.61		0.58		0.58	

Table 5.8 cont… Average orthopyroxene compositions, with cation calculations based on 6 oxygens

	Mafic Group							Intermediate Group				Stewart Hill				Host lava		
	15199	17913		17914		18002		17922		18003		19002		19003		17914		18002
n =	1	4		9		2		10		3		24		9		7		1
Sample		Ave	StDev	Ave	StDev	Ave	StDev	Ave	StDev	Ave	StDev	Ave	StDev	Ave	StDev	Ave	StDev	
Wt% O																		
SiO_2	52.08	51.69	0.20	52.80	0.50	52.53	0.15	51.08	0.35	49.83	0.14	54.00	0.38	52.14	0.74	55.16	0.92	54.51
TiO_2	0.41	0.42	0.03	0.52	0.08	0.41	0.01	0.33	0.06	0.21	0.01	0.11	0.12	0.01	0.02	0.32	0.07	0.37
Al^2O_3	2.76	1.84	0.07	2.78	0.19	2.54	0.01	1.23	0.17	0.80	0.04	2.03	0.30	2.80	0.23	2.64	0.93	3.36
FeO	20.59	24.79	0.16	18.42	0.87	19.82	0.23	29.13	0.88	34.64	1.19	17.84	0.68	24.18	1.44	10.88	0.31	10.85
MnO	0.37	0.58	0.02	0.35	0.03	0.42	-	0.64	0.02	0.91	0.08	0.35	0.03	0.36	0.03	0.18	0.02	0.18
MgO	22.73	19.56	0.13	23.97	1.15	23.14	0.23	16.01	0.55	12.25	0.55	25.47	0.47	20.12	2.18	29.18	0.34	28.48
CaO	1.55	1.62	0.10	2.02	1.34	1.56	0.03	2.07	0.59	1.79	0.01	0.50	0.27	0.61	0.21	1.97	0.09	2.31
Na_2O	0.09	0.06	0.01	0.08	0.05	0.08	-	0.07	0.01	0.06	0.02	0.02	0.02	0.03	0.01	0.10	0.01	0.09
Total	100.58	100.60	0.28	101.02	0.37	100.52	0.59	100.59	0.91	100.51	0.80	100.35	0.37	100.37	0.23	100.92	0.31	100.6
Cations (with Ferrous/ferric correction)																		
Si^{4+}	1.91	1.94		1.91		1.93		1.97		1.97		1.96		1.95		1.94		1.92
Ti^{4+}	0.01	0.01		0.01		0.01		0.01		0.01		-		-		0.01		0.01
Al^{3+}	0.12	0.08		0.12		0.11		0.06		0.04		0.09		0.12		0.11		0.14
Fe^{3+}	0.04	0.01		0.03		0.02		0.01		0.01		-		0.01		0.01		
Fe^{2+}	0.59	0.76		0.53		0.59		0.93		1.14		0.54		0.75		0.31		0.32
Mn^{2+}	0.01	0.02		0.01		0.01		0.02		0.03		0.01		0.01		0.01		0.01
Mg^{2+}	1.24	1.10		1.30		1.26		0.92		0.72		1.38		1.12		1.53		1.50
Ca^{2+}	0.06	0.07		0.08		0.06		0.09		0.08		0.02		0.02		0.07		0.09
Na^{+}	0.01	-		0.01	-	0.01		0.01		-	-	-	-	-	-	0.01		0.01
Σcat	4.00	4.00		4.00		4.00		4.00		4.00		4.00		4.00		4.00		4.00
Mg #	68	59	-	71	1	68	-	50	1	39	2	72	1	60	5	83	1	82
Al(t)	0.09	0.06	0.01	0.09	0.01	0.07	0.01	0.03	0.01	0.03	-	0.04	0.01	0.06	0.02	0.06	0.03	0.08
Al(M1)	0.03	0.02	0.01	0.03	0.01	0.04	0.01	0.02	0.01	0.01	-	0.05	0.01	0.08	0.06	0.05	0.01	0.06
Wo	2	2	-	2	3	2	-	3	1	3	-	-	-	-	-	1	1	1
En	66	58	-	69	3	67	-	48	1	38	2	73	1	61	3	82	1	82
Fs	32	40	1	28	2	31	-	49	2	59	2	28	1	41	6	17	-	17

Table 5.9 Orthopyroxene range

	Mafic Group							Intermediate Group				Stewart Hill				Host lava		
	15199	17913		17914		18002		17922		18003		19002		19003		17914		18002
n =	1	4		9		2		10		3		24		9		7		1
Sample		Low	High	Low	High	Low	High	Low	High	Low	High	Low	High	Low	High	Low	High	
Mg #	68	58	59	69	73	68	689	48	52	38	41	72	75	48	63	82	84	82
Al(t)	0.09	0.05	0.06	0.08	0.1	0.07	0.08	0.007	0.05	0.02	0.03	0.04	0.07	-	0.08	0.03	0.1	0.08
Al(M1)	0.03	0.02	0.03	0.03	0.04	0.03	0.04	0.01	0.05	0.008	0.02	0.05	0.07	0.04	0.1	0.03	0.07	0.06
Wo	2	2	2	1	10	31	32	2	7	30	36	-	-	-	-	-	2	1
En	66	57	58	64	72	67	67	46	49	36	40	71	75	48	63	81	83	82
Fs	32	40	41	26	31	31	32	44	50	57	60	25	30	37	52	16	18	17

Table 5.9 cont… Orthopyroxene range

	Felsic Group A						Felsic Group B		Felsic Subgroup	
Sample	17911		17912		17918		17921		17915	
n =	9		10		8		4		2	
	Low	High	Low	High	Low	High	Low	High	Low	High
Mg #	38	45	36	51	36	50	40	48	41	42
Al(t)	0.002	0.07	-	0.05	0.004	0.05	-	0.01	0.03	0.04
Al(M1)	0.007	0.2	0.005	0.2	0.004	0.05	0.02	0.04	0.02	0.02
Wo	-	1	-	2	1	3	1	2	3	3
En	38	45	36	51	35	49	0.39	47	40	41
Fs	55	62	49	64	50	63	52	59	56	57

Table 5.10 Average clinopyroxene compositions, with cation calculations based on 6 oxygen

Rock type	**Felsic Subgroup**		**Mafic Group**								**Intermediate Group**		**Stewart Hill**		**Host**
Sample	**17915**		**15199**		**17913**		**17914**		**18002**		**17922**		**19002**		**18002**
n =	**10**		**5**		**20**		**11**		**11**		**8**		**12**		**1**
	Ave	**StDev**	**Ave**	**StDev**	**Ave**	**StDev**	**Ave**	**StDev**	**Ave**	**StDev**	**Ave**	**StDev**	**Ave**	**StDev**	
Wt%															
SiO_2	50.07	0.33	50.57	0.44	50.28	0.28	50.52	0.37	49.89	0.74	51.22	0.31	51.83	1.31	50.12
TiO_2	0.25	0.05	1.68	0.20	1.04	0.12	1.20	0.13	1.21	0.24	0.51	0.04	0.77	0.70	1.20
Al_2O_3	2.14	0.23	3.37	0.71	4.03	0.43	4.58	0.36	4.66	0.68	2.05	0.18	3.53	1.26	5.57
FeO	18.94	0.61	7.21	0.44	12.59	1.01	8.97	0.45	10.91	0.20	16.86	0.38	7.07	0.69	8.50
MnO	0.97	0.10	0.17	0.02	0.35	0.04	0.22	0.02	0.28	0.03	0.44	0.04	0.16	0.02	0.19
MgO	9.67	0.31	14.12	0.26	12.74	0.45	14.13	0.45	13.33	0.19	11.46	0.17	14.57	0.33	15.32
CaO	17.40	0.97	21.36	0.32	18.27	0.97	18.96	0.49	18.66	0.11	16.91	0.17	21.03	1.48	18.13
Na_2O	0.33	0.02	0.49	0.03	0.65	0.05	0.70	0.03	0.75	0.04	0.55	0.02	0.01	0.01	0.64
Total	99.78	0.38	99.02	0.50	99.98	0.24	99.38	0.40	99.70	0.27	100.02	0.63	99.69	0.24	99.86
Cations (with Ferrous/ferric correction)															
Si^{4+}	1.94		1.89		1.89		1.88		1.87		1.96		1.92		1.85
Ti^{4+}	0.01		0.05		0.03		0.03		0.03		0.01		0.02		0.03
Al^{3+}	0.10		0.15		0.18		0.20		0.21		0.09		0.15		0.24
Fe^{3+}	0.03		0.01		0.03		0.01		0.05		0.01		0.02		0.04
Fe^{2+}	0.58		0.21		0.36		0.26		0.29		0.53		0.20		0.23
Mn^{2+}	0.03		0.01		0.01		0.01		0.01		0.01		0.01		0.01
Mg^{2+}	0.56		0.79		0.71		0.78		0.74		0.65		0.80		0.84
Ca^{2+}	0.72		0.86		0.74		0.76		0.75		0.69		0.83		0.72
Na^{+}	0.02		0.04		0.05		0.05		0.05		0.04		0.05		0.05
Σcat	4.00		4.00		4.00		4.00		4.00		4.00		4.00		4.00
Mg #	0.49		0.79		0.66		0.75		0.72		0.55		0.80		0.79
Al(t)	0.06		0.11		0.11		0.12		0.13		0.04		0.08		0.15
Al(M1)	0.04		0.04		0.07		0.08		0.07		0.05		0.07		0.09
Wo	35		41		35		34		36		33		39		33
En	32		46		43		49		46		37		49		53
Fs	33		13		22		17		18		30		12		14

Mg #= $100*(Mg^{2+}/(Mg^{2+}Fe^{2+})$; Al(t); Al(M1); Wo, En and Fs calculations adapted from spreadsheet of Norm Pearson (2008), which removes Na-acmite, jadite and Al and Cr Tschermak components.

Table 5.11 Clinopyroxene range

	Felsic Subgroup		Mafic Group A								Intermediate Group		Stewart Hill		Host
Sample	**17915**		**15199**		**17913**		**17914**		**18002**		**17922**		**19002**		**18002**
n =	**10**		**5**		**20**		**11**		**11**		**8**		**12**		**1**
	Low	**High**	**Low**	**High**	**Low**	**High**	**Low**	**High**	**Low**	**High**	**Low**	**High**	**Low**	**High**	
Mg #	47	51	78	80	66	72	73	77	71	73	54	56	78	82	79
Al(t)	0.04	0.08	0.08	0.1	0.09	0.1	0.1	0.1	0.09	0.1	0.04	0.05	0.02	0.2	0.2
Al(M1)	0.03	0.05	0.02	0.06	0.04	0.09	0.08	0.09	0.06	0.08	0.04	0.05	0.04	0.09	0.09
Wo	31	39	40	43	35	39	32	35	36	37	32	33	35	43	33
En	30	34	45	47	41	45	48	51	45	46	36	38	47	53	53
Fs	31	35	12	13	17	24	15	18	17	19	29	31	10	14	14

Table 5.12 Pyroxene trace element concentration (ppm) for all analyses

Mineral	**Orthopyroxene**					**Clinopyroxene**								
Group	**Felsic Group A**			**Felsic Subgroup**		**Mafic Group**								
Element	**17912**	**17912**	**17912**	**17915**	**17915**	**15199**	**15199**	**15199**	**15199**	**17914**	**17914**	**17914**	**18002**	**18002**
Li	9.5	13	57	56	24	30	19	15	6.6	18	6.8	26	27	252
Be	0.6	<0.34	1	14	6.8	<0.42	<0.42	0.5	<0.48	<0.44	<0.35	1.9	0.6	<3.43
B	0.3	<0.33	<0.45	45	22	0.7	<0.43	<0.56	<0.47	0.5	0.4	0.9	0.5	<4.34
Na	306	327	214	780	960	5839	5778	5877	5876	4453	5510	4929	5286	3982
Mg	111373	123192	108150	72520	109407	126275	135209	127615	133526	110470	163880	107250	114188	2386602
Al	9690	10869	10085	210649	98640	31860	39236	28843	38444	24105	33136	29829	21710	178094
Si	265029	325017	249195	391032	341118	279030	292324	252515	247056	203201	278017	227689	247465	3243834
P	23	18	22	452	318	103	68	117	70	105	152	115	98	623
K	428	755	232	1312	661	3.0	22	5.2	12	3.8	324	195	125	<11.06
Ca	5861	5861	5861	12579	12579	150087	150087	150087	150087	137223	137223	137223	133649	133649
Sc	120	125	120	544	714	60	63	62	62	55	58	56	51	230
Ti	1466	1485	1520	51085	76622	7905	12369	7267	11797	6422	9371	7476	5862	31251
V	38	40	48	1098	1420	425	443	386	448	346	406	384	296	1473
Cr	16	11	15	66	106	151	208	116	224	365	611	406	23	122
Mn	10621	11682	11019	15310	21693	2058	1609	2075	1696	1752	1994	1805	2164	42079
Fe	297008	332521	317398	708964	949389	89441	77435	91086	79867	78762	97934	90514	81555	1933393
Co	66	71	67	119	161	51	52	53	52	44	64	50	45	1139

Mineral	Orthopyroxene					Clinopyroxene								
Group	Felsic Group A			Felsic Subgroup		Mafic Group								
Element	17912	17912	17912	17915	17915	15199	15199	15199	15199	17914	17914	17914	18002	18002
Ni	54	59	61	431	226	44	65	46	65	100	157	121	32	683
Cu	1.7	2.4	21	170	73	1.5	1.5	4.4	1.3	1.1	2.7	25	1.5	13
Zn	830	918	884	2318	2290	86	64	91	65	77	109	130	86	3000
Ga	14	14	15	293	178	15	14	15	15	13	13	16	13	113
Ge	7.9	9.3	8.8	33	29	2.6	2.7	2.4	2.8	2.3	2.6	3.3	2.8	32
As	0.5	0.6	0.4	4.2	2.0	0.5	<0.25	<0.32	0.4	0.9	0.8	1.2	0.4	4.9
Rb	2.4	4.5	3.7	11	7.0	<0.037	0.1	<0.041	0.0	<0.031	0.2	0.8	0.1	<0.35
Sr	0.6	1.0	0.8	40	25	66	69	60	67	51	66	60	55	6.6
Y	183	188	216	575	743	24	21	25	22	26	21	26	35	72
Zr	15	16	17	150	116	97	51	116	55	90	50	85	144	154
Nb	0.4	0.9	0.9	556	647	0.4	0.3	0.4	0.3	0.4	0.7	0.5	0.4	0.5
Mo	2	1.7	1.8	6.2	8.5	0.4	0.3	0.4	0.3	0	0	0	0.5	7.6
Cs	0	0	0	4.2	2.0	<0.0184	<0.0141	<0.0195	<0.0215	<0.0184	<0.0176	0	<0.0081	<0.134
Ba	2.9	4.7	4.9	626	237	<0.129	0.3	0.2	<0.146	<0.140	7.6	10	0.5	<0.98
Hf	0.9	1.0	1.1	7.7	7.7	3.4	2.2	3.9	2.3	3.2	2.1	3.1	5.0	5.8
Ta	<0.030	0.1	<0.036	44	60	0.1	0.1	0.1	0.0	0.1	0.1	0.1	0.1	<0.178
Pb	0.6	0.6	0.7	27	14	0.1	0.1	0.1	0.1	0.1	0.1	1.2	0.1	<0.30
Th	0.1	0.9	0.4	6.4	2.5	0.3	0.1	0.3	0.2	0.1	0.1	0.1	0.2	<0.208
U	<0.033	0.1	0.1	4.2	2.6	0.1	0.0	0.1	0.0	0.0	0.1	<0.040	0.0	<0.211
La	0.6	0.8	1.1	6.2	4.1	5.8	2.3	6.8	2.8	5.6	3.0	6.1	8.8	0.6
Ce	2.4	3.3	4.1	15	8.2	19	9.3	21	10	18	11	19	29.1	3.7
Pr	0.6	0.8	0.9	2.8	1.7	3.3	1.9	3.6	2.2	3.3	2.1	3.5	5.1	1.0
Nd	4.9	5.8	6.4	17	10	18	12.1	19	13	19	13	19	27.6	7.0
Sm	4.1	4.8	5.2	10	7.3	5.3	4.3	5.6	4.6	5.7	4.2	6.0	7.9	3.9
Eu	<0.027	0.0	0.0	0.4	0.7	1.9	1.6	1.9	1.8	1.9	1.6	1.9	2.2	1.5
Gd	9.4	10	11	24	22	5.7	4.9	6.4	4.9	6.4	5.0	6.2	8.0	6.7
Tb	2.8	2.8	3.2	6.8	7.5	0.9	0.7	0.9	0.8	0.9	0.7	1.0	1.2	1.5
Dy	26	27	30	72	85	5.5	4.6	5.7	5.2	5.9	4.7	5.7	7.4	11.9
Ho	7.1	7.2	8.0	20	25	1.0	0.9	1.0	0.9	1.1	0.9	1.0	1.4	2.8
Er	26	26	28	72	98	2.5	2.0	2.5	2.2	2.8	2.1	2.7	3.6	8.7
Tm	4.6	4.5	5.2	14	20	0.3	0.3	0.3	0.3	0.3	0.3	0.3	0.5	1.5

Mineral	**Orthopyroxene**					**Clinopyroxene**								
Group	**Felsic Group A**			**Felsic Subgroup**		**Mafic Group**								
Element	**17912**	**17912**	**17912**	**17915**	**17915**	**15199**	**15199**	**15199**	**15199**	**17914**	**17914**	**17914**	**18002**	**18002**
Yb	36	36	41	109	164	2.0	1.6	1.9	1.8	2.0	1.6	2.1	3.1	12.0
Lu	6.0	6.0	6.7	19	28	0.3	0.2	0.3	0.2	0.3	0.2	0.3	0.4	1.9
∑REE	**73**	**50**	**74**	**386**	**482**	**71**	**46**	**77**	**51**	**110**	**3814**	**4764**	**106**	**65**

Table 5.13 Amphibole average composition with cations based on 23 oxygens

Rock type	**Mafic Group**	**Stewart Hill**	
Sample	**17913**	**19002**	
n =	**1**	**9**	
		Ave	**StDev**
Wt % O			
SiO_2	45.55	41.32	0.67
TiO_2	2.69	6.16	0.06
Al_2O_3	5.63	12.43	0.47
Cr_2O_3	0	0.06	0.03
Fe_2O_3	0	-	-
FeO	7.07	10.49	1.61
MnO	0.15	0.12	0.02
MgO	12.33	12.79	1.10
CaO	21.21	10.85	0.15
Na_2O	0.48	2.65	0.13
K_2O	0.01	1.39	0.05
Total	95.12	98.27	0.97
Cations			
Si^{4+}	7.16	6.05	
Ti^{4+}	0.32	0.68	
Al^{3+}	1.04	2.15	
Cr^{3+}	-	0.01	
Fe^{3+}	-	-	
Fe^{2+}	0.93	1.29	
Mn^{2+}	0.02	0.01	
Mg^{2+}	2.89	2.79	

Rock type	**Mafic Group**	**Stewart Hill**	
Sample	**17913**	**19002**	
n =	**1**	**9**	
		Ave	**StDev**
Ca^{2+}	3.57	1.70	
Na^{+}	0.15	0.75	
K^{+}	-	0.26	
Total	16.07	15.70	

Table 5.14 Average major element composition of glass

	Felsic Group A		**Felsic Group B**				**Felsic Subgroup**		**Mafic Group A**				**Intermediate**	**Stewart Hill**	
	17911		**17921 Glass**		**17921 spines**		**17915**		**17913**		**18002**		**18003**	**19002**	
n =	**15**		**10**		**11**		**2**		**2**		**2**		**1**	**3**	
wt %	**Ave**	**Std Dev**	**Ave**	**StDev**	**Ave**	**StDev**	**Ave**	**StDev**	**Ave**	**StDev**	**Ave**	**StDev**	**207 / 1 .**	**Ave**	**StDev**
SiO_2	72.00	3.10	68.88	4.17	74.21	3.59	64.89	16.07	53.99	2.23	47.56	3.56	65.98	55.42	5.96
TiO_2	0.33	0.20	0.11	0.11	0.14	0.07	0.19	0.23	0.51	0.41	2.83	1.17	0.12	2.14	2.61
Al_2O_3	15.34	2.56	17.00	3.18	13.88	2.28	19.30	11.13	26.66	0.10	10.04	5.62	19.33	8.16	10.38
FeO	0.80	0.61	0.95	0.33	0.57	0.37	0.79	0.01	1.71	0.80	8.98	2.98	0.43	10.61	8.39
MnO	0.01	0.01	0.01	0.01	0.01	0.01	0.02	0.01	0.01	-	0.14	-	-	0.19	0.16
MgO	0.01	0.01	0.01	0.01	0.01	0.01	0.06	0.08	0.13	0.04	10.62	2.21	-	17.08	14.79
CaO	0.79	0.84	1.33	1.84	0.49	0.65	6.14	8.23	10.71	0.59	18.43	3.27	1.17	1.80	0.80
Na_2O	4.05	1.37	4.74	1.33	3.99	1.15	2.68	2.56	4.70	0.44	1.25	1.06	6.45	1.69	2.81
K_2O	6.76	1.68	6.98	2.76	6.42	1.76	4.77	6.26	0.81	0.23	0.13	0.18	6.72	2.32	4.01
Total	98.64	3.63	99.73	0.52	99.80	0.34	98.67	0.72	99.25	1.23	10-	0.79	100.21	99.44	0.99

Table 5.15 Trace element concentration of the glass (ppm) for all analyses

	Felsic Group A		**Felsic Subgroup**		**Mafic Group A**						
Element	**17912**	**17912**	**17915**	**17915**	**15199**	**15199**	**17914**	**17914**	**17914**	**18002**	**18002**
Li	7.6	24	41	17	4.4	4.2	0.8	8.9	10	90	63
Be	<0.48	4.3	18	11	3.1	3.8	<0.69	1.6	15	5.8	5.6
B	<0.41	1.0	18	9.0	0.8	0.5	<0.77	1.0	6.5	4.1	2.0
Na	2417	30832	22567	23763	7136	4474	46854	1222	6269	15076	11855

	Felsic Group A		Felsic Subgroup		Mafic Group A						
Element	**17912**	**17912**	**17915**	**17915**	**15199**	**15199**	**17914**	**17914**	**17914**	**18002**	**18002**
Mg	88547	1936	148091	76005	26663	30582	274	24421	26927	112740	94256
Al	17352	93341	241440	153182	44466	32889	165024	16406	76899	105147	79337
Si	211320	511660	639538	391110	114385	101929	309072	77098	185107	333933	284558
P	103	1628	440	201	102	76	175	53	248	2686	136
K	7439	104834	4337	2549	2499	1495	7472	225	3905	20846	6047
Ca	5718	5718	71470	71470	42882	42882	71470	42882	42882	114352	114352
Sc	98	10	945	927	24	32	0	25	67	65	73
Ti	1597	2787	327426	34714	23035	24050	434	8733	59193	51154	42332
V	36	7	4960	656	473	606	1	208	880	762	906
Cr	12	1	408	55	53	60	<1.78	227	1090	44	43
Mn	8427	447	40526	14417	601	512	21	556	785	1569	1492
Fe	218269	21576	3120126	546362	71675	67860	2628	35439	135754	169396	176297
Co	55	2.6	505	98	49	36	0.2	18	42	112	99
Ni	51	8.1	441	104	56	54	<0.30	46	125	128	101
Cu	3	25	295	84	41	25	7.8	24	131	274	177
Zn	572	79	5831	1220	224	168	3.7	71	313	331	374
Ga	14	37	602	140	20	17	39	8.3	40	113	55
Ga	14	30	616	137	15	13	25	7.6	33	36	34
As	0.8	1.4	5	2.1	0.6	0.8	1.0	0.3	5.4	11	6.7
Rb	35	346	26	7.5	2.5	2.7	1.5	0.9	8.4	39	9.4
Sr	4.7	52	310	201	261	163	1753.4	34	181	616	482
Y	162	116	557	1001	13	24	0.2	12	59	100	98
Zr	24	108	735	134	79	92	0.1	45	214	290	268
Nb	6.7	48	1471	245	23	18	<0.033	7.7	81	76	37
Mo	1.6	7.8	67	3.6	0.3	0.3	<0.156	0.1	1.2	1.9	1.7
Cs	1.0	5.3	6.5	1.8	0.9	1.4	<0.032	0.1	1.6	5.9	3.0
Ba	24	275	313	132	156	116	324	18	203	1429	425
Hf	1.0	3.2	22	7.1	2.3	2.7	<0.147	1.5	6.1	9.1	8.8
Ta	0.3	2.6	121	25	1.2	1.0	<0.045	0.4	4.1	3.7	1.9
Pb	4.0	43	86	18	3.5	1.1	1.5	1.5	46	23	17
Th	25	71	9.0	3.0	0.4	0.3	<0.067	0.1	0.9	2.0	0.6
U	1.0	5.8	9.2	2.2	0.1	0.1	<0.055	0.0	0.4	1.0	0.6

	Felsic Group A		Felsic Subgroup		Mafic Group A						
Element	**17912**	**17912**	**17915**	**17915**	**15199**	**15199**	**17914**	**17914**	**17914**	**18002**	**18002**
La	37	108	27	15	6.4	5.3	5.2	3.6	57.3	70	23
Ce	59	234	48	30	17.1	17.3	7.0	8.0	41.2	191	88
Pr	9.4	27	7.0	4.7	2.6	3.6	0.6	1.8	13.9	28	17
Nd	37	99	32	26	12.3	21.2	1.7	9.3	58.0	132	92
Sm	11	22	12	16	3.2	6.4	<0.191	2.8	13.1	29	26
Eu	0.1	0.7	3.5	2.2	1.3	1.6	1.2	0.8	3.2	6.7	5
Gd	15	21	23	45	3.1	6.6	<0.227	3.1	13.6	26	25
Tb	3.3	3.3	6.3	14	0.5	0.9	<0.031	0.4	2.2	3.6	3.5
Dy	27	21	68	138	2.7	5.4	<0.178	2.9	13.0	21	21
Ho	6.2	4.2	20	37	0.5	1.0	<0.038	0.5	2.3	3.7	3.7
Er	20	11	73	121	1.3	2.2	<0.150	1.2	5.8	9.4	9.5
Tm	3.3	1.7	14	19	0.2	0.3	<0.037	0.2	0.8	1.2	1.2
Yb	25	11	106	127	1.1	1.8	<0.258	0.9	5.1	7.7	7.3
Lu	4.1	1.6	17	18	0.1	0.2	<0.038	0.1	0.7	1.0	1.0
Total REE	**257**	**566**	**458**	**612**	**52**	**74**	**16**	**36**	**230**	**531**	**324**

Table 5.16 Mica composition, with cations based on 24 oxygen

Group	**Mafic Group**	**Stewart Hill**	
Sample No	**17913**	**19002**	**19002**
n =	**1**	**1**	**1**
Wt % O			
SiO_2	37.41	51.27	51.24
TiO_2	10.22	1.32	1.07
Al_2O_3	14.30	20.47	21.09
Cr_2O_3	0.00	0.03	0.02
FeO	12.24	15.90	14.19
MnO	0.04	0.08	0.05
MgO	13.53	1.97	2.09
CaO	0.11	0.42	0.46
NiO	0.00	0.03	0.00
Na_2O	0.47	0.14	0.14
K_2O	9.03	0.59	0.57

Group	**Mafic Group**	**Stewart Hill**	
Sample No	**17913**	**19002**	**19002**
n =	**1**	**1**	**1**
Total	97.34	92.23	90.91
Cations			
Si^{4+}	5.90	10.38	10.42
Ti^{4+}	1.21	0.20	0.16
Al^{3+}	2.66	4.89	5.05
Fe^{2+}	1.61	2.69	2.41
Mn^{2+}	0.00	0.01	0.01
Mg^{2+}	3.18	0.59	0.63
Ca^{2+}	0.02	0.09	0.10
Na^{+}	0.14	0.06	0.06
K^{+}	1.82	0.15	0.15
Total	16.54	19.08	18.99

Table 5.17 Average ilmenite compositions, with cation calculations based on 6 oxygens

	Felsic Group A		**Mafic Group A**						**Intermediate**	
Sample	**17911**		**15199**		**17913**		**18002**		**17922**	
n =	**2**		**5**		**2**		**3**		**11**	
	Ave	**StDev**	**Ave**	**StDev**	**Ave**	**StDev**	**Ave**	**StDev**	**Ave**	**StDev**
Wt %										
TiO_2	50.25	0.31	49.92	1.51	50.15	0.74	48.99	0.36	50.90	0.53
Al_2O_3	0.21	-	0.23	0.12	0.24	0.02	0.30	0.14	0.15	0.04
V_2O_3	0.06	0.05	0.42	0.06	0.17	-	0.23	0.03	0.22	0.03
Fe_2O_3	5.78	0.10	5.35	3.22	7.58	1.53	9.39	0.89	4.31	1.22
FeO	40.60	-	38.10	2.04	37.40	1.13	36.80	0.69	42.22	0.99
MnO	0.90	0.03	0.41	0.09	0.48	0.09	0.39	0.05	0.49	0.03
MgO	2.05	0.02	3.62	1.20	4.05	0.22	4.00	0.28	1.64	0.40
ZnO	0.06	0.07	0.03	0.02	0.01	0.01	0.04	0.04	0.03	0.02
Total	100.02	0.28	98.22	2.20	100.12	0.01	100.17	0.17	100.06	0.28
Measured FeO	**45.80**	**0.09**	**42.91**	**1.06**	**44.22**	**0.24**	**45.25**	**0.14**	**46.10**	**0.55**
Cations										
Ti^{4+}	1.88	-	1.88		1.85		1.81		1.91	
Al^{3+}	0.01	-	0.01		0.01		0.02		0.01	
V^{3+}	-	-	0.02		0.01		0.01		0.01	
Fe^{3+}	0.22		0.20		0.28		0.35		0.16	
Fe^{2+}	1.69		1.60		1.53		1.51		1.76	
Mn^{2+}	0.03		0.01		0.02		0.01		0.02	
Mg^{2+}	0.15	-	0.27		0.30		0.29		0.12	
Total	4.00		4.00		4.00		4.00		4.00	

Table 5.18 Average magnetite compositions, with cation calculations based on 32 oxygens and compositional range

Rock type	**Mafic**		
	17914		**18002**
n =	**2**		**1**
	Ave	**StDev**	
Wt % O			
SiO_2	0.91	1.11	0.11
TiO_2	0.02	0.02	0.01
Al_2O_3	0.20	0.26	0.04
Fe_2O_3	63.82	2.21	64.90
FeO	29.50	0.85	28.80
MgO	0.14	0.09	0.02
CaO	0.10	0.08	0.06
NiO	1.15	0.96	0.46
Total	95.88	0.95	94.47
Measured			
FeO	**42.91**		**46.10**
Cations			
Si^{4+}	0.29		0.04
Ti^{4+}	-		-
Al^{3+}	0.08		0.01
Fe^{3+}	15.34		15.92
Fe^{2+}	7.88		7.85
Mg^{2+}	0.06		0.01
Ca^{2+}	0.03		0.02
Ni^{2+}	0.29		0.12
Total	24.00		24.00

Table 5.19 Average titanomagnetite compositions, with cation calculations based on 6 oxygens

Rock type	**Felsic Group A**		**Felsic Group B**		**Felsic Subgroup**		**Mafic Group**			**Intermediate Group**	
Sample	**17911**		**17921**		**17915**		**17913**		**18002**	**18003**	
n =	**6**		**7**		**4**		**11**		**1**	**6**	
	Ave	**StDev**	**Ave**	**StDev**	**Ave**	**StDev**	**Ave**	**StDev**		**Ave**	**StDev**
Wt % O											
SiO_2	0.11	0.01	0.28	0.23	0.17	0.02	0.07	0.02	0.06	0.17	0.17
TiO_2	17.28	1.30	10.37	0.72	12.81	3.01	19.69	4.29	16.01	19.29	0.24
Al_2O_3	4.65	0.20	4.22	0.69	2.95	1.28	3.83	0.89	5.27	1.95	0.26
Cr_2O_3	0.08	0.03	0.01	0.01	0.01	0.01	0.01	0.01	0.16	0.02	0.01
V_2O_3	0.29	0.06	0.08	0.02	0.23	0.05	0.47	0.07	0.59	0.08	0.03
Fe_2O_3	30.13	2.45	43.12	2.54	39.30	6.94	26.85	7.85	34.56	29.12	1.25
FeO	45.17	1.00	38.99	0.69	41.34	2.14	44.51	3.61	33.50	46.21	0.43
MnO	0.63	0.07	0.75	0.04	0.51	0.08	0.43	0.07	0.44	0.57	0.02
MgO	1.19	0.13	0.69	0.13	0.61	0.32	2.94	0.70	7.96	1.30	0.22
Total	99.68	0.52	98.81	1.23	98.06	0.27	98.92	0.63	98.71	98.92	0.93
Measured FeO	72.28	1.30	77.79	2.16	76.70	4.11	68.67	3.72	64.60	72.41	1.54
Cations											
Si^{4+}	0.03	-	0.08		0.05		0.02		0.02	0.05	
Ti^{4+}	3.82		2.34		2.92		4.33		3.39	4.34	
Al^{3+}	1.61		1.49		1.05		1.32		1.75	0.69	
Cr^{3+}	0.02		-		-		-		0.04	-	
V^{3+}	0.06		0.02		0.06		0.11		0.13	0.02	
Fe^{3+}	6.66		9.72		8.99		5.91		7.31	6.56	
Fe^{2+}	11.09		9.77		10.49		10.89		7.88	11.56	
Mn^{2+}	0.13		0.16		0.11		0.09		0.08	0.12	
Mg^{2+}	0.52		0.31		0.27		1.28		3.33	0.58	
Total	23.98	-	23.97		23.98		23.98	-	23.98	23.98	

5.3 Zircon U-Pb geochronology, trace element and Hf isotope analysis

The results are discussed in the groups determined by wholerock geochemistry.

5.3.1 Morphology – Coliban Dam Mafic Group

Morphology of the grains has been determined by microscopic observations and BSE images. Five grains from the mafic group (samples #15199 and 17913) were selected and imaged. The mafic grains are euhedral and broken (Fig. 5.13-10). Magmatic oscillatory zonation is observed in two grains (Fig. 5.13-10). It is difficult to comprehensively characterise the zircons because a small number of grains were obtained.

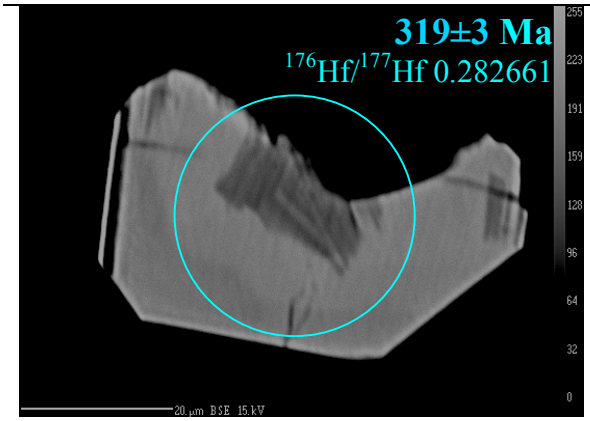


Fig. 5.13 Mafic sample #17913-03 –euhedral crystal shape with magmatic zonation and weak metamorphic domain

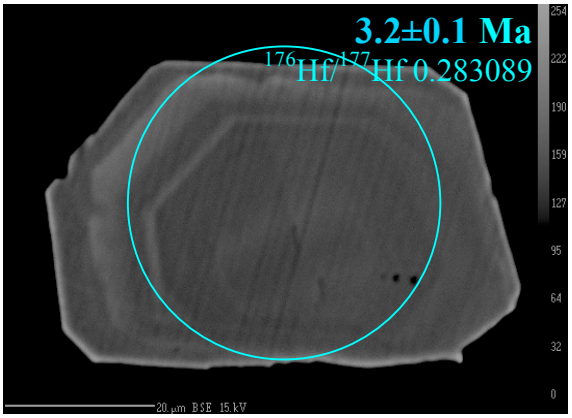


Fig. 5.14 Mafic sample 15199-04 – euhedral shape and oscillatory magmatic zonation

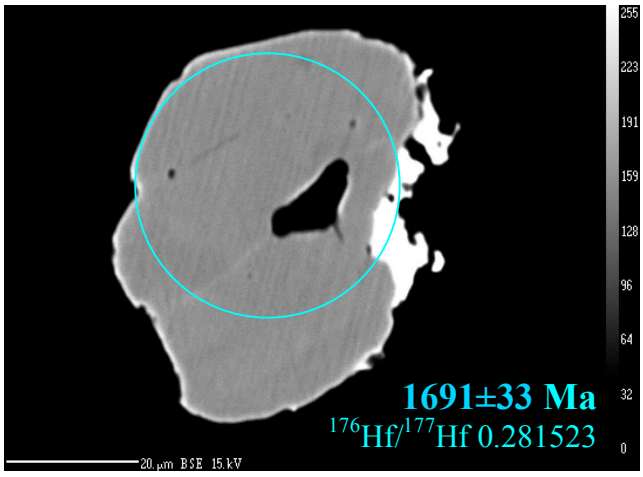


Fig. 5.15 Mafic sample #15199-02 –irregular crystal shape

5.3.2 Morphology - Coliban Dam Felsic Group

A total of 113 grains from Felsic Group A (samples #17911 and 17912) were selected and imaged. The zircon grains range in size from 20 to 50 μm and are pink to honey yellow in colour. They are euhedral to subhedral and weak to strongly rounded along the crystal edges (Fig. 5.16-13). Zircon grains from sample #17912 were slightly less rounded. Oscillatory magmatic zonation is visible in ~ 30 grains (Fig. 5.16-13). Light coloured metamorphic domains are also visible in BSE images of ~ 60 grains (Fig. 5.18-17). These domains are commonly visible at the rim with extension towards the centre of the grains and they vary from very faint (Fig. 5.18 and Fig. 5.20) to strong white BSE tones (Fig. 5.19). Eight zircons are strongly embayed (Fig. 5.21) and appear to have apatite inclusions.

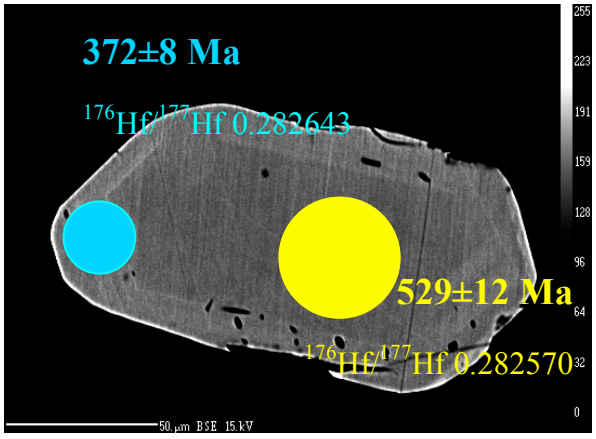


Fig. 5.16 Sample #17912-37 – weak rounding of euhedral crystal edges and magmatic zonation; the location of analyses and ages obtained for a magmatic domain (yellow spot 40 μm; 529±12 Ma) and metamorphic domain (blue spot 30 μm; 372±8 Ma) are marked.

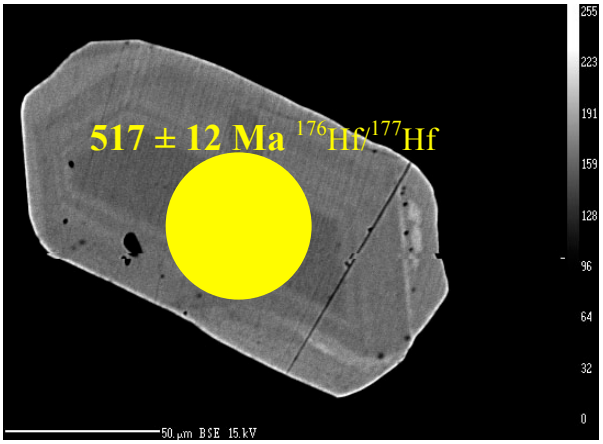


Fig. 5.17 Sample #17911-70 – oscillatory magmatic zonation with a thin metamorphic overgrowth; the location of analysis and age obtained (40 μm; 517±12 Ma) is marked. Note that the analysis location includes both the magmatic zonation and metamorphic domain.

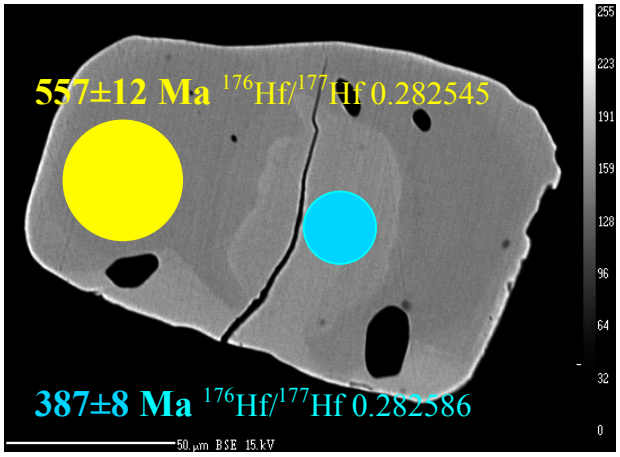


Fig. 5.18 Sample #17912-14 – metamorphic domain within a rounded grain; the location of analyses and ages obtained for the magmatic domain (yellow spot 40 µm; 557±12 Ma) and metamorphic domain (blue spot 30 µm; 387±8 Ma) are marked.

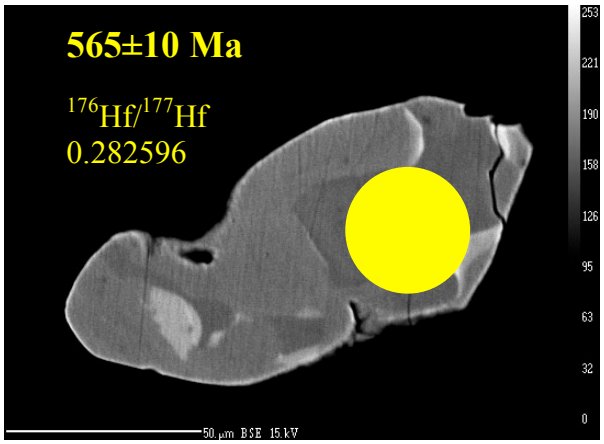


Fig. 5.19 Sample #17912-36 – metamorphic domains within a rounded grain; the location of analysis and age obtained on a magmatic domain is marked (40 µm; 565±10 Ma).

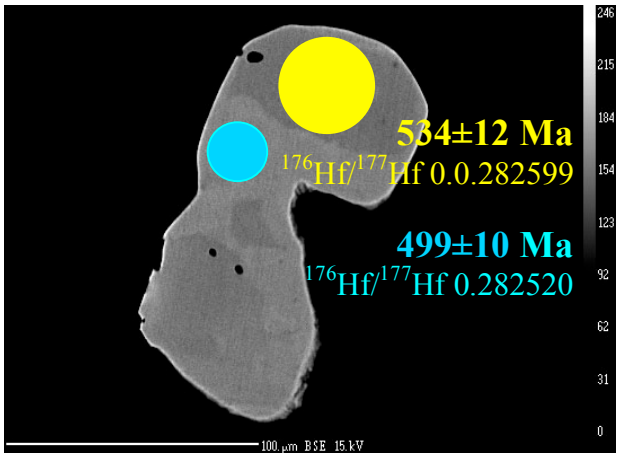


Fig. 5.20 Sample #17912-21 – rounded zircon with metamorphic domains the location of analyses and ages obtained for the magmatic zone (yellow spot 40 µm; 534±12 Ma) and metamorphic domain (blue spot 30 µm; 499±10 Ma) are marked.

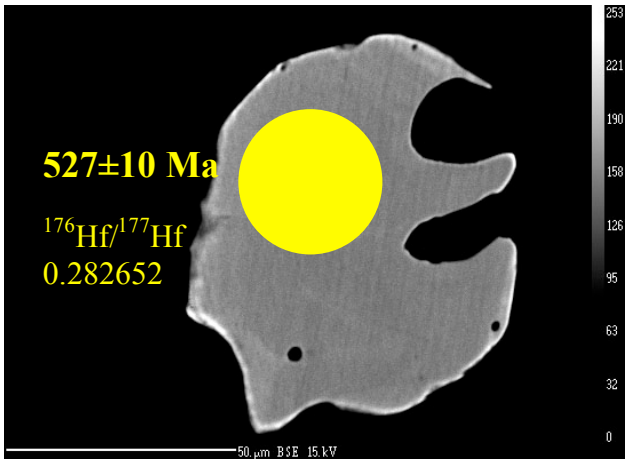


Fig. 5.21 Sample #17912-27 – rounded and embayed zircon grain with a minor metamorphic domain; the location of analysis and age obtained (40 µm; 527±10 Ma).

5.3.3 Dating – Coliban Dam Mafic Group

Five measurements were undertaken on the zircon grains from the two mafic samples, two of which are slightly discordant. No single age population was able to be determined from these as the individual zircon analyses exhibit a wide range of ages: #15199 : 3.2 ± 0.1 Ma; 1691 Ma ± 33 Ma; and #17913: 28 ± 1 Ma; 319 ±3 Ma; 349 ± 6 Ma (Fig. 5.22).

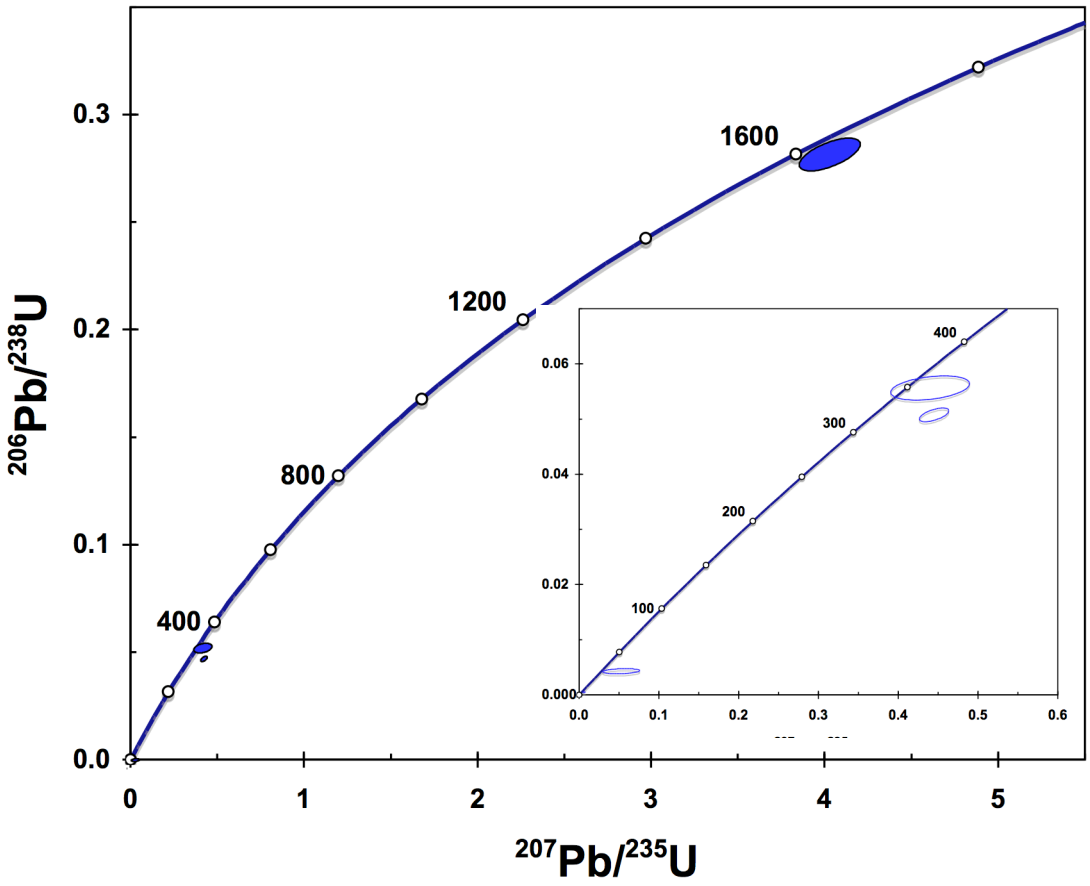


Fig. 5.22 Mafic Concordia plot with samples #15199 (1.7 Ga ± 33 Ma; 3.2 ± 0.1 Ma) and 17913 (319 ±3 Ma; 349 ± 6 Ma; 28 ± 1 Ma); Inset is the Concordia plot for grains with ages < 400 Ma.

5.3.4 Dating – Coliban Dam Felsic Group A

A summary of results from U-Pb analysis are included in Table 5.20. A more extensive table is provided in Appendix X. A total of 92 measurements were undertaken on two Felsic Group A samples. Most analyses were concordant with a few weakly discordant. A similar range of ages observed within the two samples, from 335 Ma to 577 Ma, with a scatter towards the younger ages (i.e. less than 520 Ma). Where possible, magmatic zonation and metamorphic domains were analysed separately. Younger ages (520 to 372 Ma) were recorded in the analyses with metamorphic domains (Fig. 5.16 - Fig. 5.19). In each sample, a weighted average has been used due to the lower MSWD values compared to the Concordia ages, although similar ages were obtained from both methods.

Sample #17911 has a main population at 551 ±1 Ma (n=19; MSWD = 1.14; Prob 0.30: Conc age: 551 ±1; MSWD = 3.4; Prob = 0.065), with a minor peak at ~518 Ma (Fig. 5.23).

Sample #17912 has two populations of 555 ±3 Ma (n=21; MSWD = 1.2; Prob = 0.22: Conc age: 555 ±1 Ma; MSWD = 5.7; Prob = 0.017) and 532 ±3 Ma (n=13; MSWD = 0.77; Prob = 0.68) (Fig. 5.24).

Combining the two yields a population of 553 ±2 Ma (n=43; MSWD = 1.7; Prob = 0.002), with shoulders at 535 ±3 Ma and 519 ±3 Ma (Fig. 5.25).

The peak at 532 Ma in sample #17911 and 535 Ma in the combined plot may be a mixing age because of the laser drilling through different domains.

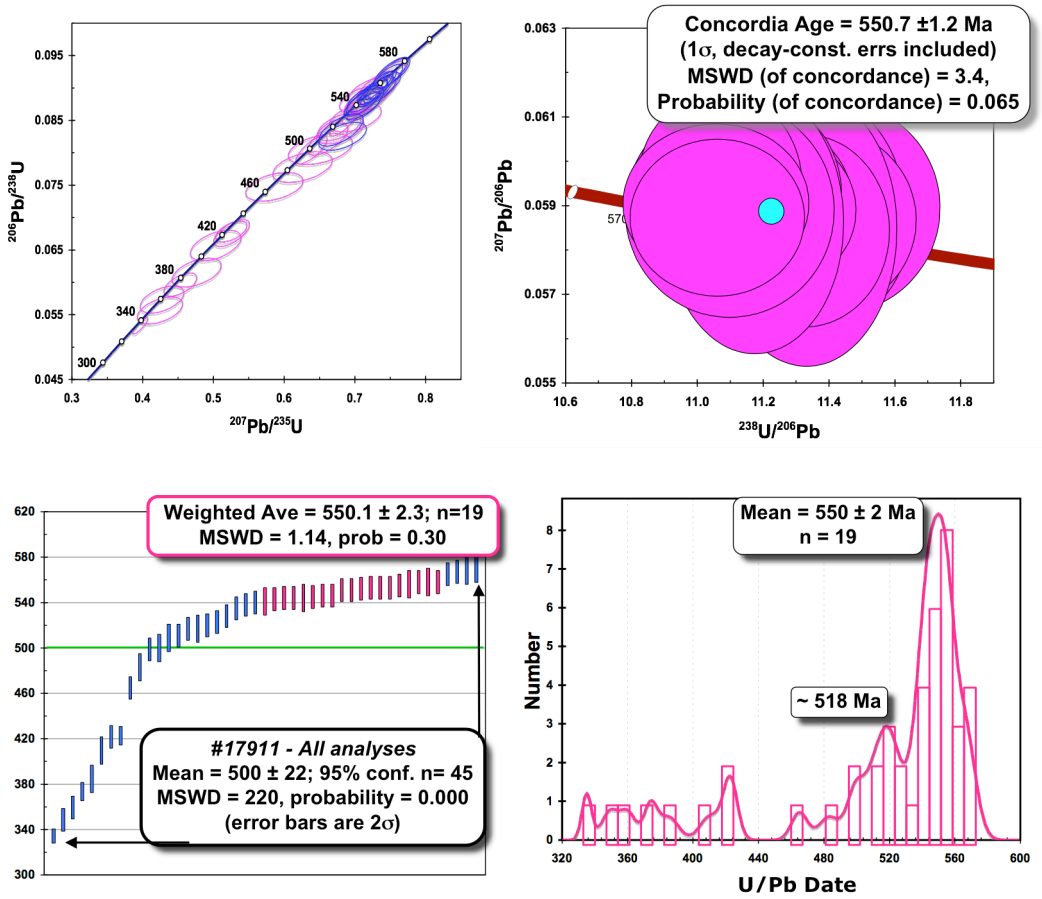


Fig. 5.23 Felsic sample #17911 – Top left - Concordia plot with all analyses for sample #17911 – Blue circles are analyses within magmatic zones, Pink circles are analyses within metamorphic domains; Top right - Inverse Concordia for main population; Bottom left Weighted average including all analyses; Bottom right – Probability.

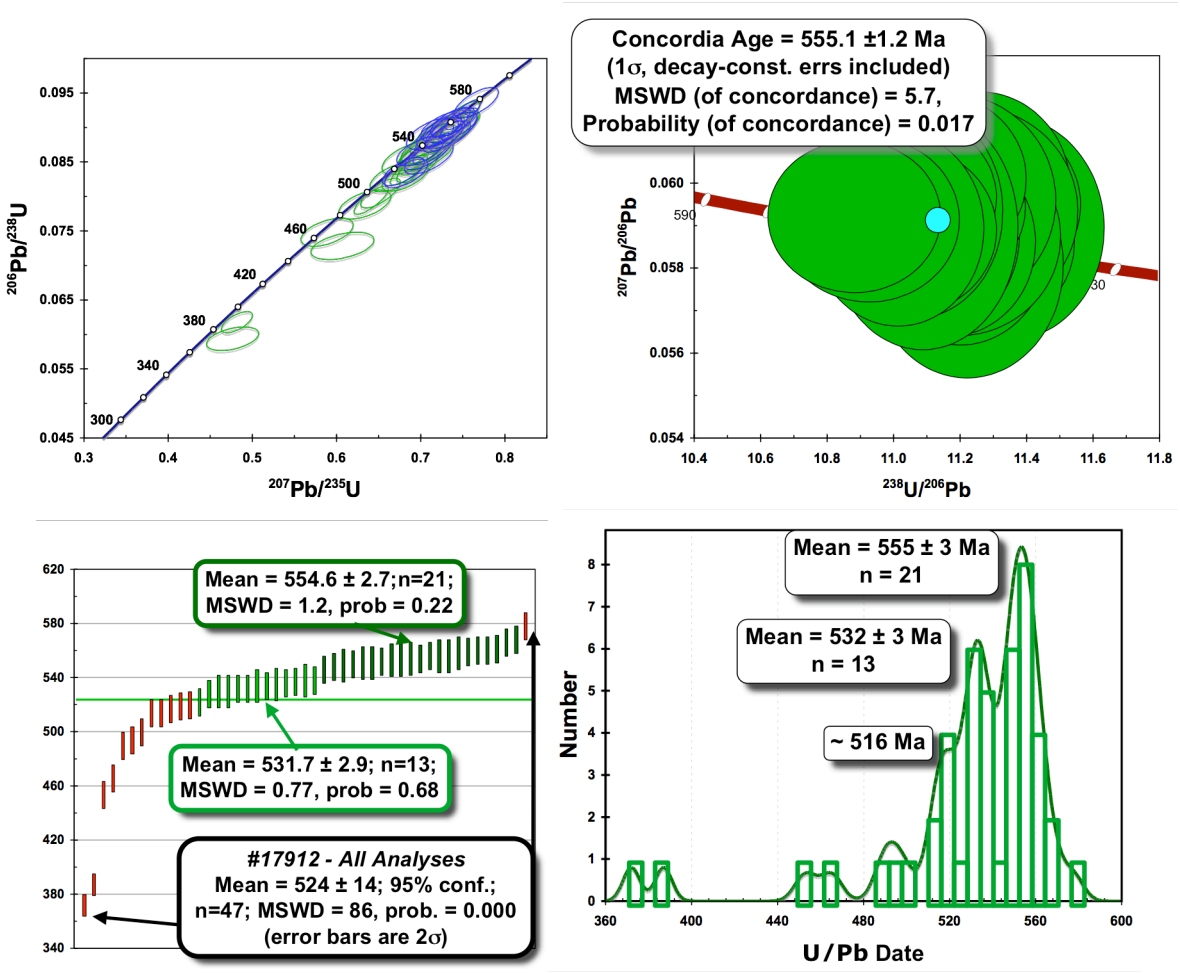


Fig. 5.24 Felsic sample #17912 – Top left - Concordia plot with all analyses for sample #17911 – Green circles are analyses within magmatic zones, Pink circles are analyses from within metamorphic domains; Top right - Inverse Concordia for main population; Bottom left Weighted average including all analyses; Bottom right – Probability.

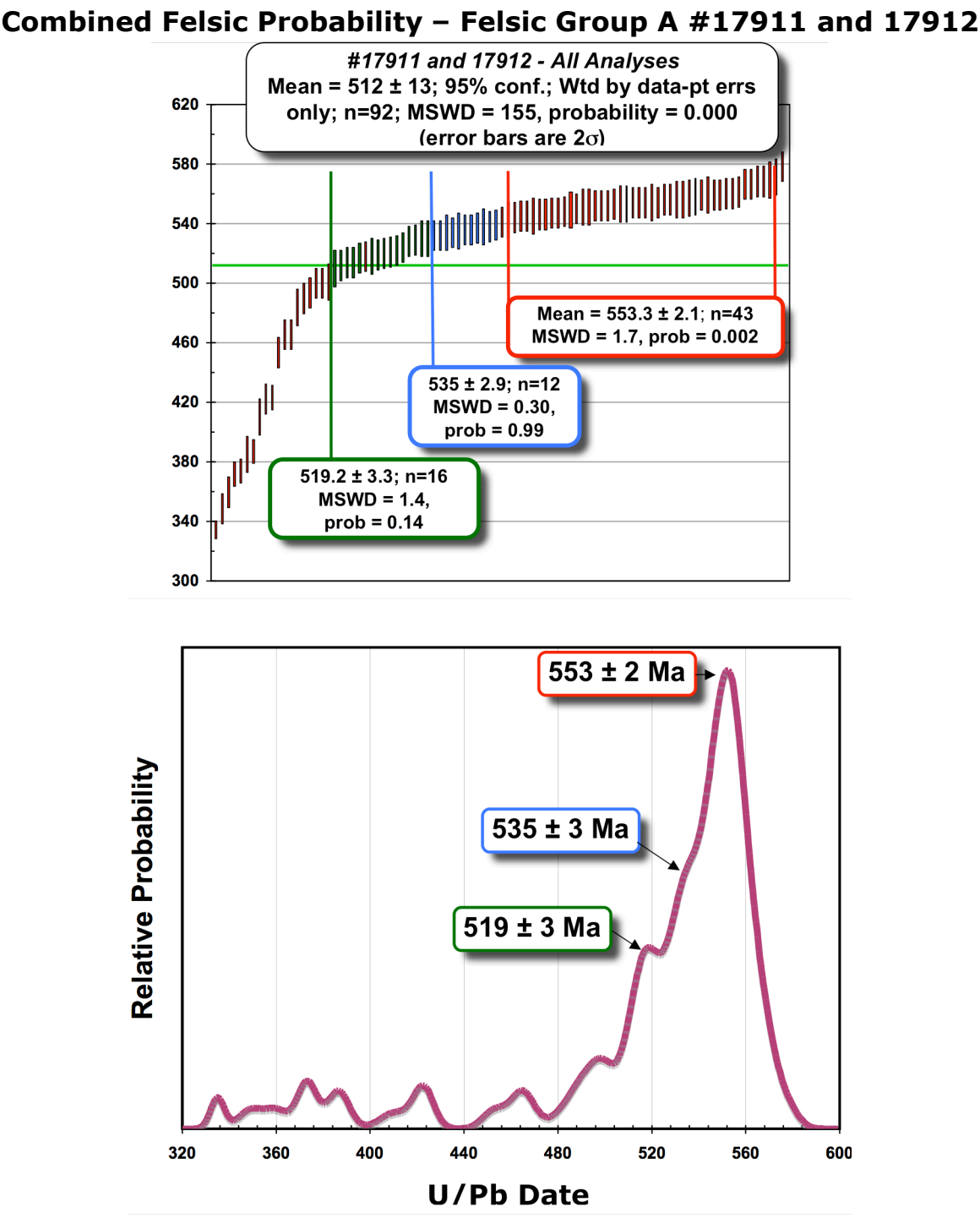


Fig. 5.25 Felsic combined probability MSWD and relative probability. The populations for MSWD calculations have been selected based on the peak and shoulders of the Relative Probability plot.

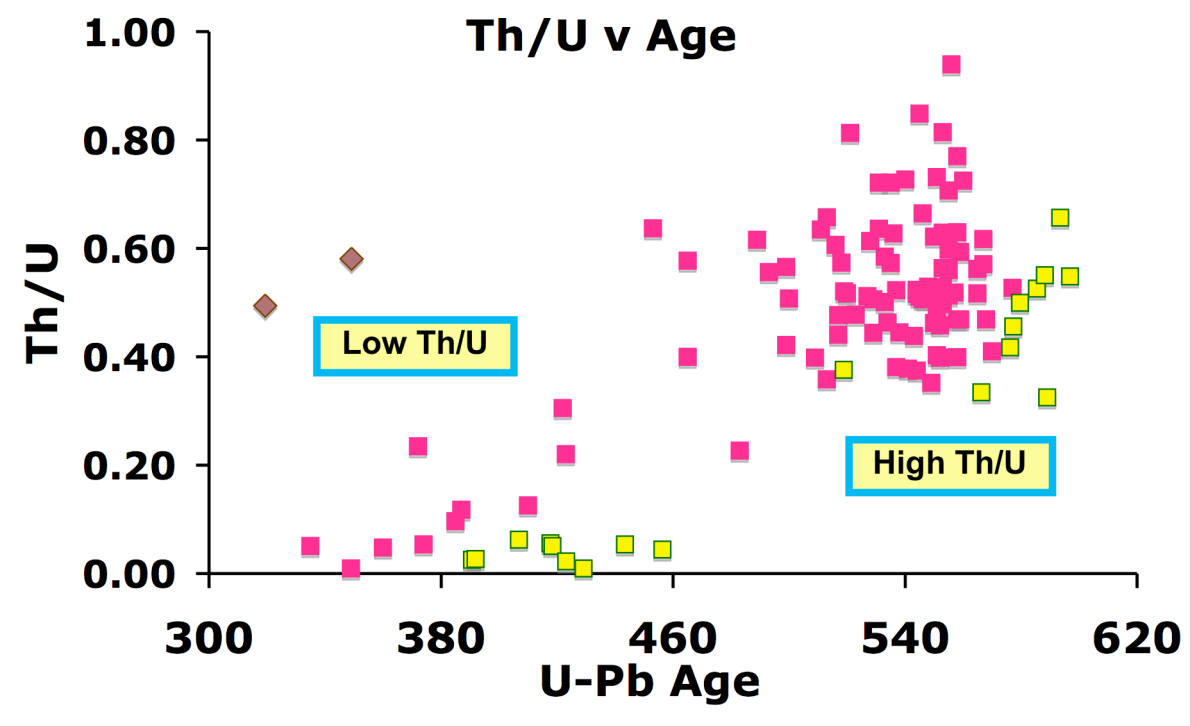


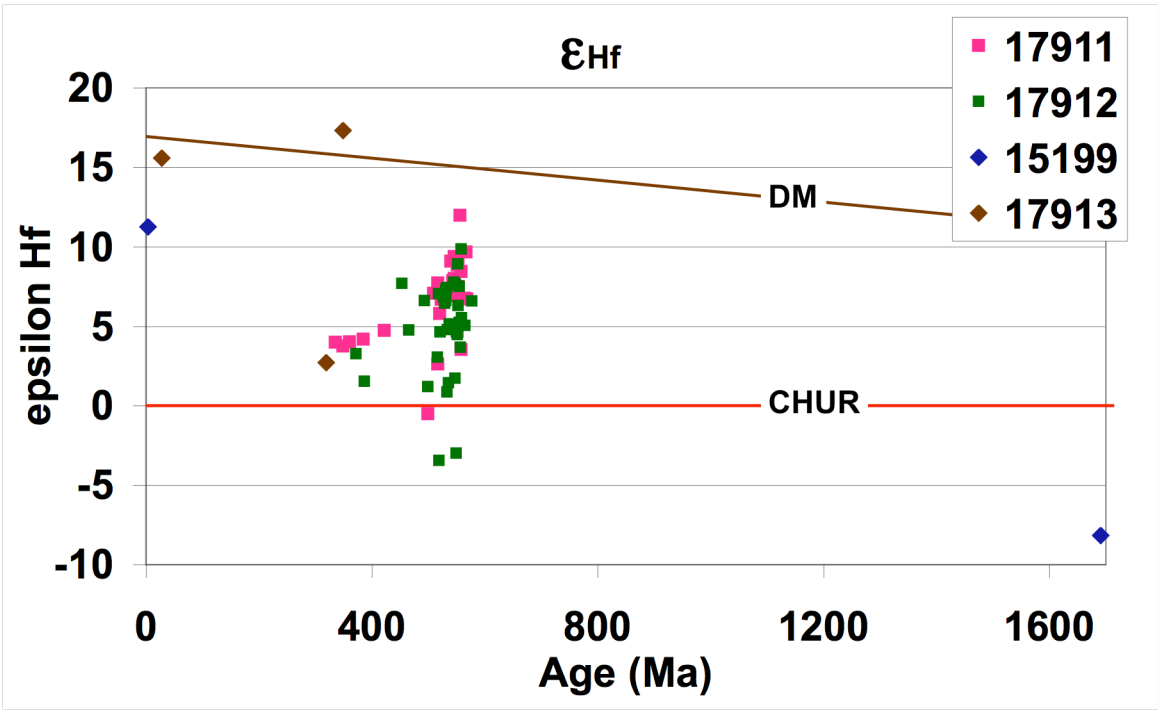
Fig. 5.26 Th/U ratio v Age, illustrating the low Th/U ratios, beginning at ~ 500 Ma.

5.3.5 Hf isotope analysis – Coliban Dam Mafic Group

Three of the zircon grains from Mafic Group A, with ages < 400 Ma have a strong juvenile signature and plot near the depleted mantle line (ε_{Hf}: 11 to 17; Fig. 5.27). One grain plots in the field defined by the zircons from the Felsic Group A rocks (ε_{Hf}: 2.7; Fig. 5.27). A single old grain (1691 Ma) has a strong crustal signature, plotting below the CHUR line (ε_{Hf}: -8.1; Fig. 5.27).

5.3.6 Hf isotope analysis – Coliban Dam Felsic Group A

A total of 67 Hf isotope measurements were undertaken on 53 of the dated grains from the felsic samples. The range of Hf isotope values was similar between the two samples, varying from $^{176}Hf/^{177}Hf$ 0.282481 to 0.282728 and ε_{Hf} -3.4 to 12 (Fig. 5.27). Once again, where possible, metamorphic zonation was targeted for separate analysis. The grains with ages less than 500 Ma form a tight line on $^{176}Hf/^{177}Hf$ values. A T_{DM}^{C} of 1.12 Ga has been determined, with the younger grains following the average crust line (Fig. 5.27 (b)).



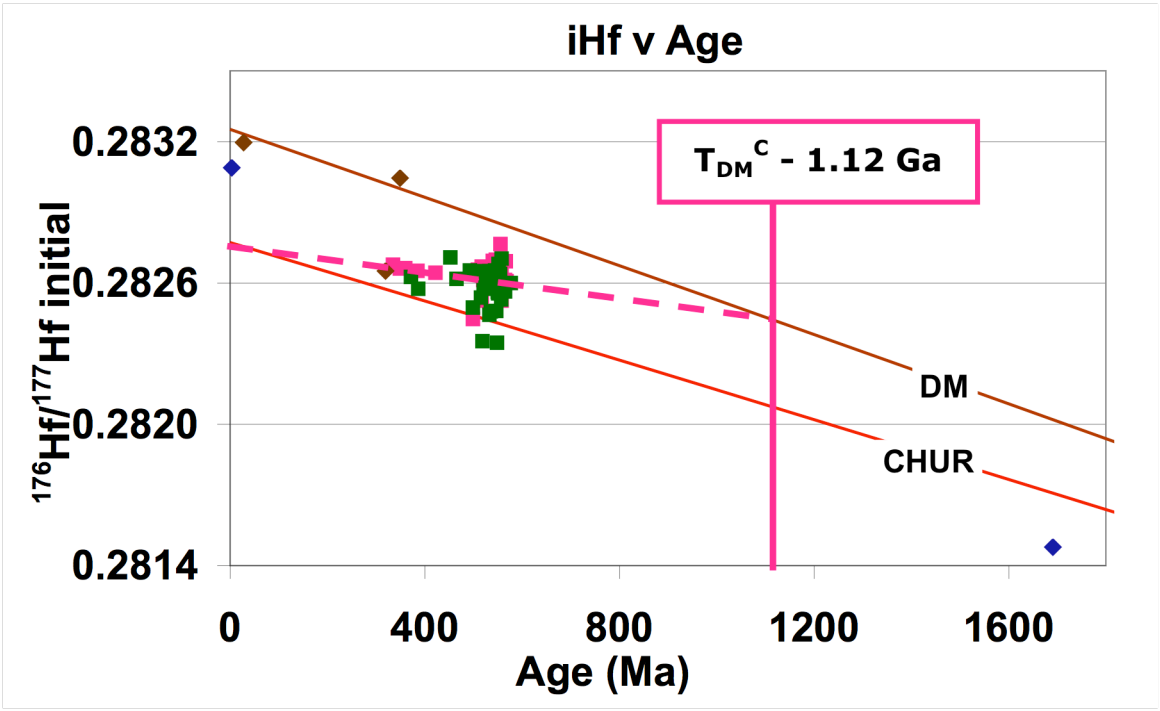


Fig. 5.27 (a) epsilon Hf plots for all samples analysed; (b) iHf v age with a with a crustal model age (T_{DM}^{C}) of 1.12 Ga for the felsic samples. To note is the distribution of the mafic grains– with a strong juvenile signature for the younger grains, with one fitting in with the evolution of the felsic samples.

5.3.7 Trace element analysis – Coliban Dam Mafic Group

The grains from the Mafic Group samples follow a similar trend to the grains from the felsic group, with enriched HREE. However, the Eu and Ce anomaly is less exaggerated.

5.3.8 Trace element analysis – Felsic Group A

A range of values for trace elements is given in Table 5.20, with all analyses included in Appendix X. A similar trend is noted for all zircons analysed. The samples are depleted in Ti, and enriched in Y, U and the HREE relative to chondrite (Fig. 5.28). Low Th/U ratios (0.01 to 0.23) are found only for grains with ages < 500 Ma (Fig. 5.26). There is a negative Eu anomaly and positive Ce anomaly within the grains of this group. Thorium concentrations range from 30 to 2022 ppm and U 85 to 6012, with Th/U ratios of 0.01 to 0.94 (Table 5.20).

Table 5.20 U-Pb analysis results

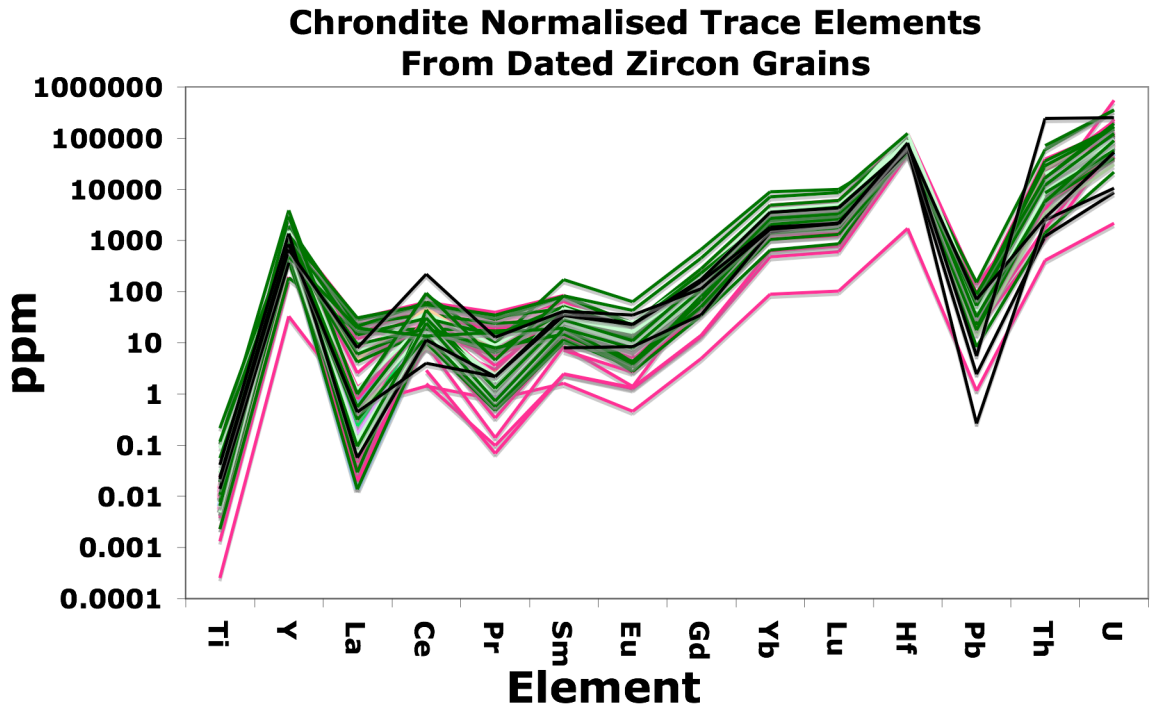
	Felsic Group A						Mafic Group				
	#17911			#17912			#15199		#17913		
Total analyses	45			47			2		3		
Population/s	551 ±1 Ma	n=19		555 ±3 Ma	n=21						
				532 ±3 Ma	n=13						
		Min	**Max**		**Min**	**Max**	**15199-02 (n=1)**	**15199-04 (n=1)**	**17913-03 (n=1)**	**17913-06 (n=1)**	**17913-07 (n=1)**
$^{207}Pb/^{206}Pb$		368 ±27-	569±32		537 ±63 -	581±33	**1691±33**	1384±179	726±38	504±101	1397±321
$^{207}Pb/^{235}U$		339±3-	569±6		396 ±9 -	578±6	1641±14	6.2±0.6	374±5	370±14	52.1±9
$^{206}Pb/^{238}U$		**335±3-**	**570±6**		**372 ±4 -**	**577±5**	1602±16	**3.2±0.1**	**319±3**	**349±6**	**27.7±1**
$^{208}Pb/^{232}Th$		342±7 -	616±19		393 ±32 -	576±20	1441±69	2.8±0.2	380±18	334±20	24.3±4
Combined #17911 and 17912 Age	553±2	n=43									
Major elements (wt %)	**Ave**	**Min**	**Max**	**Ave**	**Min**	**Max**	**n=1**	**n=1**	**n=1**	**n=1**	**n=1**
SiO_2	32.04	28.83 -	32.49	32.08	29.54	32.64	32.16	32.11	32.64	32.24	32.27
HfO_2	1.55	1.07 -	2.67	1.48	1.07	2.62	1.59	1.70	1.79	1.20	1.42
ZrO_2	65.84	65.06 -	66.95	65.95	60.13	67.15	66.21	65.86	66.88	66.88	66.19
Trace elements (ppm)	**Ave**	**Min**	**Max**	**Ave**	**Min**	**Max**	**n=1**	**n=1**	**n=1**	**n=1**	**n=1**
Ti	7	0.16 -	27	11	1.5 -	76	15	14	16	9.1	27
Y	2247	74 -	4066	2493	424 -	8763	1914	1473	3123	828	3084
La	11	0.005 -	238	6.0	0.005 -	47	0.16	2.9	42	<0.021	0.020
Ce	50	1.5 -	662	36	7.8 -	150	3.8	211	173	5.1	11
Pr	4.6	0.009 -	102	2.3	0.06 -	21	0.30	1.8	32	<0.016	0.30
Sm	14	0.37 -	141	10	2.3 -	43	8	10	81	1.8	9.4
Eu	1.7	0.04 -	25	1.2	0.24 -	5.5	2	3	25	0.723	2.0
Gd	49	1.5 -	173	49	10 -	206	48	35	133	11	53
Yb	643	22 -	1265	709	160 -	2204	450	408	783	365	885

	Felsic Group A						Mafic Group				
	#17911			#17912			#15199		#17913		
Lu	115	3.9 -	231	133	33 -	376	83	81	149	84	165
Hf	12518	306 -	22631	12842	8480 -	22214	13504	14422	11208	10216	12060
Pb	**114**	2.89	346	**116**	21	385	178	14	71	6.1	0.66
Th	426	43 -	1906	636	30 -	2202	210	14045	644	64	145
U	1241	193 -	6012	1116	85 -	3971	559	3973	1302	111	151
Th/U	0.44	0.01 -	0.94	0.56	0.12 -	0.85	0.38	3.54	0.49	0.58	0.96

Table 5.21 Summary of Hf Isotope Analysis Results

	Felsic Group A						Mafic Group				
	#17911			#17912			15199-02	15199-04	17913-03	17913-06	17913-07
Population/s	551 ± 2 Ma (n=19)			555 ± 3 Ma (n=21)	532 ±3 Ma (n=13)		1.7 Ga	3.2 Ma	319 Ma	349 Ma	28 Ma
	Ave (n=29)	**Low**	**High**	**Ave (n=34)**	**Low**	**High**					
$^{176}Hf/^{177}Hf$ measured	0.282659±56	0.282481	0.282797	0.282607±76	0.282384	0.282728	0.281523	0.283089	0.282661	0.283060	0.283198
$^{176}Lu/^{177}Hf$	0.0021	0.0005	0.0041	0.0025	0.0009	0.0079	0.0014	0.0014	0.0017	0.0023	0.0035
$^{176}Yb/^{177}Hf$	0.092	0.022	0.161	0.099	0.042	0.301	0.053	0.044	0.065	0.064	0.120
$^{176}Hf/^{177}Hf$ *	0.282639	0.282447	0.282765	0.282582	0.282346	0.282708	0.281479	0.283089	0.282651	0.283045	0.283196
epsilon Hf	6.6	-0.5	12.0	5.0	-3.4	9.9	-8.1	11.3	2.7	17.3	15.6
T(DM)	0.87	0.68	1.17	0.96	0.77	1.42	2.44	0.23	0.85	0.28	0.08
T(DM) Crustal	1.07	0.75	1.51	1.18	0.89	1.71	2.92	0.37	1.16	0.25	0.11

See Appendix ** for full data; *initial values calculated using Scherer *et al.* (2001) ^{176}Lu decay constant (1.865x10-11)



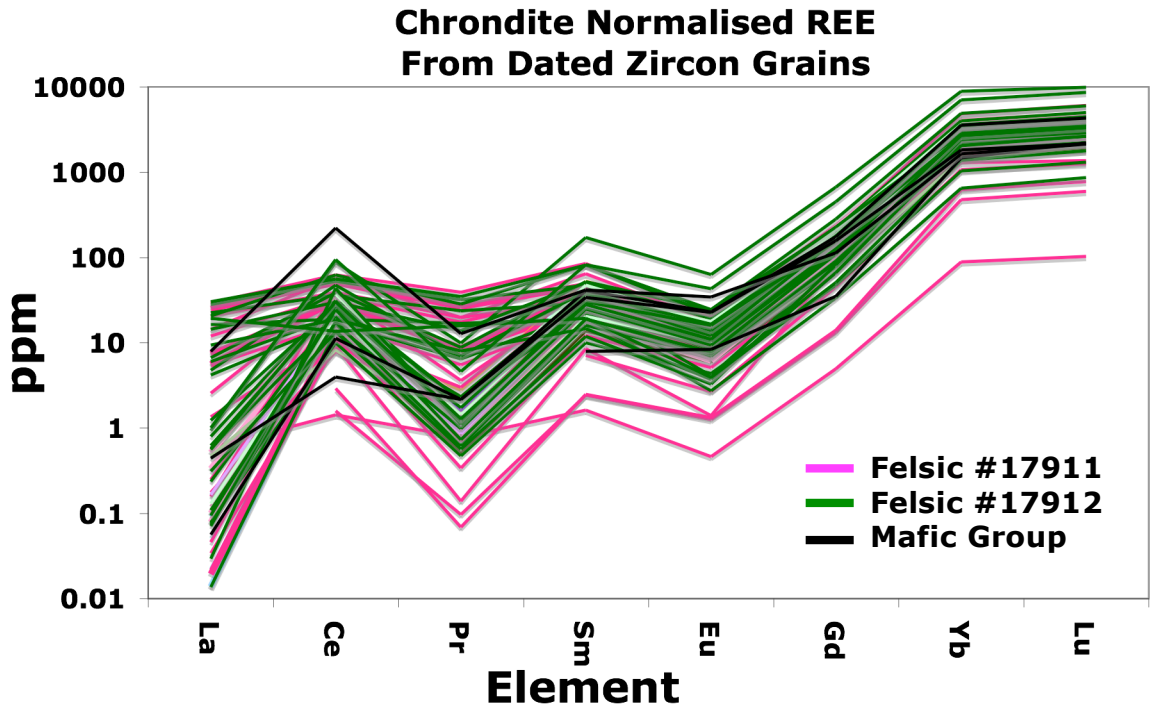


Fig. 5.28 Chondrite normalised trace elements – Pink = #17911; Green - #17912; Black – Mafic grains. A similar trend is noted for all analyses, with depletion in Ti, La, Pb and Th and enrichment in Y, Ce, Hf and U relative to chondrite.

6 Discussion

A combination of geochemistry, geochronology and isotope analysis allows the evolutionary pathway of xenoliths to be traced. For example, U-Pb zircon dating may be linked with Hf, Sr and Nd isotope analysis to provide information on the source material and a timetable of events (ie Griffin *et al.*, 2000; Dai *et al.*, 2008). Isotope analysis determines whether the xenolith is from a depleted mantle (juvenile) or enriched (crustal) source, with intermediate and/or a range of ratios suggesting magma mixing and/or reworking. When combined with U-Pb dating, isotope analysis allows crustal model ages to be derived, which gives the time that the melt was separated from the source (ie Dai *et al.*, 2008). Dai *et al.* (2008) compounded such evidence with complex bulk geochemistry to conclude that heterogeneity within the lower crust in the southern Hunan Province in China resulted from episodic juvenile growth, crustal reworking and mafic underplating.

Dodge *et al.* (1986) used the geochemistry and mineral assemblage of mafic to ultramafic lower crustal xenoliths to determine crustal processes within the Central Sierra Nevada. They correlated Al, $^{87}Rb/^{86}Sr$ and $^{87}Sr/^{86}Sr$ in a variety of xenoliths to attribute the composition of an overlying granitoid pluton to mixing of ultramafic and silicic crustal material also sampled by xenoliths. Heterogeneity in Sr ratios allowed differentiation of the overlying granitoid pluton although a similar age to the xenoliths was found. The trachybasaltic host had similar $^{87}Sr/^{86}Sr$ ratios to the ultramafic xenoliths suggesting that it, as well as other igneous-textured ultramafic xenoliths, may have resulted by partial melt of the ultramafic material.

During entrainment and transport, xenoliths are encompassed by and may react with host magma. Heating by the magma and/or decompression melting may then cause the xenolith to become assimilated into the magma. The release of water from hydrous xenolith minerals, particularly biotite, may cause low temperature granitic melts bearing hercynitic spinel, melt, sillimanite and Fe-Ti oxides (Bayhan *et al.*, 2006). However granitic melt may also occur at higher temperatures in anhydrous conditions (Steiner *et al.*, 1975; Nekvasil, 1988). Indicators of xenolith melt include increased SiO_2, the presence of glass as intergranular melt between quartz grains and dark coloured melt between foliation planes (Bayhan *et al.*, 2006).

6.1 Xenoliths from this study

Based on petrography there are two dominant groups within the xenoliths from the Upper Coliban Dam Suite: a mafic and felsic, with a rarer intermediate group. The samples within the Stewart Hill Suite are relatively uniform, with gabbroic mineralogy and texture. Overall, the wholerock major and trace element geochemistry differentiates each group of the Upper Coliban Dam and Stewart Hill suites. Groups determined petrographically are reflected in geochemistry, apart from sample #17922 which has intermediate, rather than mafic geochemistry. The trace element patterns are distinct between each group, with the closest match being strong negative anomalies in Rb, Th and K, and slight positive Sr and negative P anomalies (Fig. 6.1) within the mafic groups. The samples will be discussed in the groups determined geochemically, being: Upper Coliban Dam Mafic Group; felsic groups A and B and intermediate group; and the Stewart Hill Suite.

6.1.1 Upper Coliban Dam Mafic Group

(a) Petrography

Petrographically, this group is classified as gabbroic, which is supported by the wholerock geochemistry (TAS chart; Fig. 5.1).

Partially crystallised glass bearing a micro doleritic texture is also present interstitially throughout the sample. The major mineral phases (plagioclase, pyroxene, magnetite and ilmenite) are stable when in contact with this partially crystallised glass, inferring that the glass is related to primary processes involved in the formation of those minerals and that these minerals were crystallised from the glass. This is supported by the sharp contact between the oikyocrystic plagioclase and interstitial glass in sample #17914 (Fig. 3.15) whereby the plagioclase grains were crystallising from the glass until entrainment, when crystallisation was terminated. The above features and pyroxene clusters support formation within a cumulate environment (Fodor and Vandermeyden, 1988). Mineral stability at the contact with the host basaltic icelandite infers that the xenoliths were in equilibrium with the host. Thus, the samples in this group may be cognate xenoliths. Minor mica and amphibole abundance represent the only hydrous phase within the mafic group samples.

Samples #17914 and #17919 exhibit finer-grained size domains. Sample #17914 also exhibits the reverse ophitic texture which is less exaggerated or lacking in other samples. The finer-grained domains in sample #17919 may be attributed to brittle deformation, as an almost brecciated microstructure is apparent. This may have occurred whilst being entrained by the host material. Aside from sample #17919, only weak deformation textures are apparent within this group and strong igneous textures are retained. Hence, it may be inferred that the mafic group rocks were emplaced following deformation events that caused the stronger metamorphic textures observed in the felsic and intermediate samples.

(b) Geochemistry

Geochemically, samples of the mafic group are identical, plotting close to each other and forming linear trends in various plots v SiO_2 and Mg#. The group has a similar trend in trace elements to the host basaltic icelandite with a general decrease in trace element enrichment compared to chondrite with increasing compatibility and exaggerated positive anomalies in Sr and Ti (Fig. 6.1). Positive anomalies in HFS elements such as Nb, Ta and Ti suggest that it does not have a strong continental crustal component (Rollinson, 1993). Negative anomalies in LIL elements (Rb and K) may reflect fluid movement through the system, stripping these elements. The positive Eu and Sr anomalies reflect feldspar crystallisation. The opposite is evident within glass pockets of the mafic group samples, reflecting the partitioning of these elements (Eu and Sr) into plagioclase, thus depleting the residual melt (Fig. 6.1) and again providing evidence for a cumulate environment. The low SiO_2 values (<45 wt% in three samples) and the almost linear relationship in all elements v SiO_2 and Mg# also support the textural interpretation (Chapter 3) that the gabbros are at least in part cumulate. Whilst high Al_2O_3 suggests formation in a high temperature environment.

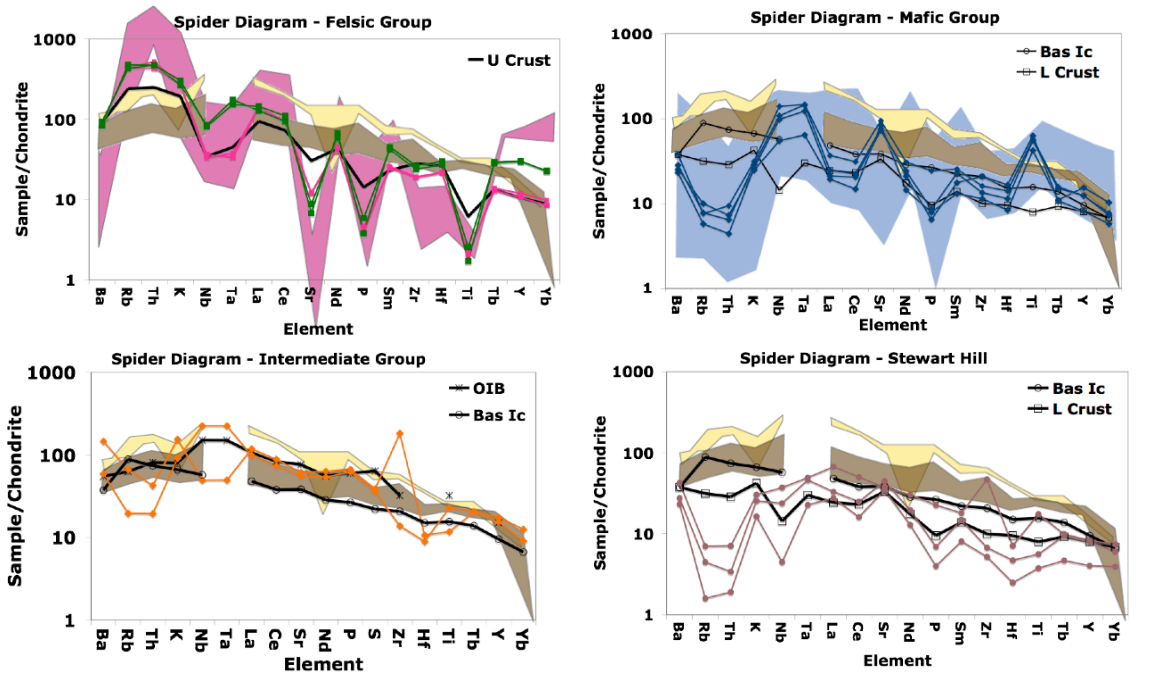


Fig. 6.1 Spider diagrams for each group normalised to chondrite values from Thompson (1982): Pink shading = felsic group glasses; Blue shading = mafic group glasses; Yellow shading = Macedon-Trentham lavas (Paul *et al.*, 2005); Brown shading = representative values of Plains Series Basalts (Price *et al.*, 1997). These diagrams show the differences within each group, particularly the intermediate group, with different trends for #17922 and 18003 and the overall difference in the Stewart Hill samples. Representative values for basaltic icelandite (Price *et al.*, 1997) and average values for Upper Crust (Rudnick and Gao, 2004) Lower Crust (Rudnick and Gao, 2004) and OIB (Sun, 1980) are included.

On basaltic tectonic discrimination plots, the mafic samples plot as within plate alkali basalts (Fig. 6.2), whilst sample #15199 suggests the influence of plume influenced MORB. These plots use relative enrichment of Zr, Y, Ti and immobility of Nb to deduce a setting. Enrichment of Ti and Zr, but not Y is assumed in within plate basalts, particularly Ti which suggests derivation from an enriched, heterogeneous mantle source relative to MORB (Pearce and Gale, 1977; Meschede, 1986; Rollinson, 1993). Whilst greater Nb is seen in enriched MORB sources, such as plume influenced regions like Iceland (Meschede, 1986). Isotopes suggest that the groups is from a mantle source with close to average values (Figs 4.7 and 4.8), with an average T_{DM} 1.28 Ga.

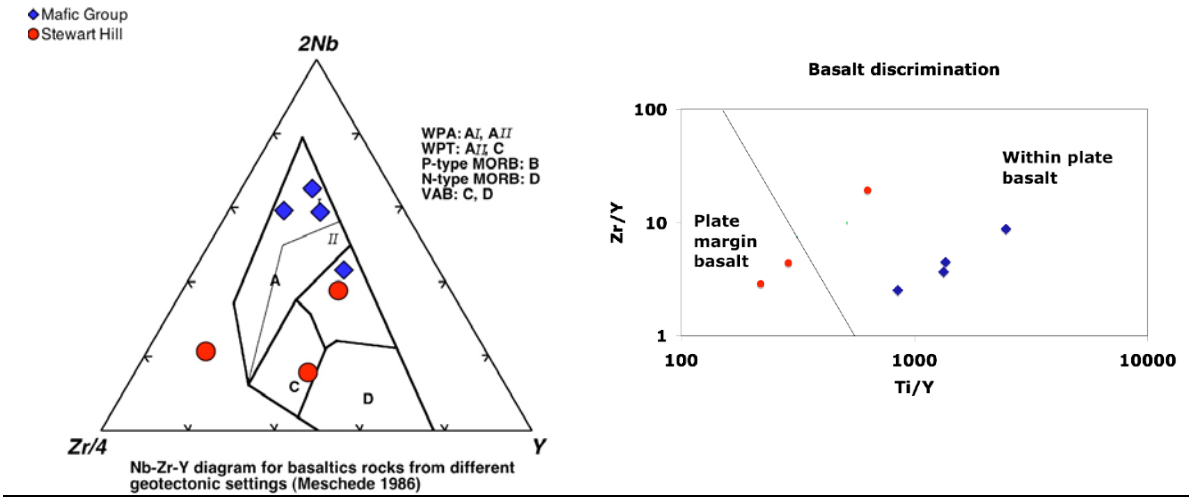


Fig. 6.2 Tectonic discrimination of the Upper Coliban Dam mafic group (blue diamond) and Stewart Hill suite (red circles). (a) Nb-Zr-Y diagram: WPA = Within plate alkali basalts; WPT = Within plate tholeiites; MORB – Mid ocean ridge basalts; N-normal; P-plume influenced; VAB = Volcanic arc basalts (Meschede, 1986); (b) Zr/Y vs Ti/Y (Pearce and Gale, 1977). The Upper Coliban Dam plots predominantly as within plate basalts in both, whilst the Stewart Hill samples show more variation, predominantly as plate margin basalts.

The composition of the orthopyroxene grains is less variable than that of the clinopyroxene grains, possibly due to exsolution within the clinopyroxene grains, as observed in the petrography chapter. There is an overlap of geochemistry with the Stewart Hill samples in orthopyroxene grains of sample #17914 and clinopyroxene grains in sample #15199. The Stewart Hill Suite mirrors the two clear geochemical clusters within the orthopyroxene grains of the mafic group.

A trend in Mg# is observed in sample #17914 - lower Mg# is recorded for both clinopyroxene (Mg# 73 to 74) and orthopyroxene (Mg# 69 to 71) when in the tight grain clusters compared to greater values in the reverse ophitic and interstitial glass textures (clinopyroxene: Mg# 71 to.73; orthopyroxene: Mg# 75 to 77; Fig. 3.20). This may be due to competition for Mg by the pyroxene grains within the clusters.

(c) Geothermometry

Geothermometry results are given in Table 6.1. Two pyroxene geothermometry suggests formation temperatures of ~ 930 (Wood and Banno, 1973) to 1017 °C (Wells, 1977). The latter will be used due to underestimation of temperatures with high Mg values in the Wood and Banno (1973) geothermometry. As a guide, a depth of 30 to 35 km (0.8 to 0.9 GPa) may be approximated using geotherms discussed by Sutherland *et al.* (O'Reilly and

Griffin, 1985; Sutherland *et al.*, 1994a; Sutherland *et al.*, 1994b; O'Reilly *et al.*, 1997; 1998). However, as the temperatures relate to igneous activity and not directly to the geotherm, the depth/pressure may be overestimated. Such depths place the samples toward the crust/mantle boundary in southeastern Australia (Cayley *et al.*, 2008).

Table 6.1 Geothermometry results

	Felsic Group A		**Mafic Group**			**Stewart Hill**
	17911	**17915**	**17913**	**17914**	**18002**	**19002**
	Temp (°C)	Temp (°C)	Temp (°C)	Temp (°C)	Temp (°C)	Temp (°C)
Fe-Ti oxide exchange (Ghiorso and Evans, In press)	851					
Two pyroxene (Wood and Banno, 1973)		874	930	962 985	963	883
Two pyroxene (Wells, 1977)		966	1005	1002 1017	1009	876

(d) Mafic Group U-Pb Zircon Dating

There is a large scatter in ages within zircon grains from the mafic samples which suggests that some, if not all, of the grains are either inherited or xenocrystic. Trace element composition of the zircon grains reflect derivation from magma with a felsic composition (Belousova *et al.*, 2002). This supports a xenocrystic nature, as does the similar age and Hf composition of one grain (sample #17913-06) to the felsic group A grains (Fig. 6.3). Considering this, the youngest age determined provides a maximum age for magmatic activity of the host xenolith. The 3.2 Ma age (sample #15199-04) is actually very close to the timing of volcanic activity within the Spring Hill Complex and proximal region, which ranges from 8.3 to 2.9 Ma (Wellman, 1974; Graham *et al.*, 2003; Sutherland and Hollis, unpublished Geotrack Reports). There is no evidence of younger events within immediately surrounding geology.

The 28 Ma age (sample #17913-07) is similar to the Older Volcanics series within the area, particularly the Nerrim Province (24.5 to 21.7 Ma) and Aberfeldy Province (26.3 to 27.9 Ma) (Wellman, 1974).

Grain #17913-06 has an age of 349 Ma and is derived from a juvenile source according to its Hf composition (ε_{Hf} 17).

Grain #17913-03 has a similar Hf composition to the zircons from the felsic xenoliths and may be derived from the felsic magma that was reset during the later metamorphic event. The 1691 Ma zircon grain provides evidence for either a basement component of the Selwyn Block or inheritance from an older source (Fig. 6.3).

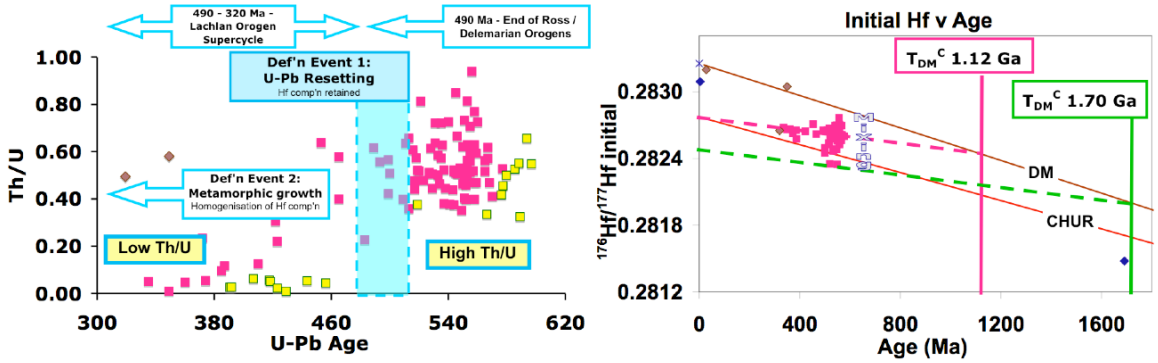


Fig. 6.3 **Left** - Th/U ratios v U-Pb Age illustrating the two deformation events. Event 1: 520 to 500 Ma with mixed Hf composition retained: Event 2: 460 onwards with homogenisation of Hf composition. SHRIMP U-Pb analyses are included in yellow (Norman *et al.*, 1996). They too exhibit a scatter in ages, with ages from 460 Ma exhibiting distinctly low Th/U ratios. **Right** - Initial Hf v Age with T_{DM}^{C} of 1.12 Ga and 1.70 Ga. The mixing signature observed in Hf composition is seen until 490 Ma. The Hf composition then becomes homogenised from ~460 Ma. The T_{DM}^{C} of 1.70 Ga suggests that the grains with a strong crustal Hf composition may be derived from melting of the rock from which the 1691 Ma grain was derived.

(e) Comparison to the NVP and Selwyn Block

Compared to the NVP plains series, the mafic group has lower SiO_2, but higher TiO_2 (almost double), Al_2O_3 and CaO, lower MgO, Na_2O and distinctly lower K_2O (Price *et al.*, 1997). The Macedon-Trentham lavas have similar SiO_2, Na_2O and CaO. The mafic group is also less enriched in LREE compared to chondrite. Strontium is higher and Rb lower, suggesting a source with less continental input and higher Ti, pointing towards a more enriched mantle source and/or accumulation of Fe-Ti oxides. Strontium isotope values are within range of the isotopically heterogeneous NVP plains series (Price *et al.*, 1997). Epsilon Nd (+1.87 to 2.91) is within range of the plains series (- 1.2 to +3.6) though lower than the cones series with values predominantly greater than + 3 (McBride *et al.*, 2001; Graham *et al.*, 2003). Although there is a correlation with isotope values, there is no evidence to support a direct evolutionary relationship between the mafic group and the NVP lavas. The MgO to SiO_2 values are too low to be the parental magma for the NVP basalts and TiO_2 is considerably higher. One possible explanation for major element variation is that the cumulate mafic group is derived from an evolved source in which

clinopyroxene has been crystallised and that Fe-Ti oxides and plagioclase have been dominant cumulus phases (Holm, 2002). It is also apparent that the mafic group has had less crustal input compared to the NVP basalts (Fig. 6.4), when considering K/Nb values (Fig. 6.4).

Young ages (~ 3 Ma) and the lack of deformation suggest that the mafic group is not part of the Selwyn Block, but rather associated with later volcanism. The outcrops of the Selwyn Block at Waratah Bay, Philip Island, Barrabool Hills, Tasmania etc have Cambrian ages and display stronger metamorphic features (Cayley *et al.*, 2002).

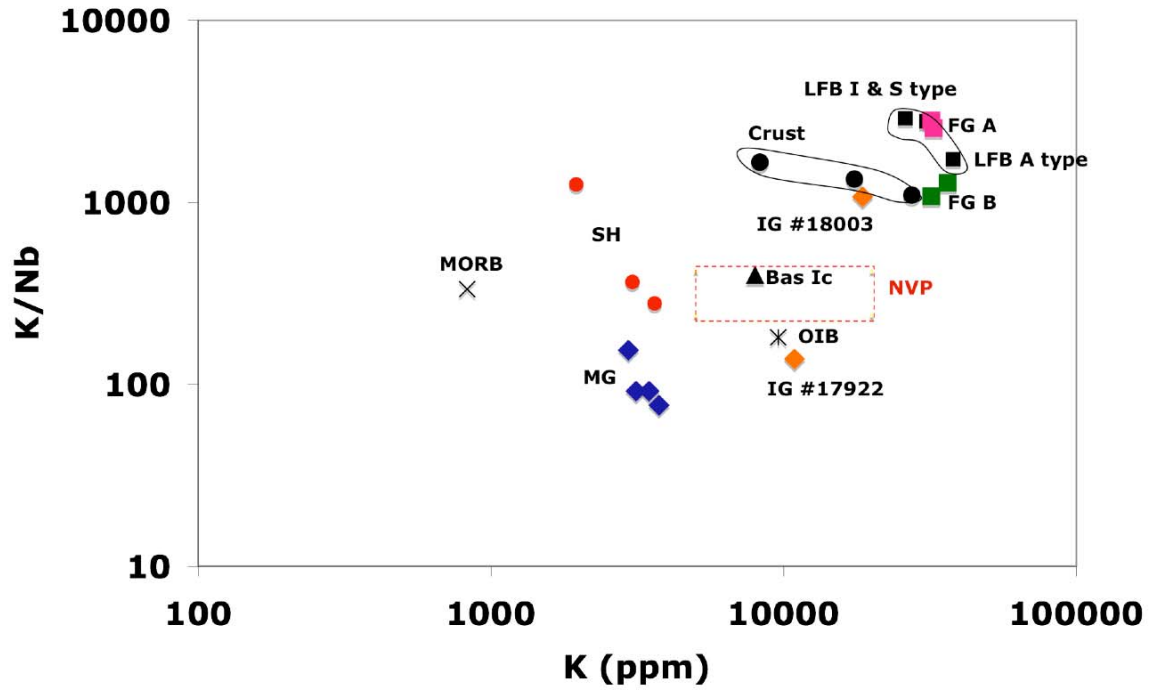


Fig. 6.4 Kb/Nb vs K used to measure crustal contamination by comparing to average crustal, MORB and OIB values (Price *et al.*, 1997). This shows strong crustal values for the felsic groups and sample #18003 of the intermediate group, with signs of minor contamination for the Stewart Hill suite and values close to MORB for the mafic group. Close affinity is seen between the LFB granites and the felsic group. Average values for Upper Crust (Taylor and McLennan, 1981) Lower Crust (Weaver and Tarney, 1984), N-type MORB (Sun, 1980; Saunders and Tarney, 1984), OIB (Sun, 1980), NVP, Basaltic icelandite (Price *et al.*, 1997) and average Lachlan Fold Belt I, S and A type granite (White and Chappell, 1983) values are also included.

6.1.2 Upper Coliban Dam Intermediate Group

(a) Petrography

The petrography for sample #17922 is similar to that of the mafic group, with plagioclase, clinopyroxene and magnetite as major phases. However, it has a larger plagioclase grains (to 4 mm) and stronger metamorphic textures in certain zones. This sample has a complex nature with intermixed fine and coarse-grained material (Fig. 3.10). It appears that the coarse-grained lighter material has intruded the finer-grained dark material.

Samples #17916 and 18003 have very different microstructures and mineralogy, dominated by polygonal aggregates of feldspar. The feldspar grains exhibit strong sieve textures, supposedly as a reaction following entrainment by the host basaltic icelandite. Some glass in sample #18003 may be attributed to alteration of pyroxene crystals, particularly those with straight edges. Other grains are highly altered and only just recognisable.

The coarse-grained band in sample #18003 at the contact with the host basaltic icelandite and the dykelet in sample #17916 have similar textures, with intergrown euhedral feldspar grains. The texture looks to be a coarser version of the host basaltic icelandite and it may be that the nucleation/growth ratio of the host basaltic icelandite has changed upon contact with and entrainment of the xenolith. This is possibly due to a change in temperature/pressure constraints and/or the xenoliths providing extra nucleation points, allowing fewer and larger grains to grow on the edge of the xenolith (Vernon, 2004).

(b) Geochemistry

The intermediate group has mixed geochemistry, as seen in the different classification on the TAS diagram (Fig. 5.1). Sample #17922 is classified as a basaltic trachyandesite and sample #18003 has a trachyandesite composition. This supports differences noted petrographically, ie with sample #17922 exhibiting more abundant mafic phases. Wholerock data was not obtained for sample #17916.

The trace element pattern of this group is relatively similar between samples, differing by anomalous Nb, Ta and Zr in sample #18003 (Fig. 6.1). The high Zr values agree with the greater abundance of zircon noted in this sample petrographically (Chapter 3). Overall,

the pattern follows that of the host basaltic icelandite, with a decrease in enrichment with increasing compatibility (Fig. 6.1). However, the negative anomalies in Rb, Th and K present the greatest difference between this group and the host. K/Nb ratios suggest that sample #18003 has greater crustal input compared to sample #17922 (Fig. 6.4).

The group is similar based on Hf and Nd isotope values (ε_{Nd}0.63 (#17922) to 1.35 (#18003)), plotting close to bulk silicate earth but initial Sr isotope values separate them ($^{87}Sr/^{88}Sr$ 0.708548 (#17922) to 0.705008 (#18003)). Sample #18003 has very close $^{87}Sr/^{88}Sr$ ratios to that of the host basaltic icelandite, each plotting close to bulk silicate earth (Figs. 4.7 and 4.8) and the ε_{Nd} is close to values for the NVP plains series (-1.6 to +3.6). The anomalous Sr values for sample #17922 may relate to superficial Rb gain or Sr loss.

The variability between samples observed in wholerock geochemistry is reflected within mineral geochemistry. Sample #18003 has similar orthopyroxene compositions to the felsic group. It also has similar K-feldspar compositions to sample #17916 but has a greater range from Na-sanidine to labradorite compared to anorthoclase to Na-sanidine for sample #17916. Sample #17922 has a limited range in feldspars, from oligoclase to labradorite, like the mafic group. However, it does have intermediate pyroxene compositions. High temperature phases up to 900°C are observed within the feldspar compositions of sample #17916 (Fig. 4.8).

The intermediate group can easily be separated based on petrography, wholerock and mineral geochemistry into: A - sample #17922; B – samples #17916 and 18003.

(c) Comparison to the NVP and/or Selwyn Block

When compared to NVP rocks, sample #17922 plots within evolution lines for Al_2O_3, MgO and K_2O (wt %) v SiO_2 (wt %) and within the trend for Sr, P and Ti (ppm) v K (ppm) (Price *et al.*, 1997). It is also very close to the range in K/Nb v K (Fig. 6.4). The REE trend fits very closely to that of the NVP rocks, with enrichment in LREE (up to 160) and a steady decrease in the HREE (down to 11) compared to chondrite (Price *et al.*, 1997), however, it does have a positive Eu anomaly that is absent in the NVP rocks. As mentioned above, εNd is within range of the NVP plains series but $^{87}Sr/^{88}Sr$ 0.708548 is

higher (possibly attributable to superficial Rb gain or Sr loss). Due to the complex physical nature of this xenolith, it was initially thought that the intermediate wholerock composition resulted from mixing of mafic and felsic components. However, the intermediate pyroxene composition and fit with the NVP rocks support its intermediate composition with complex petrography resulting from a variation of texture in intermediate material rather than two opposite end members.

It is highly likely that sample #17922 is related to NVP igneous activity. A close relationship to the NVP infers little relationship with the Selwyn Block.

Sample #18003 has a comparable REE trend, εNd (1.35) and $^{87}Sr/^{88}Sr$ (0.70500) with the NVP, however, it does not follow the evolution trends like sample #17922. They may share a similar source but it appears they have undergone different processes with greater variation in major and trace elements. Geochronology on this sample would provide valuable assistance in comparison against the NVP and Selwyn Block. Metamorphic microstructures and boudinaged zircon shape imply a certain amount of deformation upon this sample and an older age than the less deformed NVP rocks.

6.1.3 Upper Coliban Dam Felsic Group

The felsic group is divided into three groups by petrography (Chapter 3). Petrographic felsic group 1 was separated into felsic groups A and B based on the geochemical differences discussed below. These geochemical groups will be used during the discussion whilst the sample numbers will be used for #17915 (petrographic felsic group 2) and #17917 (petrographic felsic group 3) due to only one sample fulfilling a group.

6.1.4 Felsic Groups A and B

(a) Petrography

Felsic groups A and B have granitic composition based on mineralogy, including Q-Ab-Or composition and have been classified as felsic gneiss. This is supported by various geochemical evidence including TAS discrimination (Fig. 5.1) and zircon trace element composition (discussed below).

The glass bands and microstructure of felsic groups A and B present a very complex history for the xenoliths. There are two spatially discreet zones of partially crystallised glass within these xenoliths, which are likely to have been derived from different processes: (1) open system injection of melt from the host basaltic icelandite; and (2) closed system equilibrium melting of the xenolith whilst entrained in the host lava; as discussed below.

(i) Injection by host material

The texture and mineralogy of the partially crystallised glass concentrated at the contact with the host is very similar to that of the host basaltic icelandite (Price *et al.*, 1988; Price *et al.*, 1997; Graham *et al.*, 2003). Texturally, this material is distinct from the glass within bands by visible rectangular, matrix-forming, feldspar grains and the lack of quench textures. Also, these domains are spatially associated with the edge of the xenolith and so it may be inferred that they have resulted from the injection of basaltic icelandite into the xenolith upon entrainment.

(ii) Equilibrium melt

The presence of crystals with quench textures in the glass suggests that another process, apart from injection by host material, has taken place. The rounded grain shapes and dykelet form of glass pockets that embay quartz and feldspar grains suggest equilibrium melting. Additionally, the thin films of glass along grain boundaries suggest formation by equilibrium melting of the xenoliths along grain boundaries, as discussed by Bayhan *et al.* (2006). The stability of the pyroxene, opaque and zircon grains within the glass compared to textures observed at the rims of feldspar and quartz grains suggests that the latter have undergone melting. Further, the occurrence of orthopyroxene grains with straight edges within the glass supports intergrowth with a euhedral crystal, such as feldspar, that has since been melted.

The occurrence of glass throughout the sample, rather than just at the contact with the host basaltic icelandite, suggests that it does not have a limited source at thin-section scale. Variable glass abundance within samples may reflect differences in bulk composition and/or in entrainment time (ie samples #17920 and 17921 of felsic group B have more

dominant glass). The nature of the glass bands, including thickness, interlayering between feldspar and quartz-rich layers and mineralogy (ie stable pyroxene and magnetite grains) is similar to bands in gneissic rocks. Thus, it is likely that melting predominantly occurred within deformation bands formed during a metamorphic event prior to entrainment.

The cotectic for a partial melt of two feldspars and quartz with 1 % H_2O (no hydrous minerals have been observed) is ~ 900 to 1000 ºC (Steiner *et al.*, 1975; Nekvasil, 1988). This temperature may be attainable during entrainment within a high temperature melt, such as the host basaltic icelandite, of ~ 1250 ºC to 1300 ºC (Haase *et al.*, 2004; Jung *et al.*, 2006). The reaction for the melt would be:

$KAlSi_3O_8$ + $NaAlSi_3O_8$ + SiO_2 = Melt

Alkali feldspar + Plagioclase + Quartz = Melt

The difference in microstructure within the host basaltic icelandite (euhedral feldspar matrix) and glass bands (swallowtail feldspar microphenocrysts) may be explained by the more mafic host crystallising at temperature/pressure constraints suitable for partial melt of the felsic material. The felsic material could then have crystallised by quenching due to depressurisation.

(b) Geochemistry

As mentioned above, petrographic felsic group 1 is divided into two subgroups (felsic group A and B) based on geochemistry and isotopic composition with support by petrography (ie greater amounts of glass were observed in felsic group B samples #17920 and 17921). Major element geochemistry categorises felsic groups A and B as (subalkaline) granites (Fig. 5.1), as does CIPW normative Q-Ab-Or (Fig. 6.5). Once again, this is supported by petrography and zircon trace element composition.

Felsic groups A and B have a close fit with average values for the upper crust (Fig. 6.1), in particular, the enrichment in LIL elements Rb, Ba and K and negative anomalies in HFSE such as Nb, Ta and Ti. Crustal input is supported in the K/Nb vs K plot (Fig. 6.4), wholerock isotopic analysis (Fig. 4.7) and zircon Hf analysis (see below). However, these results also highlight geochemical differences of felsic group B. For example greater enrichment in Nb, Ta and HREE, more radiogenic Nd and Hf and lower K/Nb (Fig. 6.4) –

all of which reflect slightly weaker, or deeper, continental affinities and possibly more mafic input.

The exaggerated negative Sr and P anomalies suggest plagioclase and apatite fractionation and the very strong negative anomalies in Nb, Ta and Ti suggest ilmenite and/or garnet fractionation (Rollinson, 1993) has taken place and removed from the melt prior to crystallisation of these xenoliths. Tectonic discrimination plots classify felsic group A as volcanic arc granites and felsic group B as within plate granites, both being close to the boundary (Fig. 6.5 and Fig. 6.6). These plots use elements that were most effective when plotted against silica content for discrimination of 600 granites (Pearce *et al.*, 1984).

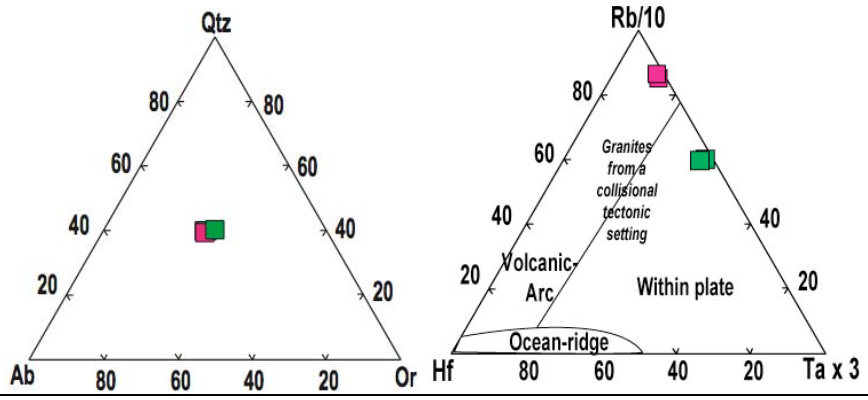


Fig. 6.5 Discrimination plots (a) Qtz-Ab-Or granite which shows an almost pure granite system; (b) tectonic setting discrimination (Harris *et al.*, 1986) – felsic group A is classified as volcanic-arc granites and felsic group B as within plate granites. Higher Hf concentration would keep the samples within the same zones.

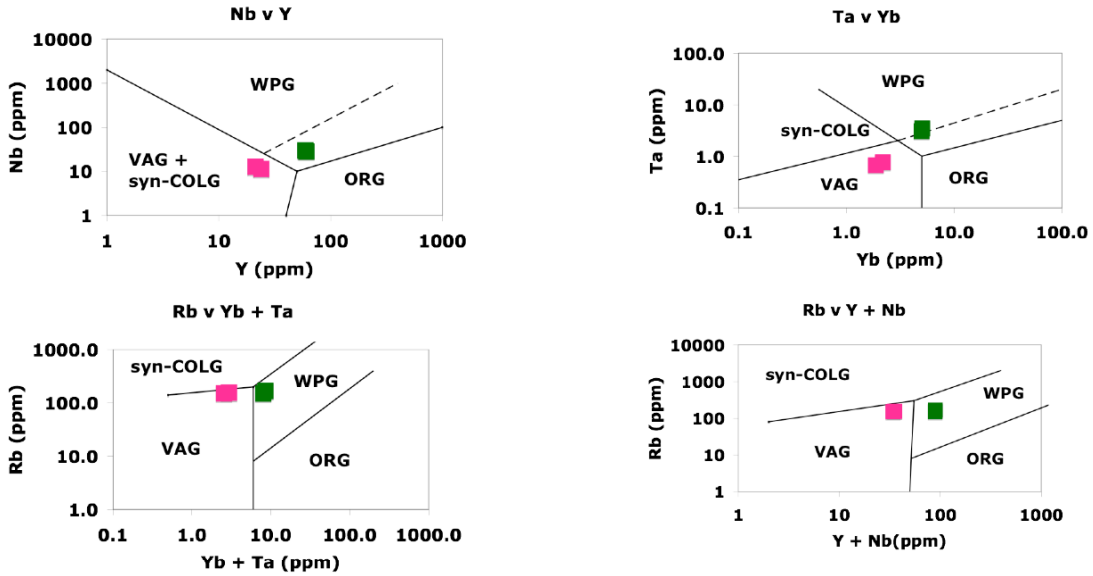


Fig. 6.6 Discrimination charts for tectonic settings (a) Nb v Y; (b) Ta v Yb; (c) Rb v Yb + Ta; (d) Rb v Y + Nb. Key as in Fig. 1. VAG = volcanic arc granites; syn-COLG = syn-collisional granites; WPG = within plate granites; ORG = ocean-ridge granites, the dashed line marks the field boundary for anomalous ridges from ORG (Pearce *et al.*, 1984). These charts are for an indication only, particularly as the samples plot very close to discrimination boundaries.

The similarity in geochemistry of the wholerock and glass within the xenoliths provides further evidence for equilibrium melting within the xenoliths (Fig. 6.1). The main difference is a slight negative anomaly in Zr and Hf within the glass (which is expected due to the two fspar + qtz equilibrium melt) and greater enrichment of compatible elements such as Tb, Y and Yb which go more easily into melt (Fig. 6.1).

The two subgroups also form distinct trends within the orthopyroxene major and trace element geochemistry. The negative Eu anomaly observed within the pyroxene grains is also observed within wholerock geochemistry. Two large euhedral grains (up to 3.5 mm) from samples #17912 and 17918 were measured and have similar compositions (Or 46 to 57; Ab 40 to 50). A euhedral grain adjacent to the large grain in #17918 has an anorthoclase composition with (Or 11; Ab 67). These provide a good indication of K-spar composition prior to deformation (Figs. 3.47-3.48).

(c) Sample #17915 Comparison to Felsic Groups A and B

The glass is less prevalent in this sample compared to felsic group A and B samples, with a dominant orthopyroxene, magnetite and plagioclase symplectite texture instead. It is possible that lower degrees of partial melting occurred due to the different composition and fewer alkali feldspar grains (observed in petrography and mineral geochemistry) required to promote the equilibrium melting of two fspar+qtz and/or less entrainment time. The greater abundance of euhedral grains reflects less exposure to deformation compared to felsic groups A and B.

The orthopyroxene, magnetite and plagioclase symplectite texture in zones with straight edges supports the occurrence of another mafic component, aside from clinopyroxene that is intergrown with feldspar and quartz throughout the sample. The symplectite texture most likely results from the breakdown of another mineral, and the common orientation of orthopyroxene and magnetite grains within this texture may follow previous cleavage planes. The coronas rimming quartz grains suggest that quartz was involved in the reaction.

The variable trace element pattern in glass from sample #17915 compared to felsic groups A and B highlights variation observed in petrography. The extreme enrichment in HREE

and positive Nb, Ta and Ti anomalies are notable differences. The latter suggests that it has a weaker crustal signature compared to the felsic group and/or that the glass is derived from melting of a source with appreciable modal garnet and/or ilmenite (Rollinson, 1993). Given this evidence, it is a possibility that garnet is the mineral that has broken down to form the symplectite texture. O'Reilly *et al.* (1989) described such textures in crustal xenoliths of southeastern Australia and Zhao *et al.* (2000) reported a decompression induced reaction of grt + qtz + O_2 = opx + plag + mag with a similar symplectic texture. As discussed by O'Reilly *et al.* (1989), Kay and Kay (1983) suggested a decrease in pressure caused garnet to breakdown and create the symplectite textures. However Rudnick and Taylor (1987) thought that olivine and pyroxene brokedown by isobaric cooling to cause the symplectites.

(d) Geothermometry

The temperatures for the last event within the felsic group range from 851 °C (sample #17911), based on Fe-Ti exchange in oxides to 966 °C (sample #17915) based on two pyroxene compositions (Wood and Banno, 1973; Wells, 1977). High temperate phases of up to 900°C are also identified within the feldspar compositions, all of which constrain the xenoliths within the granulite facies. Using the geotherms discussed by Sutherland *et al.* (1998) once again, a depth of ~ 30 km may be inferred. This is in agreement with the depth range obtained for the Selwyn Block in seismic profiles of 12 to 39 km (Cayley *et al.*, 2008). These pressure constraints also provide minimum depth regimes for the host basaltic icelandite, ie to entrain the xenoliths they must have come from at least the depth of the xenoliths.

(e) Felsic Group A U-Pb Zircon Dating

The given populations and scatter of ages present a complex evolutionary history for the felsic group A rocks. A similar range was observed in SHRIMP U-Pb zircon dating undertaken on one of these xenoliths (Graham *et al.*, 2006) (Fig. 6.3).

There are two distinct features observed within the results. Firstly, a sharp drop in the Th/U ratios at 460 Ma (Fig. 6.3); and secondly at 460 Ma, the Hf ratios form a more homogeneous trend compared to the cluster from 577 to 493 Ma which exhibits a strong mixing signature (Fig. 6.3). Given the evidence to support deformation, being

petrography, zircon morphology and Th/U ratios, it is proposed that the xenoliths have been exposed to two deformational events.

The first deformation event, from ~520 to 490 Ma, caused the U-Pb system to be reset following Pb loss, whilst retaining the mixed Hf composition of the rock. Such a process was reported by Bomparola *et al.* (2007) in a study of zircons from rocks in Antarctica, where a scatter in concordant ages similar to those in this study was observed. Deformation within the region has been reported from ~ 514 to 490 Ma, relating to the termination of the Ross/Delemarian orogens (Foden *et al.*, 2006; Berry *et al.*, 2007).

The second deformation event was rather prolonged, beginning with the sharp drop in Th/U ratios at 460 Ma, until the youngest age recorded for zircons from the felsic xenoliths, being 343 Ma (Fig. 6.3). During this time, homogenisation of Hf isotope composition occurred and metamorphic zircon growth occurred. New growth is supported by the concordant ages obtained and drastic change in Th/U ratios. It is inferred that the second deformation event relates to the Lachlan supercycle from 490 Ma to 320 Ma (Glen, 2005).

A crystallisation age for the felsic group A xenoliths is given by the combined peak at 553±2 Ma (Fig. s4.20). The Hf composition provides evidence for a mixed source, with input from both depleted mantle and crustal sources, as with the wholerock Nd. An average T_{DM}^{C} of 1.12 Ga is calculated (Fig. 6.3) which is similar to the wholerock Nd T_{DM} of 1.13 Ga. A possible T_{DM}^{C} of ~ 1.70 Ga for grains exhibiting the strongest crustal Hf signature is also apparent. This coincides with the 1691 Ma xenocrystic grain in the mafic group and provides evidence of the crustal source for the felsic rocks as the Willyama series (Broken Hill, NSW) has been dated at ~ 1700 Ma (Greenhalgh and Jeffery, 1959). 1700 Ma age peaks were also observed within the Mt Terrible Formation (SA), possibly derived from SW Gondwana (Ireland, 1997; Ireland *et al.*, 1998).

Various peaks of ~ 600 to 500 Ma have been identified in detrital zircon grains within the Lachlan Fold Belt and Hawkesbury Sandstone (NSW) and inherited grains within Lachlan Fold Belt granites (Veevers, 2003; Veevers, 2004; Veevers *et al.*, 2006; Veevers and Saeed, 2008). These grains have been traced back to the Transantarctic mountains during Gondwanan times. They exhibit low HREE and are possibly derived from carbonatite

magmas, with relatively strong crustal signatures determined by Hf isotope analysis. Although the felsic group A grains share a similar age to these grains, they are derived from a different magma type (70-75% SiO_2 by CART calculations (Belousova *et al.*, 2002)), have high HREE values and show a mixed Hf signature which is not reflected within the detrital grains of the Lachlan Orogen. At ~ 550 Ma, the Victorian microcontinent (now believed to be the Selwyn Block) was located offshore of southeastern Australia and rifting along the Kanmantoo Marginal Basin commenced (Scheibner and Veevers, 2000). This rifting and associated volcanics (Mount Arrowsmith) (Scheibner and Veevers, 2000) is likely to have provided sufficient heat for melting of the Victorian microcontinent and assimilation to produce the felsic group A rocks. This would also account for the mixed signature seen in Hf isotope composition. Within the area, Mount Arrowsmith has ages of ~ 580 Ma and Mount Wright ~ 530 Ma (Crawford *et al.*, 1997).

(f) Comparison with NVP and/or Selwyn Block

There is much evidence to support an association of the felsic group samples with the Selwyn Block. For example there are strong crustal signatures in isotopes and trace elements, Neoproterozoic/Cambrian age range and granulite facies characteristics. One distinct difference is that the composition is more felsic compared to outcrops of the Selwyn Block so far recorded on the coast of Victoria and Tasmania. However, these outcrops are 100 kms away and are easily explainable by differences in depth and/or geological processes over such a distance. This is seen in the seismic sections by Cayley (2008; Appendix 2) which identify mafic and felsic compositions separately.

Compared to the Lachlan Orogen granites, the felsic group has similar major element geochemistry to that of average values for A-type granites. However, trace elements such as Ga, Pb, Y, Zr and Zn are similar to S and I-type granites. Strontium isotope values are within range of Encounter Bay granites (0.707 to 0.719 at 500 Ma); average metasedimentary values for the Kanmantoo Group ($^{87}Sr/^{86}Sr$ ~ 0.720 at 400 Ma (Gray and Webb, 1995)), Cooma high grade terrain and Gundowring ($^{87}Sr/^{86}Sr$ ~ 0.722 at 370 Ma) (Gray, 1990) and Cooma Granodiorite (0.718 at 420 Ma; McCulloch and Chappell (1982)). However, Nd values are less radiogenic (McCulloch and Chappell, 1982). The strontium values are within range of the Heemskirk granites of western Tasmania (red granites 0.724; white A granites 0.732 at 353 Ma; (Brooks and Compston, 1965)), whilst

the Blue Tier Batholith of the Bassian granite province, NE Tasmania had stronger continental/metasedimentary affinities with lower Nd and higher Sr values (Sun and Higgins, 1996). The connection with the Kanmantoo Group provides evidence for the evolution of the Selwyn Block and its proximity to the Kanmantoo Marginal Basin.

6.1.5 Sample #17917 (Petrographic Felsic Group 3)

The textures in this sample are suggestive of high temperature metamorphism, with quartz basically forming a leucosome around feldspar grains.

The presence of the calcite in veins suggests that the carbonate was deposited from a fluid. The proximity of the calcite aggregate to contact with the host lava may suggest that the host was the source of such a fluid. However, it cannot be confirmed, and the calcite may also be of a later secondary origin. As calcite appears to be replacing plagioclase, it would suggest that the plagioclase is Ca-rich. The quartz, plagioclase and clinopyroxene appear to be in equilibrium, suggesting an equilibrium state prior to introduction of the carbonate-bearing fluid. Interestingly, calcite quartz gneiss has been identified at Mt Wright within the Ponto beds, proximal to the Mount Arrowsmith volcanics (Crawford *et al.*, 1997).

6.1.6 Stewart Hill

Glass is located throughout the samples but it has little effect on the minerals aside from the fine rims. There is no evidence for a cumulate setting for this sample as in the mafic samples, nor partial melt as in the felsic samples. This may be due to the scoriaceous host material, rather than the basaltic icelandite lava that hosts the Upper Coliban Dam suites. The spindle growths suggest quenching, either by depressurisation or cooling.

(a) Stewart Hill Suite

The samples in this suite are similar to the basaltic icelandite host based on major element geochemistry and TAS plot (Fig. 5.1) classifications. The suite shares other similarities with the host basaltic icelandite including (Mg#, TiO_2, FeO, CaO, Ba, La, Nd). It also has a similar overall trace element trend with decreasing enrichment relative to chondrite with compatibility (Fig. 6.1), except for the mobile elements such as Rb, Th and K where the xenoliths are depleted. This is characteristic of lower crust (Price *et al.*, 1997) although it may also reflect those elements being partitioned into the melt. The trace element pattern

within the Stewart Hill samples is rather sporadic, possibly resulting from a high degree of weathering of the samples.

The Stewart Hill samples are scattered and inconsistent in basaltic discrimination plots (Fig. 6.2) ranging from MORB to volcanic arc basalts, likely reflecting their basaltic andesite composition.

Based on isotopic evidence, the suite is derived from a source close to BSE, with slight enrichment. $^{87}Sr/^{86}Sr$ values are sporadic, most likely resulting from superficial contamination/weathering of the samples (Fig. 4.7).

As observed in wholerock geochemistry, this suite has the highest Mg# values in pyroxene geochemistry. The samples analysed have distinct differences in mineral geochemistry, plotting in two clusters. The negative linear trend observed in Ti within the clinopyroxene grains may be due to Ti being fractioned into kaesurtite. The large spread of Ca is most likely related to dominant exsolution within the clinopyroxene grains. Two pyroxene geothermometry yields temperatures of ~ 800 °C for formation of sample #19002 within this suite (Table 6.1).

(b) Comparison to NVP and/or Selwyn Block

As for the intermediate group, age constraints would assist when comparing the Stewart Hill Suite with both the NVP and Selwyn Block. Major element geochemistry is very similar to the basaltic icelandite. However, as discussed by Price *et al.* (1997), there is no evidence to suggest that the basaltic icelandite is directly related to the rest of the NVP rocks.

6.2 Timeline

A timeline for the evolution of the xenoliths is provided in Fig. 6.7 below. This incorporates associated tectonic activities associated with the formation and breakdown of Gondwana and NVP igneous activity.

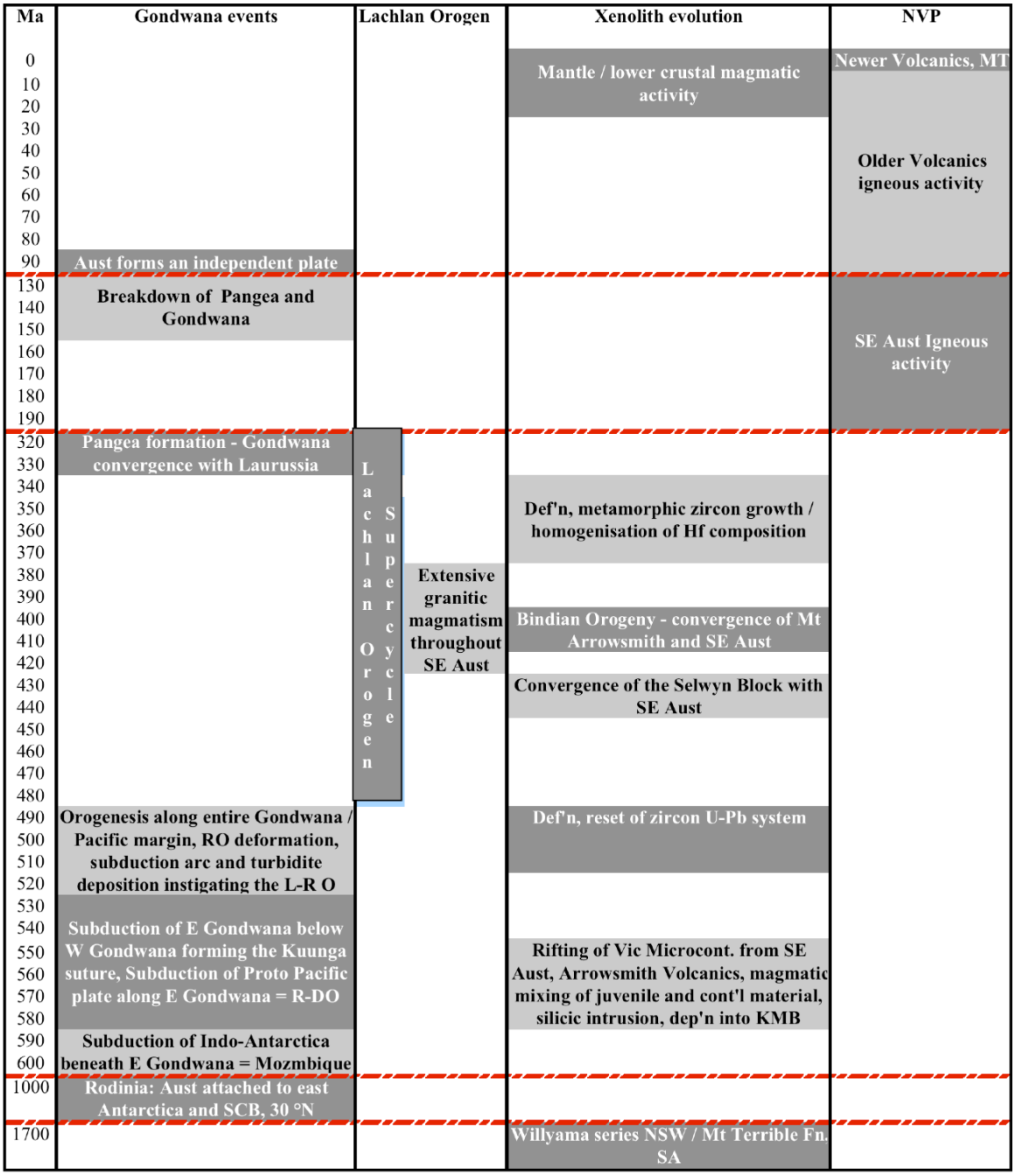


Fig. 6.7 Time line for the evolution of the xenoliths and associated tectonic activity. Red line = an interval of time; TM = Trentham-Macedon Complex; SE Aust = southeastern Australia; L-R O = Lachlan-Robertson Orogen; KMB – Kanmantoo Marginal Basin; E Gondwana – east Gondwana; W Gondwana – west Gondwana; SCB – South China Block.

7 Conclusion

The xenoliths of Upper Coliban Dam and Stewart Hill sample a diverse range of the underlying geology that reflect the complex nature of the region, including a heterogeneous mantle and transitional crust to mantle zone (Griffin *et al.*, 1984; Griffin and O'Reilly, 1986). All evidence, including petrography, isotopes, major and trace element geochemistry, suggest that each of the xenolith groups is derived from different processes and not directly related.

Zircon U-Pb dating suggests that the Upper Coliban Dam mafic group was emplaced at a similar time to NVP volcanic activity. Although there are similarities in Sr isotopes, geochemically there are no strong ties relating the mafic group with NVP activity. The mafic group xenoliths were formed in a cumulate environment within an intraplate setting similar to the NVP. It is possible that the heat source and processes that caused the NVP volcanic activity were also involved in the emplacement of the mafic group. One intermediate group sample (#17922) has strong geochemical and isotopic affinities with the NVP plains series, reflecting a more evolved composition.

The Upper Coliban Dam Felsic xenoliths crystallised at ~ 553 Ma and have experienced granulite facies deformation associated with the Delamerian and Lachlan Orogen, right up until the termination of the Lachlan Orogen at ~ 340 Ma. They are derived from a mixed source with both juvenile and crustal input, most likely in a rifting environment associated with the Kanmantoo Marginal Basin. Strontium isotope composition is a strong linking point with the Kanmantoo Group. The xenoliths experienced equilibrium melting upon entrainment with heat provided by the host basaltic icelandite. These xenoliths provide further evidence for the Selwyn Block, including both igneous and sedimentary (sample #17917) components, some of which were formed at high pressure (sample #17915).

There are similarities with the Lachlan Orogen granites, including Neoproterozoic ages of inherited grains and strontium composition. The strongest strontium isotope associations are with the Cooma granodiorite and meta-sedimentary components of the Cooma High Grade and Gundowring terrains. Hafnium isotope analyses on 550 Ma grains would provide further support for the Selwyn Block being a source for Lachlan Orogen granites

and confirm the Selwyn Block as a source for inherited grains rather than just the Transantarctic Mountains and Ross Orogen. Similarities in Sr isotope composition are also noted with Encounter Bay granites (South Australia) and Heemskirk granites of western Tasmania.

Much more information may be derived from the extensive data collected within this study. Trace element geochemistry may be investigated further to formulate melt models and gain a better understanding of magmatic processes that were involved in the formation of all of the xenoliths. Also, a more thorough comparison with the granite suites of the Lachlan Orogen will provide further evidence of the Selwyn Block being a source for these granites.

References

Aguirre-Diaz, G. J., Dubois, M., Laureyns, J. and Schaaf, P. (2002). Nature and P-T Conditions of the Crust Beneath the Central Mexican Volcanic Belt Based on a Precambrian Crustal Xenolith. *International Geology Review* **44**: 222-242.

Allaby, A. and Allaby, M. (2003). Dictionary of Earth Sciences. 2nd. Oxford, Oxford University Press**:** 608.

Bayhan, H., Aydar, E., Sen, E. and Gourgaud, A. (2006). Melting of crustal xenoliths within ascending basalt: Example from the Kula volcanic field, western Anatolia, Turkey. *Comptes Rendus Geosciences* **338**(4): 237-243.

Belousova, E. (2000). Trace elements in zircon and apatite: Applicationto petrogenesis and mineral exploration. GEMOC ARC National Key Centre, Earth and Life Science Department. Sydney, Macquarie University. **PhD:** 310.

Belousova, E. A., Griffin, W. L., O'Reilly, S. and Fisher, N. I. (2002). Igneous zircon: trace element composition as an indicator of source rock type. *Contributions to Mineralogy and Petrology* **143**: 602-622.

Berry, R. F., Chmielowski, R. M., Steele, D. A. and Meffre, S. (2007). Chemical U - Th - Pb monazite dating of the Cambrian Tyennan Orogeny, Tasmania. *Australian Journal of Earth Sciences* **54**(5): 757 - 771.

Blichert-Toft, J. (2001). On the Lu-Hf Isotope Geochemistry of Silicate Rocks. *Geostandards Newsletter* **25**(1): 41-56.

Boger, S. D. and Miller, J. M. (2004). Terminal suturing of Gondwana and the onset of the Ross-Delamerian Orogeny: the cause and effect of an Early Cambrian reconfiguration of plate motions. *Earth and Planetary Science Letters* **219**(1-2): 35-48.

Bomparola, R. M., Ghezzo, C., Belousova, E., Griffin, W. L. and O'Reilly, S. Y. (2007). Resetting of the U-Pb Zircon System in Cambro-Ordovician Intrusives of the Deep Freeze Range, Northern Victoria Land, Antarctica. *J. Petrology* **48**(2): 327-364.

Brooks, C. and Compston, W. (1965). The Age and Initial Sr87/Sr86 of the Heemskirk Granite, Western Tasmania. *Journal of Geophysical Research* **70**(24): 6249-62.

Brooks, C. and Compston, W. (1965). The Age and Initial Sr87/Sr86 of the Heemskirk Granite, Western Tasmania. *Journal of Geophysical Research* **70**(24): 6249-62.

Carmichael, I. S. E. (1964). The petrology of Thingmuili, a Tertiary volcano in Eastern Iceland. *Journal of Petrology* **5**: 435-460.

Cas, R. A. F. and Simpson, C. (1993). Excursion Guide: Newer Volcanics Province - Processes and Products of Phreatomagmatic Activity. IA VCEI General Assembly. Canberra, Australian Geological Survey Organisation.

Cayley, R. A., Korsch, R. J., Willman, C. E., Costelloe, R. D., Nakamura, A., Rawling, T. J., Morand, V. J., Skladzien, P. B. and O'Shea, P. J. (2008). Text to support the 2006 Central Victorian deep crustal seismic survey data release and 'Presentation to Industry', 22 February 2008, GeoScience Victoria, pmd*CRC and Geoscience Australia.

Cayley, R. A., Taylor, D. H., VandenBerg, A. H. M. and Moore, D. H. (2002). Proterozoic - Early Palaeozoic rocks and the Tyennan Orogeny in central Victoria: the Selwyn

Block and its tectonic implications. *Australian Journal of Earth Sciences* **49**(2): 225 - 254.

Chappell, B. W. and White, A. J. R. (1974). Two contrasting granite types. *Pacific Geology* **8**: 173-174.

Chappell, B. W. and White, A. J. R. (1985). Granites and the Victorian lithosphere. In: *Abstracts of the Victorian Lithosphere Symposium.* A. H. M. VandenBerg. Melbourne, Lithosphere Transect Studies of the Australian Continent, Victorian Working Group**:** 10-11.

Clemens, J. D. (1988). Volume and composition relationships between granites and their lower crustal source regions: An example from central Victoria, Australia. *Australian Journal of Earth Sciences* **35**(4): 445-449.

Condie, K. C. (2004). Supercontinents and superplume events: distinguishing signals in the geologic record. *Physics of the Earth and Planetary Interiors* **146**: 319-332.

Condie, K. C., Des Marais, D. J. and Abbott, D. (2000). Geologic evidence for a mantle superplume event at 1.9Ga. *Geochemistry Geophysics Geosystems* **1**.

Cox, K. G., Bell, J. D. and R.J., P. (1979). The interpretation of igneous rocks. London, George and Unwin

Crawford, A. J., Cameron, W. E. and Keays, R. R. (1984). The association boninite low-ti andesite-tholeiite in the heathcote greenstone belt, Victoria; ensimatic setting for the early lachlan fold belt. *Australian Journal of Earth Sciences* **31**(2): 161 - 175.

Crawford, A. J., Stevens, B. P. J. and Fanning, M. (1997). Geochemistry and tectonic setting of some Neoproterozoic and Early Cambrian volcanics in western New South Wales. *Australian Journal of Earth Sciences* **44**(6): 831 - 852.

Dai, B.-Z., Jiang, S.-Y., Jiang, Y.-H., Zhao, K.-D. and Liu, D.-Y. (2008). Geochronology, geochemistry and Hf-Sr-Nd isotopic compositions of Huziyan mafic xenoliths, southern Hunan Province, South China: Petrogenesis and implications for lower crust evolution. *Lithos* **102**(1-2): 65-87.

Davis, D. W., Gray, J. and Cumming, G. L. (1977). Determination of the 87Rb decay constant *Geochimica et Cosmochimica Acta* **41**: 1745-9.

Dessai, A. G., Markwick, A., Vaselli, O. and Downes, H. (2004). Granulite and pyroxenite xenoliths from the Deccan Trap: insight into the nature and composition of the lower lithosphere beneath cratonic India. *Lithos* **78**(3): 263-290.

Dickin, A. P. (2005). Radiogenic isotope geology. Cambridge, Cambridge University Press, 492pp

Dodge, F. C. W., Calk, L. C. and Kistler, R. W. (1986). Lower Crustal Xenoliths, Chinese Peak Lava Flow, Central Sierra Nevada. *J. Petrology* **27**(6): 1277-1304.

Elburg, M. A. (1996). U-Pb ages and morphologies of zircon in micrograniteoid enclaves and peraluminous host granite: evidence for magma mingling. *Contributions to Mineralogy and Petrology* **123**(2): 177-189.

Ellis, D. J. and Green, D. H. (1979). An experiemental stdy on the effect of Ca upon garnet-clinopyroxene Fe-Mg exchange equilibria. *Contributions to Mineralogy and Petrology* **71**: 13-22.

Ewart, A. (1985). Aspects of the mineralogy and chemistry of the intermediate-silicic Cainozoic volcanic rocks of eastern Australia. Part 2: Mineralogy and petrogenesis. *Australian Journal of Earth Sciences* **32**(4): 383 - 413.

Ewart, A., Chappell, B. W. and Maitre, R. W. L. (1985). Aspects of the mineralogy and chemistry of the intermediate-silicic Cainozoic volcanic rocks of eastern Australia. Part 1: Introduction and geochemistry. *Australian Journal of Earth Sciences* **32**(4): 359 - 382.

Fergusson, C. L. (2003). Ordovician, Silurian accretion tectonics of the Lachlan Fold Belt, southeastern Australia. *Australian Journal of Earth Sciences* **50**(4): 475.

Flanagan, F. J. (1984). Three USGS mafic rock reference samples, W-2, DNC-1, and BIR-1. *U.S. Geological Survey Bulletin* **1623**: 54.

Foden, J., Elburg, M. A., Dougherty-Page, J. and Burtt, A. (2006). The Timing and Duration of the Delamerian Orogeny: Correlation with the Ross Orogen and Implications for Gondwana Assembly. *The Journal of Geology* **114**(2): 189-210.

Fodor, R. V. and Vandermeyden, H. J. (1988). Petrology of gabbroic xenoliths from Mauna Kea Volcano, Hawaii. *Journal of Geophysical Research* **93**(B5): 4435-4452.

Folk, R. L. (1974). Petrology of sedimentary rocks : The University of Texas. Austin, Texas, The University of Texas, Hemphill, 182pp

Foster, D. A. and Gray, D. R. (2000). Evolution and Structure of the Lachlan Fold Belt (Orogen) of Eastern Australia. *Annual Review of Earth & Planetary Sciences* **28**(1): 47-80.

Gao, S., Liu, X., Yuan, H., Hattendorf, B., Gunther, D., Chen, L. and Hu, S. (2002). Determination of forty two major and trace elements in USGS and NIST SRM glasses by laser ablation-inductively coupled plasma-mass spectrometry. *Geostandards Newsletter* **26**: 181-196.

Ghiorso, M. S. and Evans, B. W. (In press). Thermodynamics of rhombohedral oxide solid solutions and a revision of the Fe-Ti two-oxide geothermometer and oxygenbarometer. *American Journal of Science* **308**.

Gladney, E. S. and Roelandts, I. (1988). 1987 compilation of elemental concentration data for USGS BIR-1, DNC-1, and W-2. *Geostandards Newsletter* **12**: 63-118.

Glen, R. A. (2005). The Tasmanides of eastern Australia. In: *Terrane Processes at the Margins of Gondwana.* A. P. M. Vaughan, P. T. Leat and R. J. Pankhurst. London, Geological Society Special Publications. **246:** 23-96.

Govindaraju, K. (1994). 1994 compilation of working values and descriptions for 383 geostandards. *Geostandards Newsletter* **118**: 1-158.

Graham, I. T., Hollis, J. D., Sutherland, F. L. and Joyce, E. B. (2003). Insights into the Newer Volcanics Province of Victoria. Specialist Group in Geochemistry, Mineralogy and Petrology Field Guide, Geological Society of Australia, Specialist Group in Geochemistry, Specialist Group in Geochemistry, Mineralogy and Petrology

Graham, I., Fanning, M. and Sutherland, L. (2006). Neoproterozoic charnokitic xenoliths from central Victoria: zircon SHRIMP dating and preliminary geochemistry.

Australian Earth Sciences Convention 2006. Melbourne, Geoscience Society of Australia.

Gray, C. M. (1990). A strontium isotopic traverse across the granitic rocks of southeastern Australia: Petrogenetic and tectonic implications. *Australian Journal of Earth Sciences* **37**(3): 331 - 349.

Gray, C. M. and Webb, J. A. (1995). Provenance of Palaeozoic turbidites in the Lachlan Orogenic Belt: Strontium isotopic evidence. *Australian Journal of Earth Sciences* **42**(1): 95 - 105.

Gray, D. R. and Foster, D. A. (2004). Tectonic evolution of the Lachian Orogen, southeast Australia: historical review, data synthesis and modern perspectives. *Australian Journal of Earth Sciences* **51**(6): 773-817.

Gray, D. R., Foster, D. A., Morand, V. J., Willman, C. E., Cayley, R. A., Spaggiari, C. V., Taylor, D. H., Gray, C. M., VandenBerg, A. H. M., Hendricks, M. A. and Wilson, C. J. L. (2003). Structure, metamorphism, geochronology and tectonics of Palaeozoic rocks: interpreting a complex, long lived orogenic system. In: *Geology of Victoria.* W. D. Birch. Victoria, Geological Society of Australia Special Publication**:** 361-375.

Greenhalgh, D. and Jeffery, P. M. (1959). A contribution to the pre-Cambrian chronoogy of Australia. *Geochimica et Cosmochimica Acta* **16**: 39-57.

Griffin, W. L. and O'Reilly, S. (1986). The lower crust in eastern Australia: xenolith evidence. In: *The Nature of the Lower Continental Crust.* J. B. Dawson, D. A. Carswell, J. Hall and K. H. Wedepohl. Oxford, Blackwell Scientific Publications for the Geological Society**:** 363-374.

Griffin, W. L., Belousova, E. A., Shee, S. R., Pearson, N. J. and O'Reilly, S. Y. (2004). Archean crustal evolution in the northern Yilgarn Craton: U–Pb and Hf-isotope evidence from detrital zircons. *Precambrian Research* **131**: 231-282.

Griffin, W. L., Pearson, N. J., Belousova, E. A. and Saeed, A. (2007). Reply to "Comment to short-communication 'Comment: Hf-isotope heterogeneity in zircon 91500' by W.L. Griffin, N.J. Pearson, E.A. Belousova and A. Saeed (Chemical Geology 233 (2006) 358-363)" by F. Corfu. *Chemical Geology* **244**: 354-356.

Griffin, W. L., Pearson, N. J., Belousova, E. A., Jackson, S. E., van Achterbergh, E., O'Reilly, S. Y. and Shee, S. R. (2000). The Hf isotope composition of cratonic mantle: LAM-MC-ICPMS analysis of zircon megacrysts in kimberlites. *Geochimica et Cosmochimica Acta* **64**: 133-147.

Griffin, W. L., Wass, S. Y. and Hollis, J. D. (1984). Ultramafic xenoliths from Bullenmerri and Gnotuk maars, Victoria, Australia: petrology of a sub-continental crust-mantle transition. *Journal of Petrology* **25**: 53-87.

Haase, K. M., Goldschmidt, B. and Dieter Garbe-Schonberg, C. (2004). Petrogenesis of Tertiary Continental Intra-Plate Lavas from the Westerwald Region, Germany. *Journal of Petrology* **45**(5): 883-905.

Harris, N. B. W., Pearce, J. A. and Tindle, A. G. (1986). Geochemical characteristics of collision-zone magmatism. In: *Collision tectonics.* M. P. Coward and R. C. Reis, Geological Society Special Publication. **19:** 67-81.

Hollocher, K. (2007). CIPW Norm Spreadsheet. Schenectady, Union College, hollochk@union.edu.

Holm, P. M. (2002). Data report: on the composition of the lower ocean crust—major and trace element analyses of gabbroic rocks from Hole 735B, 500–1500 mbsf. In: *Proceedings ODP, Scientific Results*. J. G. Natland, H. J. B. Dick, D. J. Miller and R. P. Von Herzen. Texas, Ocean Drilling Program. **176:** 1-13.

Hoskin, P. W. O. and Schaltegger, U. (2003). The composition of zircon and igneous and metamorphic petrogenesis. *Reviews in Mineralogy and Geochemistry* **53**: 27-62.

Ireland, T. R. (1997). Neoproterozoic history of the Southwest Pacific margin of Gondwana as recorded in Neoproterozoic-lower Paleozoic sediments. Abstracts with Programs - Geological Society of America, 1997 Annual Meeting, San Francisco, Geological Society of America.

Ireland, T. R., Flottmann, T., Fanning, C. M., Gibson, G. M. and Preiss, W. V. (1998). Development of the early Paleozoic Pacific margin of Gondwana from detrital-zircon ages across the Delamerian orogen. *Geology* **26**(3): 243-246.

Jackson, S. E., Pearson, N. J., Griffin, W. L. and Belousova, E. A. (2004). The Application of Laser Ablation Microprobe-Inductively Coupled Plasma-Mass Spectrometry (LAM-ICP MS) to In Situ U-Pb Zircon Geochronology. *Chemical Geology* **211**: 47-69.

Johnson, R. W. (1989). Intraplate volcanism and tectonics in eastern Australia and New Zealand. Cambridge, Cambridge University Press, 408pp

Joyce, E. B. (1975). Quaternary volcanism and tectonics in southeastern Australia. In: *Quaternary Studies*. R. P. Suggate and M. M. Creswell, Royal Society of New Zealand Bulletin. **13:** 169-176.

Jung, C., Jung, S., Hoffer, E. and Berndt, J. (2006). Petrogenesis of Tertiary Mafic Alkaline Magmas in the Hocheifel, Germany. *Journal of Petrology* **47**(8): 1637-1671.

Kay, S. M. and Kay, R. W. (1983). Thermal history of the deep crust inferred from granulite xenoliths, Queensland, Australia. *American Journal of Science* **283A**: 486-513.

Le Maitre, R. (2002). Igneous Rocks: A Classification and Glossary of Terms. Cambridge, Cambridge University Press

Le Maitre, R., Bateman, P., Dudek, A., Keller, J., Lameyre Le Bas, M. J., Sabine, P. A., Schmid, R., Sorensen, H., Streckeisen, A., Woolley, A. R. and Zenettin, B. (1989). A classification of igneous rocks and glossary of terms. Oxford, Blackwell

Li, Z. X. and Powell, C. M. (1993). Late Proterozoic to early Paleozoic paleomagnetism and formation of Gondwanaland. In: *Gondwana Eight Assembly, Evolution and Dispersal*. R. H. Findlay, R. Unrug, M. R. Banks, J. J. Veevers and A. A. Balkema. Rotterdam, AA Balkema**:** 9-21.

Li, Z. X. and Powell, C. M. (2001). An outline of the palaeogeographic evolution of the Australasian region since the beginning of the Neoproterozoic. *Earth-Science Reviews* **53**: 237-277.

Lister, G. S. and Etheridge, M. A. (1989). Detachment moels for uplift and volcanism in the Eastern Highlands and their applications to the origin of passive margin mountains. In: *Intraplate volcanism in Eastern Australia and New Zealand.* R. W. Johnson. Cambridge, Cambridge University Press**:** 297-313.

Lugmair, G. W. and Marti, K. (1978). Lunar initial 143Nd/144Nd: differential evolution of the lunar crust and mantle. *Earth and Planetary Science Letters* **39**: 349-357.

McBride, J. S., Lambert, D. D., Nicholls, I. A. and Price, R. C. (2001). Osmium isotopic evience for crust-mantle interaction in the genesis of continental intraplate basalts from the Newer Volcanics Province, Southeastern Australia. *Journal of Petrology* **42**(6): 1197-1218.

McCulloch, M. T. and Chappell, B. W. (1982). Nd isotopic characteristics of S- and I-type granites. *Earth and Planetary Science Letters* **58**(1): 51-64.

McDonough, W. F., McCulloch, M. T. and Sun, S. S. (1985). Isotopic and geochemical systematics in tertiary-Recent basalts from southeastern Australia and implications for the evolution of the sub-continental lithosphere. *Geochimica et Cosmochimica Acta* **49**: 2051-2067.

Meschede, M. (1986). A method of discriminating between different types of mid-ocean ridge basalts and continental tholeiites with the Nb-Zr-Y diagram. *Chemical Geology* **56**: 207-218.

Miller, J. M., Phillips, D., Wilson, C. and Dugdale, L. J. (2005). Evolution of a reworked orogenic zone: The boundary between the delamerian and lachlan fold belts, southeastern Australia *. *Australian Journal of Earth Sciences* **52**(6): 921-940.

Nekvasil, H. (1988). Calculated effect of anorthite component on the crystallization paths of H2O-undersaturated haplogranitic melts. *American Mineralogist* **73**: 966-981.

Nekvasil, H. (1990). Reaction relations in the granite system: implications for trachytic and syenitic magmas. *American Mineralogist* **75**: 560-71.

Nicholls, I. A., Greig, A. G., Gray, C. M. and Price, R. C. (1993). Excursion Guide: Newer Volcanics Province - Basalts, Xenoliths and Megacrysts (Record 1993/58). IA VCEI General Assembly. Canberra, Australian Geological Survey Organisation.

Norman, M. D., Griffin, W. L., Pearson, N. J., Garcia, M. O. and O'Reilly, S. Y. (1998). Quantitative analysis of trace element abundances in glasses and minerals: a comparison of laser ablation ICPMS, solution ICPMS, proton microprobe, and electron microprobe data. *J. Anal Atomic Spectrosc* **13**(477-482).

Norman, M. D., Pearson, N. J., Sharma, A. and Griffin, W. L. (1996). Quantitative analysis of trace elements in geological materials by laser ablation ICPMS: instrumental operating conditions and calibration values of NIST glasses. . *Geostandards Newsletter* **20**: 247-261.

Norris, K. and Hutton, J. T. (1969). *Geochimica et Cosmochimica Acta* **33**: 431-453.

O'Reilly, S. and Griffin, W. L. (1985). A xenolith-derived geotherm for southeastern australia and its geophysical implications. *Tectonophysics* **111**(1-2): 41-63.

O'Reilly, S., Griffin, W. L. and Gaul, O. (1997). Paleogeothermal gradients in Australia: key to 4-D lithosphere mapping. *AGSO Journal of Australian Geology & Geophysics* **17**: 63-72.

O'Reilly, S., Griffin, W. L. and Pearson, N. J. (1989). Xenoliths of Crustal Origin. In: *Intraplate Volcanism in Eastern Australia and New Zealand.* R. W. Johnson. Cambridge, Press Syndicate of the University of Cambridge in Association with the Australian Academy of Science**:** 408.

O'Reilly, S., Nicholls, I. A. and Griffin, W. L. (1989b). Xenoliths and Megacrysts of Mantle Origin. In: *Intraplate Volcanism in eastern Australia and New Zealand.* R. W. Johnson. Cambridge, Press Syndicate of the University of Cambridge in Association with Australian Academy of Science**:** 408.

Paul, B., Hergt, J. M. and Woodhead, J. D. (2005). Mantle heterogeneity beneath the Cenozoic volcanic provinces of central Victoria inferred from trace-element and Sr, Nd, Pb and Hf isotope data. *Australian Journal of Earth Sciences* **52**(2): 243 - 260.

Pearce, J. A. and Gale, G. H. (1977). Identification of ore-deposition enrivonment from trace element geochemistry of associated igneous host rocks. *Geological Society Special Publication* **7**: 14-24.

Pearce, J. A., Harris, N. B. W. and Tindle, A. G. (1984). Trace element discrimination diagrams for the tectonic interpretation of granitic rocks. *Journal of Petrology* **25**: 956-983.

Pin, C., Francisco, J. and Zalduegui, S. (1997). Sequential separation of light rare-earth elements, thorium and uranium by miniaturized extraction chromatography: Application to isotopic analyses of silicate rocks. *Analytica Chimica Acta* **339**: 79-89.

Powell, C. M. (1983). Tectonic Relationship between the Late Ordovician and Late Silurian palaeogeographies of southeastern Australia. *Australian Journal of Earth Sciences* **30**(3): 353 - 373.

Price, R. C., Gray, C. M. and Frey, F. A. (1997). Strontium isotopic and trace element heterogeneity in the plains basalts of the Newer Volcanic Province, Victoria, Australia. *Geochimica et Cosmochimica Acta* **61**(1): 171-192.

Price, R., Gray, C. M., Nicholls, I. A. and Day, A. (1988). Cainozoic volcanic rocks. In: *Geology of Victoria.* J. G. Douglass and J. A. Ferguson. Melbourne, Geological Soceity of Australia, Victorian Division**:** 439-451.

Price, R., Nicholls, I. A. and Gray, C. M. (2003). Cainozoic igneous activity. In: *Geology of Victoria.* W. D. Birch. Victoria, Geological Society of Australia Special Publication**:** 361-375.

Rollinson, H. R. (1993). Using Geochemical Data: Evaluation, Presentation, Interpretation. Harlow, Pearson Education Limited, 352pp

Rossiter, A. G. and Gray, C. M. (2008). Barium contents of granites: key to understanding crustal architecture in the southern Lachlan Fold Belt? *Australian Journal of Earth Sciences* **55**(4): 433 - 448.

Rudnick, R. L. and Gao, S. (2004). Composition of the Continental Crust. In: *Treatise on Geochemistry.* H. D. Holland and K. K. Turekian. Amsterdam, Elsevier. **3:** 1-64.

Rudnick, R. L. and Taylor, S. R. (1987). The composition and petrogenesis of the lower crust: a xenolith study. *Journal of Geophysical Research* **92**: 13981-14005.

Rutland, R. W. R. (1976). Orogenic evolution of Australia. *Earth Science Reviews* **12**: 161-196.

Salters, V. J. and Hart, S. R. (1991). The mantle sources of ocean ridges, islands and arcs: the Hf-isotope connection. *Earth and Planetary Science Letters* **104**: 364-80.

Saunders, A. D. and Tarney, J. (1984). Geochemical characteristics of basaltic volcanism within back-arc basins. In: *Marginal basin geology.* B. P. Kokelaar and M. F. Howells. London, Special Publication Geological Society. **16:** 59-76.

Scheibner, E. (1973). A plate tectonic model of the Palaeozoic tectonic history of New South Wales. *Journal of the Geological Society of Australia* **20**: 405-426.

Scheibner, E. (1974). Fossil fracture zones (transform faults), segmentationa nd correlation problems in the Tasman Fold Belt System. In: *The Tasman Geosyncline - a symposium in honour of Professor Dorothy Hill.* A. K. Denmead, G. W. Tweedale and A. F. Wilson. Brisbane, Geological Society of Australia, Queensland Division, Brisbane**:** 65-98.

Scheibner, E. (1985). Suspect terrans in the Tasman Fold Belt System, eastern Australia. In: *Tectonostratigraphic Terranes of the Circum-Pacific Region.* D. G. Howell. Houston, Circum-Pacific Council for Energy and Mineral Resources Earth Science Series **1**.

Scheibner, E. (1992). Influence of detachment-related passive margin Fold Belt System. *Tectonophysics* **214**: 401-416.

Scheibner, E. and Veevers, J. J. (2000). Tasman Fold Belt System. In: *Billion-year earth history of Australia and neighbours in Gondwanaland.* J. J. Veevers. Sydney, GEMOC Press**:** 388.

Scherer, E., Munker, C. and Mezger, K. (2001). Calibration of the lutetium-hafnium clock. *Science* **293**: 683-687.

Shaw, R. D., Wellman, P., Gunn, P., Whitaker, A. J., Tarlowski, C. and Morse, M. (1996). Australian Crustal Elements Map. Canberra, Australian Geological Survey Organisation**:** Record 1996/30.

Shelley, D. (1992). Igneous and metamorphic rocks under the microscope: classification, textures, microstructures and mineral preferred orientations. London, Chapman & Hall

Steiner, J. C., Jahns, R. H. and Luth, W. C. (1975). Crystallization of Alkali Feldspar and Quartz in the Haplogranite System NaAlSi3O8-KAlSi3O8-SiO2-H2O at 4 Kb. *Geological Society of America Bulletin* **86**(1): 83-98.

Streckeisen, A. (1974). Classification and nomenclature of plutonic rocks. *Geol. Rundsch.* **63**: 773–786.

Streckeisen, A. (1976). To each plutonic rock its proper name. *Earth-Science Reviews* **12**(1): 1-33.

Stump, E., White, A. J. R. and Borg, S. G. (1986). Reconstruction of Australia and Antarctica: evidence from granites and recent mapping. *Earth and Planetary Science Letters* **70**: 348-360.

Sun, S. S. (1980). Lead isotopic study of young volcanic rocks from mid-ocean ridges, ocean island and island arcs. *Phil. Trans. R. Soc.* **A297**: 409-445.

Sun, S. s. and Higgins, N. C. (1996). Neodymium and strontium isotope study of the Blue Tier Batholith, NE Tasmania, and its bearing on the origin of tin-bearing alkali feldspar granites. *Ore Geology Reviews* **10**(3-6): 339-365.

Sutherland, F. L. and Hollis, J. D. (unpublished Geotrack Reports).

Sutherland, F. L., Hollis, J. D., Birch, W. D., Pogson, R. E. and Raynor, L. R. (2004). Cumulate-rich xenolith suite in Late Cenozoic basaltic eruptives, Hepburn Lagoon, Newlyn, in relation to western Victorian lithosphere. *Australian Journal of Earth Sciences* **51**(3): 319-337.

Sutherland, F. L., Pogson, R. E., Barron, B. J., O'Reilly, S. Y., Griffin, W. L. and Gaul, O. (1998). Discussion and Reply Paleogeothermal gradients in Australia: key to 4-D lithosphere mapping. *Australian Journal of Earth Sciences* **45**(5): 817.

Sutherland, F. L., Raynor, L. R. and Pogson, R. E. (1994a). Spinel to garnet lherzolite transition in relation to high temperature palaeogeotherms, eastern Australia. *Australian Journal of Earth Sciences* **41**: 205-220.

Sutherland, F. L., Temby, P. A., Raynor, L. R. and Hollis, J. D. (1994b). A review of the East Australian diamond province. Diamonds: Characterization, Genesis and Exploration. Proceedings 5th International Kimberlite Conference, Araxa, Brazil, Compahia de Pesquisa de Recursos Minerals Special Publication 1/B.

Taylor, S. R. and McLennan, S. M. (1981). The composition and evolution of the continental crust: rare earth element evidence from sedimentary rocks. *Phil. Trans. R. Soc.* **A301**: 381-399.

Vandenberg, F. (2007). Saying goodbye to old friends- vale the Newer and Older Volcanics of Victoria. *tag: The Australian Geologist Newsletter* **143**(June 2007): 25-26.

Veevers, J. J. (2000). Billion-year earth history of Australia and neighbours in Gondwanaland Sydney, GEMOC PRESS, 388pp

Veevers, J. J., Belousova, E., Saeed, A., Sircombe, K., Cooper, A. F. and Read, S. E. (2005). Pan-Gondwanaland detrital zircons from Australia

Veevers, J. J. (2003). Pan-African is Pan-Gondwanaland: Oblique convergence drives rotation during 650-500 Ma assembly. *Geology* **31**(6): 501-504.

Veevers, J. J. (2004). Gondwanaland from 650-500 Ma assembly through 320 Ma merger in Pangea to 185-100 Ma breakup: supercontinental tectonics via stratigraphy and radiometric dating. *Earth-Science Reviews* **68**(1-2): 1-132.

Veevers, J. J. and Powell, C. M. (1984). Uluru and Adelaidean regimes: (d) Epi-Adelaidean: regional shear, (e) Cambrian: plate divergence on the east and north-west, followed by plate convergence on the east. In: *Phanerozoic Earth history of Australia.* J. J. Veevers. Oxford, Oxford University Press**:** 278-289.

Veevers, J. J. and Saeed, A. (2008). Gamburtsev Subglacial Mountains provenance of Permian-Triassic sandstones in the Prince Charles Mountains and offshore Prydz Bay: Integrated U-Pb and TDM ages and host-rock affinity from detrital zircons. *Gondwana Research* **14**(3): 316-342.

Veevers, J. J., Belousova, E. A., Saeed, A., Sircombe, K., Cooper, A. F. and Read, S. E. (2006). Pan-Gondwanaland detrital zircons from Australia analysed for Hf-isotopes and trace elements reflect an ice-covered Antarctic provenance of 700-500 Ma age, TDM of 2.0-1.0 Ga, and alkaline affinity. *Earth-Science Reviews* **76**(3-4): 135-174.

Veevers, J. J., Saeed, A. and O'Brien, P. E. (2008). Provenance of the Gamburtsev Subglacial Mountains from U-Pb and Hf analysis of detrital zircons in Cretaceous to Quaternary sediments in Prydz Bay and beneath the Amery Ice Shelf. *Sedimentary Geology* **211**(1-2): 12-32.

Vernon, R. H. (2004). A practical guide to Rock Microstructure. Cambridge, Cambridge University Press, 594pp

Vogel, D. C. and Keays, R. R. (1997). The petrogenesis and platinum-group element geochemistry of the Newer Volcanic Province, Victoria, Australia. *Chemical Geology* **136**(3-4): 181-204.

Weaver, B. L. and Tarney, J. (1984). Empirical approach to estimating the composition of the continental crust. *Nature* **310**: 557-75.

Weber, M. B. I., Tarney, J., Kempton, P. D. and Kent, R. W. (2002). Crustal make-up of the northern Andes: evidence based on deep crustal xenolith suites, Mercaderes, SW Colombia. *Tectonophysics* **345**(1-4): 49-82.

Wellman, P. (1974). Potassium-argon ages on the Cainozoic Volcanic rocks of Eastern Victoria, Australia. *Australian Journal of Earth Sciences* **21**(4): 359 - 376.

Wellman, P. and McDougall, I. (1974). Cainozoic igneous activity in eastern australia. *Tectonophysics* **23**(1-2): 49-65.

Wells, P. R. A. (1977). Pyroxene thermometry in simple and complex systems. *Contributions to Mineralogy and Petrology* **62**: 129-139.

White, A. J. R. and Chappell, B. W. (1983). Granitoid types and their distribution in the Lachlan Fold Belt, southeastern Australia. *Geological Society of America Bulletin* **159**: 21-34.

Wilshire, H. G. and Shervais, J. W. (1975). Al-augite and Cr-diopside ultramafic xenoliths in basaltic rocks from western United States. In: *Phisics and Chemistry or the Earth, 9*. L. H. Ahrens. New York, Pergamon Press**:** 257-272.

Wilson, M. (1989). Igneous Petrogenesis. London, Unwin Hyman

Winter, J. D. (2001). An introduction to igneous and metamorphic petrology. New Jersey, Prentice-Hall, 697pp

Wood, B. J. and Banno (1973). Garnet-orthopyroxene and orthopyroxene-clinopyroxene relationships in simple and complex systems. *Contributions to Mineralogy and Petrology* **42**: 109-121.

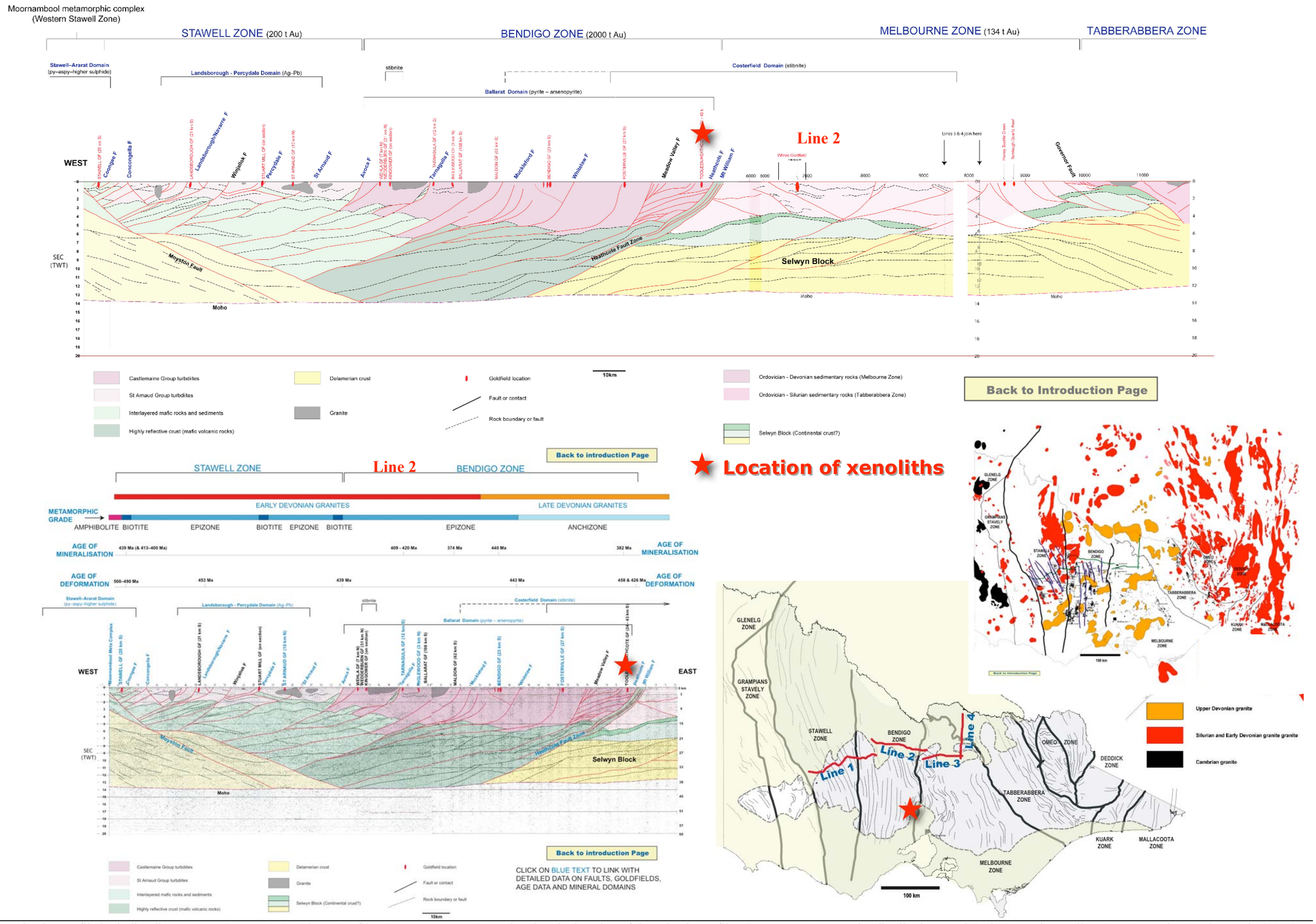
Wysoczanski, R. J., Gamble, J. A., Kyle, P. R. and Thirlwall, M. F. (1995). The petrology of lower crustal xenoliths from the Executive Committee Range, Marie Byrd Land Volcanic Province, West Antarctica. *Lithos* **36**(3-4): 185-201.

Zhao, G. C., Wilde, S. A., Cawood, P. A. and Lu, L. Z. (2000). Petrology and P-T path of the Fuping mafic granulites: implications for tectonic evolution of the central zone of the North China craton. *Journal of Metamorphic Geology* **18**: 375-391.

Appendix 1 Table of Acronyms

Acronym	Description
BSE	Back scattered electron
BSE	Bulk silicate earth
CHUR	Chondritic unfractionated reservoir
DM	Depleted mantle (juvenile magmas)
EMP	Electron microprobe
ε_{Hf} / ε_{Nd}	Difference between the sample's initial isotope ratios ($^{176}Hf/^{177}Hf$ or $^{143}Nd/^{144}Nd$) and the value for CHUR at that time, in parts per thousand
HFSE	High field strength elements
HREE	Heavy rare earth elements
ICP-MS	Inductively coupled plasma mass spectrometer
LAM	Laser ablation microprobe
LILE	Large ion lithophile elements
LREE	Light rare earth elements
MC-ICP-MS	Multi collector ICP-MS
MOHO	Mohorovičić discontinuity, being the boundary between the crust and mantle
MORB	Mid ocean ridge basalt
NVP	Newer volcanic province
OIB	Ocean island basalt
REE	Rare earth elements
TIMS	Thermal ionisation mass spectrometer

Appendix 2 – Seismic profile (Cayley *et al.*, 2008)



Top – composite seismics profile including lines 1 to 4**; Bottom left** - Line 1 Profile; **Bottom centre**– Map showing the location of the seismic profiles; **Bottom right** – granite distribution – red Early Devonian; yellow Late Devonian Cayley et al., (2008)

Appendix 3 Physical volcanology and geochemistry of the NVP

Physical volcanology

The two subprovinces, being the Central Highlands Subprovince and Western Plains Subprovince have been created based on their geomorphology (Nicholls and Joyce, 1989). The Central Highlands Province has approximately 250 volcanic centres with the most prominent features being narrow lava plains and valley filling flows. Phreatomagmatic deposits within the subprovince have been poorly preserved and are less common than the lava flows mentioned (Price *et al.*, 2003b). The Central Highlands Subprovince includes approximately 80% of lava shields and 75% of the scoria dominated volcanoes within the WDP (Nicholls and Joyce, 1989). The resulting rocks cover Ordovician metasedimentary rocks within the Lachlan Orogen (Graham et al., 2003).

Within the Western Plains Subprovince, lava shields, cones and maars to 100m height reflect the most recent activity, whilst older activity is reflected by lava flows up to 60m thick that cover the plains. Maars, cones and shields are common and most prominent within the landscape, and cover a Late Neogene surface (Graham *et al.*, 2003).

The scoria cones are usually associated with Strombolian type activity and consist of massive deposits of vesiculated basaltic scoria deposited by air fall. The ejected basaltic material ranges in size from ash to blocks and bombs. The scoriaceous material is present as moderate to highly vesicular angular lapilli sized clasts, 2-64 mm. The coarser blocks and bombs (>64mm) tend to vary in morphology depending on the liquid properties of the lava whilst moving through the air. They may vary from spindle to ribbon shaped and consist of dense to semi vesicular basaltic material. The blocks and bombs commonly contain cores of entrained xenoliths or country rock and display vesicular zoning, with micro vesicles in the shells and larger vesicles in the core (Nicholls *et al.*, 1993; Graham *et al.*, 2003).

Geochemistry

Vogel and Keays (1997) identified three main suites within the NVP:

- Tholeiitic Plains Suite - >50wt% SiO_2 with highly fractionated S saturated rocks and low, MORB like, PGE concentrations. However they are enriched in incompatible elements relative to MORB. Concentrations of Ni were 128ppm, whilst Cr was 236ppm, lower than the Transitional suite.
- Transitional Plains Suite - <50 wt% SiO_2 with transitional. Lower compositions and less fractionation. Greater trace elements than the tholeiitic suite (Ni 209ppm, Cr 306ppm), with low Pd suggesting crystallisation under S saturated conditions, though the behaviour of Ni and Au as well as elevated Pt suggest fewer sulfides were precipitated than the tholeiitic suite magmas.
- Alkalic Cones Suite – undersaturated (44-48wt%) SiO_2 with variable compositions with Ni ranging from 165-496ppm and Cr 219-1030ppm. Upper mantle xenoliths abundant at some locations. Rocks of the suite are S saturated with surface features suggesting that these basalts were the last to erupt in the province.

The Plains Series Basalts have TiO_2 (1.69-2.43wt%), P_2O_5 (0.31-0.78wt%) and K_2O (0.75-2.08wt%) and depleted CaO (6.91-9.24wt%), which is suggestive of ocean island basalts rather than MORB (Frey *et al.*, 1978).

Strontium ($^{87}Sr/^{86}Sr$) ratios appear to be controlled by the underlying material, with a sharp change west of the Mortlake Discontinuity from 0.7040-0.7058 in the east to 0.7037-0.7050 in the west (Price *et al*., 1997; 1998). The difference in Sr ratios infers crustal contamination of different lithologies around the Mortlake Discontinuity (Nicholls, 1993). The Plains Series basalts typically have ε_{Nd} between -1.2-+3.6 whilst the Cones series basalts have ε_{Nd} between +2.9-+4.2 (McDonough *et al.*, 1985). 206Pb/204Pb values ranged from 18.57-18.84 for Plains Series olivine tholeiites and Cones Series nepheline hawaiites. Typical values over the NVP were 18.4 to 18.9 (Price *et al.*, 1997).

Variable $^{187}Re/^{188}Os$ ratios of 10.92-80.24 were noted for the Plains Series olivine tholeiites whilst tighter values of 3.55-6.88 were noted for the Cones series nepheline hawaiites.

$^{206}Pb/^{204}Pb$ ratios for the rocks are similar to ocean island basalts, with a Os concentration v Re/Os plot suggesting that the basalts were derived from mantle melts. The Cones Series nepheline had Os values representative of ocean island basalts (ϒOs+6-+8) with the Plains Series olivine tholeiites being more radiogenic with (ϒOs+42-+250).

For the basalts, a trend of LREE enrichment is evidence for a source of metasomatised lithosphere, without plagioclase as a major fractionating phase due to the lack of an Eu anomaly. This is further suggested due to the composition of the upper mantle xenoliths located within the alkalic cones. LILE and HFSE enrichment together with the lack of Ta or Nb anomalies suggests that basaltic suites within the region represent an intraplate environment with limited lower crust assimilation or input of fluid related to subduction (Vogel and Keays, 1997; Graham *et al.*, 2006).

Differences in Zr/Nb values, REE slopes and compatible trace elements with similar Mg numbers demonstrate that there is no magmatic relationship between two end members of the basaltic plains suites. Whilst alkalic cones, with variable composition, have resulted from lower degrees of partial melt (~3-6%) of an enriched mantle source (Vogel and Keays, 1997; Graham *et al.*, 2006).

The basaltic rocks of the NVP have low Mg to Fe ratios suggesting that they may not be the result of melting of mantle peridotites and it is argued that modification may have occurred during ascent through the crust and crystal fractionation (Price et al., 2003a). A Sr isotope discontinuity is observed within the Western Plains Subprovince, now known as the Mortlake discontinuity. This coincides with the transition between the Lachlan and Delamerian fold belts (Price et al., 2003a).

Appendix 4 List of samples collected with xenolith size, analyses undertaken and a petrographic summary, in groups determined by petrography

Coliban Dam Suite			Petrographic summary				
Sample No	**Size (cm)**	**Analyses**	**Mineral**	**Mode (% vol)**	**Size (mm)**	**Crystal habit**	**Comment**
Mafic Group							
15199	15 x 10	Full*	Fspar	30 – 60	0.5 to 4	Euhedral to subhedral	Predominantly plag, growth and def twinning, 'moth eaten' rims
17913	5 x 5	Full	Px	25 – 65	0.4 to 3.2	Euhedral, some with irregular edges	Orthopyroxene and clinopyroxene present, 'moth eaten' reaction rims to glass/host lava
17914	4 x 8	Thin section EMP*	Mag	Acc.	0.04 to 2	Interstitial, rounded	At grain boundaries or as rounded inclusions in plag and px, with titanomagnetite exsolution
17919	10 x 5	Thin section whole-rock	Ilm	Acc.	0.04 to 2	Interstitial, rounded	At grain boundaries or as rounded inclusions in plag and px
17922	20 x 12	Thin section EMP whole-rock	Bt	Acc.	Up to 0.4	Subhedral	As inclusion within px, following cleavage, also growing from glass
18001	4 x 2	Thin section	Apt	Acc.	Up to 0.05	Euhedral	Inclusions within px and plag
18002	5 x 2	Thin section whole-rock, EMP*	Glass			Interstitial	Interstitial along grain boundaries and in fractures; in lieu of plag in sub ophitic texture; sometimes altering pseudomorphed mineral
18005	3 x 2						

Coliban Dam Suite			Petrographic summary				
Sample No	**Size (cm)**	**Analyses**	**Mineral**	**Mode (% vol)**	**Size (mm)**	**Crystal habit**	**Comment**
Felsic Group 1							
17911	30 x 30	Full	Fspar	55-65	0.2 to 4	Most with smooth rounded edges Some larger euhedral	Sieve like texture on the rims when in contact with glass, growth and deformation twinning though brokendown with reaction rims
17912	> 10 x 10	Full*	Qtz	35	0.1 to 1.6	Rounded and interstitial	Glass forms films along qtz rims
17918	5 x 5	Thin section EMP	Px	Acc.	0.02 to 2	Anhedral, some look like have old shape	Mainly ortho (hypersthene), often rimming quartz and associated with glass, magnetite and ilmenite
17920	5 x 5	Thin section whole-rock	Zrc	Acc.	0.2 to 0.1	euhedral to subhedral	Embedded in quartz or feldspar grains and less common in glass
17921	8 x 5	Thin section whole-rock, EMP	Mag	Acc.	0.01 to 0.8	Anhedral, interstitial	Rounded inclusion in px, usually associated with glass, with titanomagnetite exsolution
17923	5 x 5	XRD - **Result** carbonate, Mg and Ca	Ilm	Acc.	0.02 to 0.2	Anhedral, interstitial	Rounded inclusion in px, usually associated with glass
18000	10 x 5	Thin section	Apte	Acc.	0.02 to 0.5	Euhedral, elongate	Inclusions in fspar or zrc
			Glass			Banded	Up to 1 width ~ 0.5 apart; along grain boundaries, has fspar quench textures incl microphenocrysts of fspar
Felsic Group 2							
17915	8 x 5	Thin section, EMP*	Mineralogy as for Felsic Group 1 except for the following				

Coliban Dam Suite			Petrographic summary				
Sample No	**Size (cm)**	**Analyses**	**Mineral**	**Mode (% vol)**	**Size (mm)**	**Crystal habit**	**Comment**
			Symplectic texture		Up to 2		In discreet domains, some with straight sides consisting of opx + mag enveloped by plag
			Glass				Irregularly distributed in small domains up to 0.5 or as films along grain boundaries
Felsic Group 3							
17917	5 x 5	Thin section	Qtz	90	0.08 to 4	Irregular edges	
			Plag	Acc.	0.04 to 0.08	Irregular edges	Inclusion in qtz
			Px	Acc.	0.06 to 0.10	Subhedral	Inclusion in qtz
			Cal	Acc.	<0.04	Polygonal aggregates or veins	Located at points of breakdown in plag
Intermediate Group							
17916	3 x 5	Thin section	Plag	Up to 70	0.08 to 2		
		Thin section EMP	K spar	15	0.08 to 2		
18003	6 x 4	whole-rock					
18004	3 x 1		Px	10	0.04 to 1		
			Mag	Acc.	Up to 0.08		Titanomagnetite exsolution
			Apt	Acc.	Up to 0.3		
			Zrc	Acc.	Up to 8		
			Glass			Irregularly distributed	Along grain boundaries

Stewart Hill Suite			**Petrographic Summary**				
Sample No	**Size (cm)**	**Analyses**	Mineral	**Mode (vol)**	**Size**	**Crystal habit**	**Coent**
19000	5 x 10	Thin section	Plag	40 to 50	Up to 2	Subhedral	Intergrown texture with pyroxene
19001	5 x 10	Thin section	Px	40 to 60	Up to 1.2	Subhedral	Intergrown texture with plagioclase, abundant inclusions and exsolution along cleavage
19002	10 x 10	Thin section, whole-rock	Kaes	Acc.	Up to 0.8	Subhedral	
19003	10 x 10	Thin section, whole-rock	Mag	Acc.		Rounded	Inclusions
19004	15 x 10	Thin section, whole-rock	Glass	Acc.		Interstitial	Quench textures including spiky outgrowths of plagioclase
19005	15 x 10	Thin section					

Acc. = Accessory; Full analysis = Thin section, EMP mineral geochemistry, ICP-MS wholerock geochemistry and isotope analysis, zircon geochronology and Hf isotope analysis, * = LAM-ICP-MS mineral trace element geochemistry

Appendix 5
Feldspar EMP data - cation calculations based on 32 oxygen

No	15199 1.6 plag	15199 1.7 plag	15199 2.11 ksp	15199 2.12 pla	15199 2.7 plag	15199 2.8 plag	15199 2.9 plag	15199 3.1 plag	15199 3.2 plag
Mineral	**Plagioclase**	**Plagioclase**	**Kspar**	**Plagioclase**	**Plagioclase**	**Plagioclase**	**Plagioclase**	**Plagioclase**	**Plagioclase**
Wt %									
SiO2	53.85	54.29	62.22	60.98	52.51	52.57	53.14	54.84	52.75
TiO2	0.10	0.10	0.30	0.22	0.14	0.16	0.13	0.10	0.10
Al2O3	28.44	28.89	22.82	23.52	29.55	29.65	29.32	27.98	29.43
Cr2O3	0.00	0.02	0.03	0.00	0.00	0.02	0.01	0.00	0.01
FeO	0.24	0.27	0.82	0.90	0.48	0.57	0.52	0.27	0.40
MnO	0.00	0.02	0.00	0.00	0.00	0.01	0.00	0.00	0.02
MgO	0.00	0.00	0.19	0.23	0.00	0.00	0.00	0.00	0.00
CaO	10.98	11.56	4.68	5.68	12.81	12.86	12.52	10.89	12.89
Na2O	5.19	4.95	7.82	7.34	4.12	4.16	4.40	5.42	4.15
K2O	0.49	0.49	1.96	1.63	0.36	0.41	0.44	0.54	0.42
NiO	0.00	0.00	0.00	0.00	0.00	0.02	0.02	0.00	0.02
Total	**99.30**	**100.60**	**100.83**	**100.50**	**99.97**	**100.42**	**100.51**	**100.04**	**100.18**
Cations									
Si^{4+}	9.82	9.78	11.06	10.89	9.56	9.54	9.62	9.93	9.58
Ti^{4+}	0.01	0.01	0.04	0.03	0.02	0.02	0.02	0.01	0.01
Al^{3+}	6.11	6.14	4.78	4.95	6.34	6.34	6.26	5.97	6.30
Cr^{3+}	0.00	0.00	0.00	0.00	0.00	0.00	0.00	0.00	0.00
Fe^{2+}	0.04	0.04	0.12	0.13	0.07	0.09	0.08	0.04	0.06
Mn^{2+}	0.00	0.00	0.00	0.00	0.00	0.00	0.00	0.00	0.00
Mg^{2+}	0.00	0.00	0.05	0.06	0.00	0.00	0.00	0.00	0.00
Ca^{2+}	2.15	2.23	0.89	1.09	2.50	2.50	2.43	2.11	2.51
Na^{+}	1.84	1.73	2.69	2.54	1.45	1.46	1.54	1.90	1.46
K^{+}	0.11	0.11	0.44	0.37	0.08	0.09	0.10	0.13	0.10
Ni^{+}	0.00	0.00	0.00	0.00	0.00	0.00	0.00	0.00	0.00
Zn	0.00	0.00	0.00	0.00	0.00	0.00	0.00	0.00	0.00
V	0.00	0.00	0.00	0.00	0.00	0.00	0.00	0.00	0.00
Σcat	**20.08**	**20.05**	**20.08**	**20.06**	**20.02**	**20.05**	**20.06**	**20.09**	**20.03**
Or	3	3	11	9	2	2	2	3	2
Ab	45	42	67	64	36	36	38	46	36
An	52	55	22	27	62	62	60	51	62

Appendix 5
Feldspar EMP data - cation calculations based on 32 oxygen

No	15199 3.3 plag	15199 3.3 plag	15199 3.3 plag	15199 3.3 plag	15199 3.3 plag	15199 3.3 plag	15199 3.3 plag	15199 3.3 plag	15199 3.3 plag
Mineral	**Plagioclase**	**Plagioclase**	**Plagioclase**	**Plagioclase**	**Plagioclase**	**Plagioclase**	**Plagioclase**	**Plagioclase**	**Plagioclase**
Wt %									
SiO2	52.54	54.16	54.66	54.71	54.71	54.71	54.72	54.75	54.77
TiO2	0.14	0.10	0.10	0.12	0.09	0.12	0.15	0.11	0.08
Al2O3	29.40	28.49	28.00	28.17	28.04	28.01	28.03	28.00	27.92
Cr2O3	0.00	0.02	0.00	0.00	0.01	0.00	0.00	0.00	0.01
FeO	0.57	0.26	0.26	0.25	0.25	0.33	0.28	0.26	0.28
MnO	0.02	0.03	0.00	0.01	0.00	0.02	0.00	0.00	0.01
MgO	0.00	0.00	0.00	0.00	0.00	0.00	0.00	0.00	0.00
CaO	13.02	11.48	11.05	11.12	10.91	11.04	10.84	11.21	10.91
Na2O	4.06	4.98	5.22	5.24	5.32	5.15	5.28	5.20	5.29
K2O	0.45	0.47	0.51	0.46	0.54	0.51	0.55	0.50	0.54
NiO	0.00	0.01	0.01	0.05	0.01	0.00	0.00	0.02	0.02
Total	**100.21**	**99.97**	**99.80**	**100.13**	**99.88**	**99.88**	**99.85**	**100.06**	**99.82**
Cations									
Si^{4+}	9.56	9.82	9.91	9.89	9.92	9.92	9.92	9.91	9.93
Ti^{4+}	0.02	0.01	0.01	0.02	0.01	0.02	0.02	0.02	0.01
Al^{3+}	6.30	6.09	5.99	6.00	5.99	5.98	5.99	5.97	5.97
Cr^{3+}	0.00	0.00	0.00	0.00	0.00	0.00	0.00	0.00	0.00
Fe^{2+}	0.09	0.04	0.04	0.04	0.04	0.05	0.04	0.04	0.04
Mn^{2+}	0.00	0.00	0.00	0.00	0.00	0.00	0.00	0.00	0.00
Mg^{2+}	0.00	0.00	0.00	0.00	0.00	0.00	0.00	0.00	0.00
Ca^{2+}	2.54	2.23	2.15	2.15	2.12	2.14	2.11	2.17	2.12
Na^{+}	1.43	1.75	1.84	1.84	1.87	1.81	1.86	1.83	1.86
K^{+}	0.11	0.11	0.12	0.11	0.13	0.12	0.13	0.12	0.12
Ni^{+}	0.00	0.00	0.00	0.01	0.00	0.00	0.00	0.00	0.00
Zn	0.00	0.00	0.00	0.00	0.00	0.00	0.00	0.00	0.00
V	0.00	0.00	0.00	0.00	0.00	0.00	0.00	0.00	0.00
Σcat	**20.04**	**20.05**	**20.06**	**20.06**	**20.07**	**20.04**	**20.06**	**20.06**	**20.06**
Or	3	3	3	3	3	3	3	3	3
Ab	35	43	45	45	45	44	45	44	45
An	62	55	52	53	51	53	51	53	52

Appendix 5
Feldspar EMP data - cation calculations based on 32 oxygen

No	15199 3.3 plag	15199 3.3 plag	15199 3.3 plag	15199 3.3 plag	15199 3.3 plag	15199 3.3 plag	15199 3.4 plag	15199 3.5 plag	17911 1.7 plag
Mineral	**Plagioclase**	**Plagioclase**	**Plagioclase**	**Plagioclase**	**Plagioclase**	**Plagioclase**	**Plagioclase**	**Plagioclase**	**Plagioclase**
Wt %									
SiO2	54.80	54.85	54.91	54.97	54.99	55.12	54.81	56.06	63.19
TiO2	0.09	0.11	0.11	0.09	0.09	0.11	0.08	0.27	0.06
Al2O3	27.72	28.00	28.04	28.04	27.89	27.85	28.01	27.36	22.73
Cr2O3	0.04	0.01	0.01	0.02	0.01	0.04	0.00	0.02	0.00
FeO	0.24	0.28	0.24	0.28	0.28	0.23	0.28	0.99	0.29
MnO	0.01	0.01	0.00	0.00	0.04	0.02	0.00	0.00	0.00
MgO	0.00	0.00	0.00	0.00	0.00	0.00	0.00	0.05	0.00
CaO	10.69	11.13	11.04	11.06	10.98	10.90	11.03	10.41	5.02
Na2O	5.21	5.17	5.26	5.10	5.26	5.24	5.22	5.34	7.92
K2O	0.59	0.55	0.49	0.64	0.51	0.54	0.61	0.70	1.57
NiO	0.03	0.00	0.00	0.00	0.03	0.03	0.02	0.00	0.00
Total	**99.42**	**100.11**	**100.10**	**100.20**	**100.07**	**100.07**	**100.06**	**101.20**	**100.78**
Cations									
Si^{4+}	9.97	9.92	9.93	9.93	9.95	9.96	9.92	10.04	11.17
Ti^{4+}	0.01	0.01	0.01	0.01	0.01	0.01	0.01	0.04	0.01
Al^{3+}	5.94	5.97	5.97	5.97	5.95	5.93	5.98	5.78	4.74
Cr^{3+}	0.01	0.00	0.00	0.00	0.00	0.01	0.00	0.00	0.00
Fe^{2+}	0.04	0.04	0.04	0.04	0.04	0.03	0.04	0.15	0.04
Mn^{2+}	0.00	0.00	0.00	0.00	0.01	0.00	0.00	0.00	0.00
Mg^{2+}	0.00	0.00	0.00	0.00	0.00	0.00	0.00	0.01	0.00
Ca^{2+}	2.08	2.16	2.14	2.14	2.13	2.11	2.14	2.00	0.95
Na^{+}	1.84	1.81	1.84	1.79	1.85	1.84	1.83	1.85	2.71
K^{+}	0.14	0.13	0.11	0.15	0.12	0.12	0.14	0.16	0.35
Ni^{+}	0.00	0.00	0.00	0.00	0.00	0.01	0.00	0.00	0.00
Zn	0.00	0.00	0.00	0.00	0.00	0.00	0.00	0.00	0.00
V	0.00	0.00	0.00	0.00	0.00	0.00	0.00	0.00	0.00
Σcat	**20.03**	**20.05**	**20.05**	**20.04**	**20.05**	**20.03**	**20.06**	**20.04**	**19.98**
Or	3	3	3	4	3	3	3	4	9
Ab	45	44	45	44	45	45	45	46	68
An	51	53	52	53	52	52	52	50	24

Appendix 5
Feldspar EMP data - cation calculations based on 32 oxygen

No	17911 1.8 kspa	17911 5.7 kspa	17911 5.8 kspa	17911 8.1 kspa	17911 8.2 kspa	17911 8.3 kspa	17911 8.4 kspa	17911 8.5 kspa	17911 8.6 kspa
Mineral	**Kspar**	**Kspar**	**Kspar**	**Kspar**	**Kspar**	**Kspar**	**Kspar**	**Kspar**	**Kspar**
Wt %									
SiO2	63.03	62.99	62.83	62.57	62.48	66.47	66.46	66.51	62.79
TiO2	0.02	0.00	0.00	0.00	0.01	0.01	0.03	0.00	0.01
Al2O3	22.67	22.67	22.62	22.51	22.62	19.15	19.04	18.58	22.44
Cr2O3	0.00	0.00	0.00	0.00	0.03	0.00	0.00	0.00	0.00
FeO	0.19	0.17	0.16	0.18	0.22	0.13	0.09	0.12	0.18
MnO	0.03	0.00	0.04	0.00	0.00	0.00	0.00	0.01	0.00
MgO	0.00	0.00	0.00	0.00	0.00	0.03	0.00	0.00	0.00
CaO	4.74	4.74	4.72	4.74	4.86	0.95	0.91	0.55	4.69
Na2O	7.52	7.32	7.41	7.16	7.04	5.21	5.44	4.83	7.12
K2O	2.11	2.81	2.61	3.04	3.05	8.65	8.31	9.48	2.83
NiO	0.00	0.01	0.00	0.00	0.00	0.00	0.00	0.00	0.00
Total	**100.31**	**100.71**	**100.39**	**100.21**	**100.32**	**100.61**	**100.28**	**100.08**	**100.05**
Cations									
Si^{4+}	11.20	11.19	11.19	11.18	11.16	11.91	11.93	12.00	11.22
Ti^{4+}	0.00	0.00	0.00	0.00	0.00	0.00	0.00	0.00	0.00
Al^{3+}	4.75	4.75	4.75	4.74	4.76	4.04	4.03	3.95	4.72
Cr^{3+}	0.00	0.00	0.00	0.00	0.00	0.00	0.00	0.00	0.00
Fe^{2+}	0.03	0.03	0.02	0.03	0.03	0.02	0.01	0.02	0.03
Mn^{2+}	0.00	0.00	0.01	0.00	0.00	0.00	0.00	0.00	0.00
Mg^{2+}	0.00	0.00	0.00	0.00	0.00	0.01	0.00	0.00	0.00
Ca^{2+}	0.90	0.90	0.90	0.91	0.93	0.18	0.17	0.11	0.90
Na^{+}	2.59	2.52	2.56	2.48	2.44	1.81	1.89	1.69	2.47
K^{+}	0.48	0.64	0.59	0.69	0.70	1.98	1.90	2.18	0.64
Ni^{+}	0.00	0.00	0.00	0.00	0.00	0.00	0.00	0.00	0.00
Zn	0.00	0.00	0.00	0.00	0.00	0.00	0.00	0.00	0.00
V	0.00	0.00	0.00	0.00	0.00	0.00	0.00	0.00	0.00
Σcat	**19.96**	**20.02**	**20.02**	**20.03**	**20.02**	**19.96**	**19.95**	**19.96**	**19.98**
Or	12	16	15	17	17	50	48	55	16
Ab	65	62	63	61	60	46	48	42	62
An	23	22	22	22	23	5	4	3	22

Appendix 5
Feldspar EMP data - cation calculations based on 32 oxygen

No	17911 9.1 kspa	17911 9.2 kspa	17911 9.3 kspa	17911 9.4 kspa	17912 1.6 kspa	17912 2.1 euh	17912 2.2 euh	17912 2.3 euh	17912 2.4 euh
Mineral	**Kspar**	**Kspar**	**Kspar**	**Kspar**	**Kspar**	**Kspar**	**Kspar**	**Kspar**	**Kspar**
Wt %									
SiO2	62.63	61.83	62.74	63.31	63.31	66.60	66.19	66.75	66.22
TiO2	0.00	0.00	0.00	0.02	0.00	0.00	0.00	0.00	0.00
Al2O3	22.05	22.38	22.61	22.73	22.83	19.00	19.34	19.18	19.46
Cr2O3	0.00	0.02	0.01	0.03	0.01	0.00	0.00	0.00	0.01
FeO	0.17	0.21	0.21	0.20	0.19	0.14	0.14	0.11	0.12
MnO	0.00	0.01	0.00	0.00	0.05	0.00	0.00	0.00	0.00
MgO	0.00	0.00	0.00	0.00	0.00	0.00	0.00	0.00	0.00
CaO	4.76	4.78	4.72	4.76	4.84	0.45	1.00	0.82	0.95
Na2O	7.08	6.91	7.47	7.75	7.37	4.78	5.35	5.08	5.29
K2O	2.84	2.99	2.64	2.18	2.87	10.13	8.71	8.86	8.73
NiO	0.00	0.03	0.01	0.04	0.02	0.00	0.00	0.01	0.05
Total	**99.54**	**99.16**	**100.40**	**101.02**	**101.49**	**101.11**	**100.73**	**100.82**	**100.84**
Cations									
Si^{4+}	11.25	11.17	11.18	11.19	11.17	11.94	11.87	11.94	11.86
Ti^{4+}	0.00	0.00	0.00	0.00	0.00	0.00	0.00	0.00	0.00
Al^{3+}	4.67	4.76	4.75	4.73	4.75	4.02	4.09	4.04	4.11
Cr^{3+}	0.00	0.00	0.00	0.00	0.00	0.00	0.00	0.00	0.00
Fe^{2+}	0.03	0.03	0.03	0.03	0.03	0.02	0.02	0.02	0.02
Mn^{2+}	0.00	0.00	0.00	0.00	0.01	0.00	0.00	0.00	0.00
Mg^{2+}	0.00	0.00	0.00	0.00	0.00	0.00	0.00	0.00	0.00
Ca^{2+}	0.92	0.93	0.90	0.90	0.91	0.09	0.19	0.16	0.18
Na^{+}	2.46	2.42	2.58	2.65	2.52	1.66	1.86	1.76	1.84
K^{+}	0.65	0.69	0.60	0.49	0.65	2.32	1.99	2.02	1.99
Ni^{+}	0.00	0.00	0.00	0.01	0.00	0.00	0.00	0.00	0.01
Zn	0.00	0.00	0.00	0.00	0.00	0.00	0.00	0.00	0.00
V	0.00	0.00	0.00	0.00	0.00	0.00	0.00	0.00	0.00
Σcat	**19.97**	**20.00**	**20.04**	**20.01**	**20.04**	**20.04**	**20.02**	**19.94**	**20.00**
Or	16	17	15	12	16	57	49	51	50
Ab	61	60	63	66	62	41	46	45	46
An	23	23	22	22	22	2	5	4	5

Appendix 5
Feldspar EMP data - cation calculations based on 32 oxygen

No	17912 2.6 euh	17912 2.7 kspa	17912 4.8 kspa	17912 4sub6 k	17912 4sub7ks	17913 1.12 pla	17913 1.13 pla	17913 1.16 pla	17913 1.5 plag
Mineral	**Kspar**	**Kspar**	**Kspar**	**Kspar**	**Kspar**	**Plagioclase**	**Plagioclase**	**Plagioclase**	**Plagioclase**
Wt %									
SiO2	66.39	63.00	63.03	63.19	62.99	57.56	55.97	57.33	57.11
TiO2	0.00	0.02	0.00	0.00	0.00	0.05	0.09	0.04	0.09
Al2O3	18.86	22.82	22.72	22.32	22.34	26.01	27.00	26.32	26.44
Cr2O3	0.01	0.00	0.01	0.03	0.02	0.00	0.02	0.00	0.01
FeO	0.12	0.17	0.19	0.24	0.20	0.24	0.26	0.23	0.39
MnO	0.00	0.00	0.00	0.01	0.00	0.01	0.00	0.00	0.00
MgO	0.01	0.00	0.00	0.00	0.00	0.00	0.00	0.00	0.00
CaO	0.48	4.80	4.67	4.78	4.80	8.69	9.86	8.96	9.14
Na2O	4.74	7.17	7.52	7.38	7.27	6.40	5.75	6.18	6.32
K2O	10.13	3.12	2.75	2.86	2.80	0.79	0.65	0.74	0.74
NiO	0.00	0.00	0.00	0.00	0.03	0.06	0.02	0.04	0.00
Total	**100.75**	**101.10**	**100.90**	**100.83**	**100.46**	**99.82**	**99.62**	**99.84**	**100.24**
Cations									
Si^{4+}	11.95	11.16	11.18	11.22	11.22	10.38	10.14	10.33	10.28
Ti^{4+}	0.00	0.00	0.00	0.00	0.00	0.01	0.01	0.00	0.01
Al^{3+}	4.00	4.77	4.75	4.67	4.69	5.53	5.77	5.59	5.61
Cr^{3+}	0.00	0.00	0.00	0.00	0.00	0.00	0.00	0.00	0.00
Fe^{2+}	0.02	0.02	0.03	0.04	0.03	0.04	0.04	0.03	0.06
Mn^{2+}	0.00	0.00	0.00	0.00	0.00	0.00	0.00	0.00	0.00
Mg^{2+}	0.00	0.00	0.00	0.00	0.00	0.00	0.00	0.00	0.00
Ca^{2+}	0.09	0.91	0.89	0.91	0.92	1.68	1.91	1.73	1.76
Na^{+}	1.66	2.46	2.59	2.54	2.51	2.24	2.02	2.16	2.21
K^{+}	2.32	0.70	0.62	0.65	0.64	0.18	0.15	0.17	0.17
Ni^{+}	0.00	0.00	0.00	0.00	0.00	0.01	0.00	0.01	0.00
Zn	0.00	0.00	0.00	0.00	0.00	0.00	0.00	0.00	0.00
V	0.00	0.00	0.00	0.00	0.00	0.00	0.00	0.00	0.00
Σcat	**20.04**	**20.04**	**20.05**	**20.04**	**20.01**	**20.06**	**20.05**	**20.03**	**20.09**
Or	57	17	15	16	16	4	4	4	4
Ab	41	60	63	62	62	55	49	53	53
An	2	22	22	22	23	41	47	43	43

Appendix 5
Feldspar EMP data - cation calculations based on 32 oxygen

No	17913 1.6 plag	17913 1.9 plag	17913 2.4 plag	17913 2.8 plag	17913 3.1 plag	17913 3.11 pla	17913 3.12 pla	17913 3.14 pla	17913 3.15 pla
Mineral	**Plagioclase**	**Plagioclase**	**Plagioclase**	**Plagioclase**	**Plagioclase**	**Plagioclase**	**Plagioclase**	**Plagioclase**	**Plagioclase**
Wt %									
SiO2	56.84	57.46	58.43	58.29	57.97	57.26	56.75	57.72	57.46
TiO2	0.02	0.05	0.06	0.06	0.05	0.05	0.06	0.03	0.06
Al2O3	26.41	25.97	25.38	25.31	25.57	26.36	26.44	25.95	25.96
Cr2O3	0.00	0.00	0.00	0.00	0.00	0.00	0.00	0.00	0.01
FeO	0.26	0.25	0.28	0.23	0.25	0.24	0.25	0.21	0.22
MnO	0.00	0.01	0.00	0.00	0.03	0.03	0.00	0.01	0.01
MgO	0.00	0.00	0.00	0.00	0.00	0.00	0.00	0.00	0.00
CaO	9.22	8.80	8.16	7.89	8.19	8.90	9.09	8.65	8.85
Na2O	6.07	6.21	6.45	6.45	6.54	6.05	5.94	6.32	6.17
K2O	0.66	0.74	0.98	0.98	0.82	0.97	1.07	0.78	0.73
NiO	0.01	0.03	0.01	0.00	0.00	0.06	0.00	0.00	0.00
Total	**99.48**	**99.52**	**99.76**	**99.22**	**99.42**	**99.91**	**99.60**	**99.67**	**99.48**
Cations									
Si^{4+}	10.29	10.38	10.52	10.54	10.47	10.32	10.28	10.41	10.39
Ti^{4+}	0.00	0.01	0.01	0.01	0.01	0.01	0.01	0.00	0.01
Al^{3+}	5.63	5.53	5.39	5.39	5.44	5.60	5.64	5.52	5.53
Cr^{3+}	0.00	0.00	0.00	0.00	0.00	0.00	0.00	0.00	0.00
Fe^{2+}	0.04	0.04	0.04	0.04	0.04	0.04	0.04	0.03	0.03
Mn^{2+}	0.00	0.00	0.00	0.00	0.00	0.00	0.00	0.00	0.00
Mg^{2+}	0.00	0.00	0.00	0.00	0.00	0.00	0.00	0.00	0.00
Ca^{2+}	1.79	1.70	1.57	1.53	1.58	1.72	1.76	1.67	1.71
Na^{+}	2.13	2.18	2.25	2.26	2.29	2.11	2.09	2.21	2.16
K^{+}	0.15	0.17	0.23	0.23	0.19	0.22	0.25	0.18	0.17
Ni^{+}	0.00	0.00	0.00	0.00	0.00	0.01	0.00	0.00	0.00
Zn	0.00	0.00	0.00	0.00	0.00	0.00	0.00	0.00	0.00
V	0.00	0.00	0.00	0.00	0.00	0.00	0.00	0.00	0.00
Σcat	**20.03**	**20.02**	**20.01**	**20.00**	**20.04**	**20.04**	**20.06**	**20.02**	**20.01**
Or	4	4	6	6	5	6	6	4	4
Ab	52	54	56	56	56	52	51	54	53
An	44	42	39	38	39	42	43	41	42

Appendix 5
Feldspar EMP data - cation calculations based on 32 oxygen

No	17913 3.3 plag	17913 4.1 plag	17913 4.2 plag	17913 4.3 plag	17913 4.3 plag	17913 4.4 plag	17913 4.4 plag	17913 4.4 plag	17913 5.1 plag
Mineral	**Plagioclase**	**Plagioclase**	**Plagioclase**	**Plagioclase**	**Plagioclase**	**Plagioclase**	**Plagioclase**	**Plagioclase**	**Plagioclase**
Wt %									
SiO2	57.02	56.09	56.95	56.20	56.73	56.12	55.92	56.26	57.49
TiO2	0.05	0.08	0.05	0.09	0.06	0.07	0.05	0.07	0.08
Al2O3	26.61	27.04	26.45	26.89	26.36	26.51	27.16	26.42	25.67
Cr2O3	0.00	0.00	0.00	0.00	0.00	0.00	0.00	0.05	0.03
FeO	0.23	0.27	0.30	0.23	0.25	0.23	0.25	0.25	0.25
MnO	0.02	0.00	0.00	0.00	0.00	0.01	0.00	0.00	0.00
MgO	0.00	0.00	0.00	0.00	0.00	0.00	0.00	0.00	0.00
CaO	9.08	9.85	9.15	9.74	9.33	9.74	10.21	9.65	8.84
Na2O	6.18	5.80	6.06	5.76	5.78	5.79	5.55	5.78	6.05
K2O	0.74	0.53	0.79	0.57	0.87	0.50	0.48	0.60	0.88
NiO	0.00	0.03	0.01	0.00	0.01	0.00	0.03	0.00	0.01
Total	**99.93**	**99.70**	**99.75**	**99.48**	**99.38**	**98.96**	**99.66**	**99.08**	**99.31**
Cations									
Si^{4+}	10.28	10.15	10.29	10.18	10.28	10.22	10.12	10.23	10.42
Ti^{4+}	0.01	0.01	0.01	0.01	0.01	0.01	0.01	0.01	0.01
Al^{3+}	5.65	5.77	5.63	5.74	5.63	5.69	5.79	5.66	5.48
Cr^{3+}	0.00	0.00	0.00	0.00	0.00	0.00	0.00	0.01	0.00
Fe^{2+}	0.03	0.04	0.05	0.03	0.04	0.03	0.04	0.04	0.04
Mn^{2+}	0.00	0.00	0.00	0.00	0.00	0.00	0.00	0.00	0.00
Mg^{2+}	0.00	0.00	0.00	0.00	0.00	0.00	0.00	0.00	0.00
Ca^{2+}	1.75	1.91	1.77	1.89	1.81	1.90	1.98	1.88	1.72
Na^{+}	2.16	2.04	2.12	2.02	2.03	2.04	1.95	2.04	2.12
K^{+}	0.17	0.12	0.18	0.13	0.20	0.12	0.11	0.14	0.20
Ni^{+}	0.00	0.00	0.00	0.00	0.00	0.00	0.00	0.00	0.00
Zn	0.00	0.00	0.00	0.00	0.00	0.00	0.00	0.00	0.00
V	0.00	0.00	0.00	0.00	0.00	0.00	0.00	0.00	0.00
Σcat	**20.06**	**20.04**	**20.04**	**20.01**	**20.01**	**20.01**	**20.00**	**20.01**	**19.99**
Or	4	3	4	3	5	3	3	3	5
Ab	53	50	52	50	50	50	48	50	53
An	43	47	43	47	45	47	49	46	42

Appendix 5
Feldspar EMP data - cation calculations based on 32 oxygen

No	17913 5.12 pla	17913 5.2 plag	17913 5.3 plag	17913 5.4 plag	17913 6.2 plag	17913 6.3 plag	17913 6.4 plag	17913 6.5 plag	17913 6.6 plag
Mineral	**Plagioclase**	**Plagioclase**	**Plagioclase**	**Plagioclase**	**Plagioclase**	**Plagioclase**	**Plagioclase**	**Plagioclase**	**Plagioclase**
Wt %									
SiO2	56.91	56.74	55.74	55.35	56.19	55.60	55.66	56.03	57.01
TiO2	0.06	0.05	0.04	0.06	0.04	0.07	0.03	0.05	0.02
Al2O3	26.35	26.37	27.13	27.08	26.60	27.31	27.07	27.08	26.31
Cr2O3	0.00	0.00	0.02	0.00	0.00	0.01	0.02	0.00	0.00
FeO	0.30	0.25	0.20	0.24	0.21	0.26	0.24	0.24	0.22
MnO	0.00	0.00	0.00	0.00	0.01	0.00	0.00	0.02	0.00
MgO	0.00	0.00	0.00	0.00	0.00	0.00	0.00	0.00	0.00
CaO	9.04	9.34	9.96	9.95	9.50	10.32	10.09	9.84	9.05
Na2O	6.00	5.99	5.57	5.67	5.89	5.49	5.61	5.77	6.08
K2O	0.86	0.65	0.62	0.58	0.65	0.56	0.56	0.62	0.76
NiO	0.00	0.00	0.00	0.01	0.01	0.03	0.00	0.02	0.00
Total	**99.52**	**99.38**	**99.28**	**98.94**	**99.10**	**99.65**	**99.27**	**99.67**	**99.47**
Cations									
Si^{4+}	10.30	10.28	10.13	10.10	10.22	10.08	10.12	10.14	10.32
Ti^{4+}	0.01	0.01	0.00	0.01	0.00	0.01	0.00	0.01	0.00
Al^{3+}	5.62	5.63	5.81	5.82	5.70	5.83	5.80	5.78	5.61
Cr^{3+}	0.00	0.00	0.00	0.00	0.00	0.00	0.00	0.00	0.00
Fe^{2+}	0.05	0.04	0.03	0.04	0.03	0.04	0.04	0.04	0.03
Mn^{2+}	0.00	0.00	0.00	0.00	0.00	0.00	0.00	0.00	0.00
Mg^{2+}	0.00	0.00	0.00	0.00	0.00	0.00	0.00	0.00	0.00
Ca^{2+}	1.75	1.81	1.94	1.95	1.85	2.00	1.97	1.91	1.76
Na^{+}	2.10	2.11	1.96	2.00	2.08	1.93	1.98	2.02	2.13
K^{+}	0.20	0.15	0.14	0.14	0.15	0.13	0.13	0.14	0.18
Ni^{+}	0.00	0.00	0.00	0.00	0.00	0.00	0.00	0.00	0.00
Zn	0.00	0.00	0.00	0.00	0.00	0.00	0.00	0.00	0.00
V	0.00	0.00	0.00	0.00	0.00	0.00	0.00	0.00	0.00
Σcat	**20.03**	**20.02**	**20.02**	**20.05**	**20.04**	**20.03**	**20.03**	**20.05**	**20.03**
Or	5	4	4	3	4	3	3	4	4
Ab	52	52	49	49	51	47	49	50	52
An	43	45	48	48	45	49	48	47	43

Appendix 5
Feldspar EMP data - cation calculations based on 32 oxygen

No	17913 6.7 plag	17913 6.8 plag	17914 1.17 pla	17914 1.17 pla	17914 1.17 pla	17914 1.17 pla	17914 1.17 pla	17914 1.17 pla	17914 1.17 pla
Mineral	**Plagioclase**	**Plagioclase**	**Plagioclase**	**Plagioclase**	**Plagioclase**	**Plagioclase**	**Plagioclase**	**Plagioclase**	**Plagioclase**
Wt %									
SiO2	56.73	55.88	54.88	55.25	55.89	55.86	55.43	55.19	55.60
TiO2	0.06	0.09	0.07	0.10	0.06	0.07	0.09	0.09	0.06
Al2O3	25.89	27.14	27.92	27.29	27.51	27.31	27.44	27.26	27.56
Cr2O3	0.00	0.01	0.00	0.01	0.00	0.00	0.01	0.03	0.01
FeO	0.21	0.27	0.32	0.28	0.29	0.32	0.28	0.32	0.30
MnO	0.00	0.01	0.03	0.00	0.02	0.01	0.00	0.01	0.02
MgO	0.00	0.00	0.00	0.00	0.00	0.00	0.00	0.00	0.00
CaO	9.08	10.04	10.85	10.57	10.39	10.52	10.60	10.61	10.21
Na2O	5.97	5.77	5.18	5.25	5.47	5.46	5.48	5.30	5.48
K2O	0.77	0.64	0.48	0.49	0.51	0.52	0.53	0.54	0.55
NiO	0.00	0.00	0.03	0.01	0.00	0.01	0.00	0.00	0.01
Total	**98.70**	**99.84**	**99.76**	**99.24**	**100.14**	**100.10**	**99.85**	**99.34**	**99.80**
Cations									
Si^{4+}	10.34	10.11	9.95	10.05	10.07	10.08	10.04	10.04	10.06
Ti^{4+}	0.01	0.01	0.01	0.01	0.01	0.01	0.01	0.01	0.01
Al^{3+}	5.56	5.79	5.97	5.85	5.84	5.81	5.86	5.85	5.88
Cr^{3+}	0.00	0.00	0.00	0.00	0.00	0.00	0.00	0.00	0.00
Fe^{2+}	0.03	0.04	0.05	0.04	0.04	0.05	0.04	0.05	0.05
Mn^{2+}	0.00	0.00	0.00	0.00	0.00	0.00	0.00	0.00	0.00
Mg^{2+}	0.00	0.00	0.00	0.00	0.00	0.00	0.00	0.00	0.00
Ca^{2+}	1.77	1.95	2.11	2.06	2.01	2.04	2.06	2.07	1.98
Na^{+}	2.11	2.03	1.82	1.85	1.91	1.91	1.92	1.87	1.92
K^{+}	0.18	0.15	0.11	0.11	0.12	0.12	0.12	0.12	0.13
Ni^{+}	0.00	0.00	0.00	0.00	0.00	0.00	0.00	0.00	0.00
Zn	0.00	0.00	0.00	0.00	0.00	0.00	0.00	0.00	0.00
V	0.00	0.00	0.00	0.00	0.00	0.00	0.00	0.00	0.00
Σcat	**20.01**	**20.07**	**20.02**	**19.99**	**20.01**	**20.02**	**20.05**	**20.02**	**20.02**
Or	4	4	3	3	3	3	3	3	3
Ab	52	49	45	46	47	47	47	46	48
An	44	47	52	51	50	50	50	51	49

Appendix 5
Feldspar EMP data - cation calculations based on 32 oxygen

No	17914 1.17 pla	17914 1.17 pla	17914 1.17 pla	17914 1.17 pla	17914 1.17 pla	17914 1.17 pla	17914 4.10 pla	17914 4.11 pla	17914 4.12 pla
Mineral	**Plagioclase**	**Plagioclase**	**Plagioclase**	**Plagioclase**	**Plagioclase**	**Plagioclase**	**Plagioclase**	**Plagioclase**	**Plagioclase**
Wt %									
SiO2	56.00	56.46	56.84	56.83	56.46	57.54	56.14	56.60	56.79
TiO2	0.04	0.06	0.05	0.07	0.08	0.04	0.06	0.05	0.07
Al2O3	26.96	26.31	26.31	26.55	25.86	25.67	26.75	26.54	26.43
Cr2O3	0.00	0.00	0.04	0.01	0.01	0.00	0.00	0.00	0.01
FeO	0.34	0.29	0.31	0.30	0.99	0.29	0.33	0.46	0.41
MnO	0.01	0.00	0.00	0.02	0.02	0.00	0.03	0.01	0.00
MgO	0.00	0.00	0.00	0.00	0.10	0.00	0.00	0.01	0.00
CaO	10.17	9.69	9.50	9.69	9.17	9.00	10.08	9.66	9.63
Na2O	5.56	5.69	5.79	5.75	5.50	6.04	5.51	5.76	5.74
K2O	0.57	0.65	0.70	0.75	0.73	0.80	0.66	0.62	0.74
NiO	0.00	0.00	0.00	0.02	0.02	0.04	0.03	0.00	0.00
Total	**99.65**	**99.16**	**99.54**	**99.98**	**98.94**	**99.43**	**99.59**	**99.70**	**99.82**
Cations									
Si^{4+}	10.14	10.26	10.29	10.25	10.30	10.41	10.18	10.24	10.26
Ti^{4+}	0.01	0.01	0.01	0.01	0.01	0.01	0.01	0.01	0.01
Al^{3+}	5.76	5.64	5.61	5.64	5.56	5.48	5.71	5.66	5.63
Cr^{3+}	0.00	0.00	0.01	0.00	0.00	0.00	0.00	0.00	0.00
Fe^{2+}	0.05	0.04	0.05	0.04	0.15	0.04	0.05	0.07	0.06
Mn^{2+}	0.00	0.00	0.00	0.00	0.00	0.00	0.00	0.00	0.00
Mg^{2+}	0.00	0.00	0.00	0.00	0.03	0.00	0.00	0.00	0.00
Ca^{2+}	1.97	1.89	1.84	1.87	1.79	1.75	1.96	1.87	1.86
Na^{+}	1.95	2.00	2.03	2.01	1.94	2.12	1.94	2.02	2.01
K^{+}	0.13	0.15	0.16	0.17	0.17	0.18	0.15	0.14	0.17
Ni^{+}	0.00	0.00	0.00	0.00	0.00	0.01	0.00	0.00	0.00
Zn	0.00	0.00	0.00	0.00	0.00	0.00	0.00	0.00	0.00
V	0.00	0.00	0.00	0.00	0.00	0.00	0.00	0.00	0.00
Σcat	**20.01**	**19.99**	**19.99**	**20.01**	**19.96**	**19.99**	**20.00**	**20.01**	**20.01**
Or	3	4	4	4	4	5	4	4	4
Ab	48	50	50	50	50	52	48	50	50
An	49	47	46	46	46	43	48	46	46

Appendix 5
Feldspar EMP data - cation calculations based on 32 oxygen

No	17914 4.13 pla	17915 1.18 pla	17915 1.8 plag	17915 2.9 plag	17915 3.4 plag	17915 3.5 plag	17915 3.6 plag	17915 5.4 plag	17915 5.5 plag
Mineral	**Plagioclase**	**Plagioclase**	**Plagioclase**	**Plagioclase**	**Plagioclase**	**Plagioclase**	**Plagioclase**	**Plagioclase**	**Plagioclase**
Wt %									
SiO2	57.16	56.82	58.06	56.01	56.92	56.57	57.87	58.39	58.36
TiO2	0.06	0.01	0.01	0.00	0.02	0.00	0.01	0.02	0.01
Al2O3	26.40	26.12	25.26	26.04	26.19	26.21	25.47	24.64	24.43
Cr2O3	0.00	0.00	0.00	0.03	0.04	0.00	0.02	0.00	0.01
FeO	0.32	0.45	0.44	0.42	0.46	0.48	0.42	0.43	0.45
MnO	0.00	0.00	0.02	0.03	0.04	0.03	0.01	0.03	0.00
MgO	0.00	0.00	0.00	0.00	0.00	0.00	0.00	0.00	0.00
CaO	9.48	9.96	9.37	10.41	10.25	10.43	9.51	9.03	9.13
Na2O	5.82	5.49	5.86	5.19	5.40	5.30	5.72	6.02	5.67
K2O	0.72	0.61	0.60	0.52	0.60	0.57	0.72	0.57	0.74
NiO	0.02	0.01	0.02	0.02	0.00	0.01	0.00	0.03	0.01
Total	**99.98**	**99.46**	**99.63**	**98.67**	**99.91**	**99.59**	**99.75**	**99.17**	**98.81**
Cations									
Si^{4+}	10.30	10.30	10.48	10.24	10.28	10.25	10.44	10.58	10.61
Ti^{4+}	0.01	0.00	0.00	0.00	0.00	0.00	0.00	0.00	0.00
Al^{3+}	5.61	5.58	5.37	5.61	5.57	5.60	5.42	5.26	5.23
Cr^{3+}	0.00	0.00	0.00	0.00	0.01	0.00	0.00	0.00	0.00
Fe^{2+}	0.05	0.07	0.07	0.06	0.07	0.07	0.06	0.07	0.07
Mn^{2+}	0.00	0.00	0.00	0.00	0.01	0.00	0.00	0.00	0.00
Mg^{2+}	0.00	0.00	0.00	0.00	0.00	0.00	0.00	0.00	0.00
Ca^{2+}	1.83	1.93	1.81	2.04	1.98	2.03	1.84	1.75	1.78
Na^{+}	2.03	1.93	2.05	1.84	1.89	1.86	2.00	2.11	2.00
K^{+}	0.17	0.14	0.14	0.12	0.14	0.13	0.17	0.13	0.17
Ni^{+}	0.00	0.00	0.00	0.00	0.00	0.00	0.00	0.00	0.00
Zn	0.00	0.00	0.00	0.00	0.00	0.00	0.00	0.00	0.00
V	0.00	0.00	0.00	0.00	0.00	0.00	0.00	0.00	0.00
Σcat	**19.99**	**19.95**	**19.93**	**19.93**	**19.94**	**19.95**	**19.93**	**19.91**	**19.86**
Or	4	4	3	3	3	3	4	3	4
Ab	50	48	51	46	47	46	50	53	51
An	45	48	45	51	49	50	46	44	45

Appendix 5
Feldspar EMP data - cation calculations based on 32 oxygen

No	17916 1.4 kspa	17916 1b.6 ksp	17916 2.4 kspa	17916 3.2 kspa	17916 4.4 kspa	17916 4.5 kspa	17918 2.1 euh	17918 2.2 euh	17918 2.3 kspa
Mineral	**Kspar**	**Kspar**	**Kspar**	**Kspar**	**Kspar**	**Kspar**	**Kspar**	**Kspar**	**Kspar**
Wt %									
SiO2	64.95	63.74	64.70	64.20	64.39	63.14	67.28	66.50	62.94
TiO2	0.00	0.00	0.00	0.00	0.00	0.03	0.00	0.00	0.00
Al2O3	21.63	21.29	21.42	21.11	21.26	17.83	18.68	18.90	22.64
Cr2O3	0.00	0.00	0.00	0.00	0.00	0.02	0.01	0.02	0.01
FeO	0.13	0.24	0.22	0.20	0.24	4.41	0.16	0.13	0.23
MnO	0.03	0.00	0.00	0.01	0.00	0.04	0.01	0.00	0.02
MgO	0.00	0.00	0.00	0.00	0.00	0.67	0.01	0.00	0.01
CaO	3.36	3.44	3.26	3.24	3.22	1.27	0.71	0.75	4.79
Na2O	7.59	7.38	7.56	7.40	7.35	4.25	5.79	5.83	7.91
K2O	3.40	3.77	3.80	3.58	3.83	6.74	8.02	8.16	1.93
NiO	0.00	0.00	0.02	0.03	0.01	0.02	0.01	0.00	0.04
Total	**101.09**	**99.87**	**100.99**	**99.78**	**100.29**	**98.41**	**100.68**	**100.29**	**100.53**
Cations									
Si^{4+}	11.46	11.42	11.46	11.49	11.47	11.72	12.01	11.94	11.18
Ti^{4+}	0.00	0.00	0.00	0.00	0.00	0.00	0.00	0.00	0.00
Al^{3+}	4.50	4.50	4.47	4.45	4.47	3.90	3.93	4.00	4.74
Cr^{3+}	0.00	0.00	0.00	0.00	0.00	0.00	0.00	0.00	0.00
Fe^{2+}	0.02	0.04	0.03	0.03	0.04	0.68	0.02	0.02	0.03
Mn^{2+}	0.00	0.00	0.00	0.00	0.00	0.01	0.00	0.00	0.00
Mg^{2+}	0.00	0.00	0.00	0.00	0.00	0.19	0.00	0.00	0.00
Ca^{2+}	0.64	0.66	0.62	0.62	0.61	0.25	0.14	0.14	0.91
Na^{+}	2.60	2.57	2.60	2.57	2.54	1.53	2.00	2.03	2.72
K^{+}	0.77	0.86	0.86	0.82	0.87	1.60	1.83	1.87	0.44
Ni^{+}	0.00	0.00	0.00	0.00	0.00	0.00	0.00	0.00	0.01
Zn	0.00	0.00	0.00	0.00	0.00	0.00	0.00	0.00	0.00
V	0.00	0.00	0.00	0.00	0.00	0.00	0.00	0.00	0.00
Σcat	**19.98**	**20.04**	**20.04**	**19.98**	**20.00**	**19.89**	**19.94**	**20.01**	**20.03**
Or	19	21	21	20	22	47	46	46	11
Ab	65	63	64	64	63	45	50	50	67
An	16	16	15	16	15	7	3	4	22

Appendix 5
Feldspar EMP data - cation calculations based on 32 oxygen

No	17918 2.5 fspa	17918 2.6 kspa	17918 3.6 kspa	17918 3.7 kspa	17918 5.5 kspa	17921 1.13 ksp	17921 2.7 kspa	17921 3.16 ksp	17921 3.17 ksp
Mineral	**Kspar**	**Kspar**	**Kspar**	**Kspar**	**Kspar**	**Kspar**	**Kspar**	**Kspar**	**Kspar**
Wt %									
SiO2	62.54	63.19	63.40	62.82	59.88	63.25	62.36	67.10	62.86
TiO2	0.00	0.00	0.00	0.00	0.00	0.00	0.00	0.00	0.00
Al2O3	22.89	22.53	22.58	22.72	25.19	21.66	22.21	18.34	22.35
Cr2O3	0.00	0.00	0.00	0.00	0.00	0.02	0.01	0.00	0.01
FeO	0.22	0.21	0.22	0.16	0.57	0.25	0.25	0.14	0.24
MnO	0.02	0.00	0.00	0.04	0.02	0.00	0.00	0.00	0.01
MgO	0.00	0.00	0.00	0.01	0.00	0.00	0.00	0.00	0.00
CaO	5.15	4.62	4.54	4.88	7.73	4.48	5.14	0.47	4.95
Na2O	7.73	7.85	7.75	7.57	5.33	7.97	7.22	5.29	7.18
K2O	1.78	2.20	2.68	2.06	0.03	1.80	2.09	8.59	2.28
NiO	0.00	0.02	0.00	0.00	0.00	0.00	0.01	0.00	0.00
Total	**100.32**	**100.62**	**101.16**	**100.28**	**98.78**	**99.43**	**99.27**	**99.93**	**99.87**
Cations									
Si^{4+}	11.13	11.21	11.21	11.17	10.75	11.33	11.21	12.07	11.23
Ti^{4+}	0.00	0.00	0.00	0.00	0.00	0.00	0.00	0.00	0.00
Al^{3+}	4.80	4.71	4.71	4.76	5.33	4.57	4.70	3.89	4.70
Cr^{3+}	0.00	0.00	0.00	0.00	0.00	0.00	0.00	0.00	0.00
Fe^{2+}	0.03	0.03	0.03	0.02	0.09	0.04	0.04	0.02	0.04
Mn^{2+}	0.00	0.00	0.00	0.01	0.00	0.00	0.00	0.00	0.00
Mg^{2+}	0.00	0.00	0.00	0.00	0.00	0.00	0.00	0.00	0.00
Ca^{2+}	0.98	0.88	0.86	0.93	1.49	0.86	0.99	0.09	0.95
Na^{+}	2.67	2.70	2.66	2.61	1.86	2.77	2.51	1.85	2.49
K^{+}	0.40	0.50	0.60	0.47	0.01	0.41	0.48	1.97	0.52
Ni^{+}	0.00	0.00	0.00	0.00	0.00	0.00	0.00	0.00	0.00
Zn	0.00	0.00	0.00	0.00	0.00	0.00	0.00	0.00	0.00
V	0.00	0.00	0.00	0.00	0.00	0.00	0.00	0.00	0.00
Σcat	**20.01**	**20.03**	**20.07**	**19.98**	**19.52**	**19.98**	**19.94**	**19.89**	**19.92**
Or	10	12	15	12	0	10	12	50	13
Ab	66	66	64	65	55	69	63	47	63
An	24	22	21	23	44	21	25	2	24

Appendix 5
Feldspar EMP data - cation calculations based on 32 oxygen

No	17921 3.18 ksp	17921 3.8 kspa	17922 1.10 pla	17922 1.14 pla	17922 1.2 plag	17922 1.24 fpla	17922 1.26 pla	17922 1.27 pla	17922 1.34 pla
Mineral	**Kspar**	**Kspar**	**Plagioclase**	**Plagioclase**	**Plagioclase**	**Plagioclase**	**Plagioclase**	**Plagioclase**	**Plagioclase**
Wt %									
SiO2	63.49	63.15	56.95	58.79	57.68	62.37	60.26	60.36	61.80
TiO2	0.02	0.00	0.05	0.04	0.08	0.03	0.00	0.04	0.04
Al2O3	21.97	22.15	26.30	24.98	25.71	22.64	24.09	24.36	22.70
Cr2O3	0.02	0.01	0.01	0.00	0.00	0.02	0.03	0.02	0.02
FeO	0.28	0.23	0.26	0.26	0.38	0.25	0.33	0.28	0.34
MnO	0.01	0.00	0.00	0.02	0.02	0.00	0.00	0.01	0.00
MgO	0.00	0.00	0.00	0.00	0.00	0.00	0.00	0.00	0.00
CaO	4.43	4.65	9.73	7.77	8.80	5.29	7.22	7.00	5.70
Na2O	7.30	7.25	5.81	6.72	6.24	7.56	6.82	6.97	7.60
K2O	2.61	2.56	0.60	0.88	0.68	1.66	1.01	1.06	1.29
NiO	0.02	0.00	0.00	0.00	0.00	0.00	0.00	0.00	0.01
Total	**100.16**	**100.00**	**99.72**	**99.45**	**99.59**	**99.83**	**99.75**	**100.10**	**99.49**
Cations									
Si^{4+}	11.31	11.27	10.29	10.60	10.42	11.14	10.81	10.79	11.09
Ti^{4+}	0.00	0.00	0.01	0.00	0.01	0.00	0.00	0.01	0.01
Al^{3+}	4.61	4.66	5.60	5.31	5.47	4.77	5.09	5.13	4.80
Cr^{3+}	0.00	0.00	0.00	0.00	0.00	0.00	0.00	0.00	0.00
Fe^{2+}	0.04	0.03	0.04	0.04	0.06	0.04	0.05	0.04	0.05
Mn^{2+}	0.00	0.00	0.00	0.00	0.00	0.00	0.00	0.00	0.00
Mg^{2+}	0.00	0.00	0.00	0.00	0.00	0.00	0.00	0.00	0.00
Ca^{2+}	0.85	0.89	1.88	1.50	1.70	1.01	1.39	1.34	1.10
Na^{+}	2.52	2.51	2.03	2.35	2.19	2.62	2.37	2.42	2.64
K^{+}	0.59	0.58	0.14	0.20	0.16	0.38	0.23	0.24	0.29
Ni^{+}	0.00	0.00	0.00	0.00	0.00	0.00	0.00	0.00	0.00
Zn	0.00	0.00	0.00	0.00	0.00	0.00	0.00	0.00	0.00
V	0.00	0.00	0.00	0.00	0.00	0.00	0.00	0.00	0.00
Σcat	**19.94**	**19.95**	**19.99**	**20.01**	**20.01**	**19.97**	**19.94**	**19.97**	**19.98**
Or	15	15	3	5	4	9	6	6	7
Ab	64	63	50	58	54	65	59	60	66
An	21	22	46	37	42	25	35	34	27

Appendix 5
Feldspar EMP data - cation calculations based on 32 oxygen

No	17922 1.34 pla	17922 1.35 pla	17922 1.8 plag	17922 1.9 plag	17922 2.1 plag	17922 2.10 pla	17922 2.14 pla	17922 2.16 pla	17922 2.17 pla
Mineral	**Plagioclase**	**Plagioclase**	**Plagioclase**	**Plagioclase**	**Plagioclase**	**Plagioclase**	**Plagioclase**	**Plagioclase**	**Plagioclase**
Wt %									
SiO2	61.69	60.87	58.60	56.97	56.41	57.05	60.93	56.64	56.19
TiO2	0.02	0.04	0.02	0.03	0.05	0.05	0.02	0.03	0.05
Al2O3	23.53	23.18	25.15	26.17	26.53	26.26	23.79	25.79	26.46
Cr2O3	0.00	0.00	0.02	0.00	0.02	0.00	0.00	0.00	0.00
FeO	0.31	0.31	0.20	0.23	0.24	0.27	0.25	0.24	0.26
MnO	0.00	0.00	0.00	0.02	0.02	0.02	0.00	0.00	0.00
MgO	0.00	0.00	0.00	0.00	0.00	0.00	0.00	0.00	0.00
CaO	5.91	6.45	8.26	9.57	10.13	9.41	6.18	9.52	10.14
Na2O	7.45	7.03	6.48	5.79	5.52	5.94	7.22	5.76	5.55
K2O	1.34	1.24	0.80	0.58	0.53	0.68	1.34	0.61	0.59
NiO	0.00	0.00	0.00	0.00	0.00	0.02	0.01	0.03	0.02
Total	**100.24**	**99.12**	**99.53**	**99.36**	**99.44**	**99.70**	**99.74**	**98.61**	**99.25**
Cations									
Si^{4+}	10.99	10.97	10.56	10.32	10.22	10.31	10.91	10.34	10.21
Ti^{4+}	0.00	0.01	0.00	0.00	0.01	0.01	0.00	0.00	0.01
Al^{3+}	4.94	4.92	5.34	5.59	5.67	5.59	5.02	5.55	5.67
Cr^{3+}	0.00	0.00	0.00	0.00	0.00	0.00	0.00	0.00	0.00
Fe^{2+}	0.05	0.05	0.03	0.03	0.04	0.04	0.04	0.04	0.04
Mn^{2+}	0.00	0.00	0.00	0.00	0.00	0.00	0.00	0.00	0.00
Mg^{2+}	0.00	0.00	0.00	0.00	0.00	0.00	0.00	0.00	0.00
Ca^{2+}	1.13	1.24	1.60	1.86	1.97	1.82	1.19	1.86	1.97
Na^{+}	2.57	2.46	2.26	2.03	1.94	2.08	2.51	2.04	1.95
K^{+}	0.31	0.28	0.18	0.13	0.12	0.16	0.31	0.14	0.14
Ni^{+}	0.00	0.00	0.00	0.00	0.00	0.00	0.00	0.00	0.00
Zn	0.00	0.00	0.00	0.00	0.00	0.00	0.00	0.00	0.00
V	0.00	0.00	0.00	0.00	0.00	0.00	0.00	0.00	0.00
Σcat	**19.98**	**19.93**	**19.98**	**19.97**	**19.97**	**20.01**	**19.98**	**19.97**	**19.99**
Or	8	7	5	3	3	4	8	3	3
Ab	64	62	56	51	48	51	63	50	48
An	28	31	39	46	49	45	30	46	49

Appendix 5
Feldspar EMP data - cation calculations based on 32 oxygen

No	17922 2.2 plag	17922 2.3 plag	17922 2.4 plag	17922 2.5 plag	17922 3.1 plag	17922 3.10plag	17922 3.11plag	17922 3.12 pla	17922 3.13 pla
Mineral	**Plagioclase**	**Plagioclase**	**Plagioclase**	**Plagioclase**	**Plagioclase**	**Plagioclase**	**Plagioclase**	**Plagioclase**	**Plagioclase**
Wt %									
SiO2	56.18	55.95	56.04	55.94	55.90	56.10	56.37	56.33	56.20
TiO2	0.05	0.04	0.03	0.06	0.14	0.04	0.05	0.02	0.04
Al2O3	26.60	26.48	26.63	26.61	26.25	26.52	26.39	26.33	26.29
Cr2O3	0.00	0.00	0.02	0.03	0.02	0.01	0.00	0.00	0.00
FeO	0.21	0.21	0.24	0.31	0.46	0.26	0.24	0.28	0.21
MnO	0.00	0.00	0.02	0.01	0.00	0.00	0.00	0.00	0.01
MgO	0.00	0.00	0.00	0.00	0.00	0.00	0.00	0.00	0.00
CaO	10.17	10.08	10.16	10.08	9.82	9.78	9.88	9.76	10.02
Na2O	5.42	5.56	5.51	5.54	5.56	5.67	5.71	5.56	5.48
K2O	0.52	0.58	0.55	0.56	0.64	0.59	0.63	0.65	0.60
NiO	0.00	0.00	0.00	0.00	0.01	0.00	0.00	0.02	0.00
Total	**99.15**	**98.89**	**99.19**	**99.13**	**98.79**	**98.97**	**99.29**	**98.95**	**98.84**
Cations									
Si^{4+}	10.21	10.20	10.19	10.18	10.21	10.22	10.24	10.26	10.24
Ti^{4+}	0.01	0.01	0.00	0.01	0.02	0.01	0.01	0.00	0.01
Al^{3+}	5.70	5.69	5.71	5.71	5.65	5.69	5.65	5.65	5.65
Cr^{3+}	0.00	0.00	0.00	0.00	0.00	0.00	0.00	0.00	0.00
Fe^{2+}	0.03	0.03	0.04	0.05	0.07	0.04	0.04	0.04	0.03
Mn^{2+}	0.00	0.00	0.00	0.00	0.00	0.00	0.00	0.00	0.00
Mg^{2+}	0.00	0.00	0.00	0.00	0.00	0.00	0.00	0.00	0.00
Ca^{2+}	1.98	1.97	1.98	1.97	1.92	1.91	1.92	1.90	1.96
Na^{+}	1.91	1.97	1.94	1.95	1.97	2.00	2.01	1.96	1.94
K^{+}	0.12	0.13	0.13	0.13	0.15	0.14	0.15	0.15	0.14
Ni^{+}	0.00	0.00	0.00	0.00	0.00	0.00	0.00	0.00	0.00
Zn	0.00	0.00	0.00	0.00	0.00	0.00	0.00	0.00	0.00
V	0.00	0.00	0.00	0.00	0.00	0.00	0.00	0.00	0.00
Σcat	**19.95**	**20.00**	**19.99**	**20.00**	**20.00**	**20.00**	**20.01**	**19.97**	**19.96**
Or	3	3	3	3	4	3	4	4	3
Ab	48	48	48	48	49	49	49	49	48
An	49	48	49	49	48	47	47	47	49

Appendix 5
Feldspar EMP data - cation calculations based on 32 oxygen

No	17922 3.14 pla	17922 3.15 pla	17922 3.16 pla	17922 3.17 pla	17922 3.18 pla	17922 3.19 pla	17922 3.2 plag	17922 3.20 pla	17922 3.21 pla
Mineral	**Plagioclase**	**Plagioclase**	**Plagioclase**	**Plagioclase**	**Plagioclase**	**Plagioclase**	**Plagioclase**	**Plagioclase**	**Plagioclase**
Wt %									
SiO2	58.02	59.37	56.26	56.49	56.40	56.47	56.61	56.59	56.33
TiO2	0.05	0.02	0.04	0.04	0.04	0.05	0.04	0.05	0.04
Al2O3	25.59	24.93	26.70	26.64	26.62	26.75	26.21	26.69	26.74
Cr2O3	0.00	0.00	0.02	0.00	0.01	0.00	0.00	0.02	0.00
FeO	0.30	0.23	0.27	0.23	0.27	0.22	0.20	0.28	0.28
MnO	0.00	0.00	0.00	0.01	0.03	0.00	0.00	0.03	0.00
MgO	0.00	0.00	0.00	0.00	0.00	0.00	0.00	0.00	0.00
CaO	8.85	7.72	9.80	9.79	9.80	9.87	9.89	9.78	9.83
Na2O	6.12	6.53	5.69	5.70	5.61	5.68	5.63	5.65	5.82
K2O	0.68	0.85	0.65	0.62	0.62	0.57	0.59	0.56	0.47
NiO	0.00	0.00	0.02	0.00	0.00	0.00	0.00	0.00	0.01
Total	**99.61**	**99.66**	**99.44**	**99.54**	**99.39**	**99.62**	**99.18**	**99.66**	**99.53**
Cations									
Si^{4+}	10.46	10.66	10.20	10.23	10.22	10.21	10.28	10.23	10.20
Ti^{4+}	0.01	0.00	0.01	0.01	0.00	0.01	0.01	0.01	0.01
Al^{3+}	5.44	5.28	5.71	5.68	5.69	5.70	5.61	5.69	5.71
Cr^{3+}	0.00	0.00	0.00	0.00	0.00	0.00	0.00	0.00	0.00
Fe^{2+}	0.04	0.04	0.04	0.04	0.04	0.03	0.03	0.04	0.04
Mn^{2+}	0.00	0.00	0.00	0.00	0.00	0.00	0.00	0.00	0.00
Mg^{2+}	0.00	0.00	0.00	0.00	0.00	0.00	0.00	0.00	0.00
Ca^{2+}	1.71	1.49	1.90	1.90	1.90	1.91	1.92	1.89	1.91
Na^{+}	2.14	2.27	2.00	2.00	1.97	1.99	1.98	1.98	2.04
K^{+}	0.16	0.19	0.15	0.14	0.14	0.13	0.14	0.13	0.11
Ni^{+}	0.00	0.00	0.00	0.00	0.00	0.00	0.00	0.00	0.00
Zn	0.00	0.00	0.00	0.00	0.00	0.00	0.00	0.00	0.00
V	0.00	0.00	0.00	0.00	0.00	0.00	0.00	0.00	0.00
Σcat	**19.96**	**19.93**	**20.01**	**20.00**	**19.98**	**19.99**	**19.97**	**19.97**	**20.02**
Or	4	5	4	4	4	3	3	3	3
Ab	53	58	49	49	49	49	49	49	50
An	43	38	47	47	47	47	48	47	47

Appendix 5
Feldspar EMP data - cation calculations based on 32 oxygen

No	17922 3.22 pla	17922 3.23 pla	17922 3.24 pla	17922 3.25 pla	17922 3.27 pla	17922 3.28 pla	17922 3.4 plag	17922 3.5 plag	17922 3.6 plag
Mineral	**Plagioclase**	**Plagioclase**	**Plagioclase**	**Plagioclase**	**Plagioclase**	**Plagioclase**	**Plagioclase**	**Plagioclase**	**Plagioclase**
Wt %									
SiO2	56.64	55.95	56.69	56.52	56.45	57.33	56.62	56.22	56.10
TiO2	0.04	0.29	0.05	0.03	0.06	0.04	0.05	0.02	0.05
Al2O3	26.88	26.69	26.70	26.75	26.71	26.18	26.84	26.69	26.74
Cr2O3	0.00	0.01	0.00	0.00	0.00	0.01	0.00	0.00	0.00
FeO	0.26	0.84	0.27	0.21	0.22	0.26	0.24	0.24	0.24
MnO	0.00	0.00	0.02	0.02	0.00	0.01	0.02	0.02	0.01
MgO	0.00	0.00	0.00	0.00	0.00	0.00	0.00	0.00	0.00
CaO	9.86	9.74	9.85	9.83	9.89	9.22	9.96	9.79	9.84
Na2O	5.75	5.64	5.71	5.63	5.64	6.03	5.63	5.74	5.71
K2O	0.57	0.58	0.57	0.61	0.61	0.70	0.61	0.64	0.61
NiO	0.01	0.00	0.02	0.01	0.03	0.01	0.00	0.01	0.00
Total	**100.01**	**99.74**	**99.87**	**99.62**	**99.62**	**99.79**	**99.96**	**99.38**	**99.29**
Cations									
Si^{4+}	10.21	10.14	10.23	10.22	10.21	10.34	10.21	10.20	10.19
Ti^{4+}	0.00	0.04	0.01	0.00	0.01	0.01	0.01	0.00	0.01
Al^{3+}	5.71	5.70	5.68	5.70	5.70	5.57	5.70	5.71	5.72
Cr^{3+}	0.00	0.00	0.00	0.00	0.00	0.00	0.00	0.00	0.00
Fe^{2+}	0.04	0.13	0.04	0.03	0.03	0.04	0.04	0.04	0.04
Mn^{2+}	0.00	0.00	0.00	0.00	0.00	0.00	0.00	0.00	0.00
Mg^{2+}	0.00	0.00	0.00	0.00	0.00	0.00	0.00	0.00	0.00
Ca^{2+}	1.90	1.89	1.90	1.90	1.92	1.78	1.92	1.90	1.91
Na^{+}	2.01	1.98	2.00	1.98	1.98	2.11	1.97	2.02	2.01
K^{+}	0.13	0.13	0.13	0.14	0.14	0.16	0.14	0.15	0.14
Ni^{+}	0.00	0.00	0.00	0.00	0.00	0.00	0.00	0.00	0.00
Zn	0.00	0.00	0.00	0.00	0.00	0.00	0.00	0.00	0.00
V	0.00	0.00	0.00	0.00	0.00	0.00	0.00	0.00	0.00
Σcat	**20.00**	**20.02**	**19.99**	**19.98**	**19.99**	**20.01**	**19.99**	**20.03**	**20.02**
Or	3	3	3	4	3	4	3	4	3
Ab	50	49	50	49	49	52	49	50	49
An	47	47	47	47	48	44	48	47	47

Appendix 5
Feldspar EMP data - cation calculations based on 32 oxygen

No	17922 3.7 plag	17922 3.8 plag	17922 3.9 plag	18002 2.6 plag	18002 2.7 plag	18002 3.2 plag	18002 3.2 plag	18002 3.2 plag	18002 3.2 plag
Mineral	**Plagioclase**	**Plagioclase**	**Plagioclase**	**Plagioclase**	**Plagioclase**	**Plagioclase**	**Plagioclase**	**Plagioclase**	**Plagioclase**
Wt %									
SiO2	56.29	56.41	56.45	54.97	56.65	55.04	55.61	55.47	56.33
TiO2	0.05	0.06	0.02	0.09	0.08	0.07	0.09	0.12	0.08
Al2O3	26.73	26.57	26.55	27.66	26.70	27.83	27.56	27.27	26.87
Cr2O3	0.01	0.01	0.03	0.00	0.00	0.00	0.00	0.00	0.00
FeO	0.26	0.25	0.30	0.29	0.35	0.27	0.28	0.58	0.24
MnO	0.02	0.01	0.00	0.00	0.01	0.00	0.00	0.00	0.02
MgO	0.00	0.00	0.00	0.00	0.00	0.00	0.00	0.00	0.00
CaO	9.90	9.86	9.83	10.69	9.35	10.55	10.33	10.19	9.53
Na2O	5.68	5.63	5.61	5.35	5.89	5.36	5.37	5.53	5.39
K2O	0.61	0.63	0.58	0.56	0.76	0.61	0.75	0.61	0.61
NiO	0.02	0.02	0.00	0.00	0.00	0.00	0.00	0.00	0.00
Total	**99.57**	**99.45**	**99.37**	**99.62**	**99.79**	**99.72**	**99.98**	**99.77**	**99.07**
Cations									
Si^{4+}	10.20	10.22	10.24	9.98	10.23	9.98	10.05	10.06	10.22
Ti^{4+}	0.01	0.01	0.00	0.01	0.01	0.01	0.01	0.02	0.01
Al^{3+}	5.71	5.68	5.67	5.92	5.69	5.95	5.87	5.83	5.75
Cr^{3+}	0.00	0.00	0.00	0.00	0.00	0.00	0.00	0.00	0.00
Fe^{2+}	0.04	0.04	0.05	0.04	0.05	0.04	0.04	0.09	0.04
Mn^{2+}	0.00	0.00	0.00	0.00	0.00	0.00	0.00	0.00	0.00
Mg^{2+}	0.00	0.00	0.00	0.00	0.00	0.00	0.00	0.00	0.00
Ca^{2+}	1.92	1.91	1.91	2.08	1.81	2.05	2.00	1.98	1.85
Na^{+}	1.99	1.98	1.97	1.88	2.06	1.88	1.88	1.94	1.90
K^{+}	0.14	0.14	0.13	0.13	0.18	0.14	0.17	0.14	0.14
Ni^{+}	0.00	0.00	0.00	0.00	0.00	0.00	0.00	0.00	0.00
Zn	0.00	0.00	0.00	0.00	0.00	0.00	0.00	0.00	0.00
V	0.00	0.00	0.00	0.00	0.00	0.00	0.00	0.00	0.00
Σcat	**20.01**	**19.99**	**19.98**	**20.05**	**20.03**	**20.05**	**20.03**	**20.06**	**19.91**
Or	3	4	3	3	4	3	4	3	4
Ab	49	49	49	46	51	46	46	48	49
An	47	47	48	51	45	50	49	49	48

Appendix 5
Feldspar EMP data - cation calculations based on 32 oxygen

No	18002 3.2 plag	18002 3.2 plag	18002 3.2 plag	18002 3.2 plag	18002 3.2 plag	18002 4.1 plag	18002 4.2 plag	18002 4.7 plag	18002 4.7 plag
Mineral	**Plagioclase**	**Plagioclase**	**Plagioclase**	**Plagioclase**	**Plagioclase**	**Plagioclase**	**Plagioclase**	**Plagioclase**	**Plagioclase**
Wt %									
SiO2	56.31	57.20	57.07	57.07	56.77	55.52	55.21	55.04	54.98
TiO2	0.07	0.05	0.08	0.09	0.06	0.08	0.08	0.08	0.09
Al2O3	26.88	26.36	26.45	26.43	26.76	27.23	27.26	27.43	27.43
Cr2O3	0.01	0.00	0.00	0.00	0.02	0.00	0.00	0.00	0.00
FeO	0.28	0.34	0.26	0.37	0.34	0.30	0.26	0.34	0.27
MnO	0.00	0.02	0.00	0.00	0.01	0.01	0.01	0.00	0.02
MgO	0.00	0.00	0.00	0.00	0.00	0.00	0.00	0.00	0.00
CaO	9.67	8.93	8.96	8.94	9.34	10.45	10.51	10.58	10.67
Na2O	5.95	5.93	6.02	6.04	6.10	5.36	5.41	5.28	5.24
K2O	0.69	1.18	1.06	1.04	0.74	0.53	0.53	0.55	0.52
NiO	0.00	0.02	0.05	0.02	0.01	0.00	0.03	0.02	0.01
Total	**99.85**	**100.04**	**99.95**	**99.99**	**100.13**	**99.49**	**99.30**	**99.31**	**99.23**
Cations									
Si^{4+}	10.18	10.31	10.29	10.29	10.23	10.08	10.05	10.02	10.01
Ti^{4+}	0.01	0.01	0.01	0.01	0.01	0.01	0.01	0.01	0.01
Al^{3+}	5.73	5.60	5.62	5.62	5.68	5.83	5.85	5.88	5.89
Cr^{3+}	0.00	0.00	0.00	0.00	0.00	0.00	0.00	0.00	0.00
Fe^{2+}	0.04	0.05	0.04	0.06	0.05	0.05	0.04	0.05	0.04
Mn^{2+}	0.00	0.00	0.00	0.00	0.00	0.00	0.00	0.00	0.00
Mg^{2+}	0.00	0.00	0.00	0.00	0.00	0.00	0.00	0.00	0.00
Ca^{2+}	1.87	1.73	1.73	1.73	1.80	2.03	2.05	2.06	2.08
Na^{+}	2.09	2.07	2.11	2.11	2.13	1.89	1.91	1.86	1.85
K^{+}	0.16	0.27	0.24	0.24	0.17	0.12	0.12	0.13	0.12
Ni^{+}	0.00	0.00	0.01	0.00	0.00	0.00	0.00	0.00	0.00
Zn	0.00	0.00	0.00	0.00	0.00	0.00	0.00	0.00	0.00
V	0.00	0.00	0.00	0.00	0.00	0.00	0.00	0.00	0.00
Σcat	**20.07**	**20.05**	**20.06**	**20.06**	**20.07**	**20.00**	**20.03**	**20.02**	**20.02**
Or	4	7	6	6	4	3	3	3	3
Ab	51	51	52	52	52	47	47	46	46
An	45	42	42	42	44	50	50	51	51

Appendix 5
Feldspar EMP data - cation calculations based on 32 oxygen

No	18002 4.7 plag	18002 4.7 plag	18002 4.7 plag	18002 4.7 plag	18002 5.1 plag	18002 5.6 plag	18002 6.1 plag	18002 6.4 plag	18003 1.1 kspa
Mineral	**Plagioclase**	**Plagioclase**	**Plagioclase**	**Plagioclase**	**Plagioclase**	**Plagioclase**	**Plagioclase**	**Plagioclase**	**Kspar**
Wt %									
SiO2	55.45	55.56	55.80	55.92	57.07	57.22	54.73	55.16	66.51
TiO2	0.07	0.09	0.10	0.06	0.08	0.05	0.09	0.08	0.05
Al2O3	26.89	27.08	27.07	26.98	26.39	25.92	27.84	27.39	18.12
Cr2O3	0.01	0.00	0.02	0.00	0.00	0.00	0.00	0.01	0.00
FeO	0.32	0.27	0.29	0.29	0.28	0.30	0.30	0.31	0.52
MnO	0.01	0.02	0.01	0.02	0.02	0.00	0.01	0.02	0.02
MgO	0.00	0.00	0.00	0.00	0.00	0.00	0.00	0.00	0.14
CaO	10.22	10.27	10.20	10.18	9.31	9.09	10.69	10.33	0.50
Na2O	5.38	5.49	5.53	5.57	5.88	5.99	5.43	5.43	4.93
K2O	0.62	0.56	0.54	0.60	0.88	0.80	0.55	0.58	9.05
NiO	0.03	0.05	0.02	0.01	0.02	0.00	0.00	0.00	0.00
Total	**99.00**	**99.39**	**99.60**	**99.63**	**99.93**	**99.37**	**99.65**	**99.31**	**99.83**
Cations									
Si^{4+}	10.12	10.10	10.11	10.13	10.29	10.37	9.94	10.04	12.03
Ti^{4+}	0.01	0.01	0.01	0.01	0.01	0.01	0.01	0.01	0.01
Al^{3+}	5.78	5.80	5.78	5.76	5.61	5.53	5.96	5.87	3.86
Cr^{3+}	0.00	0.00	0.00	0.00	0.00	0.00	0.00	0.00	0.00
Fe^{2+}	0.05	0.04	0.04	0.04	0.04	0.05	0.05	0.05	0.08
Mn^{2+}	0.00	0.00	0.00	0.00	0.00	0.00	0.00	0.00	0.00
Mg^{2+}	0.00	0.00	0.00	0.00	0.00	0.00	0.00	0.00	0.04
Ca^{2+}	2.00	2.00	1.98	1.98	1.80	1.76	2.08	2.01	0.10
Na^{+}	1.90	1.93	1.94	1.96	2.06	2.10	1.91	1.91	1.73
K^{+}	0.14	0.13	0.13	0.14	0.20	0.18	0.13	0.13	2.09
Ni^{+}	0.00	0.01	0.00	0.00	0.00	0.00	0.00	0.00	0.00
Zn	0.00	0.00	0.00	0.00	0.00	0.00	0.00	0.00	0.00
V	0.00	0.00	0.00	0.00	0.00	0.00	0.00	0.00	0.00
Σcat	**20.01**	**20.02**	**20.01**	**20.03**	**20.02**	**20.00**	**20.08**	**20.04**	**19.94**
Or	4	3	3	3	5	5	3	3	53
Ab	47	48	48	48	51	52	46	47	44
An	49	49	49	49	44	44	51	50	2

Appendix 5
Feldspar EMP data - cation calculations based on 32 oxygen

No	18003 1.4 kspa	18003 1.7 kspa	18003 2.3 kspa	18003 2.4 kspa	18003 2.8 kspa	18003 3.4 kspa	18003 4.1 kspa	18003 4.2 kspa	18003 4.4 kspa
Mineral	**Kspar**	**Kspar**	**Kspar**	**Kspar**	**Kspar**	**Kspar**	**Kspar**	**Kspar**	**Kspar**
Wt %									
SiO2	68.65	64.51	63.10	62.88	63.78	64.43	61.27	60.36	61.57
TiO2	0.22	0.00	0.00	0.03	0.03	0.01	0.02	0.02	0.04
Al2O3	17.51	21.24	22.23	22.51	21.73	21.54	23.86	24.00	23.48
Cr2O3	0.00	0.00	0.02	0.02	0.00	0.00	0.01	0.01	0.00
FeO	0.94	0.19	0.19	0.18	0.17	0.14	0.25	0.20	0.28
MnO	0.00	0.00	0.04	0.02	0.00	0.00	0.02	0.00	0.00
MgO	0.06	0.00	0.00	0.00	0.00	0.00	0.00	0.00	0.00
CaO	1.39	3.34	4.69	4.93	3.81	3.36	5.96	6.54	5.80
Na2O	6.09	7.78	7.66	7.53	7.73	7.76	7.61	7.08	7.62
K2O	5.12	3.01	2.15	1.93	2.84	3.20	1.42	1.23	1.45
NiO	0.01	0.01	0.00	0.00	0.03	0.00	0.00	0.01	0.00
Total	**99.99**	**100.09**	**100.08**	**100.02**	**100.12**	**100.45**	**100.43**	**99.44**	**100.22**
Cations									
Si^{4+}	12.20	11.48	11.25	11.20	11.37	11.44	10.91	10.85	10.98
Ti^{4+}	0.03	0.00	0.00	0.00	0.00	0.00	0.00	0.00	0.00
Al^{3+}	3.67	4.46	4.67	4.73	4.56	4.51	5.01	5.08	4.93
Cr^{3+}	0.00	0.00	0.00	0.00	0.00	0.00	0.00	0.00	0.00
Fe^{2+}	0.14	0.03	0.03	0.03	0.03	0.02	0.04	0.03	0.04
Mn^{2+}	0.00	0.00	0.01	0.00	0.00	0.00	0.00	0.00	0.00
Mg^{2+}	0.01	0.00	0.00	0.00	0.00	0.00	0.00	0.00	0.00
Ca^{2+}	0.26	0.64	0.90	0.94	0.73	0.64	1.14	1.26	1.11
Na^{+}	2.10	2.69	2.65	2.60	2.67	2.67	2.63	2.47	2.63
K^{+}	1.16	0.68	0.49	0.44	0.64	0.73	0.32	0.28	0.33
Ni^{+}	0.00	0.00	0.00	0.00	0.00	0.00	0.00	0.00	0.00
Zn	0.00	0.00	0.00	0.00	0.00	0.00	0.00	0.00	0.00
V	0.00	0.00	0.00	0.00	0.00	0.00	0.00	0.00	0.00
Σcat	**19.57**	**19.97**	**19.98**	**19.95**	**20.01**	**20.00**	**20.06**	**19.98**	**20.03**
Or	33	17	12	11	16	18	8	7	8
Ab	60	67	66	65	66	66	64	62	65
An	7	16	22	24	18	16	28	31	27

Appendix 5
Feldspar EMP data - cation calculations based on 32 oxygen

No	18003 5.2 kspa	18003 5.3 kspa	19002 1.12 pla	19002 1.13 pla	19002 1.14 pla	19002 1.16 pla	19002 1.17 pla	19002 2.18 pla	19002 2.25 pla
Mineral	**Kspar**	**Kspar**	**Plagioclase**	**Plagioclase**	**Plagioclase**	**Plagioclase**	**Plagioclase**	**Plagioclase**	**Plagioclase**
Wt %									
SiO2	59.55	59.46	53.66	53.47	53.75	53.65	52.75	56.58	51.72
TiO2	0.03	0.00	0.00	0.00	0.01	0.00	0.00	0.06	0.09
Al2O3	25.44	24.73	28.42	28.30	28.67	28.63	28.91	26.39	29.17
Cr2O3	0.02	0.00	0.02	0.02	0.00	0.00	0.00	0.02	0.02
FeO	0.35	0.22	0.12	0.14	0.19	0.14	0.09	0.15	0.11
MnO	0.01	0.02	0.01	0.00	0.03	0.05	0.00	0.00	0.00
MgO	0.04	0.00	0.00	0.00	0.00	0.00	0.00	0.00	0.00
CaO	7.63	7.30	11.96	11.68	11.74	11.78	12.18	9.55	13.75
Na2O	6.89	6.99	4.81	4.91	4.96	4.92	4.67	6.00	3.71
K2O	0.84	1.01	0.43	0.40	0.41	0.44	0.43	0.75	0.30
NiO	0.00	0.00	0.02	0.01	0.00	0.00	0.00	0.00	0.00
Total	**100.81**	**99.72**	**99.45**	**98.93**	**99.75**	**99.60**	**99.04**	**99.50**	**98.86**
Cations									
Si^{4+}	10.59	10.68	9.79	9.80	9.77	9.77	9.67	10.25	9.52
Ti^{4+}	0.00	0.00	0.00	0.00	0.00	0.00	0.00	0.01	0.01
Al^{3+}	5.33	5.24	6.11	6.11	6.14	6.14	6.25	5.64	6.33
Cr^{3+}	0.00	0.00	0.00	0.00	0.00	0.00	0.00	0.00	0.00
Fe^{2+}	0.05	0.03	0.02	0.02	0.03	0.02	0.01	0.02	0.02
Mn^{2+}	0.00	0.00	0.00	0.00	0.00	0.01	0.00	0.00	0.00
Mg^{2+}	0.01	0.00	0.00	0.00	0.00	0.00	0.00	0.00	0.00
Ca^{2+}	1.45	1.40	2.34	2.29	2.29	2.30	2.39	1.85	2.71
Na^{+}	2.38	2.43	1.70	1.75	1.75	1.74	1.66	2.11	1.33
K^{+}	0.19	0.23	0.10	0.09	0.10	0.10	0.10	0.17	0.07
Ni^{+}	0.00	0.00	0.00	0.00	0.00	0.00	0.00	0.00	0.00
Zn	0.00	0.00	0.00	0.00	0.00	0.00	0.00	0.00	0.00
V	0.00	0.00	0.00	0.00	0.00	0.00	0.00	0.00	0.00
Σcat	**20.02**	**20.03**	**20.06**	**20.07**	**20.08**	**20.08**	**20.09**	**20.06**	**20.00**
Or	5	6	2	2	2	2	2	4	2
Ab	59	60	41	42	42	42	40	51	32
An	36	35	56	55	55	56	58	45	66

Appendix 5
Feldspar EMP data - cation calculations based on 32 oxygen

No	19002 4.3 plag	19002 4.4 plag	19002 4.9 plag	19002 5.4 kspa	19003 1.2 plag	19003 1.7 plag	19003 2.3 plag	19003 3.4 plag	19003 3.7 plag
Mineral	**Plagioclase**	**Plagioclase**	**Plagioclase**	**Kspar**	**Plagioclase**	**Plagioclase**	**Plagioclase**	**Plagioclase**	**Plagioclase**
Wt %									
SiO2	54.46	57.92	49.80	63.00	54.40	54.13	57.07	55.25	54.32
TiO2	0.00	0.04	0.01	0.03	0.00	0.00	0.02	0.00	0.02
Al2O3	27.92	25.57	30.87	22.15	28.56	28.55	26.33	27.42	28.44
Cr2O3	0.00	0.00	0.01	0.00	0.00	0.02	0.00	0.00	0.00
FeO	0.21	0.15	0.20	0.16	**0.15**	0.16	**0.25**	**0.22**	**0.21**
MnO	0.00	0.00	0.00	0.01	0.02	0.00	0.00	0.00	0.00
MgO	0.00	0.00	0.00	0.00	0.00	0.00	0.00	0.00	0.00
CaO	11.60	8.71	14.75	4.45	11.41	11.68	9.11	10.45	11.52
Na2O	4.86	6.13	3.13	7.86	4.93	4.85	6.03	5.48	4.93
K2O	0.46	0.97	0.23	2.07	0.63	0.52	0.99	0.74	0.57
NiO	0.02	0.00	0.01	0.00	0.04	0.00	0.00	0.02	0.00
Total	**99.53**	**99.49**	**99.02**	**99.92**	**100.14**		**99.80**	**99.60**	**100.02**
Cations									
Si^{4+}	9.91	10.46	9.19	11.26	9.84	9.82	10.31	10.04	9.84
Ti^{4+}	0.00	0.01	0.00	0.00	0.00	0.00	0.00	0.00	0.00
Al^{3+}	5.99	5.44	6.72	4.67	6.09	6.10	5.60	5.87	6.07
Cr^{3+}	0.00	0.00	0.00	0.00	0.00	0.00	0.00	0.00	0.00
Fe^{2+}	0.03	0.02	0.03	0.02	0.02	0.02	0.04	0.03	0.03
Mn^{2+}	0.00	0.00	0.00	0.00	0.00	0.00	0.00	0.00	0.00
Mg^{2+}	0.00	0.00	0.00	0.00	0.00	0.00	0.00	0.00	0.00
Ca^{2+}	2.26	1.69	2.92	0.85	2.21	2.27	1.76	2.03	2.24
Na^{+}	1.72	2.15	1.12	2.72	1.73	1.71	2.11	1.93	1.73
K^{+}	0.11	0.22	0.05	0.47	0.14	0.12	0.23	0.17	0.13
Ni^{+}	0.00	0.00	0.00	0.00	0.01	0.00	0.00	0.00	0.00
Zn	0.00	0.00	0.00	0.00	0.00	0.00	0.00	0.00	0.00
V	0.00	0.00	0.00	0.00	0.00	0.00	0.00	0.00	0.00
Σcat	**20.01**	**19.99**	**20.04**	**20.00**	**20.05**	**20.04**	**20.06**	**20.08**	**20.05**
Or	3	6	1	12	4	3	6	4	3
Ab	42	53	27	67	42	42	51	47	42
An	55	42	71	21	54	55	43	49	55

Appendix 5
Pyroxene EMP data - cation calculations based on 6 oxygen

No	**15199 2.10 cp**	**15199 2.2 opx**	**15199 2.3 cpx**	**15199 2.4 cpx**	**15199 2.5 cpx**	**15199 2.6 cpx**	**17911 1.4 opx**	**17911 1.6 opx**	**17911 2.3 px**
Mineral	**Cpx**	**Opx**	**Cpx**	**Cpx**	**Cpx**	**Cpx**	**Opx**	**Opx**	**Opx**
wt %									
SiO2	49.95	52.08	50.97	50.29	50.95	50.67	49.34	49.69	49.07
TiO2	1.92	0.41	1.60	1.40	1.66	1.82	0.24	0.32	0.23
Al2O3	4.41	2.76	2.70	3.77	3.10	2.88	1.58	1.57	1.39
Cr2O3	0.01	0.00	0.02	0.03	0.01	0.05	0.00	0.01	0.02
FeO	7.13	20.59	6.50	7.25	7.60	7.55	35.50	33.85	35.99
MnO	0.13	0.37	0.17	0.18	0.19	0.17	1.23	1.25	1.22
MgO	14.22	22.73	14.19	13.78	14.45	13.97	12.39	13.87	12.18
CaO	21.27	1.55	21.69	21.42	20.87	21.57	0.67	0.71	0.74
Na2O	0.44	0.09	0.49	0.50	0.52	0.50	0.02	0.04	0.03
K2O	0.02	0.01	0.01	0.01	0.02	0.02	0.00	0.02	0.03
NiO	0.00	0.00	0.00	0.03	0.04	0.00	0.00	0.02	0.00
Total	**99.49**	**100.58**	**98.34**	**98.66**	**99.42**	**99.19**	**100.99**	**101.36**	**100.90**
Cations									
Si	1.86	1.91	1.92	1.89	1.90	1.90	1.95	1.93	1.94
Ti	0.05	0.01	0.05	0.04	0.05	0.05	0.01	0.01	0.01
Al	0.19	0.12	0.12	0.17	0.14	0.13	0.07	0.07	0.06
Cr	0.00	0.00	0.00	0.00	0.00	0.00	0.00	0.00	0.00
Fe3+	0.02	0.04	0.00	0.01	0.01	0.01	0.02	0.04	0.04
Fe2+	0.21	0.59	0.20	0.21	0.23	0.22	1.15	1.06	1.15
Mn	0.00	0.01	0.01	0.01	0.01	0.01	0.04	0.04	0.04
Mg	0.79	1.24	0.80	0.77	0.80	0.78	0.73	0.81	0.72
Ca	0.85	0.06	0.87	0.86	0.83	0.87	0.03	0.03	0.03
Na	0.03	0.01	0.04	0.04	0.04	0.04	0.00	0.00	0.00
K	0.00	0.00	0.00	0.00	0.00	0.00	0.00	0.00	0.00
Ni	0.00	0.00	0.00	0.00	0.00	0.00	0.00	0.00	0.00
Σcat w/ Fe3+	**4.00**	**4.00**	**4.00**	**4.00**	**4.00**	**4.00**	**4.00**	**4.00**	**4.00**
Mg #	79.25	67.66	79.56	78.25	78.10	77.69	38.76	43.19	38.42
Al(t)	0.14	0.09	0.08	0.11	0.10	0.10	0.05	0.07	0.06
Al(M1)	0.05	0.03	0.04	0.06	0.03	0.02	0.02	0.01	0.01
Wo	41	2	42	41	40	43	0	1	1
En	47	66	46	46	46	45	39	43	38
Fs	12	32	12	13	13	13	61	56	61

Appendix 5
Pyroxene EMP data - cation calculations based on 6 oxygen

No	17911 2.4 px	17911 3.1 px	17911 3.2 px r	17911 3.5 opx	17911 5.1 opx	17911 6.1 px	17912 1.1 px	17912 3.1 px r	17912 3.2 px r
Mineral	**Opx**	**Opx**	**Opx**	**Opx**	**Opx**	**Opx**	**Opx**	**Opx**	**Opx**
wt %									
SiO2	49.63	49.35	48.93	50.09	50.10	48.80	49.39	49.23	49.43
TiO2	0.21	0.24	0.26	0.26	0.09	0.27	0.01	0.01	0.02
Al2O3	1.32	1.58	1.58	1.63	1.20	4.17	1.55	1.43	1.71
Cr2O3	0.00	0.01	0.01	0.01	0.00	0.03	0.02	0.00	0.03
FeO	34.89	34.30	35.91	32.34	33.77	32.34	35.61	35.28	34.06
MnO	1.29	1.31	1.21	1.24	1.15	1.20	1.17	1.23	1.19
MgO	12.87	13.38	12.00	14.68	12.54	11.02	12.24	12.02	12.95
CaO	0.72	0.71	0.72	0.63	0.59	0.68	0.78	0.80	0.86
Na2O	0.03	0.04	0.05	0.04	0.04	0.06	0.04	0.05	0.04
K2O	0.02	0.01	0.03	0.02	0.08	0.08	0.01	0.00	0.00
NiO	0.00	0.01	0.00	0.01	0.00	0.02	0.01	0.00	0.00
Total	**100.98**	**100.95**	**100.69**	**100.94**	**99.56**	**98.67**	**100.83**	**100.06**	**100.31**
Cations									
Si	1.95	1.94	1.94	1.95	2.00	1.96	1.95	1.96	1.95
Ti	0.01	0.01	0.01	0.01	0.00	0.01	0.00	0.00	0.00
Al	0.06	0.07	0.07	0.07	0.06	0.20	0.07	0.07	0.08
Cr	0.00	0.00	0.00	0.00	0.00	0.00	0.00	0.00	0.00
Fe3+	0.02	0.05	0.03	0.02	0.00	0.00	0.03	0.01	0.02
Fe2+	1.12	1.08	1.16	1.03	1.13	1.09	1.15	1.16	1.11
Mn	0.04	0.04	0.04	0.04	0.04	0.04	0.04	0.04	0.04
Mg	0.76	0.78	0.71	0.85	0.75	0.66	0.72	0.71	0.76
Ca	0.03	0.03	0.03	0.03	0.03	0.03	0.03	0.03	0.04
Na	0.00	0.00	0.00	0.00	0.00	0.00	0.00	0.00	0.00
K	0.00	0.00	0.00	0.00	0.00	0.00	0.00	0.00	0.00
Ni	0.00	0.00	0.00	0.00	0.00	0.00	0.00	0.00	0.00
Σcat w/ Fe3+	**4.00**	**4.00**	**4.00**	**4.00**	**4.00**	**4.00**	**4.00**	**4.00**	**4.00**
Mg #	40.18	42.02	37.98	45.24	39.82	37.78	38.53	38.01	40.76
Al(t)	0.05	0.06	0.06	0.05	0.00	0.04	0.05	0.04	0.05
Al(M1)	0.01	0.01	0.02	0.02	0.05	0.16	0.02	0.03	0.03
Wo	1	1	1	0	0	0	1	0	0
En	40	42	38	45	40	38	38	38	41
Fs	59	57	61	55	60	62	61	62	59

Appendix 5
Pyroxene EMP data - cation calculations based on 6 oxygen

No	17912 4.3 px	17912 4.7 opx	17912 4 px su	17912 4 px su	17912 4 px su	17912 4 px su	17912 4 px su	17913 1.10 px	17913 1.11 px
Mineral	**Opx**	**Opx**	**Opx**	**Opx**	**Opx**	**Opx**	**Opx**	**Cpx**	**Cpx**
wt %									
SiO2	54.15	51.36	49.25	49.31	49.19	49.42	50.15	49.94	50.34
TiO2	0.00	0.00	0.04	0.03	0.01	0.00	0.03	1.10	0.90
Al2O3	4.57	1.40	1.30	1.26	1.42	1.23	0.65	4.21	3.37
Cr2O3	0.02	0.00	0.00	0.02	0.00	0.00	0.00	0.01	0.00
FeO	28.90	29.01	35.42	35.49	35.13	35.54	33.72	12.74	14.66
MnO	0.91	0.94	1.29	1.27	1.16	1.28	1.28	0.35	0.41
MgO	12.64	16.93	11.99	11.33	12.24	11.85	13.60	12.50	13.67
CaO	0.60	0.87	0.85	0.82	0.85	0.81	0.94	18.02	16.17
Na2O	1.01	0.03	0.03	0.03	0.04	0.04	0.02	0.61	0.61
K2O	0.96	0.01	0.00	0.00	0.00	0.00	0.01	0.01	0.00
NiO	0.00	0.00	0.00	0.00	0.00	0.03	0.03	0.00	0.00
Total	**103.74**	**100.56**	**100.18**	**99.71**	**100.03**	**100.33**	**100.43**	**99.49**	**100.13**
Cations									
Si	2.02	1.97	1.96	1.98	1.96	1.97	1.97	1.89	1.89
Ti	0.00	0.00	0.00	0.00	0.00	0.00	0.00	0.03	0.03
Al	0.20	0.06	0.06	0.06	0.07	0.06	0.03	0.19	0.15
Cr	0.00	0.00	0.00	0.00	0.00	0.00	0.00	0.00	0.00
Fe3+	0.00	0.00	0.01	0.00	0.02	0.00	0.02	0.02	0.06
Fe2+	0.90	0.93	1.17	1.19	1.15	1.19	1.09	0.38	0.40
Mn	0.03	0.03	0.04	0.04	0.04	0.04	0.04	0.01	0.01
Mg	0.70	0.97	0.71	0.68	0.73	0.70	0.80	0.70	0.77
Ca	0.02	0.04	0.04	0.04	0.04	0.03	0.04	0.73	0.65
Na	0.07	0.00	0.00	0.00	0.00	0.00	0.00	0.04	0.04
K	0.05	0.00	0.00	0.00	0.00	0.00	0.00	0.00	0.00
Ni	0.00	0.00	0.00	0.00	0.00	0.00	0.00	0.00	0.00
Σcat w/ Fe3+	**4.00**	**4.00**	**4.00**	**4.00**	**4.00**	**4.00**	**4.00**	**4.00**	**4.00**
Mg #	43.81	50.98	37.90	36.26	38.67	37.28	42.29	64.72	65.78
Al(t)	0.00	0.03	0.04	0.02	0.04	0.03	0.03	0.11	0.11
Al(M1)	0.20	0.03	0.02	0.04	0.03	0.03	0.00	0.08	0.04
Wo	0	0	1	0	1	0	2	34	33
En	44	51	38	36	38	37	42	43	44
Fs	56	49	62	64	61	63	57	23	23

Appendix 5
Pyroxene EMP data - cation calculations based on 6 oxygen

No	**17913 1.12 px**	**17913 1.14 px**	**17913 1.15 px**	**17913 1.7 px**	**17913 1.8 px**	**17913 2.1 px i**	**17913 2.3 px i**	**17913 2.6 px**	**17913 2.7 px**
Mineral	**Cpx**	**Cpx**	**Cpx**	**Cpx**	**Cpx**	**Cpx**	**Cpx**	**Cpx**	**Cpx**
wt %									
SiO2	49.81	50.52	50.36	50.40	50.34	50.08	50.41	50.32	50.40
TiO2	1.21	1.02	0.98	0.83	0.98	0.95	0.82	1.02	1.04
Al2O3	4.67	3.79	3.65	3.52	3.66	4.10	3.73	4.05	3.92
Cr2O3	0.00	0.00	0.00	0.02	0.00	0.00	0.03	0.00	0.01
FeO	12.56	13.41	13.27	14.12	13.91	13.14	12.83	12.79	12.48
MnO	0.37	0.39	0.37	0.41	0.38	0.34	0.37	0.40	0.39
MgO	12.32	12.80	12.70	13.73	12.95	12.08	12.46	12.78	12.64
CaO	18.46	17.55	17.78	15.84	17.20	18.71	18.85	18.17	18.44
Na2O	0.68	0.64	0.70	0.56	0.62	0.62	0.62	0.65	0.68
K2O	0.01	0.02	0.00	0.00	0.00	0.02	0.00	0.02	0.01
NiO	0.00	0.00	0.00	0.05	0.03	0.00	0.02	0.00	0.03
Total	**100.09**	**100.14**	**99.81**	**99.49**	**100.07**	**100.03**	**100.14**	**100.19**	**100.03**
Cations									
Si	1.87	1.90	1.90	1.90	1.89	1.89	1.89	1.89	1.89
Ti	0.03	0.03	0.03	0.02	0.03	0.03	0.02	0.03	0.03
Al	0.21	0.17	0.16	0.16	0.16	0.18	0.17	0.18	0.17
Cr	0.00	0.00	0.00	0.00	0.00	0.00	0.00	0.00	0.00
Fe3+	0.03	0.02	0.04	0.03	0.04	0.04	0.05	0.04	0.03
Fe2+	0.36	0.40	0.38	0.42	0.40	0.38	0.36	0.36	0.36
Mn	0.01	0.01	0.01	0.01	0.01	0.01	0.01	0.01	0.01
Mg	0.69	0.72	0.71	0.77	0.73	0.68	0.70	0.71	0.71
Ca	0.74	0.71	0.72	0.64	0.69	0.76	0.76	0.73	0.74
Na	0.05	0.05	0.05	0.04	0.05	0.05	0.05	0.05	0.05
K	0.00	0.00	0.00	0.00	0.00	0.00	0.00	0.00	0.00
Ni	0.00	0.00	0.00	0.00	0.00	0.00	0.00	0.00	0.00
Σcat w/ Fe3+	**4.00**	**4.00**	**4.00**	**4.00**	**4.00**	**4.00**	**4.00**	**4.00**	**4.00**
Mg #	65.60	64.34	65.21	64.96	64.58	64.29	66.10	66.34	66.23
Al(t)	0.13	0.10	0.10	0.10	0.11	0.11	0.11	0.11	0.11
Al(M1)	0.08	0.07	0.06	0.06	0.06	0.07	0.06	0.07	0.07
Wo	35	33	35	30	34	36	37	35	35
En	43	43	43	45	43	41	42	43	43
Fs	22	24	23	24	23	23	21	22	22

Appendix 5
Pyroxene EMP data - cation calculations based on 6 oxygen

No	**17913 3.10 op**	**17913 3.2 opx**	**17913 3.6 opx**	**17913 3.7 opx**	**17913 4.6 px r**	**17913 4.7 px r**	**17913 5.11**	**17913 6.10 px**	**17913 6.9 px**
Mineral	**Cpx**	**Cpx**	**Cpx**	**Cpx**	**Cpx**	**Cpx**	**Cpx**	**Cpx**	**Cpx**
wt %									
SiO2	50.22	51.14	50.35	50.45	49.97	50.04	50.28	50.02	50.19
TiO2	1.15	0.89	1.15	1.01	1.15	1.21	1.19	1.09	1.09
Al2O3	4.37	3.37	4.33	4.03	4.67	4.85	3.75	4.21	4.43
Cr2O3	0.03	0.00	0.00	0.01	0.00	0.03	0.03	0.01	0.03
FeO	11.79	11.58	12.08	12.18	11.83	10.48	11.10	12.31	12.49
MnO	0.29	0.32	0.35	0.33	0.33	0.27	0.30	0.32	0.30
MgO	12.85	13.03	12.50	12.52	12.24	12.67	13.49	12.51	12.44
CaO	18.72	19.05	18.82	18.83	19.07	19.53	19.48	18.47	18.20
Na2O	0.73	0.70	0.68	0.67	0.64	0.78	0.59	0.64	0.68
K2O	0.00	0.02	0.00	0.01	0.00	0.02	0.00	0.00	0.01
NiO	0.00	0.00	0.05	0.04	0.00	0.00	0.01	0.00	0.00
Total	**100.15**	**100.09**	**100.32**	**100.06**	**99.90**	**99.87**	**100.22**	**99.59**	**99.85**
Cations									
Si	1.88	1.91	1.88	1.89	1.88	1.87	1.87	1.89	1.89
Ti	0.03	0.03	0.03	0.03	0.03	0.03	0.03	0.03	0.03
Al	0.19	0.15	0.19	0.18	0.21	0.21	0.16	0.19	0.20
Cr	0.00	0.00	0.00	0.00	0.00	0.00	0.00	0.00	0.00
Fe3+	0.04	0.03	0.03	0.03	0.02	0.03	0.06	0.02	0.01
Fe2+	0.33	0.34	0.35	0.35	0.35	0.29	0.29	0.36	0.38
Mn	0.01	0.01	0.01	0.01	0.01	0.01	0.01	0.01	0.01
Mg	0.72	0.73	0.70	0.70	0.69	0.71	0.75	0.70	0.70
Ca	0.75	0.76	0.75	0.76	0.77	0.78	0.78	0.75	0.73
Na	0.05	0.05	0.05	0.05	0.05	0.06	0.04	0.05	0.05
K	0.00	0.00	0.00	0.00	0.00	0.00	0.00	0.00	0.00
Ni	0.00	0.00	0.00	0.00	0.00	0.00	0.00	0.00	0.00
Σcat w/ Fe3+	**4.00**	**4.00**	**4.00**	**4.00**	**4.00**	**4.00**	**4.00**	**4.00**	**4.00**
Mg #	68.51	68.42	66.42	66.37	66.03	70.57	72.45	65.94	64.84
Al(t)	0.12	0.09	0.12	0.11	0.12	0.13	0.13	0.11	0.11
Al(M1)	0.07	0.06	0.08	0.07	0.08	0.08	0.04	0.07	0.08
Wo	36	36	35	36	35	37	39	35	33
En	44	43	43	43	43	45	44	43	43
Fs	20	20	22	22	22	19	17	22	24

Appendix 5
Pyroxene EMP data - cation calculations based on 6 oxygen

No	**17913 8.1 px**	**17913 8.2 px**	**17913 8.3 px**	**17913 8.4 px**	**Host 17914 1.**	**Host 17914 1.**	**Host 17914 1.**	**Host 17914 1.**	**Host 17914 1.**
Mineral	**Opx**	**Opx**	**Opx**	**Opx**	**Opx**	**Opx**	**Opx**	**Opx**	**Opx**
wt %									
SiO2	51.69	51.74	51.91	51.43	54.59	54.00	54.50	56.14	56.16
TiO2	0.39	0.46	0.39	0.44	0.30	0.37	0.39	0.26	0.25
Al2O3	1.82	1.93	1.77	1.82	3.23	4.14	2.82	1.65	1.63
Cr2O3	0.00	0.04	0.01	0.01	0.44	0.47	0.45	0.30	0.24
FeO	25.02	24.71	24.72	24.70	10.33	10.65	11.13	10.89	10.88
MnO	0.59	0.56	0.59	0.58	0.18	0.16	0.20	0.19	0.20
MgO	19.74	19.50	19.45	19.53	29.33	28.73	29.06	29.47	29.42
CaO	1.49	1.74	1.64	1.60	1.85	1.97	1.97	2.09	1.97
Na2O	0.08	0.07	0.06	0.06	0.10	0.12	0.09	0.11	0.09
K2O	0.00	0.01	0.01	0.00	0.01	0.00	0.01	0.01	0.01
NiO	0.03	0.00	0.00	0.05	0.13	0.14	0.11	0.13	0.09
Total	**100.86**	**100.76**	**100.55**	**100.22**	**100.49**	**100.76**	**100.72**	**101.23**	**100.94**
Cations									
Si	1.94	1.94	1.95	1.94	1.92	1.90	1.92	1.97	1.97
Ti	0.01	0.01	0.01	0.01	0.01	0.01	0.01	0.01	0.01
Al	0.08	0.09	0.08	0.08	0.13	0.17	0.12	0.07	0.07
Cr	0.00	0.00	0.00	0.00	0.01	0.01	0.01	0.01	0.01
Fe3+	0.03	0.01	0.00	0.02	0.01	0.01	0.02	0.00	0.00
Fe2+	0.75	0.76	0.78	0.76	0.30	0.30	0.31	0.32	0.32
Mn	0.02	0.02	0.02	0.02	0.01	0.00	0.01	0.01	0.01
Mg	1.10	1.09	1.09	1.10	1.54	1.50	1.52	1.54	1.54
Ca	0.06	0.07	0.07	0.06	0.07	0.07	0.07	0.08	0.07
Na	0.01	0.01	0.00	0.00	0.01	0.01	0.01	0.01	0.01
K	0.00	0.00	0.00	0.00	0.00	0.00	0.00	0.00	0.00
Ni	0.00	0.00	0.00	0.00	0.00	0.00	0.00	0.00	0.00
Σcat w/ Fe3+	**4.00**	**4.00**	**4.00**	**4.00**	**4.00**	**4.00**	**4.00**	**4.00**	**4.00**
Mg #	59.38	58.78	58.38	59.07	83.78	83.26	83.23	82.82	82.81
Al(t)	0.06	0.06	0.05	0.06	0.08	0.10	0.08	0.03	0.03
Al(M1)	0.02	0.03	0.03	0.02	0.05	0.07	0.04	0.03	0.04
Wo	2	2	2	2	1	0	2	2	1
En	58	57	57	58	83	83	82	81	82
Fs	40	40	41	40	16	17	16	17	17

Appendix 5
Pyroxene EMP data - cation calculations based on 6 oxygen

No	**Host 17914 1.**	**Host 17914 1.**	**17914**	**17914 1.16 cp**	**17914 2.18 cp**	**17914 2.19 cp**	**17914 2.20 cp**	**17914 2.21 op**	**17914 2.22 op**
Mineral	**Opx**	**Opx**	**Opx**	**Cpx**	**Cpx**	**Cpx**	**Cpx**	**Opx**	**Opx**
wt %									
SiO2	56.05	54.68	53.15	50.05	50.58	50.84	50.13	53.26	52.86
TiO2	0.23	0.41	0.53	1.20	1.15	1.18	1.33	0.41	0.47
Al2O3	1.98	3.03	2.63	4.92	4.53	4.46	4.97	2.55	2.90
Cr2O3	0.28	0.43	0.03	0.05	0.10	0.08	0.11	0.00	0.07
FeO	11.16	11.15	17.85	10.13	8.55	9.55	8.25	17.68	17.71
MnO	0.15	0.21	0.34	0.24	0.22	0.24	0.24	0.30	0.30
MgO	29.50	28.74	24.90	12.72	14.20	14.88	14.52	25.24	24.79
CaO	1.86	2.06	1.54	19.04	19.16	17.99	18.71	1.45	1.41
Na2O	0.09	0.09	0.06	0.81	0.71	0.63	0.70	0.05	0.05
K2O	0.00	0.03	0.01	0.05	0.01	0.00	0.00	0.00	0.01
NiO	0.08	0.10	0.02	0.01	0.01	0.02	0.03	0.03	0.03
Total	**101.38**	**100.93**	**101.06**	**99.22**	**99.22**	**99.88**	**99.00**	**100.98**	**100.58**
Cations									
Si	1.96	1.92	1.92	1.88	1.89	1.88	1.87	1.92	1.92
Ti	0.01	0.01	0.01	0.03	0.03	0.03	0.04	0.01	0.01
Al	0.08	0.13	0.11	0.22	0.20	0.19	0.22	0.11	0.12
Cr	0.01	0.01	0.00	0.00	0.00	0.00	0.00	0.00	0.00
Fe3+	0.00	0.00	0.03	0.01	0.01	0.01	0.02	0.03	0.02
Fe2+	0.33	0.33	0.51	0.30	0.25	0.28	0.24	0.50	0.52
Mn	0.00	0.01	0.01	0.01	0.01	0.01	0.01	0.01	0.01
Mg	1.54	1.51	1.34	0.71	0.79	0.82	0.81	1.36	1.34
Ca	0.07	0.08	0.06	0.77	0.77	0.71	0.75	0.06	0.05
Na	0.01	0.01	0.00	0.06	0.05	0.05	0.05	0.00	0.00
K	0.00	0.00	0.00	0.00	0.00	0.00	0.00	0.00	0.00
Ni	0.00	0.00	0.00	0.00	0.00	0.00	0.00	0.00	0.00
Σcat w/ Fe3+	**4.00**	**4.00**	**4.00**	**4.00**	**4.00**	**4.00**	**4.00**	**4.00**	**4.00**
Mg #	82.49	82.21	72.33	70.07	75.77	74.52	76.92	72.98	72.14
Al(t)	0.04	0.08	0.08	0.12	0.11	0.12	0.13	0.08	0.08
Al(M1)	0.04	0.05	0.03	0.10	0.08	0.08	0.09	0.03	0.04
Wo	1	1	2	34	35	32	34	2	1
En	82	81	71	46	50	50	51	72	72
Fs	17	18	27	20	16	17	15	27	28

Appendix 5
Pyroxene EMP data - cation calculations based on 6 oxygen

No	**17914 2.23 cp**	**17914 2.24 cp**	**17914 2.27 op**	**17914 2.28 cp**	**17914 3.1 opx**	**17914 4.1 cpx**	**17914 4.2 opx**	**17914 4.4 opx**	**17914 4.5 opx**
Mineral	**Cpx**	**Cpx**	**Opx**	**Cpx**	**Opx**	**Cpx**	**Cpx**	**Opx**	**Opx**
wt %									
SiO2	50.17	50.67	53.47	50.30	52.65	50.49	50.95	53.05	52.38
TiO2	1.27	1.12	0.49	1.45	0.56	1.17	1.01	0.48	0.49
Al2O3	4.76	4.53	2.83	5.12	2.78	4.67	3.92	2.66	2.67
Cr2O3	0.09	0.08	0.00	0.11	0.12	0.01	0.08	0.06	0.03
FeO	8.45	9.13	17.73	8.55	18.84	9.13	9.25	19.53	19.47
MnO	0.20	0.20	0.34	0.21	0.37	0.24	0.25	0.36	0.37
MgO	14.10	14.84	24.93	14.04	23.62	13.75	13.87	23.76	23.44
CaO	19.10	18.06	1.46	19.44	2.33	19.10	19.31	1.52	1.45
Na2O	0.70	0.67	0.07	0.69	0.08	0.77	0.71	0.07	0.07
K2O	0.02	0.00	0.01	0.01	0.00	0.01	0.01	0.01	0.01
NiO	0.04	0.00	0.05	0.03	0.01	0.02	0.05	0.00	0.04
Total	**98.89**	**99.29**	**101.37**	**99.94**	**101.36**	**99.35**	**99.40**	**101.51**	**100.40**
Cations									
Si	1.88	1.89	1.92	1.86	1.91	1.88	1.90	1.92	1.92
Ti	0.04	0.03	0.01	0.04	0.02	0.03	0.03	0.01	0.01
Al	0.21	0.20	0.12	0.22	0.12	0.21	0.17	0.11	0.12
Cr	0.00	0.00	0.00	0.00	0.00	0.00	0.00	0.00	0.00
Fe3+	0.02	0.01	0.01	0.02	0.04	0.02	0.01	0.02	0.02
Fe2+	0.25	0.27	0.52	0.25	0.53	0.27	0.27	0.57	0.57
Mn	0.01	0.01	0.01	0.01	0.01	0.01	0.01	0.01	0.01
Mg	0.79	0.82	1.34	0.78	1.28	0.77	0.77	1.28	1.28
Ca	0.77	0.72	0.06	0.77	0.09	0.76	0.77	0.06	0.06
Na	0.05	0.05	0.00	0.05	0.01	0.06	0.05	0.01	0.00
K	0.00	0.00	0.00	0.00	0.00	0.00	0.00	0.00	0.00
Ni	0.00	0.00	0.00	0.00	0.00	0.00	0.00	0.00	0.00
Σcat w/ Fe3+	**4.00**	**4.00**	**4.00**	**4.00**	**4.00**	**4.00**	**4.00**	**4.00**	**4.00**
Mg #	75.93	75.24	71.92	75.67	70.51	74.04	73.79	69.20	69.09
Al(t)	0.12	0.11	0.08	0.14	0.09	0.12	0.10	0.08	0.08
Al(M1)	0.09	0.08	0.04	0.09	0.03	0.09	0.08	0.04	0.03
Wo	35	32	1	35	3	35	35	1	1
En	50	51	71	49	68	48	48	68	68
Fs	16	17	28	16	29	17	17	30	31

Appendix 5
Pyroxene EMP data - cation calculations based on 6 oxygen

No	**17914 4.6 cpx**	**17914 4.7 opx**	**17914 4.8 cpx**	**17914 4.9 cpx**	**17914 host**	**17915 1.1 px**	**17915 1.2 cpx**	**17915 1.3 cpx**	**17915 1.4 opx**
Mineral	**Cpx**	**Opx**	**Cpx**	**Cpx**	**Opx**	**Cpx**	**Cpx**	**Cpx**	**Opx**
wt %									
SiO2	49.88	52.50	50.59	51.09	55.16	50.23	50.15	49.89	49.29
TiO2	1.31	0.57	1.16	1.02	0.32	0.19	0.19	0.19	0.12
Al2O3	4.83	2.82	4.52	4.04	2.64	1.89	1.96	1.91	1.26
Cr2O3	0.06	0.04	0.07	0.05	0.37	0.01	0.00	0.00	0.01
FeO	9.05	19.40	9.55	9.25	10.88	18.68	19.62	19.07	32.91
MnO	0.19	0.40	0.22	0.23	0.18	1.05	1.11	1.01	1.56
MgO	13.57	23.54	13.68	13.98	29.18	9.60	9.69	9.54	12.76
CaO	19.15	1.56	19.19	19.32	1.97	17.74	16.83	17.45	1.76
Na2O	0.71	0.09	0.70	0.72	0.10	0.34	0.32	0.31	0.03
K2O	0.02	0.00	0.01	0.00	0.01	0.00	0.00	0.01	0.01
NiO	0.00	0.00	0.00	0.01	0.11	0.00	0.00	0.00	0.03
Total	**98.77**	**100.93**	**99.69**	**99.72**	**100.92**	**99.74**	**99.88**	**99.38**	**99.74**
Cations									
Si	1.87	1.91	1.89	1.90	1.94	1.95	1.95	1.94	1.96
Ti	0.04	0.02	0.03	0.03	0.01	0.01	0.01	0.01	0.00
Al	0.21	0.12	0.20	0.18	0.11	0.09	0.09	0.09	0.06
Cr	0.00	0.00	0.00	0.00	0.01	0.00	0.00	0.00	0.00
Fe3+	0.02	0.03	0.01	0.01	0.01	0.03	0.03	0.04	0.02
Fe2+	0.27	0.56	0.28	0.27	0.31	0.58	0.61	0.59	1.07
Mn	0.01	0.01	0.01	0.01	0.01	0.03	0.04	0.03	0.05
Mg	0.76	1.28	0.76	0.77	1.53	0.56	0.56	0.55	0.76
Ca	0.77	0.06	0.77	0.77	0.07	0.74	0.70	0.73	0.07
Na	0.05	0.01	0.05	0.05	0.01	0.03	0.02	0.02	0.00
K	0.00	0.00	0.00	0.00	0.00	0.00	0.00	0.00	0.00
Ni	0.00	0.00	0.00	0.00	0.00	0.00	0.00	0.00	0.00
Σcat w/ Fe3+	**4.00**	**4.00**	**4.00**	**4.00**	**4.00**	**4.00**	**4.00**	**4.00**	**4.00**
Mg #	73.90	69.42	72.86	73.94	82.94	49.06	48.00	48.60	41.37
Al(t)	0.13	0.09	0.11	0.10	0.06	0.05	0.05	0.06	0.04
Al(M1)	0.09	0.03	0.08	0.08	0.05	0.04	0.04	0.03	0.02
Wo	35	2	35	35	1	36	34	36	3
En	48	68	48	48	82	31	32	31	40
Fs	17	30	18	17	17	32	34	33	57

Appendix 5
Pyroxene EMP data - cation calculations based on 6 oxygen

No	**17915 1.5 opx**	**17915 2.4 cpx**	**17915 2.5 cpx**	**17915 3.1 cpx**	**17915 3.10 cp**	**17915 3.2 cpx**	**17915 5.1 cpx**	**17915 5.2 cpx**	**17918 2.11 px**
Mineral	**Opx**	**Cpx**	**Cpx**	**Cpx**	**Cpx**	**Cpx**	**Cpx**	**Cpx**	**Opx**
wt %									
SiO2	50.13	49.51	49.64	50.54	50.36	49.85	50.28	50.21	52.26
TiO2	0.15	0.33	0.29	0.21	0.27	0.33	0.25	0.26	0.02
Al2O3	1.21	2.50	2.46	1.99	2.02	2.35	2.08	2.19	1.01
Cr2O3	0.00	0.01	0.00	0.00	0.02	0.00	0.03	0.00	0.04
FeO	32.56	19.81	19.73	18.25	19.05	18.54	18.19	18.46	29.23
MnO	1.59	1.02	1.03	0.89	0.97	0.95	0.84	0.81	1.16
MgO	13.24	9.70	9.58	10.15	10.16	9.71	9.27	9.25	16.05
CaO	1.77	16.44	16.41	17.89	16.17	17.40	19.07	18.65	1.54
Na2O	0.03	0.36	0.30	0.33	0.33	0.37	0.36	0.31	0.08
K2O	0.02	0.00	0.00	0.00	0.01	0.01	0.00	0.00	0.03
NiO	0.00	0.05	0.00	0.01	0.00	0.00	0.00	0.00	0.00
Total	**100.71**	**99.71**	**99.44**	**100.28**	**99.37**	**99.50**	**100.35**	**100.16**	**101.44**
Cations									
Si	1.97	1.92	1.94	1.94	1.96	1.94	1.94	1.94	2.00
Ti	0.00	0.01	0.01	0.01	0.01	0.01	0.01	0.01	0.00
Al	0.06	0.11	0.11	0.09	0.09	0.11	0.09	0.10	0.05
Cr	0.00	0.00	0.00	0.00	0.00	0.00	0.00	0.00	0.00
Fe3+	0.01	0.05	0.02	0.04	0.00	0.03	0.04	0.03	0.00
Fe2+	1.06	0.60	0.62	0.55	0.62	0.57	0.54	0.57	0.93
Mn	0.05	0.03	0.03	0.03	0.03	0.03	0.03	0.03	0.04
Mg	0.77	0.56	0.56	0.58	0.59	0.56	0.53	0.53	0.91
Ca	0.07	0.68	0.69	0.74	0.67	0.72	0.79	0.77	0.06
Na	0.00	0.03	0.02	0.02	0.02	0.03	0.03	0.02	0.01
K	0.00	0.00	0.00	0.00	0.00	0.00	0.00	0.00	0.00
Ni	0.00	0.00	0.00	0.00	0.00	0.00	0.00	0.00	0.00
Σcat w/ Fe3+	**4.00**	**4.00**	**4.00**	**4.00**	**4.00**	**4.00**	**4.00**	**4.00**	**4.00**
Mg #	42.14	48.41	47.22	51.35	48.73	49.58	49.46	48.37	49.46
Al(t)	0.03	0.08	0.06	0.06	0.04	0.06	0.06	0.06	0.00
Al(M1)	0.02	0.04	0.05	0.03	0.05	0.04	0.03	0.04	0.04
Wo	3	34	33	36	31	35	39	38	1
En	41	32	32	33	34	32	30	30	49
Fs	56	34	35	31	35	33	31	32	50

Appendix 5
Pyroxene EMP data - cation calculations based on 6 oxygen

No	**17918 3.2 px**	**17918 3.3 px**	**17918 4.2 px**	**17918 4.3 plag**	**17918 4.5 px**	**17918 4.6 px**	**17918 5.1 px**	**17921 1.20 op**	**17921 1.21 ??**
Mineral	**Opx**	**Opx**	**Opx**	**Opx**	**Opx**	**Opx**	**Opx**	**Opx**	**Opx**
wt %									
SiO2	49.64	49.41	49.72	49.52	49.78	49.81	50.03	50.89	50.16
TiO2	0.04	0.00	0.00	0.03	0.00	0.00	0.04	0.15	0.13
Al2O3	0.73	2.09	0.65	0.71	0.68	0.73	0.75	0.83	0.78
Cr2O3	0.02	0.00	0.00	0.03	0.03	0.03	0.00	0.03	0.02
FeO	35.88	33.61	35.12	34.46	35.37	35.12	35.94	32.11	33.12
MnO	1.67	1.56	1.59	1.77	1.70	1.73	1.72	2.01	1.99
MgO	11.39	12.28	11.76	12.20	11.62	11.69	11.23	12.91	12.40
CaO	1.42	1.47	1.37	1.41	1.39	1.44	1.47	1.58	1.53
Na2O	0.08	0.06	0.06	0.04	0.04	0.04	0.05	0.05	0.05
K2O	0.00	0.02	0.00	0.01	0.01	0.01	0.00	0.02	0.03
NiO	0.00	0.00	0.00	0.00	0.02	0.00	0.00	0.02	0.00
Total	**100.86**	**100.50**	**100.27**	**100.17**	**100.65**	**100.60**	**101.24**	**100.59**	**100.20**
Cations									
Si	1.97	1.95	1.98	1.97	1.98	1.98	1.98	2.00	1.99
Ti	0.00	0.00	0.00	0.00	0.00	0.00	0.00	0.00	0.00
Al	0.03	0.10	0.03	0.03	0.03	0.03	0.03	0.04	0.04
Cr	0.00	0.00	0.00	0.00	0.00	0.00	0.00	0.00	0.00
Fe3+	0.02	0.01	0.01	0.03	0.01	0.01	0.00	0.00	0.00
Fe2+	1.17	1.10	1.16	1.12	1.17	1.16	1.19	1.06	1.10
Mn	0.06	0.05	0.05	0.06	0.06	0.06	0.06	0.07	0.07
Mg	0.67	0.72	0.70	0.72	0.69	0.69	0.66	0.76	0.73
Ca	0.06	0.06	0.06	0.06	0.06	0.06	0.06	0.07	0.07
Na	0.01	0.00	0.00	0.00	0.00	0.00	0.00	0.00	0.00
K	0.00	0.00	0.00	0.00	0.00	0.00	0.00	0.00	0.00
Ni	0.00	0.00	0.00	0.00	0.00	0.00	0.00	0.00	0.00
Σcat w/ Fe3+	**4.00**	**4.00**	**4.00**	**4.00**	**4.00**	**4.00**	**4.00**	**4.00**	**4.00**
Mg #	36.55	39.58	37.56	39.24	37.15	37.36	35.77	41.74	40.03
Al(t)	0.03	0.05	0.02	0.03	0.02	0.02	0.02	0.00	0.01
Al(M1)	0.01	0.05	0.01	0.00	0.01	0.02	0.02	0.04	0.03
Wo	3	1	3	3	2	2	2	1	2
En	35	39	37	38	36	36	35	41	39
Fs	62	60	61	59	61	61	63	58	59

Appendix 5
Pyroxene EMP data - cation calculations based on 6 oxygen

No	**17921 2.5 cpx**	**17921 3.12 op**	**17922 1.1 opx**	**17922 1.11 op**	**17922 1.12 op**	**17922 1.13 op**	**17922 1.13 op**	**17922 1.17 cp**	**17922 1.18 cp**
Mineral	**Opx**	**Opx**	**Opx**	**Opx**	**Opx**	**Opx**	**Opx**	**Cpx**	**Cpx**
wt %									
SiO2	50.42	51.48	51.11	51.38	51.15	50.85	51.31	51.19	51.65
TiO2	0.18	0.06	0.26	0.34	0.33	0.32	0.31	0.50	0.49
Al2O3	0.86	0.37	1.15	1.23	1.28	1.62	1.18	2.01	2.03
Cr2O3	0.03	0.00	0.02	0.00	0.02	0.00	0.00	0.01	0.02
FeO	33.32	30.18	28.99	29.49	29.41	29.46	29.21	17.20	17.12
MnO	1.86	1.65	0.69	0.65	0.64	0.61	0.63	0.42	0.41
MgO	12.21	15.32	16.26	16.10	16.28	16.20	16.17	11.55	11.53
CaO	1.54	1.00	1.76	1.82	1.88	1.80	1.87	16.79	16.75
Na2O	0.10	0.07	0.08	0.08	0.07	0.06	0.08	0.53	0.56
K2O	0.16	0.02	0.00	0.01	0.01	0.01	0.00	0.00	0.00
NiO	0.00	0.00	0.02	0.00	0.00	0.00	0.00	0.00	0.00
Total	**100.69**	**100.14**	**100.33**	**101.10**	**101.07**	**100.95**	**100.76**	**100.20**	**100.57**
Cations									
Si	1.99	2.01	1.97	1.97	1.96	1.95	1.97	1.95	1.96
Ti	0.01	0.00	0.01	0.01	0.01	0.01	0.01	0.01	0.01
Al	0.04	0.02	0.05	0.06	0.06	0.07	0.05	0.09	0.09
Cr	0.00	0.00	0.00	0.00	0.00	0.00	0.00	0.00	0.00
Fe3+	0.00	0.00	0.00	0.00	0.01	0.02	0.00	0.02	0.00
Fe2+	1.10	0.98	0.93	0.94	0.93	0.93	0.94	0.53	0.54
Mn	0.06	0.05	0.02	0.02	0.02	0.02	0.02	0.01	0.01
Mg	0.72	0.89	0.93	0.92	0.93	0.93	0.93	0.66	0.65
Ca	0.07	0.04	0.07	0.07	0.08	0.07	0.08	0.69	0.68
Na	0.01	0.01	0.01	0.01	0.00	0.00	0.01	0.04	0.04
K	0.01	0.00	0.00	0.00	0.00	0.00	0.00	0.00	0.00
Ni	0.00	0.00	0.00	0.00	0.00	0.00	0.00	0.00	0.00
Σcat w/ Fe3+	**4.00**	**4.00**	**4.00**	**4.00**	**4.00**	**4.00**	**4.00**	**4.00**	**4.00**
Mg #	39.51	47.50	49.99	49.31	49.96	49.91	49.67	55.24	54.55
Al(t)	0.01	0.00	0.03	0.03	0.04	0.05	0.03	0.05	0.04
Al(M1)	0.03	0.02	0.02	0.02	0.02	0.02	0.02	0.04	0.05
Wo	2	1	2	3	3	3	3	33	31
En	39	47	49	48	48	49	48	37	37
Fs	59	52	49	49	48	49	49	30	31

Appendix 5
Pyroxene EMP data - cation calculations based on 6 oxygen

No	**17922 1.19 cp**	**17922 1.19 cp**	**17922 1.20 cp**	**17922 1.3 cpx**	**17922 1.4 cpx**	**17922 2.11 op**	**17922 2.12 op**	**17922 2.13 cp**	**17922 2.8 opx**
Mineral	**Cpx**	**Cpx**	**Cpx**	**Cpx**	**Cpx**	**Opx**	**Opx**	**Cpx**	**Opx**
wt %									
SiO2	51.51	50.85	51.51	51.03	50.87	50.88	50.32	51.14	50.92
TiO2	0.49	0.57	0.51	0.47	0.51	0.27	0.43	0.55	0.31
Al2O3	1.79	2.20	2.13	1.87	2.01	1.22	1.16	2.35	1.29
Cr2O3	0.02	0.05	0.02	0.02	0.01	0.00	0.00	0.03	0.00
FeO	16.75	16.82	16.75	16.55	16.25	29.71	28.04	17.42	29.89
MnO	0.44	0.51	0.39	0.44	0.42	0.63	0.63	0.49	0.64
MgO	11.70	11.47	11.48	11.48	11.36	15.92	14.53	11.10	16.01
CaO	17.09	16.80	17.22	16.92	16.90	1.75	2.82	16.81	1.74
Na2O	0.54	0.55	0.56	0.52	0.54	0.08	0.10	0.59	0.05
K2O	0.00	0.00	0.00	0.01	0.01	0.01	0.10	0.01	0.00
NiO	0.00	0.00	0.00	0.00	0.00	0.00	0.02	0.00	0.00
Total	**100.33**	**99.82**	**100.58**	**99.29**	**98.90**	**100.47**	**98.13**	**100.48**	**100.86**
Cations									
Si	1.96	1.94	1.95	1.96	1.96	1.96	1.99	1.95	1.96
Ti	0.01	0.02	0.01	0.01	0.01	0.01	0.01	0.02	0.01
Al	0.08	0.10	0.10	0.08	0.09	0.06	0.05	0.11	0.06
Cr	0.00	0.00	0.00	0.00	0.00	0.00	0.00	0.00	0.00
Fe3+	0.01	0.02	0.01	0.00	0.00	0.01	0.00	0.01	0.01
Fe2+	0.52	0.52	0.52	0.53	0.52	0.95	0.93	0.54	0.95
Mn	0.01	0.02	0.01	0.01	0.01	0.02	0.02	0.02	0.02
Mg	0.66	0.65	0.65	0.66	0.65	0.92	0.86	0.63	0.92
Ca	0.70	0.69	0.70	0.70	0.70	0.07	0.12	0.69	0.07
Na	0.04	0.04	0.04	0.04	0.04	0.01	0.01	0.04	0.00
K	0.00	0.00	0.00	0.00	0.00	0.00	0.01	0.00	0.00
Ni	0.00	0.00	0.00	0.00	0.00	0.00	0.00	0.00	0.00
Σcat w/ Fe3+	**4.00**	**4.00**	**4.00**	**4.00**	**4.00**	**4.00**	**4.00**	**4.00**	**4.00**
Mg #	56.08	55.70	55.30	55.47	55.48	49.07	48.03	53.68	49.14
Al(t)	0.04	0.06	0.05	0.04	0.04	0.04	0.01	0.05	0.04
Al(M1)	0.04	0.04	0.05	0.05	0.05	0.02	0.05	0.05	0.02
Wo	33	33	33	33	32	3	4	32	3
En	37	37	37	37	38	48	46	36	48
Fs	29	30	30	30	30	49	50	31	49

Appendix 5
Pyroxene EMP data - cation calculations based on 6 oxygen

No	17922 2.9 opx	18002 1.3 px i	Host 18002 2.	18002 2.4 px	18002 2.5 px c	18002 3.5 px	18002 3.6 px	18002 4.3 px	18002 4.4 px c
Mineral	**Opx**	**Cpx**	**Opx**	**Opx**	**Opx**	**Cpx**	**Cpx**	**Cpx**	**Cpx**
wt %									
SiO2	51.36	50.12	54.51	52.64	52.43	51.19	50.79	48.92	49.86
TiO2	0.30	1.20	0.37	0.42	0.40	0.89	0.89	1.63	1.17
Al2O3	1.17	5.57	3.36	2.55	2.54	3.61	3.62	5.74	4.60
Cr2O3	0.02	0.19	0.31	0.02	0.01	0.01	0.04	0.00	0.00
FeO	29.91	8.50	10.85	19.98	19.66	11.15	11.04	10.48	10.96
MnO	0.63	0.19	0.18	0.42	0.42	0.32	0.31	0.24	0.27
MgO	16.07	15.32	28.48	23.30	22.98	13.54	13.51	13.14	13.31
CaO	1.79	18.13	2.31	1.54	1.58	18.78	18.59	18.84	18.73
Na2O	0.07	0.64	0.09	0.08	0.07	0.73	0.71	0.76	0.67
K2O	0.00	0.00	0.01	0.00	0.00	0.00	0.00	0.01	0.00
NiO	0.00	0.01	0.15	0.00	0.00	0.02	0.00	0.02	0.00
Total	**101.32**	**99.86**	**100.62**	**100.94**	**100.11**	**100.23**	**99.49**	**99.79**	**99.58**
Cations									
Si	1.97	1.85	1.92	1.92	1.93	1.91	1.90	1.83	1.87
Ti	0.01	0.03	0.01	0.01	0.01	0.02	0.03	0.05	0.03
Al	0.05	0.24	0.14	0.11	0.11	0.16	0.16	0.25	0.20
Cr	0.00	0.01	0.01	0.00	0.00	0.00	0.00	0.00	0.00
Fe3+	0.00	0.04	0.00	0.03	0.01	0.03	0.03	0.06	0.04
Fe2+	0.95	0.23	0.32	0.58	0.59	0.31	0.31	0.27	0.30
Mn	0.02	0.01	0.01	0.01	0.01	0.01	0.01	0.01	0.01
Mg	0.92	0.84	1.50	1.27	1.26	0.75	0.76	0.73	0.74
Ca	0.07	0.72	0.09	0.06	0.06	0.75	0.75	0.75	0.75
Na	0.01	0.05	0.01	0.01	0.01	0.05	0.05	0.05	0.05
K	0.00	0.00	0.00	0.00	0.00	0.00	0.00	0.00	0.00
Ni	0.00	0.00	0.00	0.00	0.00	0.00	0.00	0.00	0.00
Σcat w/ Fe3+	**4.00**	**4.00**	**4.00**	**4.00**	**4.00**	**4.00**	**4.00**	**4.00**	**4.00**
Mg #	49.02	78.81	82.38	68.58	67.98	70.56	70.59	73.20	71.28
Al(t)	0.03	0.15	0.08	0.08	0.07	0.09	0.10	0.17	0.13
Al(M1)	0.02	0.09	0.06	0.03	0.04	0.06	0.06	0.08	0.07
Wo	3	33	1	2	1	36	36	36	36
En	48	53	82	67	67	45	45	46	45
Fs	49	14	17	31	32	19	19	17	18

Appendix 5
Pyroxene EMP data - cation calculations based on 6 oxygen

No	18002 4.5 px r	18002 4.6 px r	18002 5.3 px	18002 5.4 px	18002 6.2 px	18002 6.3 px	18003 1.3 px b	18003 4.3 px	18003 4.7 px
Mineral	**Cpx**	**Cpx**	**Cpx**	**Cpx**	**Cpx**	**Cpx**	**Opx**	**Opx**	**Opx**
wt %									
SiO2	49.69	48.71	49.83	49.81	49.94	50.17	49.97	49.84	49.69
TiO2	1.20	1.56	1.12	1.30	1.19	1.11	0.20	0.22	0.19
Al2O3	4.62	5.52	4.66	4.95	4.75	4.51	0.82	0.83	0.75
Cr2O3	0.03	0.01	0.03	0.00	0.02	0.02	0.02	0.00	0.00
FeO	11.05	10.81	10.99	10.71	10.90	11.01	35.58	35.02	33.31
MnO	0.26	0.23	0.28	0.28	0.30	0.28	0.84	0.89	1.00
MgO	13.31	12.99	13.41	13.09	13.41	13.53	11.96	11.90	12.88
CaO	18.59	18.63	18.62	18.74	18.55	18.49	1.79	1.78	1.80
Na2O	0.78	0.77	0.73	0.82	0.79	0.74	0.06	0.08	0.05
K2O	0.00	0.00	0.00	0.01	0.00	0.02	0.00	0.00	0.00
NiO	0.00	0.00	0.02	0.00	0.02	0.01	0.02	0.00	0.01
Total	**99.55**	**99.23**	**99.70**	**99.71**	**99.86**	**99.89**	**101.28**	**100.57**	**99.69**
Cations									
Si	1.86	1.83	1.86	1.86	1.86	1.87	1.97	1.98	1.97
Ti	0.03	0.04	0.03	0.04	0.03	0.03	0.01	0.01	0.01
Al	0.20	0.24	0.21	0.22	0.21	0.20	0.04	0.04	0.04
Cr	0.00	0.00	0.00	0.00	0.00	0.00	0.00	0.00	0.00
Fe3+	0.06	0.06	0.06	0.05	0.05	0.05	0.01	0.00	0.01
Fe2+	0.28	0.28	0.29	0.29	0.29	0.29	1.16	1.16	1.10
Mn	0.01	0.01	0.01	0.01	0.01	0.01	0.03	0.03	0.03
Mg	0.74	0.73	0.75	0.73	0.75	0.75	0.70	0.70	0.76
Ca	0.75	0.75	0.75	0.75	0.74	0.74	0.08	0.08	0.08
Na	0.06	0.06	0.05	0.06	0.06	0.05	0.00	0.01	0.00
K	0.00	0.00	0.00	0.00	0.00	0.00	0.00	0.00	0.00
Ni	0.00	0.00	0.00	0.00	0.00	0.00	0.00	0.00	0.00
Σcat w/ Fe3+	**4.00**	**4.00**	**4.00**	**4.00**	**4.00**	**4.00**	**4.00**	**4.00**	**4.00**
Mg #	72.41	72.40	72.33	71.57	72.29	71.98	37.75	37.71	40.99
Al(t)	0.14	0.17	0.14	0.14	0.14	0.13	0.03	0.02	0.03
Al(M1)	0.06	0.07	0.07	0.08	0.07	0.07	0.01	0.02	0.01
Wo	37	37	36	36	36	36	4	3	4
En	46	46	46	46	46	46	36	37	40
Fs	17	18	18	18	18	18	60	60	57

Appendix 5
Pyroxene EMP data - cation calculations based on 6 oxygen

No	**19002 1.10 op**	**19002 1.11 cp**	**19002 1.15 op**	**19002 1.18 px**	**19002 1.20 op**	**19002 1.4 opx**	**19002 1.5 opx**	**19002 1.6 opx**	**19002 1.7 opx**
Mineral	**Opx**	**Cpx**	**Opx**	**Opx**	**Opx**	**Opx**	**Opx**	**Opx**	**Opx**
wt %									
SiO2	53.88	50.79	54.04	54.23	54.30	54.40	53.92	53.53	54.29
TiO2	0.04	1.12	0.03	0.07	0.07	0.05	0.04	0.43	0.16
Al2O3	1.92	4.55	1.97	2.00	1.87	1.97	1.92	2.47	1.85
Cr2O3	0.04	0.04	0.05	0.04	0.03	0.01	0.03	0.04	0.03
FeO	18.19	7.52	17.43	17.60	17.49	16.63	18.32	16.63	16.72
MnO	0.35	0.16	0.34	0.37	0.36	0.33	0.35	0.29	0.35
MgO	25.52	14.47	26.21	25.87	25.61	25.71	25.27	25.11	26.88
CaO	0.31	20.04	0.34	0.29	0.42	0.40	0.34	1.25	0.35
Na2O	0.03	0.62	0.02	0.04	0.04	0.03	0.01	0.08	0.03
K2O	0.00	0.01	0.01	0.00	0.01	0.01	0.01	0.01	0.01
NiO	0.00	0.00	0.00	0.04	0.00	0.05	0.00	0.05	0.00
Total	**100.28**	**99.32**	**100.44**	**100.54**	**100.21**	**99.58**	**100.22**	**99.88**	**100.67**
Cations									
Si	1.96	1.89	1.95	1.96	1.97	1.98	1.96	1.95	1.95
Ti	0.00	0.03	0.00	0.00	0.00	0.00	0.00	0.01	0.00
Al	0.08	0.20	0.08	0.09	0.08	0.08	0.08	0.11	0.08
Cr	0.00	0.00	0.00	0.00	0.00	0.00	0.00	0.00	0.00
Fe3+	0.00	0.01	0.01	0.00	0.00	0.00	0.00	0.00	0.02
Fe2+	0.55	0.22	0.51	0.53	0.53	0.51	0.56	0.51	0.49
Mn	0.01	0.01	0.01	0.01	0.01	0.01	0.01	0.01	0.01
Mg	1.38	0.80	1.41	1.39	1.39	1.40	1.37	1.36	1.44
Ca	0.01	0.80	0.01	0.01	0.02	0.02	0.01	0.05	0.01
Na	0.00	0.04	0.00	0.00	0.00	0.00	0.00	0.01	0.00
K	0.00	0.00	0.00	0.00	0.00	0.00	0.00	0.00	0.00
Ni	0.00	0.00	0.00	0.00	0.00	0.00	0.00	0.00	0.00
Σcat w/ Fe3+	**4.00**	**4.00**	**4.00**	**4.00**	**4.00**	**4.00**	**4.00**	**4.00**	**4.00**
Mg #	71.58	78.21	73.27	72.38	72.30	73.37	71.09	72.91	74.73
Al(t)	0.04	0.11	0.05	0.04	0.03	0.02	0.04	0.05	0.05
Al(M1)	0.04	0.09	0.04	0.04	0.05	0.07	0.04	0.05	0.03
Wo	0	36	0	0	0	0	0	0	0
En	72	50	73	72	72	73	71	73	75
Fs	28	14	27	28	28	27	29	27	25

Appendix 5
Pyroxene EMP data - cation calculations based on 6 oxygen

No	**19002 1.9 cpx**	**19002 2.10 op**	**19002 2.11 op**	**19002 2.12 op**	**19002 2.13 op**	**19002 2.14 op**	**19002 2.15 cp**	**19002 2.16 cp**	**19002 2.17 op**
Mineral	**Cpx**	**Opx**	**Opx**	**Opx**	**Opx**	**Opx**	**Cpx**	**Cpx**	**Opx**
wt %									
SiO2	48.45	53.06	53.44	54.29	54.25	54.56	52.13	52.26	54.38
TiO2	2.80	0.36	0.43	0.06	0.08	0.06	0.48	0.74	0.04
Al2O3	6.57	3.04	2.75	1.87	1.80	2.00	3.04	3.53	1.81
Cr2O3	0.06	0.03	0.02	0.04	0.03	0.01	0.05	0.05	0.01
FeO	8.63	16.88	16.83	17.51	18.48	17.92	7.13	7.08	18.02
MnO	0.18	0.31	0.29	0.33	0.36	0.39	0.21	0.17	0.38
MgO	14.09	25.27	25.43	26.13	25.37	24.92	14.38	14.58	25.95
CaO	17.46	0.92	1.20	0.34	0.42	0.36	22.01	20.87	0.34
Na2O	1.25	0.07	0.05	0.01	0.01	0.00	0.54	0.65	0.02
K2O	0.33	0.00	0.01	0.00	0.01	0.00	0.00	0.00	0.01
NiO	0.00	0.00	0.01	0.00	0.01	0.00	0.01	0.00	0.00
Total	**99.83**	**99.94**	**100.45**	**100.58**	**100.83**	**100.23**	**99.99**	**99.94**	**100.96**
Cations									
Si	1.79	1.93	1.93	1.96	1.96	1.99	1.92	1.93	1.96
Ti	0.08	0.01	0.01	0.00	0.00	0.00	0.01	0.02	0.00
Al	0.29	0.13	0.12	0.08	0.08	0.09	0.13	0.15	0.08
Cr	0.00	0.00	0.00	0.00	0.00	0.00	0.00	0.00	0.00
Fe3+	0.08	0.00	0.00	0.00	0.00	0.00	0.03	0.00	0.00
Fe2+	0.19	0.51	0.51	0.53	0.56	0.55	0.19	0.22	0.54
Mn	0.01	0.01	0.01	0.01	0.01	0.01	0.01	0.01	0.01
Mg	0.78	1.37	1.37	1.41	1.37	1.35	0.79	0.80	1.39
Ca	0.69	0.04	0.05	0.01	0.02	0.01	0.87	0.82	0.01
Na	0.09	0.00	0.00	0.00	0.00	0.00	0.04	0.05	0.00
K	0.02	0.00	0.00	0.00	0.00	0.00	0.00	0.00	0.00
Ni	0.00	0.00	0.00	0.00	0.00	0.00	0.00	0.00	0.00
Σcat w/ Fe3+	**4.00**	**4.00**	**4.00**	**4.00**	**4.00**	**4.00**	**4.00**	**4.00**	**4.00**
Mg #	80.73	72.75	72.93	72.68	70.98	71.25	80.51	78.60	72.13
Al(t)	0.21	0.07	0.07	0.04	0.04	0.01	0.08	0.07	0.04
Al(M1)	0.08	0.06	0.05	0.04	0.04	0.07	0.06	0.08	0.04
Wo	35	0	0	0	0	0	42	37	0
En	53	73	73	73	71	71	47	49	72
Fs	13	27	27	27	29	29	11	13	28

Appendix 5
Pyroxene EMP data - cation calculations based on 6 oxygen

No	**19002 2.7 opx**	**19002 2.8 opx**	**19002 2.9 opx**	**19002 3.1 opx**	**19002 3.2 opx**	**19002 3.3 cpx**	**19002 3.4 cpx**	**19002 3.5 cpx**	**19002 3.6 opx**
Mineral	**Opx**	**Opx**	**Opx**	**Opx**	**Opx**	**Cpx**	**Cpx**	**Cpx**	**Opx**
wt %									
SiO2	53.79	53.72	54.05	53.65	53.49	52.43	51.64	51.66	53.94
TiO2	0.06	0.07	0.06	0.07	0.07	0.44	0.69	0.92	0.05
Al2O3	1.92	1.94	1.91	1.82	1.89	2.92	3.84	3.75	1.95
Cr2O3	0.03	0.01	0.03	0.01	0.02	0.01	0.03	0.03	0.03
FeO	18.17	18.53	18.57	18.28	18.57	7.16	7.22	7.28	18.25
MnO	0.37	0.40	0.39	0.40	0.42	0.12	0.15	0.18	0.36
MgO	25.48	25.18	25.20	25.25	24.96	14.97	14.94	14.66	25.14
CaO	0.36	0.72	0.38	0.36	0.45	20.79	20.60	20.40	0.42
Na2O	0.01	0.01	0.01	0.01	0.02	0.59	0.61	0.71	0.02
K2O	0.00	0.01	0.00	0.01	0.01	0.00	0.00	0.01	0.01
NiO	0.00	0.02	0.00	0.00	0.04	0.00	0.01	0.03	0.01
Total	**100.19**	**100.63**	**100.60**	**99.86**	**99.93**	**99.44**	**99.73**	**99.63**	**100.18**
Cations									
Si	1.96	1.95	1.96	1.96	1.96	1.94	1.91	1.91	1.96
Ti	0.00	0.00	0.00	0.00	0.00	0.01	0.02	0.03	0.00
Al	0.08	0.08	0.08	0.08	0.08	0.13	0.17	0.16	0.08
Cr	0.00	0.00	0.00	0.00	0.00	0.00	0.00	0.00	0.00
Fe3+	0.00	0.02	0.00	0.00	0.01	0.01	0.03	0.02	0.00
Fe2+	0.55	0.55	0.56	0.56	0.56	0.21	0.20	0.21	0.56
Mn	0.01	0.01	0.01	0.01	0.01	0.00	0.00	0.01	0.01
Mg	1.38	1.36	1.36	1.37	1.36	0.83	0.82	0.81	1.36
Ca	0.01	0.03	0.01	0.01	0.02	0.82	0.81	0.81	0.02
Na	0.00	0.00	0.00	0.00	0.00	0.04	0.04	0.05	0.00
K	0.00	0.00	0.00	0.00	0.00	0.00	0.00	0.00	0.00
Ni	0.00	0.00	0.00	0.00	0.00	0.00	0.00	0.00	0.00
Σcat w/ Fe3+	**4.00**	**4.00**	**4.00**	**4.00**	**4.00**	**4.00**	**4.00**	**4.00**	**4.00**
Mg #	71.51	71.41	70.75	71.11	70.76	79.53	80.75	79.41	71.05
Al(t)	0.04	0.05	0.04	0.04	0.04	0.06	0.09	0.09	0.04
Al(M1)	0.04	0.03	0.04	0.04	0.04	0.07	0.07	0.07	0.05
Wo	0	0	0	0	0	38	38	37	0
En	72	71	71	71	71	49	50	50	71
Fs	28	29	29	29	29	13	12	13	29

Appendix 5
Pyroxene EMP data - cation calculations based on 6 oxygen

No	**19002 3.7 cpx**	**19002 4.1 opx**	**19002 4.2 cpx**	**19002 4.2.3 cp**	**19002 4.2.4 cp**	**19002 4.2.5 cp**	**19002 4.2.6 cp**	**19002 4.6 cpx**	**19002 4.8 opx**
Mineral	**Cpx**	**Opx**	**Cpx**	**Cpx**	**Opx**	**Cpx**	**Opx**	**Cpx**	**Opx**
wt %									
SiO2	52.55	54.34	53.91	51.46	53.91	52.53	54.46	52.10	54.00
TiO2	0.34	0.06	0.07	0.79	0.09	0.37	0.06	0.49	0.06
Al2O3	2.78	1.88	1.39	4.20	1.97	2.84	1.98	2.97	2.12
Cr2O3	0.05	0.01	0.04	0.00	0.01	0.03	0.01	0.05	0.04
FeO	6.39	18.30	5.82	7.33	18.22	6.52	17.92	6.79	18.73
MnO	0.14	0.34	0.15	0.18	0.31	0.14	0.37	0.15	0.38
MgO	14.40	25.29	15.25	14.27	25.01	14.53	24.96	14.33	25.44
CaO	22.62	0.38	22.90	20.39	0.69	22.14	0.48	22.13	0.36
Na2O	0.54	0.02	0.39	0.67	0.01	0.54	0.02	0.54	0.02
K2O	0.01	0.00	0.01	0.02	0.00	0.02	0.00	0.00	0.00
NiO	0.04	0.03	0.03	0.02	0.04	0.02	0.02	0.03	0.00
Total	**99.85**	**100.66**	**99.97**	**99.33**	**100.25**	**99.68**	**100.29**	**99.57**	**101.14**
Cations									
Si	1.94	1.97	1.98	1.91	1.96	1.94	1.98	1.93	1.95
Ti	0.01	0.00	0.00	0.02	0.00	0.01	0.00	0.01	0.00
Al	0.12	0.08	0.06	0.18	0.08	0.12	0.09	0.13	0.09
Cr	0.00	0.00	0.00	0.00	0.00	0.00	0.00	0.00	0.00
Fe3+	0.02	0.00	0.00	0.00	0.00	0.01	0.00	0.02	0.01
Fe2+	0.18	0.55	0.18	0.23	0.55	0.19	0.55	0.19	0.55
Mn	0.00	0.01	0.00	0.01	0.01	0.00	0.01	0.00	0.01
Mg	0.79	1.37	0.84	0.79	1.36	0.80	1.35	0.79	1.37
Ca	0.89	0.01	0.90	0.81	0.03	0.88	0.02	0.88	0.01
Na	0.04	0.00	0.03	0.05	0.00	0.04	0.00	0.04	0.00
K	0.00	0.00	0.00	0.00	0.00	0.00	0.00	0.00	0.00
Ni	0.00	0.00	0.00	0.00	0.00	0.00	0.00	0.00	0.00
Σcat w/ Fe3+	**4.00**	**4.00**	**4.00**	**4.00**	**4.00**	**4.00**	**4.00**	**4.00**	**4.00**
Mg #	81.60	71.12	82.37	77.66	70.98	80.84	71.28	80.54	71.21
Al(t)	0.06	0.03	0.02	0.09	0.04	0.06	0.02	0.07	0.05
Al(M1)	0.06	0.05	0.04	0.09	0.05	0.07	0.07	0.06	0.04
Wo	43	0	43	36	0	41	0	42	0
En	47	71	47	50	71	48	71	47	71
Fs	11	29	10	14	29	11	29	11	29

Appendix 5
Pyroxene EMP data - cation calculations based on 6 oxygen

No	Host 19002 5.	19003 1. px	19003 1.3 px	19003 1.8 plag	19003 1.8 px	19003 2.1 px	19003 2.4 px	19003 2.6 px b	19003 3 1 px
Mineral	**Cpx**	**Opx**	**Opx**	**Opx**	**Opx**	**Opx**	**Opx**	**Opx**	**Opx**
wt %									
SiO2	49.62	51.60	51.53	51.74	52.10	51.94	52.55	53.93	51.87
TiO2	1.71	0.01	0.00	0.00	0.00	0.02	0.02	0.04	0.00
Al2O3	4.89	2.79	2.79	2.97	3.00	2.72	3.00	3.01	2.36
Cr2O3	0.14	0.09	0.09	0.11	0.08	0.06	0.08	0.07	0.09
FeO	8.62	23.76	24.49	24.20	23.82	23.96	22.32	27.64	23.45
MnO	0.17	0.38	0.36	0.36	0.41	0.35	0.38	0.30	0.38
MgO	14.15	21.04	20.71	20.58	20.53	21.10	20.96	14.34	21.20
CaO	19.31	0.70	0.53	0.46	0.49	0.44	1.10	0.73	0.51
Na2O	0.62	0.04	0.01	0.05	0.04	0.04	0.02	0.02	0.05
K2O	0.01	0.02	0.02	0.00	0.01	0.01	0.00	0.00	0.02
NiO	0.00	0.03	0.02	0.00	0.02	0.01	0.00	0.00	0.03
Total	**99.25**	**100.45**	**100.56**	**100.47**	**100.51**	**100.65**	**100.44**	**100.10**	**99.95**
Cations									
Si	1.85	1.92	1.92	1.93	1.94	1.93	1.95	2.09	1.94
Ti	0.05	0.00	0.00	0.00	0.00	0.00	0.00	0.00	0.00
Al	0.22	0.12	0.12	0.13	0.13	0.12	0.13	0.14	0.10
Cr	0.00	0.00	0.00	0.00	0.00	0.00	0.00	0.00	0.00
Fe3+	0.02	0.03	0.03	0.01	0.00	0.02	0.00	0.00	0.02
Fe2+	0.24	0.71	0.73	0.75	0.74	0.73	0.69	0.90	0.72
Mn	0.01	0.01	0.01	0.01	0.01	0.01	0.01	0.01	0.01
Mg	0.79	1.17	1.15	1.15	1.14	1.17	1.16	0.83	1.18
Ca	0.77	0.03	0.02	0.02	0.02	0.02	0.04	0.03	0.02
Na	0.04	0.00	0.00	0.00	0.00	0.00	0.00	0.00	0.00
K	0.00	0.00	0.00	0.00	0.00	0.00	0.00	0.00	0.00
Ni	0.00	0.00	0.00	0.00	0.00	0.00	0.00	0.00	0.00
Σcat w/ Fe3+	**4.00**	**4.00**	**4.00**	**4.00**	**4.00**	**4.00**	**4.00**	**4.00**	**4.00**
Mg #	76.28	62.32	61.08	60.45	60.57	61.67	62.59	48.04	62.28
Al(t)	0.15	0.08	0.08	0.07	0.06	0.07	0.05	0.00	0.06
Al(M1)	0.07	0.04	0.05	0.06	0.08	0.05	0.08	0.14	0.04
Wo	36	0	0	0	0	0	0	0	0
En	49	62	61	60	61	62	63	48	62
Fs	15	38	39	40	39	38	37	52	38

Appendix 5
Pyroxene EMP data - cation calculations based on 6 oxygen

No	**19003 3.8 px**
Mineral	**Opx**
wt %	
SiO2	51.98
TiO2	0.03
Al2O3	2.58
Cr2O3	0.10
FeO	23.94
MnO	0.33
MgO	20.65
CaO	0.53
Na2O	0.02
K2O	0.00
NiO	0.04
Total	**100.21**
Cations	
Si	1.95
Ti	0.00
Al	0.11
Cr	0.00
Fe3+	0.00
Fe2+	0.75
Mn	0.01
Mg	1.15
Ca	0.02
Na	0.00
K	0.00
Ni	0.00
Σcat w/ Fe3+	**4.00**
Mg #	60.59
Al(t)	0.05
Al(M1)	0.06
Wo	0
En	61
Fs	39

Appendix 5
Amphibole EMP data - cation calculations based on 23 oxygen

No	19002 1.1	19002 1.2	19002 1.3	19002 1.8	19002 2.1	19002 2.2	19002 2.3	19002 2.4	19002 5.1	17913 5.13
Mineral	**Kaersutite**	**Kaersutite**	**Kaersutite**	**Kaersutite**	**Kaersutite**	**Kaersutite**	**Kaersutite**	**Kaersutite**	**Kaersutite**	**Ferropargasitic**
wt %										
SiO_2	41.60	41.88	41.75	41.89	41.64	40.55	41.22	41.41	39.92	45.55
TiO_2	6.25	6.21	6.19	6.02	6.15	6.18	6.14	6.15	6.16	2.69
Al_2O_3	12.78	12.70	12.51	12.63	12.53	11.46	11.85	12.57	12.85	5.63
Cr_2O_3	0.05	0.11	0.09	0.06	0.03	0.04	0.04	0.04	0.03	0.00
FeO	9.59	9.11	9.22	10.44	10.50	10.32	10.36	10.39	14.53	7.07
MnO	0.10	0.09	0.09	0.12	0.14	0.12	0.13	0.13	0.16	0.15
MgO	13.18	13.58	13.42	13.31	13.07	12.70	12.96	12.91	9.95	12.33
CaO	11.01	10.94	11.05	10.80	10.82	10.90	10.82	10.84	10.51	21.21
NiO	0.03	0.00	0.02	0.04	0.01	0.01	0.02	0.01	0.00	0.01
Na_2O	2.78	2.74	2.69	2.63	2.67	2.47	2.43	2.70	2.77	0.48
K_2O	1.33	1.41	1.39	1.41	1.42	1.43	1.38	1.42	1.29	0.01
Total	**98.69**	**98.75**	**98.42**	**99.37**	**99.00**	**96.17**	**97.34**	**98.56**	**98.16**	**95.12**
Cations										
Si^{4+}	6.00	6.06	6.07	6.06	6.05	6.08	6.09	6.05	5.97	7.16
Ti^{4+}	0.68	0.68	0.68	0.66	0.67	0.70	0.68	0.68	0.69	0.32
Al^{3+}	2.17	2.17	2.14	2.15	2.15	2.03	2.06	2.16	2.27	1.04
Cr^{3+}	0.01	0.01	0.01	0.01	0.00	0.01	0.00	0.01	0.00	0.00
Fe^{2+}	1.15	1.10	1.12	1.26	1.28	1.29	1.28	1.27	1.82	0.93
Mn^{2+}	0.01	0.01	0.01	0.01	0.01	0.01	0.01	0.01	0.02	0.02
Mg^{2+}	2.83	2.93	2.91	2.87	2.83	2.84	2.85	2.81	2.22	2.89
Ca^{2+}	1.70	1.70	1.72	1.67	1.69	1.75	1.71	1.70	1.69	3.57
Ni^{2+}	0.00	0.00	0.00	0.00	0.00	0.00	0.00	0.00	0.00	0.00
Na^{+}	0.78	0.77	0.76	0.74	0.75	0.72	0.70	0.77	0.80	0.15
K^{+}	0.24	0.26	0.26	0.26	0.26	0.27	0.26	0.26	0.25	0.00
Total	**15.58**	**15.69**	**15.68**	**15.70**	**15.71**	**15.70**	**15.67**	**15.71**	**15.72**	**16.07**

Appendix 5
Glass EMP data

	17921 1.3 g	17921 1.4 glass	17921 1.5 glass	17921 2.14 ? gl	17921 2.25? glass	17921 1.6 glas	17921 1.18 ?	17921 1.19	17921 2.3	17921 2.13
wt %										
SiO2	71.10	71.82	67.63	74.29	74.08	63.71	66.69	61.76	67.62	70.12
TiO2	0.14	0.14	0.07	0.37	0.20	0.01	0.04	0.02	0.02	0.09
Al2O3	15.12	14.58	17.75	13.09	13.57	21.38	18.17	22.66	17.60	16.04
FeO	0.80	0.82	0.41	1.74	1.04	0.26	0.36	0.35	0.26	0.44
MnO	0.00	0.03	0.01	0.00	0.02	0.00	0.00	0.00	0.00	0.01
MgO	0.02	0.03	0.00	0.04	0.02	0.00	0.01	0.00	0.00	0.03
CaO	0.57	0.53	0.26	0.72	0.59	3.93	0.60	5.55	0.12	0.44
Na2O	4.02	3.47	4.48	3.92	3.79	6.91	5.08	7.32	4.20	4.17
K2O	7.48	7.36	9.93	5.19	6.67	3.82	8.87	1.59	10.20	8.68
Total	**99.27**	**98.82**	**100.54**	**99.35**	**100.11**	**100.05**	**99.82**	**99.28**	**100.03**	**100.01**

Appendix 5
Glass EMP data

	17921 3.5 s	17921 3.7.3	17921 3.7.6	17921 3.2 s	17921 3.3 sp	17911 1.9 me	17911 1.10	17911 2.5 n	17911 2.6 n	17911 3.10	17911 3.11 m
wt %											
SiO2	68.17	76.06	74.43	75.73	**78.28**	72.91	72.13	73.41	67.83	68.10	73.38
TiO2	0.07	0.10	0.14	0.12	**0.14**	0.56	0.48	0.24	0.11	0.19	0.75
Al2O3	17.34	12.61	13.48	12.97	**11.75**	14.19	15.33	15.42	17.96	19.59	14.14
FeO	0.22	0.27	0.93	0.52	0.28	1.29	1.19	0.73	0.40	0.35	0.79
MnO	0.01	0.00	0.00	0.00	**0.01**	0.03	0.01	0.01	0.00	0.01	0.04
MgO	0.00	0.00	0.03	0.00	**0.00**	0.02	0.00	0.00	0.01	0.00	0.03
CaO	0.24	0.25	0.27	0.38	**0.13**	0.64	0.66	1.08	0.70	1.04	0.48
Na2O	4.71	3.25	3.59	3.76	**2.80**	3.94	4.54	4.92	4.40	5.05	3.34
K2O	9.06	6.62	7.02	6.12	**6.60**	6.62	6.50	5.45	9.03	8.70	6.63
Total	**99.88**	**99.22**	**99.97**	**99.66**	**100.03**	**100.21**	**100.85**	**101.26**	**100.46**	**103.05**	**99.62**

Appendix 5
Glass EMP data

	17911 3.1	17911 4.1	17911 4.3	17911 4.4	17911 4.5	17911 5.3	17911 9.7	17911 9.6	17911 2.2	17914 1.1	17914 1.4	17914 1.9	17914 1.2
wt %													
SiO2	70.42	75.12	75.37	64.69	74.20	73.20	75.01	70.50	73.66	60.54	62.44	57.02	67.94
TiO2	0.53	0.57	0.26	0.07	0.35	0.14	0.20	0.28	0.25	0.11	0.13	0.17	0.10
Al2O3	15.62	12.39	12.50	21.56	13.61	15.26	13.40	14.96	14.14	22.47	23.41	24.80	18.20
FeO	0.66	2.75	0.82	0.30	0.77	0.45	0.37	0.72	0.41	0.63	0.74	0.86	0.49
MnO	0.03	0.00	0.02	0.00	0.02	0.00	0.00	0.01	0.01	0.00	0.00	0.04	0.01
MgO	0.03	0.02	0.04	0.00	0.01	0.00	0.00	0.00	0.01	0.00	0.00	0.00	0.03
CaO	0.77	0.26	0.62	3.65	0.31	0.62	0.19	0.77	0.10	5.53	6.47	8.54	0.45
Na2O	4.56	2.75	3.24	7.92	2.96	3.99	2.68	4.16	2.27	6.08	6.36	6.20	5.39
K2O	6.12	6.69	6.20	2.14	6.51	7.21	7.79	6.74	9.07	3.26	2.39	0.55	8.40
Total	**98.78**	**100.55**	**99.08**	**100.34**	**98.77**	**100.89**	**99.64**	**98.14**	**99.95**	**98.64**	**101.94**	**98.17**	**101.03**

Appendix 5
Glass EMP data

	17914 1.5	17914 1.8	17914 1.6	Host 1791	Host 1791	Host 1791	17913 3.9	17913 3.1	Host 1800	Host 1800	Host 1800	18002 3.1	18002 5.5
wt %													
SiO2	68.66	66.93	36.24	57.50	65.73	72.48	55.56	52.41	59.39	71.31	58.76	45.05	50.08
TiO2	0.19	0.14	7.10	0.10	0.17	0.15	0.22	0.80	0.18	0.28	0.11	3.66	2.00
Al2O3	16.22	18.50	7.79	24.37	16.57	17.01	26.73	26.59	23.16	15.58	24.59	6.06	14.01
FeO	0.38	0.49	41.80	0.77	0.94	0.61	1.14	2.27	1.09	0.57	0.86	11.09	6.87
MnO	0.01	0.00	0.48	0.03	0.01	0.00	0.00	0.01	0.00	0.01	0.04	0.14	0.14
MgO	0.01	0.00	0.78	0.01	0.20	0.07	0.16	0.10	0.19	0.12	0.00	12.19	9.06
CaO	0.53	0.85	0.79	7.29	2.23	0.89	10.30	11.13	6.97	0.66	8.03	20.75	16.12
Na2O	4.36	6.53	2.71	6.50	4.75	6.53	5.01	4.38	6.47	4.42	6.69	0.50	1.99
K2O	7.72	6.10	1.98	1.07	4.86	4.55	0.98	0.65	0.91	7.46	0.67	0.00	0.25
Total	**98.10**	**99.54**	**99.69**	**97.65**	**95.47**	**102.30**	**100.12**	**98.39**	**98.40**	**100.41**	**99.76**	**99.44**	**100.56**

Appendix 5
Mica EMP data - cation calculations based on 24 oxygen

No	**17913 5.7**	**19002 2.5**	**19002 2.22**
Mneral	**Phlogopite-biot**	**Biotite**	**Biotite**
wt %			
SiO_2	37.41	51.27	51.24
TiO_2	10.22	1.32	1.07
Al_2O_3	14.30	20.47	21.09
Cr_2O_3	0.00	0.03	0.02
FeO	12.24	15.90	14.19
MnO	0.04	0.08	0.05
MgO	13.53	1.97	2.09
CaO	0.11	0.42	0.46
NiO	0.00	0.03	0.00
Na_2O	0.47	0.14	0.14
K_2O	9.03	0.59	0.57
Total	**97.34**	**92.23**	**90.91**
Cations			
Si^{4+}	5.90	10.38	10.42
Ti^{4+}	1.21	0.20	0.16
Al^{3+}	2.66	4.89	5.05
Cr^{3+}	0.00	0.01	0.00
Fe^{2+}	1.61	2.69	2.41
Mn^{2+}	0.00	0.01	0.01
Mg^{2+}	3.18	0.59	0.63
Ca^{2+}	0.02	0.09	0.10
Ni^{2+}	0.00	0.01	0.00
Na^{+}	0.14	0.06	0.06
K^{+}	1.82	0.15	0.15
Total	**16.54**	**19.08**	**18.99**

Appendix 5
Ilmenite EMP data - cation calculations based on 6 oxygen

No	**15199 1.1**	**15199 1.2**	**15199 2.16c**	**15199 2.17r**	**15199 2.18**	**17922 1.5 inc**	**17922 1.6 inc**	**17922 1.15**
Mineral	Ilmenite	Ilmenite	Ilmenite	Ilmenite	Ilmenite	Ilmenite	Ilmenite	Ilmenite
wt %								
SiO_2	0.00	0.01	0.02	0.06	0.04	0.03	0.03	0.01
TiO_2	49.91	49.89	50.97	47.49	51.35	50.85	50.92	50.74
Al_2O_3	0.35	0.35	0.13	0.17	0.13	0.19	0.19	0.11
Cr_2O_3	0.01	0.04	0.08	0.09	0.09	0.03	0.06	0.02
Fe_2O_3	7.90	8.16	0.37	6.20	4.11	4.68	4.47	4.89
FeO	36.50	36.50	41.50	38.00	38.00	41.80	42.00	42.00
MnO	0.36	0.30	0.38	0.50	0.50	0.48	0.53	0.49
MgO	4.50	4.62	2.29	2.34	4.36	1.83	1.78	1.80
CaO	0.01	0.00	0.05	0.05	0.06	0.05	0.06	0.01
NiO	0.01	0.00	0.00	0.01	0.00	0.00	0.02	0.00
ZnO	0.01	0.05	0.04	0.01	0.02	0.05	0.02	0.04
Na_2O	0.00	0.01	0.00	0.00	0.04	0.00	0.00	0.00
K_2O	0.01	0.00	0.00	0.01	0.02	0.00	0.00	0.00
Total	**99.95**	**100.29**	**96.32**	**95.44**	**99.10**	**100.25**	**100.32**	**100.31**
Total FeO	**43.61**	**43.84**	**41.83**	**43.58**	**41.69**	**46.01**	**46.02**	**46.40**
Cations								
Si^{4+}	0.00	0.00	0.00	0.00	0.00	0.00	0.00	0.00
Ti^{4+}	1.84	1.83	1.97	1.86	1.91	1.90	1.90	1.90
Al^{3+}	0.02	0.02	0.01	0.01	0.01	0.01	0.01	0.01
Cr^{3+}	0.00	0.00	0.00	0.00	0.00	0.00	0.00	0.00
Fe^{3+}	0.29	0.30	0.01	0.24	0.15	0.18	0.17	0.18
Fe^{2+}	1.49	1.49	1.79	1.65	1.57	1.74	1.75	1.75
Mn^{2+}	0.01	0.01	0.01	0.02	0.02	0.02	0.02	0.02
Mg^{2+}	0.33	0.34	0.18	0.18	0.32	0.14	0.13	0.13
Ca^{2+}	0.00	0.00	0.00	0.00	0.00	0.00	0.00	0.00
Ni^{2+}	0.00	0.00	0.00	0.00	0.00	0.00	0.00	0.00
Zn^{2+}	0.00	0.00	0.00	0.00	0.00	0.00	0.00	0.00
Na^{+}	0.00	0.00	0.00	0.00	0.00	0.00	0.00	0.00
K^{+}	0.00	0.00	0.00	0.00	0.00	0.00	0.00	0.00
Total	**4.00**	**4.00**	**4.00**	**4.00**	**4.00**	**4.00**	**4.00**	**4.00**

Appendix 5
Ilmenite EMP data - cation calculations based on 6 oxygen

No	**17922 1.16**	**17922 1.21 inc**	**17922 1.22 inc**	**17922 1.23 inc**	**17922 1.29**	**17922 2.6**	**17922 2.7**	**17922 2.15**
Mineral	Ilmenite	Ilmenite	Ilmenite	Ilmenite	Ilmenite	Ilmenite	Ilmenite	Ilmenite
wt %								
SiO_2	0.02	0.01	0.01	0.02	0.02	0.02	0.00	0.03
TiO_2	50.21	50.74	50.78	51.05	51.19	51.91	51.49	50.02
Al_2O_3	0.11	0.17	0.13	0.14	0.12	0.21	0.11	0.17
Cr_2O_3	0.06	0.05	0.00	0.00	0.08	0.02	0.02	0.03
Fe_2O_3	5.32	4.75	4.29	4.00	4.11	2.10	2.41	6.42
FeO	41.40	42.00	42.80	43.20	41.40	43.20	44.00	40.60
MnO	0.48	0.50	0.47	0.49	0.44	0.50	0.54	0.50
MgO	1.86	1.61	1.17	1.27	2.27	1.55	0.89	1.96
CaO	0.02	0.02	0.00	0.00	0.03	0.02	0.00	0.08
NiO	0.01	0.04	0.00	0.00	0.02	0.03	0.01	0.03
ZnO	0.03	0.02	0.02	0.04	0.00	0.03	0.01	0.08
Na_2O	0.01	0.00	0.00	0.01	0.00	0.01	0.00	0.00
K_2O	0.00	0.00	0.01	0.00	0.00	0.01	0.00	0.00
Total	**99.72**	**100.14**	**99.89**	**100.45**	**99.91**	**99.76**	**99.67**	**100.21**
Total FeO	**46.19**	**46.28**	**46.66**	**46.80**	**45.10**	**45.09**	**46.17**	**46.37**
Cations								
Si^{4+}	0.00	0.00	0.00	0.00	0.00	0.00	0.00	0.00
Ti^{4+}	1.89	1.90	1.92	1.92	1.92	1.95	1.95	1.87
Al^{3+}	0.01	0.01	0.01	0.01	0.01	0.01	0.01	0.01
Cr^{3+}	0.00	0.00	0.00	0.00	0.00	0.00	0.00	0.00
Fe^{3+}	0.20	0.18	0.16	0.15	0.15	0.08	0.09	0.24
Fe^{2+}	1.73	1.75	1.80	1.80	1.72	1.81	1.85	1.69
Mn^{2+}	0.02	0.02	0.02	0.02	0.02	0.02	0.02	0.02
Mg^{2+}	0.14	0.12	0.09	0.09	0.17	0.12	0.07	0.15
Ca^{2+}	0.00	0.00	0.00	0.00	0.00	0.00	0.00	0.00
Ni^{2+}	0.00	0.00	0.00	0.00	0.00	0.00	0.00	0.00
Zn^{2+}	0.00	0.00	0.00	0.00	0.00	0.00	0.00	0.00
Na^{+}	0.00	0.00	0.00	0.00	0.00	0.00	0.00	0.00
K^{+}	0.00	0.00	0.00	0.00	0.00	0.00	0.00	0.00
Total	**4.00**	**4.00**	**4.00**	**4.00**	**4.00**	**4.00**	**4.00**	**4.00**

Appendix 5
Ilmenite EMP data - cation calculations based on 6 oxygen

No	**17911 3.8**	**17911 3.9 blade**	**17913 4.8 inc**	**17913 1.3**	**18002 6.5**	**18002 6.6**	**18002 3.4**
Mineral	Ilmenite	Ilmenite	Ilmenite	Ilmenite	Ilmenite	Ilmenite	Ilmenite
wt %							
SiO_2	0.04	0.02	0.04	0.00	0.00	0.01	0.01
TiO_2	50.04	50.47	49.62	50.67	49.28	49.11	48.59
Al_2O_3	0.21	0.21	0.25	0.22	0.18	0.45	0.26
Cr_2O_3	0.01	0.03	0.01	0.02	0.04	0.00	0.01
Fe_2O_3	5.70	5.85	8.66	6.50	8.77	8.99	10.41
FeO	40.60	40.60	36.60	38.20	37.20	37.20	36.00
MnO	0.92	0.88	0.54	0.42	0.37	0.45	0.36
MgO	2.07	2.04	4.20	3.89	3.88	3.79	4.31
CaO	0.01	0.01	0.00	0.00	0.00	0.00	0.01
NiO	0.00	0.04	0.03	0.02	0.00	0.00	0.00
ZnO	0.11	0.01	0.00	0.02	0.00	0.08	0.04
Na_2O	0.00	0.00	0.00	0.00	0.00	0.01	0.00
K_2O	0.02	0.03	0.00	0.00	0.00	0.00	0.00
Total	**99.82**	**100.22**	**100.12**	**100.12**	**99.97**	**100.30**	**100.23**
Total FeO	**45.73**	**45.86**	**44.39**	**44.05**	**45.09**	**45.29**	**45.36**
Cations							
Si^{4+}	0.00	0.00	0.00	0.00	0.00	0.00	0.00
Ti^{4+}	1.88	1.89	1.83	1.87	1.83	1.81	1.79
Al^{3+}	0.01	0.01	0.01	0.01	0.01	0.03	0.01
Cr^{3+}	0.00	0.00	0.00	0.00	0.00	0.00	0.00
Fe^{3+}	0.21	0.22	0.32	0.24	0.32	0.33	0.38
Fe^{2+}	1.70	1.69	1.50	1.57	1.53	1.53	1.48
Mn^{2+}	0.03	0.03	0.02	0.01	0.01	0.02	0.01
Mg^{2+}	0.15	0.15	0.31	0.28	0.29	0.28	0.31
Ca^{2+}	0.00	0.00	0.00	0.00	0.00	0.00	0.00
Ni^{2+}	0.00	0.00	0.00	0.00	0.00	0.00	0.00
Zn^{2+}	0.00	0.00	0.00	0.00	0.00	0.00	0.00
Na^{+}	0.00	0.00	0.00	0.00	0.00	0.00	0.00
K^{+}	0.00	0.00	0.00	0.00	0.00	0.00	0.00
Total	**4.00**	**4.00**	**4.00**	**4.00**	**4.00**	**4.00**	**4.00**

Appendix 5
Magnetite and titanomagnetite EMP data - cation calculations based on 32 oxygen

No	**17914 4.14**	**17914 2.29**	**18002 6.7**	**17921 2.9**	**17921 2.10**	**17921 2.11**	**'921 2.12 px exs**	**17921 3.13**	**17921 3.14 c**
Mineral	Magnetite	Magnetite	Magnetite inc	Titanomagnetite	Titanomagnetite	Titanomagnetite	Titanomagnetite	Titanomagnetite	Titanomagnetite
wt %									
SiO_2	1.70	0.13	0.11	0.20	0.19	0.18	0.21	0.20	0.19
TiO_2	0.00	0.03	0.01	9.78	9.63	10.13	9.89	11.51	10.53
Al_2O_3	0.39	0.02	0.04	3.77	3.88	3.52	3.52	4.90	4.86
Cr_2O_3	0.01	0.02	0.00	0.02	0.00	0.00	0.00	0.01	0.01
Fe_2O_3	62.26	65.38	64.90	45.19	45.29	45.07	44.16	40.78	42.58
FeO	30.10	28.90	28.80	38.60	38.57	39.10	38.49	40.40	39.24
MnO	0.01	0.00	0.00	0.74	0.76	0.73	0.70	0.83	0.77
MgO	0.20	0.07	0.02	0.66	0.67	0.56	0.58	0.68	0.77
CaO	0.04	0.15	0.06	0.01	0.00	0.00	0.00	0.01	0.01
NiO	1.83	0.47	0.46	0.01	0.02	0.00	0.03	0.03	0.04
ZnO	0.00	0.00	0.07	0.26	0.24	0.26	0.19	0.27	0.26
Na_2O	0.01	0.02	0.00	0.01	0.00	0.00	0.01	0.00	0.02
K_2O	0.01	0.02	0.00	0.02	0.01	0.01	0.02	0.02	0.01
Total	**96.55**	**95.21**	**94.47**	**99.31**	**99.35**	**99.64**	**97.90**	**99.71**	**99.37**
Total FeO	**86.12**	**87.73**	**87.20**	**79.26**	**79.33**	**79.65**	**78.23**	**77.09**	**77.55**
Cations									
Si^{4+}	0.54	0.04	0.04	0.06	0.06	0.05	0.07	0.06	0.06
Ti^{4+}	0.00	0.01	0.00	2.20	2.17	2.28	2.26	2.56	2.35
Al^{3+}	0.14	0.01	0.01	1.33	1.37	1.24	1.26	1.71	1.70
Cr^{3+}	0.00	0.00	0.00	0.00	0.00	0.00	0.00	0.00	0.00
Fe^{3+}	14.79	15.90	15.92	10.18	10.20	10.14	10.11	9.08	9.52
Fe^{2+}	7.94	7.81	7.85	9.67	9.65	9.78	9.79	10.00	9.75
Mn^{2+}	0.00	0.00	0.00	0.15	0.16	0.15	0.15	0.17	0.16
Mg^{2+}	0.10	0.03	0.01	0.29	0.30	0.25	0.26	0.30	0.34
Ca^{2+}	0.01	0.05	0.02	0.00	0.00	0.00	0.00	0.00	0.00
Ni^{2+}	0.46	0.12	0.12	0.00	0.00	0.00	0.01	0.01	0.01
Zn^{2+}	0.00	0.00	0.02	0.06	0.05	0.06	0.04	0.06	0.06
Na^{+}	0.00	0.01	0.00	0.01	0.00	0.00	0.00	0.00	0.01
K^{+}	0.00	0.01	0.00	0.01	0.00	0.00	0.01	0.01	0.00
Total	**24.00**	**24.00**	**24.00**	**23.98**	**23.98**	**23.97**	**23.98**	**23.98**	**23.98**

Appendix 5
Magnetite and titanomagnetite EMP data - cation calculations based on 32 oxygen

No	**17921 3.14 r**	**17915 1.14**	**17915 1.15**	**17915 3.3**	**17915 5.3**	**17911 3.7**	**17911 1.1 incl**	**17911 1.2 incl**	**17911 1.3 incl r**
Mineral	Titanomagnetite	Titanomagnetite	Titanomagnetite	Titanomagnetite	Titanomagnetite	Titanomagnetite	Titanomagnetite	Titanomagnetite	Titanomagnetite
wt %									
SiO_2	0.80	0.18	0.19	0.17	0.14	0.10	0.13	0.09	0.10
TiO_2	11.13	8.96	12.61	13.37	16.29	19.31	17.58	17.43	17.67
Al_2O_3	5.07	1.19	3.75	2.84	4.01	4.74	4.35	4.54	4.58
Cr_2O_3	0.02	0.01	0.03	0.00	0.02	0.04	0.07	0.10	0.07
Fe_2O_3	38.74	48.46	38.89	38.25	31.60	26.57	29.84	29.55	29.01
FeO	38.54	38.60	41.21	41.76	43.80	46.90	45.45	44.95	45.30
MnO	0.74	0.41	0.55	0.50	0.60	0.76	0.59	0.62	0.60
MgO	0.94	0.26	0.57	0.56	1.03	1.42	1.14	1.24	1.21
CaO	0.02	0.01	0.01	0.05	0.02	0.00	0.01	0.01	0.02
NiO	0.04	0.00	0.00	0.01	0.01	0.00	0.09	0.02	0.04
ZnO	0.24	0.00	0.13	0.05	0.22	0.00	0.19	0.22	0.16
Na_2O	0.01	0.00	0.00	0.01	0.00	0.00	0.00	0.01	0.00
K_2O	0.01	0.00	0.00	0.00	0.00	0.02	0.00	0.02	0.01
Total	**96.38**	**98.35**	**98.20**	**97.76**	**97.93**	**99.86**	**99.78**	**99.11**	**99.08**
Total FeO	**73.40**	**82.20**	**76.20**	**76.17**	**72.23**	**70.81**	**72.30**	**71.54**	**71.40**
Cations									
Si^{4+}	0.24	0.06	0.06	0.05	0.04	0.03	0.04	0.03	0.03
Ti^{4+}	2.54	2.08	2.86	3.06	3.68	4.24	3.89	3.87	3.92
Al^{3+}	1.81	0.43	1.33	1.02	1.42	1.63	1.51	1.58	1.59
Cr^{3+}	0.01	0.00	0.01	0.00	0.00	0.01	0.02	0.02	0.02
Fe^{3+}	8.84	11.23	8.83	8.76	7.14	5.84	6.60	6.57	6.45
Fe^{2+}	9.77	9.94	10.40	10.63	11.00	11.46	11.17	11.10	11.19
Mn^{2+}	0.16	0.09	0.11	0.10	0.12	0.15	0.12	0.13	0.12
Mg^{2+}	0.43	0.12	0.25	0.26	0.46	0.62	0.50	0.55	0.53
Ca^{2+}	0.01	0.00	0.00	0.02	0.01	0.00	0.00	0.00	0.01
Ni^{2+}	0.01	0.00	0.00	0.00	0.00	0.00	0.02	0.00	0.01
Zn^{2+}	0.05	0.00	0.03	0.01	0.05	0.00	0.04	0.05	0.03
Na^{+}	0.01	0.00	0.00	0.01	0.00	0.00	0.00	0.00	0.00
K^{+}	0.00	0.00	0.00	0.00	0.00	0.01	0.00	0.01	0.00
Total	**23.89**	**24.00**	**23.96**	**23.97**	**23.98**	**23.99**	**23.98**	**23.98**	**23.98**

Appendix 5
Magnetite and titanomagnetite EMP data - cation calculations based on 32 oxygen

No	**17911 5.4**	**17911 5.5**	**17913 1.4**	**17913 2.2 incl**	**17913 2.5**	**17913 3.4**	**17913 4.9 incl**	**17913 5.5**	**17913 5.6**
Mineral	Titanomagnetite	Titanomagnetite	Titanomagnetite	Titanomagnetite	Titanomagnetite	Titanomagnetite	Titanomagnetite	Titanomagnetite	Titanomagnetite
wt %									
SiO_2	0.11	0.11	0.05	0.05	0.06	0.05	0.07	0.08	0.08
TiO_2	15.81	15.88	19.85	22.60	13.87	19.20	24.49	23.02	12.95
Al_2O_3	4.80	4.90	4.32	2.87	4.24	2.58	4.12	4.02	3.85
Cr_2O_3	0.08	0.13	0.01	0.01	0.03	0.03	0.02	0.01	0.00
Fe_2O_3	33.28	32.54	26.50	21.48	37.10	28.96	17.07	20.84	40.16
FeO	44.22	44.20	45.20	47.86	39.85	43.46	46.57	44.70	38.26
MnO	0.64	0.58	0.38	0.51	0.40	0.56	0.50	0.49	0.30
MgO	1.09	1.06	2.83	2.21	2.43	3.04	4.22	4.70	3.05
CaO	0.00	0.00	0.01	0.01	0.01	0.01	0.00	0.00	0.01
NiO	0.06	0.01	0.00	0.00	0.00	0.07	0.01	0.00	0.00
ZnO	0.13	0.13	0.16	0.10	0.13	0.06	0.14	0.16	0.08
Na_2O	0.00	0.02	0.01	0.01	0.00	0.00	0.01	0.01	0.00
K_2O	0.02	0.01	0.00	0.00	0.00	0.01	0.00	0.00	0.00
Total	**100.45**	**99.80**	**99.74**	**98.26**	**98.62**	**98.46**	**97.73**	**98.47**	**99.22**
Total FeO	**74.17**	**73.48**	**69.04**	**67.18**	**73.23**	**69.52**	**61.93**	**63.45**	**74.39**
Cations									
Si^{4+}	0.03	0.03	0.02	0.01	0.02	0.01	0.02	0.02	0.02
Ti^{4+}	3.47	3.51	4.33	5.04	3.08	4.27	5.37	5.00	2.85
Al^{3+}	1.65	1.70	1.48	1.00	1.48	0.90	1.41	1.37	1.33
Cr^{3+}	0.02	0.03	0.00	0.00	0.01	0.01	0.00	0.00	0.00
Fe^{3+}	7.31	7.19	5.78	4.80	8.25	6.45	3.74	4.53	8.86
Fe^{2+}	10.80	10.85	10.95	11.88	9.84	10.75	11.34	10.79	9.38
Mn^{2+}	0.13	0.12	0.08	0.11	0.08	0.11	0.10	0.10	0.06
Mg^{2+}	0.47	0.46	1.22	0.98	1.07	1.34	1.83	2.02	1.33
Ca^{2+}	0.00	0.00	0.00	0.00	0.00	0.00	0.00	0.00	0.00
Ni^{2+}	0.01	0.00	0.00	0.00	0.00	0.02	0.00	0.00	0.00
Zn^{2+}	0.03	0.03	0.03	0.02	0.03	0.01	0.03	0.03	0.02
Na^{+}	0.00	0.01	0.00	0.00	0.00	0.00	0.01	0.01	0.00
K^{+}	0.01	0.00	0.00	0.00	0.00	0.00	0.00	0.00	0.00
Total	**23.98**	**23.98**	**23.98**	**23.98**	**23.98**	**23.99**	**23.98**	**23.98**	**23.97**

Appendix 5
Magnetite and titanomagnetite EMP data - cation calculations based on 32 oxygen

No	**17913 5.8**	**17913 7.1**	**17913 7.2 r**	**17913 7.3 c**	**17913 7.4 r**	**17913 7.5 c**	**17913 7.6 r**	**18002 4.8 incl**	**18003 1.6**
Mineral	Titanomagnetite	Titanomagnetite	Titanomagnetite	Titanomagnetite	Titanomagnetite	Titanomagnetite	Titanomagnetite	Titanomagnetite	Titanomagnetite
wt %									
SiO_2	0.06	0.09	0.05	0.09	0.07	0.10	0.05	0.06	0.10
TiO_2	21.93	16.98	21.80	18.39	28.09	19.66	18.41	16.01	19.08
Al_2O_3	2.98	4.97	4.57	4.67	2.73	4.65	4.90	5.27	2.08
Cr_2O_3	0.02	0.02	0.03	0.01	0.00	0.00	0.00	0.16	0.01
Fe_2O_3	23.28	31.00	21.61	28.22	11.59	26.30	28.14	34.56	30.01
FeO	45.27	43.30	47.15	44.00	51.85	45.34	44.48	33.50	46.65
MnO	0.48	0.40	0.41	0.38	0.48	0.39	0.39	0.44	0.57
MgO	3.59	2.46	2.57	2.59	3.00	2.62	2.45	7.96	1.13
CaO	0.00	0.00	0.01	0.00	0.00	0.00	0.03	0.10	0.01
NiO	0.00	0.00	0.01	0.01	0.02	0.02	0.00	0.05	0.04
ZnO	0.08	0.04	0.13	0.13	0.09	0.13	0.08	0.00	0.15
Na_2O	0.01	0.01	0.01	0.00	0.00	0.01	0.01	0.00	0.00
K_2O	0.00	0.00	0.00	0.00	0.00	0.00	0.00	0.01	0.01
Total	**98.28**	**99.82**	**98.83**	**98.96**	**98.32**	**99.62**	**99.34**	**98.71**	**99.95**
Total FeO	**66.22**	**71.19**	**66.59**	**69.39**	**62.28**	**69.01**	**69.80**	**64.60**	**73.65**
Cations									
Si^{4+}	0.02	0.03	0.01	0.03	0.02	0.03	0.02	0.02	0.03
Ti^{4+}	4.84	3.70	4.78	4.04	6.20	4.29	4.03	3.39	4.26
Al^{3+}	1.03	1.70	1.57	1.61	0.94	1.59	1.68	1.75	0.73
Cr^{3+}	0.00	0.01	0.01	0.00	0.00	0.00	0.00	0.04	0.00
Fe^{3+}	5.14	6.76	4.74	6.20	2.56	5.74	6.16	7.31	6.70
Fe^{2+}	11.12	10.50	11.51	10.75	12.73	10.99	10.83	7.88	11.57
Mn^{2+}	0.10	0.08	0.08	0.08	0.10	0.08	0.08	0.08	0.12
Mg^{2+}	1.57	1.06	1.12	1.13	1.31	1.13	1.06	3.33	0.50
Ca^{2+}	0.00	0.00	0.00	0.00	0.00	0.00	0.01	0.03	0.00
Ni^{2+}	0.00	0.00	0.00	0.00	0.01	0.01	0.00	0.01	0.01
Zn^{2+}	0.02	0.01	0.03	0.03	0.02	0.03	0.02	0.00	0.03
Na^{+}	0.01	0.00	0.00	0.00	0.00	0.01	0.00	0.00	0.00
K^{+}	0.00	0.00	0.00	0.00	0.00	0.00	0.00	0.00	0.00
Total	**23.98**	**23.98**	**23.98**	**23.97**	**23.98**	**23.98**	**23.98**	**23.98**	**23.98**

Appendix 5
Magnetite and titanomagnetite EMP data - cation calculations based on 32 oxygen

No	**18003 2.5**	**18003 2.7**	**18003 4.5**	**18003 4.5 opq**	**18003 5.4 opq**
Mineral	Titanomagnetite	Titanomagnetite	Titanomagnetite	Titanomagnetite	Titanomagnetite
wt %					
SiO_2	0.52	0.09	0.09	0.11	0.12
TiO_2	19.61	19.48	19.05	19.10	19.43
Al_2O_3	2.36	2.06	1.67	1.72	1.81
Cr_2O_3	0.01	0.00	0.04	0.00	0.03
Fe_2O_3	26.76	29.02	29.96	29.95	29.01
FeO	45.45	46.14	46.40	46.50	46.10
MnO	0.57	0.60	0.55	0.58	0.55
MgO	1.59	1.45	1.09	1.09	1.43
CaO	0.03	0.04	0.01	0.01	0.09
NiO	0.02	0.00	0.00	0.00	0.00
ZnO	0.19	0.27	0.15	0.10	0.13
Na_2O	0.01	0.00	0.01	0.00	0.02
K_2O	0.00	0.00	0.01	0.00	0.00
Total	**97.18**	**99.23**	**99.13**	**99.21**	**98.79**
Total FeO	**69.53**	**72.25**	**73.36**	**73.45**	**72.20**
Cations					
Si^{4+}	0.16	0.03	0.03	0.03	0.04
Ti^{4+}	4.45	4.37	4.30	4.30	4.38
Al^{3+}	0.84	0.72	0.59	0.61	0.64
Cr^{3+}	0.00	0.00	0.01	0.00	0.01
Fe^{3+}	6.08	6.51	6.76	6.75	6.54
Fe^{2+}	11.48	11.50	11.64	11.65	11.55
Mn^{2+}	0.12	0.12	0.11	0.12	0.11
Mg^{2+}	0.72	0.64	0.49	0.49	0.64
Ca^{2+}	0.01	0.01	0.00	0.00	0.03
Ni^{2+}	0.00	0.00	0.00	0.00	0.00
Zn^{2+}	0.04	0.06	0.03	0.02	0.03
Na^{+}	0.00	0.00	0.01	0.00	0.01
K^{+}	0.00	0.00	0.00	0.00	0.00
Total	**23.92**	**23.98**	**23.99**	**23.98**	**23.99**

Appendix 6
Results for Zircon U-Pb Dating

				RATIOS (common-Pb corrected)								AGES (common-Pb corrected, Ma)								
Analysis No.	Th (ppm)	U (ppm)	Th/U	$^{207}Pb/^{206}Pb$	± 1σ	$^{207}Pb/^{235}U$	± 1σ	$^{206}Pb/^{238}U$	± 1σ	$^{208}Pb/^{232}Th$	± 1σ	$^{207}Pb/^{206}Pb$	± 1σ	$^{207}Pb/^{235}U$	± 1σ	$^{206}Pb/^{238}U$	± 1σ	$^{208}Pb/^{232}Th$	± 1σ	Disc.
Felsic Group																				
17911-01	171	429	0.40	0.05953	0.00083	0.742	0.009	0.09035	0.00083	0.02832	0.00071	587	31	563	5	558	5	564	14	5.2
17911-03	1120	2343	0.48	0.05866	0.00073	0.684	0.008	0.08458	0.00082	0.02756	0.00064	555	28	529	5	523	5	550	13	5.9
17911-03B	291	1318	0.22	0.05614	0.00105	0.525	0.009	0.06785	0.00066	0.02310	0.00105	458	42	429	6	423	4	462	21	7.8
17911-05	482	1209	0.40	0.05847	0.00102	0.661	0.012	0.08208	0.00100	0.02819	0.00107	547	39	516	7	509	6	562	21	7.4
17911-06	373	736	0.51	0.05870	0.00072	0.716	0.008	0.08843	0.00082	0.02899	0.00063	556	27	548	5	546	5	578	12	1.8
17911-07	500	1005	0.50	0.05937	0.00074	0.734	0.009	0.08965	0.00087	0.02903	0.00066	581	28	559	5	553	5	578	13	4.9
17911-12	203	2102	0.10	0.05615	0.00172	0.476	0.014	0.06152	0.00091	0.02818	0.00242	458	70	395	10	385	6	562	48	16.5
17911-13	268	519	0.52	0.05905	0.00077	0.745	0.009	0.09155	0.00087	0.02914	0.00070	569	29	566	5	565	5	581	14	0.8
17911-13B	258	499	0.52	0.05851	0.00117	0.678	0.013	0.08400	0.00086	0.02692	0.00127	549	45	525	8	520	5	537	25	5.5
17911-14	266	711	0.37	0.05848	0.00088	0.710	0.010	0.08802	0.00088	0.02685	0.00084	548	34	545	6	544	5	536	17	0.8
17911-14B	44	193	0.23	0.05836	0.00170	0.626	0.017	0.07779	0.00097	0.02285	0.00145	543	65	494	11	483	6	457	29	11.5
17911-15	1906	2029	0.94	0.05895	0.00097	0.732	0.012	0.09011	0.00105	0.02857	0.00111	565	37	558	7	556	6	569	22	1.7
17911-19	536	1015	0.53	0.05929	0.00089	0.732	0.010	0.08959	0.00090	0.02780	0.00092	578	33	558	6	553	5	554	18	4.5
17911-19B	436	686	0.64	0.05996	0.00129	0.683	0.014	0.08255	0.00088	0.02608	0.00142	602	48	528	8	511	5	520	28	15.7
17911-20	129	2395	0.05	0.05508	0.00118	0.453	0.009	0.05966	0.00073	0.03063	0.00190	415	49	379	7	374	4	610	37	10.4
17911-20B	188	371	0.51	0.05861	0.00180	0.651	0.019	0.08058	0.00097	0.02569	0.00235	553	69	509	11	500	6	513	46	10.0
17911-21	43	4393	0.01	0.05531	0.00175	0.424	0.013	0.05567	0.00085	0.01702	0.00206	425	72	359	9	349	5	341	41	18.3
17911-22	496	1038	0.48	0.05899	0.00130	0.679	0.014	0.08349	0.00086	0.02507	0.00180	567	49	526	8	517	5	500	35	9.2
17911-22B	407	1019	0.40	0.05687	0.00176	0.586	0.017	0.07475	0.00090	0.02272	0.00248	486	70	468	11	465	5	454	49	4.6
17911-23	878	1394	0.63	0.05909	0.00072	0.737	0.009	0.09045	0.00094	0.02859	0.00061	570	27	561	5	558	6	570	12	2.2
17911-24	320	637	0.50	0.05874	0.00078	0.725	0.009	0.08947	0.00084	0.02904	0.00071	557	30	553	5	552	5	579	14	0.9

Appendix 6
Results for Zircon U-Pb Dating

				R A T I O S (common-Pb corrected)								A G E S (common-Pb corrected, Ma)								
Analysis No.	Th (ppm)	U (ppm)	Th/U	$^{207}Pb/^{206}Pb$	± 1σ	$^{207}Pb/^{235}U$	± 1σ	$^{206}Pb/^{238}U$	± 1σ	$^{208}Pb/^{232}Th$	± 1σ	$^{207}Pb/^{206}Pb$	± 1σ	$^{207}Pb/^{235}U$	± 1σ	$^{206}Pb/^{238}U$	± 1σ	$^{208}Pb/^{232}Th$	± 1σ	Disc.
17911-28	541	880	0.61	0.05949	0.00139	0.701	0.015	0.08541	0.00089	0.02693	0.00211	585	52	539	9	528	5	537	42	10.1
17911-30	407	868	0.47	0.05906	0.00079	0.751	0.010	0.09219	0.00101	0.03001	0.00076	569	30	569	6	568	6	598	15	0.2
17911-33	364	637	0.57	0.05898	0.00081	0.748	0.010	0.09193	0.00090	0.02949	0.00078	566	31	567	6	567	5	587	15	-0.1
17911-34	538	809	0.67	0.05849	0.00087	0.712	0.010	0.08831	0.00082	0.02804	0.00090	548	33	546	6	546	5	559	18	0.5
17911-36	420	876	0.48	0.05900	0.00078	0.725	0.009	0.08915	0.00083	0.02897	0.00078	567	29	554	5	551	5	577	15	3.0
17911-38	292	724	0.40	0.05894	0.00072	0.725	0.008	0.08919	0.00087	0.02986	0.00067	565	27	553	5	551	5	595	13	2.6
17911-40	196	4072	0.05	0.05405	0.00164	0.427	0.013	0.05736	0.00085	0.01689	0.00155	373	70	361	9	360	5	339	31	3.7
17911-44	490	1043	0.47	0.05878	0.00071	0.733	0.008	0.09041	0.00088	0.02908	0.00067	559	27	558	5	558	5	579	13	0.2
17911-48	271	659	0.41	0.05904	0.00085	0.752	0.011	0.09237	0.00097	0.03096	0.00097	569	32	569	6	570	6	616	19	-0.2
17911-51	423	739	0.57	0.05886	0.00079	0.703	0.009	0.08661	0.00083	0.02827	0.00081	562	30	541	5	535	5	563	16	4.9
17911-52	276	2187	0.13	0.05556	0.00165	0.503	0.015	0.06569	0.00097	0.02635	0.00211	435	68	414	10	410	6	526	42	5.9
17911-52B	431	842	0.51	0.05852	0.00124	0.712	0.014	0.08826	0.00087	0.02794	0.00193	549	47	546	8	545	5	557	38	0.8
17911-53	364	610	0.60	0.05911	0.00072	0.733	0.009	0.08994	0.00089	0.02735	0.00053	571	27	558	5	555	5	545	10	2.9
17911-55	573	1358	0.42	0.05757	0.00082	0.639	0.009	0.08047	0.00089	0.02470	0.00070	513	32	501	6	499	5	493	14	2.9
17911-55B	671	1283	0.52	0.05891	0.00104	0.715	0.012	0.08804	0.00085	0.02750	0.00149	564	39	548	7	544	5	548	29	3.7
17911-56	192	629	0.31	0.05637	0.00112	0.526	0.010	0.06762	0.00085	0.02685	0.00109	467	45	429	7	422	5	536	21	10.0
17911-58	221	497	0.45	0.05935	0.00085	0.713	0.010	0.08710	0.00089	0.02671	0.00079	580	32	546	6	538	5	533	16	7.5
17911-59	305	6012	0.05	0.05392	0.00064	0.396	0.004	0.05332	0.00052	0.01704	0.00037	368	27	339	3	335	3	342	7	9.2
17911-62	512	993	0.52	0.05872	0.00086	0.713	0.010	0.08808	0.00098	0.02640	0.00079	557	33	547	6	544	6	527	16	2.4
17911-63	257	679	0.38	0.05900	0.00096	0.713	0.011	0.08760	0.00100	0.02666	0.00091	567	36	546	7	541	6	532	18	4.8
17911-66	750	1031	0.73	0.05891	0.00077	0.710	0.009	0.08740	0.00088	0.02717	0.00068	564	29	545	5	540	5	542	13	4.4
17911-66B	703	863	0.81	0.05868	0.00119	0.724	0.013	0.08950	0.00088	0.02667	0.00167	555	45	553	8	553	5	532	33	0.5

Appendix 6
Results for Zircon U-Pb Dating

				R A T I O S (common-Pb corrected)								A G E S (common-Pb corrected, Ma)								
Analysis No.	Th (ppm)	U (ppm)	Th/U	$^{207}Pb/^{206}Pb$	± 1σ	$^{207}Pb/^{235}U$	± 1σ	$^{206}Pb/^{238}U$	± 1σ	$^{208}Pb/^{232}Th$	± 1σ	$^{207}Pb/^{206}Pb$	± 1σ	$^{207}Pb/^{235}U$	± 1σ	$^{206}Pb/^{238}U$	± 1σ	$^{208}Pb/^{232}Th$	± 1σ	Disc.
17911-67	187	426	0.44	0.05873	0.00082	0.712	0.009	0.08790	0.00087	0.02762	0.00075	557	31	546	6	543	5	551	15	2.6
17911-70	477	1082	0.44	0.05905	0.00112	0.680	0.013	0.08353	0.00102	0.02634	0.00120	569	42	527	8	517	6	525	24	9.5
17912-01	241	526	0.46	0.05878	0.00080	0.725	0.010	0.08948	0.00093	0.02724	0.00071	559	30	554	6	552	6	543	14	1.2
17912-03	2202	3765	0.58	0.05943	0.00114	0.707	0.014	0.08627	0.00107	0.02716	0.00105	583	43	543	8	533	6	542	21	8.9
17912-04	309	593	0.52	0.05930	0.00078	0.686	0.009	0.08388	0.00090	0.02598	0.00069	578	29	530	5	519	5	518	14	10.6
17912-05	607	1200	0.51	0.05866	0.00082	0.717	0.009	0.08860	0.00083	0.02789	0.00076	555	31	549	5	547	5	556	15	1.4
17912-08	415	1089	0.38	0.05965	0.00083	0.715	0.010	0.08693	0.00093	0.02676	0.00074	591	31	548	6	537	6	534	15	9.5
17912-11	287	515	0.56	0.05851	0.00078	0.641	0.008	0.07947	0.00083	0.02533	0.00065	549	30	503	5	493	5	506	13	10.6
17912-12	103	258	0.40	0.05877	0.00094	0.724	0.011	0.08934	0.00101	0.02662	0.00085	559	36	553	7	552	6	531	17	1.3
17912-14	242	467	0.52	0.05896	0.00115	0.733	0.014	0.09019	0.00095	0.02825	0.00118	566	43	558	8	557	6	563	23	1.7
17912-14B	98	835	0.12	0.05653	0.00094	0.482	0.008	0.06179	0.00063	0.02832	0.00123	473	38	399	5	387	4	564	24	18.9
17912-15	340	663	0.51	0.05882	0.00095	0.730	0.011	0.08998	0.00088	0.02680	0.00095	560	36	556	6	555	5	535	19	0.9
17912-18	561	1109	0.51	0.06018	0.00104	0.710	0.012	0.08552	0.00093	0.02652	0.00102	610	38	544	7	529	6	529	20	13.8
17912-20	30	85	0.35	0.05987	0.00092	0.733	0.011	0.08882	0.00088	0.02780	0.00099	599	34	558	6	549	5	554	19	8.8
17912-21	409	883	0.46	0.05955	0.00096	0.709	0.012	0.08638	0.00102	0.02605	0.00085	587	36	544	7	534	6	520	17	9.4
17912-21B	616	1089	0.57	0.05877	0.00088	0.652	0.010	0.08050	0.00088	0.02507	0.00075	559	33	510	6	499	5	500	15	11.1
17912-23	650	1094	0.59	0.05968	0.00076	0.745	0.009	0.09060	0.00091	0.02776	0.00066	592	28	566	5	559	5	553	13	5.8
17912-24	477	951	0.50	0.05841	0.00080	0.694	0.009	0.08613	0.00082	0.02702	0.00075	545	31	535	5	533	5	539	15	2.4
17912-24B	1603	2268	0.71	0.05943	0.00076	0.737	0.009	0.08997	0.00093	0.02740	0.00070	583	28	561	5	555	6	546	14	4.9
17912-25	1838	3971	0.46	0.05811	0.00107	0.714	0.013	0.08911	0.00094	0.02585	0.00142	534	41	547	7	550	6	516	28	-3.2
17912-27	306	598	0.51	0.05945	0.00092	0.698	0.010	0.08521	0.00085	0.02723	0.00090	584	34	538	6	527	5	543	18	10.1
17912-30	476	766	0.62	0.05934	0.00100	0.728	0.012	0.08904	0.00105	0.02717	0.00103	580	37	556	7	550	6	542	20	5.4

Appendix 6
Results for Zircon U-Pb Dating

				R A T I O S (common-Pb corrected)								A G E S (common-Pb corrected, Ma)								
Analysis No.	Th (ppm)	U (ppm)	Th/U	$^{207}Pb/^{206}Pb$	± 1σ	$^{207}Pb/^{235}U$	± 1σ	$^{206}Pb/^{238}U$	± 1σ	$^{208}Pb/^{232}Th$	± 1σ	$^{207}Pb/^{206}Pb$	± 1σ	$^{207}Pb/^{235}U$	± 1σ	$^{206}Pb/^{238}U$	± 1σ	$^{208}Pb/^{232}Th$	± 1σ	Disc.
17912-30B	286	465	0.62	0.05828	0.00125	0.634	0.013	0.07885	0.00086	0.02385	0.00118	540	48	498	8	489	5	476	23	9.8
17912-35	665	783	0.85	0.05896	0.00106	0.717	0.012	0.08815	0.00092	0.02765	0.00118	566	40	549	7	545	5	551	23	3.9
17912-36	437	778	0.56	0.05916	0.00078	0.747	0.010	0.09153	0.00093	0.02853	0.00077	573	29	566	6	565	5	569	15	1.5
17912-37	604	996	0.61	0.05942	0.00097	0.683	0.011	0.08335	0.00085	0.02626	0.00101	583	36	529	6	516	5	524	20	11.9
17912-37B	109	466	0.23	0.05820	0.00165	0.476	0.013	0.05939	0.00070	0.01961	0.00160	537	63	396	9	372	4	393	32	31.7
17912-37B	1020	2293	0.44	0.05817	0.00115	0.686	0.013	0.08555	0.00097	0.02570	0.00143	536	44	530	8	529	6	513	28	1.4
17912-42	407	648	0.63	0.05961	0.00102	0.736	0.013	0.08959	0.00107	0.02721	0.00095	589	38	560	7	553	6	543	19	6.4
17912-42B	337	513	0.66	0.05856	0.00111	0.668	0.012	0.08279	0.00085	0.02492	0.00103	551	42	520	7	513	5	498	20	7.2
17912-47	324	575	0.56	0.05864	0.00089	0.724	0.010	0.08954	0.00085	0.02773	0.00089	554	34	553	6	553	5	553	18	0.2
17912-49	607	983	0.62	0.05923	0.00072	0.751	0.009	0.09190	0.00090	0.02818	0.00062	576	27	569	5	567	5	562	12	1.6
17912-50	1183	1640	0.72	0.05909	0.00080	0.700	0.009	0.08588	0.00083	0.02642	0.00076	570	30	539	5	531	5	527	15	7.2
17912-50B	1290	1676	0.77	0.05935	0.00101	0.740	0.012	0.09039	0.00089	0.02802	0.00137	580	38	562	7	558	5	559	27	4.0
17912-51	445	795	0.56	0.06010	0.00083	0.746	0.010	0.08999	0.00095	0.02745	0.00075	607	31	566	6	555	6	547	15	8.9
17912-51B	628	1087	0.58	0.05706	0.00133	0.589	0.013	0.07483	0.00083	0.02363	0.00145	494	53	470	8	465	5	472	29	6.0
17912-56	355	757	0.47	0.05892	0.00079	0.736	0.009	0.09057	0.00090	0.02847	0.00078	564	30	560	5	559	5	567	15	1.0
17912-60	506	692	0.73	0.05868	0.00099	0.722	0.011	0.08927	0.00089	0.02779	0.00110	555	38	552	7	551	5	554	22	0.8
17912-61	783	1230	0.64	0.05883	0.00088	0.696	0.010	0.08578	0.00083	0.02597	0.00089	561	33	536	6	531	5	518	18	5.6
17912-61B	507	1413	0.36	0.05964	0.00103	0.681	0.011	0.08286	0.00084	0.02749	0.00133	591	38	528	7	513	5	548	26	13.6
17912-62	393	742	0.53	0.05951	0.00084	0.728	0.010	0.08870	0.00093	0.02601	0.00077	586	31	555	6	548	6	519	15	6.8
17912-63	1502	2873	0.52	0.05879	0.00099	0.704	0.011	0.08686	0.00084	0.02670	0.00131	559	38	541	7	537	5	533	26	4.2
17912-66	1787	2198	0.81	0.05992	0.00088	0.696	0.010	0.08424	0.00091	0.02481	0.00082	601	33	536	6	521	5	495	16	13.7
17912-66B	1121	1785	0.63	0.05906	0.00110	0.706	0.012	0.08675	0.00091	0.02638	0.00134	569	41	543	7	536	5	526	26	6.0

Appendix 6
Results for Zircon U-Pb Dating

				RATIOS (common-Pb corrected)								AGES (common-Pb corrected, Ma)								
Analysis No.	Th (ppm)	U (ppm)	Th/U	$^{207}Pb/^{206}Pb$	± 1σ	$^{207}Pb/^{235}U$	± 1σ	$^{206}Pb/^{238}U$	± 1σ	$^{208}Pb/^{232}Th$	± 1σ	$^{207}Pb/^{206}Pb$	± 1σ	$^{207}Pb/^{235}U$	± 1σ	$^{206}Pb/^{238}U$	± 1σ	$^{208}Pb/^{232}Th$	± 1σ	Disc.
17912-66BE	644	1010	0.64	0.06043	0.00164	0.607	0.015	0.07284	0.00081	0.02073	0.00164	619	60	482	10	453	5	415	32	27.7
17912-70	385	731	0.53	0.05937	0.00089	0.766	0.011	0.09362	0.00090	0.02891	0.00104	581	33	578	6	577	5	576	20	0.7
17912-74	552	762	0.73	0.05895	0.00092	0.738	0.011	0.09080	0.00087	0.02778	0.00107	565	35	561	6	560	5	554	21	0.9
17912-76	602	1048	0.57	0.05891	0.00093	0.679	0.010	0.08365	0.00084	0.02493	0.00098	564	35	526	6	518	5	498	19	8.5
17912-77	576	798	0.72	0.05855	0.00101	0.699	0.011	0.08659	0.00086	0.02650	0.00118	550	39	538	7	535	5	529	23	2.9
Mafic Group																				
15199-02	210	559	0.38	0.10367	0.00189	4.031	0.070	0.28212	0.00309	0.07389	0.00364	1691	33	1641	14	1602	16	1441	69	6.0
15199-04	14045	3973	3.54	0.08807	0.00874	0.006	0.001	0.00050	0.00002	0.00014	0.00001	1384	179	6.2	1	3.2	0	2.8	0.2	99.8
17913-03	644	1302	0.49	0.06352	0.00116	0.445	0.008	0.05078	0.00051	0.01896	0.00091	725.8	38	374	5	319	3	380	18	0.0
17913-06	64	111	0.58	0.05734	0.00272	0.440	0.020	0.05565	0.00090	0.01667	0.00102	504.2	101	370	14	349	6	334	20	31.7
17913-07	145	151	0.96	0.08865	0.01653	0.053	0.010	0.00431	0.00019	0.00120	0.00018	1397	321	52.1	9	28	1	24.3	3.7	98.2

Appendix 7
Results for Zircon Hf isotope analysis

						Scherer et al., 2001 - ^{176}Lu decay constant (1.865×10^{-11})							
Analysis No.	Age (Ma)	$^{176}Hf/^{177}Hf$	2se	$^{176}Lu/^{177}Hf$	$^{176}Yb/^{177}Hf$	$^{176}Hf/^{177}Hf$ initial	epsilon Hf	1 se	T(DM) (Ga)	T(DM) crustal	Residence Time	Hf Chur (t)	Hf DM (t)
17911-01	558	0.282685	0.000050	0.002077	0.08662	0.282663	8.45	0.875	0.83	0.98	0.27	0.282425	0.282849
17911-03	523	0.282655	0.000028	0.001992	0.11139	0.282635	6.69	0.49	0.87	1.07	0.35	0.282447	0.282875
17911-05	509	0.282673	0.000030	0.001850	0.09820	0.282655	7.08	0.525	0.84	1.03	0.33	0.282455	0.282885
17911-06	546	0.282718	0.000022	0.001994	0.09886	0.282698	9.40	0.385	0.78	0.91	0.23	0.282432	0.282858
17911-07	553	0.282638	0.000017	0.001439	0.07485	0.282623	6.91	0.2905	0.88	1.08	0.33	0.282428	0.282853
17911-12	385	0.282666	0.000024	0.002032	0.09466	0.282651	4.20	0.42	0.85	1.12	0.47	0.282533	0.282974
17911-13	565	0.282630	0.000022	0.001725	0.08213	0.282612	6.78	0.385	0.90	1.10	0.33	0.282420	0.282844
~~17911-13b1~~	~~520~~	~~0.282425~~	~~0.000025~~	~~0.003565~~	~~0.129412~~	~~0.282390~~	~~-2.06~~	~~0.875~~	~~1.26~~	~~1.62~~	~~0.73507~~	~~0.282448~~	~~0.282877~~
17911-13b2c	520	0.282631	0.000019	0.001936	0.08906	0.282612	5.79	0.329	0.90	1.12	0.38	0.282448	0.282877
17911-14	544	0.282676	0.000026	0.001985	0.09294	0.282656	7.87	0.455	0.84	1.01	0.29	0.282433	0.282859
17911-15	556	0.282797	0.000052	0.003095	0.10924	0.282765	12.00	0.91	0.68	0.75	0.13	0.282426	0.282851
17911-19	553	0.282655	0.000019	0.001474	0.07002	0.282640	7.50	0.336	0.86	1.04	0.30	0.282428	0.282853
17911-21	349	0.282673	0.000019	0.001744	0.08471	0.282662	3.77	0.3325	0.84	1.12	0.49	0.282555	0.283000
17911-22	517	0.282561	0.000040	0.003766	0.13782	0.282525	2.63	0.7	1.06	1.32	0.54	0.282450	0.282879
17911-23	558	0.282568	0.000044	0.004132	0.16149	0.282525	3.54	0.77	1.06	1.30	0.50	0.282425	0.282849
17911-30	568	0.282636	0.000028	0.002610	0.09771	0.282608	6.72	0.49	0.91	1.10	0.34	0.282418	0.282842
17911-33	567	0.282710	0.000024	0.001642	0.08358	0.282693	9.68	0.42	0.78	0.91	0.21	0.282419	0.282843
17911-34	546	0.282676	0.000024	0.001682	0.08937	0.282659	8.02	0.42	0.83	1.00	0.29	0.282432	0.282858
17911-36	551	0.282590	0.000038	0.002800	0.09805	0.282561	4.67	0.665	0.98	1.22	0.43	0.282429	0.282854
17911-36	551	0.282698	0.000020	0.001775	0.09035	0.282680	8.87	0.35	0.80	0.95	0.25	0.282429	0.282854
17911-40	360	0.282667	0.000019	0.000710	0.03242	0.282662	4.03	0.3255	0.82	1.11	0.46	0.282548	0.282992

Appendix 7
Results for Zircon Hf isotope analysis

						Scherer et al., 2001 - ^{176}Lu decay constant (1.865×10^{-11})							
Analysis No.	Age (Ma)	$^{176}Hf/^{177}Hf$	2se	$^{176}Lu/^{177}Hf$	$^{176}Yb/^{177}Hf$	$^{176}Hf/^{177}Hf$ initial	epsilon Hf	1 se	T(DM) (Ga)	T(DM) crustal	Residence Time	Hf Chur (t)	Hf DM (t)
17911-52	545	0.282664	0.000022	0.001978	0.08162	0.282644	7.47	0.385	0.86	1.04	0.31	0.282433	0.282859
17911-55r	499	0.282481	0.000034	0.003583	0.13044	0.282447	-0.50	0.595	1.17	1.51	0.67	0.282462	0.282892
17911-55bc	544	0.282657	0.000024	0.002195	0.10179	0.282635	7.12	0.42	0.87	1.06	0.33	0.282433	0.282859
17911-56	422	0.282660	0.000054	0.002058	0.07177	0.282644	4.75	0.945	0.86	1.11	0.44	0.282510	0.282948
17911-59	335	0.282680	0.000013	0.000465	0.02226	0.282677	4.00	0.2345	0.80	1.09	0.46	0.282564	0.283010
17911-66r	540	0.282709	0.000016	0.001589	0.08542	0.282693	9.10	0.2835	0.78	0.93	0.24	0.282436	0.282862
17911-66bc	553	0.282698	0.000026	0.001619	0.08612	0.282681	8.97	0.455	0.80	0.94	0.25	0.282428	0.282853
17911-67	543	0.282678	0.000022	0.002203	0.11475	0.282656	7.84	0.385	0.84	1.01	0.30	0.282434	0.282860
17911-70	517	0.282689	0.000046	0.002110	0.10333	0.282669	7.73	0.805	0.82	1.00	0.31	0.282450	0.282879
~~17911-70b~~	~~517~~	~~0.282659~~	~~0.000028~~	~~0.001502~~	~~0.08028~~	~~0.282644~~	~~6.87~~	~~0.49~~	~~0.85~~	~~1.05~~	~~0.34~~	~~0.282450~~	~~0.282879~~
17912-01	552	0.282606	0.000019	0.003485	0.12121	0.282570	5.01	0.3325	0.98	1.20	0.43	0.282428	0.282854
17912-03	533	0.282665	0.000018	0.001470	0.07813	0.282650	7.43	0.315	0.84	1.03	0.31	0.282440	0.282867
17912-04	519	0.282429	0.000074	0.007888	0.30118	0.282352	-3.43	1.295	1.42	1.71	0.90	0.282449	0.282878
17912-05	547	0.282516	0.000044	0.003434	0.12406	0.282481	1.74	0.77	1.11	1.40	0.57	0.282432	0.282857
17912-08	537	0.282607	0.000026	0.002314	0.10268	0.282584	5.17	0.455	0.95	1.18	0.41	0.282438	0.282864
17912-11	493	0.282672	0.000018	0.002145	0.09813	0.282652	6.62	0.3115	0.85	1.05	0.36	0.282465	0.282896
17912-12	552	0.282704	0.000036	0.002215	0.10119	0.282681	8.94	0.63	0.80	0.95	0.25	0.282428	0.282854
17912-14	557	0.282545	0.000032	0.001475	0.05695	0.282530	3.69	0.56	1.01	1.29	0.46	0.282425	0.282850
17912-14B	387	0.282586	0.000024	0.001486	0.05948	0.282575	1.55	0.42	0.96	1.29	0.57	0.282532	0.282973
17912-15	555	0.282590	0.000015	0.001480	0.06456	0.282575	5.24	0.2555	0.95	1.19	0.40	0.282427	0.282851
17912-18	529	0.282640	0.000026	0.001481	0.06649	0.282625	6.46	0.455	0.88	1.09	0.35	0.282443	0.282870

Appendix 7
Results for Zircon Hf isotope analysis

						Scherer et al., 2001 - ^{176}Lu decay constant ($1.865x10^{-11}$)							
Analysis No.	Age (Ma)	$^{176}Hf/^{177}Hf$	2se	$^{176}Lu/^{177}Hf$	$^{176}Yb/^{177}Hf$	$^{176}Hf/^{177}Hf$ initial	epsilon Hf	1 se	T(DM) (Ga)	T(DM) crustal	Residence Time	Hf Chur (t)	Hf DM (t)
17912-20	549	0.282384	0.000028	0.003671	0.12585	0.282346	-2.98	0.49	1.32	1.70	0.77	0.282430	0.282856
17912-21	534	0.282599	0.000022	0.002396	0.08879	0.282575	4.79	0.385	0.96	1.20	0.43	0.282440	0.282867
17912-21b	499	0.282520	0.000050	0.002597	0.08689	0.282496	1.21	0.875	1.08	1.40	0.58	0.282462	0.282892
17912-23	559	0.282603	0.000028	0.002142	0.07947	0.282581	5.54	0.49	0.95	1.17	0.39	0.282424	0.282849
17912-24	533	0.282499	0.000036	0.003375	0.11491	0.282465	0.88	0.63	1.14	1.45	0.60	0.282440	0.282867
~~17912-24bcore~~	~~555~~	~~0.282242~~	~~0.000019~~	~~0.003361~~	~~0.117737~~	~~0.28221~~	~~-7.77~~	~~0.67~~	~~1.5208~~	~~2.01~~	~~0.97~~	~~0.28~~	~~0.28~~
17912-24bcore	555	0.282661	0.000036	0.002119	0.09473	0.282639	7.52	0.63	0.86	1.04	0.31	0.282427	0.282851
17912-27	527	0.282652	0.000020	0.001520	0.05928	0.282637	6.83	0.35	0.86	1.06	0.34	0.282444	0.282872
17912-30	550	0.282593	0.000034	0.003043	0.09888	0.282562	4.67	0.595	0.99	1.22	0.44	0.282430	0.282855
17912-35	545	0.282679	0.000036	0.002562	0.11201	0.282653	7.79	0.63	0.85	1.01	0.30	0.282433	0.282859
17912-36	565	0.282596	0.000034	0.003082	0.11116	0.282563	5.06	0.595	0.98	1.20	0.42	0.282420	0.282844
17912-37	516	0.282570	0.000026	0.003328	0.12008	0.282538	3.08	0.455	1.03	1.29	0.51	0.282451	0.282880
17912-37B	372	0.282643	0.000019	0.002445	0.08581	0.282626	3.01	0.665	0.90	1.19	0.53	0.282984	0.282870
17912-47	553	0.282615	0.000011	0.000867	0.04229	0.282606	6.31	0.1995	0.90	1.12	0.35	0.282428	0.282853
17912-50	531	0.282645	0.000020	0.001652	0.08366	0.282629	6.62	0.35	0.88	1.08	0.34	0.282442	0.282869
17912-50B	558	0.282725	0.000032	0.002024	0.10039	0.282704	9.88	0.56	0.77	0.89	0.21	0.282425	0.282849
17912-51	465	0.282629	0.000026	0.001292	0.06399	0.282618	4.78	0.455	0.89	1.15	0.42	0.282483	0.282917
17912-60	551	0.282577	0.000032	0.002058	0.07228	0.282556	4.48	0.56	0.98	1.23	0.43	0.282429	0.282854
17912-61	531	0.282666	0.000017	0.001747	0.07985	0.282649	7.33	0.301	0.85	1.03	0.32	0.282442	0.282869
17912-63	548	0.282681	0.000032	0.003285	0.14341	0.282647	7.66	0.56	0.86	1.03	0.31	0.282431	0.282857
17912-66	521	0.282620	0.000036	0.004175	0.14844	0.282579	4.65	0.63	0.98	1.20	0.46	0.282448	0.282876

Appendix 7
Results for Zircon Hf isotope analysis

						Scherer et al., 2001 - ^{176}Lu decay constant (1.865×10^{-11})							
Analysis No.	Age (Ma)	$^{176}Hf/^{177}Hf$	2se	$^{176}Lu/^{177}Hf$	$^{176}Yb/^{177}Hf$	$^{176}Hf/^{177}Hf$ initial	epsilon Hf	1 se	T(DM) (Ga)	T(DM) crustal	Residence Time	Hf Chur (t)	Hf DM (t)
17912-66BCOI	536	0.282514	0.000042	0.003430	0.11242	0.282480	1.45	0.735	1.12	1.41	0.58	0.282438	0.282865
17912-66BCOI	453	0.282728	0.000036	0.002351	0.11496	0.282708	7.71	0.63	0.77	0.95	0.32	0.282490	0.282925
17912-70	577	0.282613	0.000010	0.001273	0.06331	0.282599	6.60	0.182	0.91	1.12	0.34	0.282413	0.282836
17912-76	518	0.282667	0.000026	0.001851	0.09302	0.282649	7.06	0.455	0.85	1.04	0.33	0.282450	0.282878
15199-02	1691	0.281523	0.000044	0.001372	0.05260	0.281479	-8.14	0.77	2.44	2.92	0.75	0.281708	0.282021
15199-04	3	0.283089	0.000026	0.001359	0.04425	0.283089	11.28	0.455	0.23	0.37	0.23	0.282770	0.283249
17913-03	319	0.282661	0.000036	0.001703	0.06482	0.282651	2.73	0.63	0.85	1.16	0.53	0.282574	0.283022
17913-06	349	0.283060	0.000070	0.002286	0.06403	0.283045	17.34	1.225	0.28	0.25	-0.07	0.282555	0.283000
17913-07	28	0.283198	0.000052	0.003489	0.11967	0.283196	15.61	0.91	0.08	0.11	0.05	0.282755	0.283231